FABRICATION, SIMULATION AND TECHNO-ECONOMIC EVALUATION OF THIN FILM NANOCOMPOSITE MEMBRANE FOR ACID MINE DRAINAGE TREATMENT

BY

SELAELO KHOLOFELO RAMOKGOPA

Dissertation in fulfilment of the requirements of the degree

Master of Technology (MTech)

In

Chemical Engineering

Faculty of Engineering and the Built Environment (FEBE)

at the

University of Johannesburg

Supervisor: Prof K. Moothi

Co-Supervisors: Prof R. Moutloali and Dr K. Sikhwivhilu

DEDICATION

To my loving family

My parents: Nkhensani Ramokgopa, Mashakgene Ramokgopa, Victoria Moloi and Peter Moloi

My siblings: Khanyisa, Tshepo, Karabo, Themba and Palesa and my nephews Ntwanano and Oratile

ACKNOWLEDGEMENTS

I would like to express my sincere gratitude to Prof Kapil Moothi for giving me the opportunity to embark on such meaningful research in nanotechnology and wastewater treatment. Thank you for believing in me.

Secondly, I would like to thank my co-supervisor Prof Richard Moutloali for always being willing to help and for introducing me to the world of thin film membranes and also thank my co-supervisor Dr Keneiloe Sikhwivhilu for allowing me to use Mintek facilities for my research.

Thank you to Dr. Selby Maphutha for allowing me to express my thoughts and creativity through this research and for his constructive criticism during the development and proposal stages of the project.

Thank you to the DSI/Mintek Nanotechnology Innovation Centre (NIC) for their feedback and suggestions that helped to improve my work. I would like to give a special thanks to Dr Poslet Shumbula, Mr Bongani Mlasi and Ms Linah Shapo for their assistance with analysis.

I would like to thank Prof Peter Olubambi for providing NRF funding for the research project.

Thank you to my friend and fellow researcher, Lizzie Mampane, who held me together when I felt like I was about to lose my mind.

Lastly, I would like to thank my family for all their love and support. I do not know how I would have managed without you.

ABSTRACT

Thin Film Composite (TFC) membrane technology has been applied in the removal of various pollutants from wastewater. TFC membranes have small pore sizes which enable the rejection of multivalent ions such as those found in Acid Mine Drainage (AMD). Also, nanoparticles with desirable properties have been added to TFC membranes to form Thin Film Nanocomposite (TFN) membranes with potentially enhanced properties. A great opportunity is provided for novel and sustainable development of TFN membranes with Carbon Nanotube (CNTs) for the treatment of AMD. CNT-Infused TFN membranes were synthesized to investigate the feasibility for use in synthetic AMD treatment. Flux and rejection under various operating conditions were measured. The addition of CNTs improved flux by up to 50% and reduced heavy metal concentration in AMD up to 95%. Furthermore, rejection followed the sequence $Mg^{2+}>Fe^{3+}>Al^{3+}$. Design of Experiments (DOE) was used to determine the effects of process parameters (heavy metal concentration, pressure and MWCNT loading) on process optimisation and semi-empirical modelling techniques were conducted on the experimental data. Response Surface Methodology (RSM) was used to evaluate model outputs and Analysis of variance (ANOVA) was used for model validation. Iron concentration, pressure and CNT loading were found to have the most significance on the process followed by magnesium concentration and aluminium concentration according to RSM results. From the RSM model optimum parameters of 20 bar and CNT loading of 0.3% were found. The optimum parameters obtained from RSM were used to optimise flux and rejection of heavy metals at lab scale. In order to determine if the process would be feasible on an industrial scale, process simulation was conducted. Mathematical models were generated through mass balance equations that included the effect of membrane area and length on flux. Processes were simulated with CAPE-OPEN chemical engineering design software along with mass and energy balances. Design parameters (pressure, flowrate, number of passes) were varied in order optimise process conditions including energy requirements. The simulation could effectively be used for scale-up of TFN treatment systems.

Economic risk factors such as interest rate, inflation rate and electricity price are barriers that prevent potential investment in membrane-based technology. Therefore, an economic risk evaluation of the simulated TFN membrane treatment plant was conducted considering variables which could affect membrane plant Capital Expenditure (CAPEX) and Operating Expenditure

(OPEX). The variables were stochastically modelled using Monte Carlo simulation. Historical data was used to model the variables and they were incorporated into equations for determining CAPEX and OPEX costs. The CAPEX costs and OPEX costs for the Double-Pass-System (DPS) were found to be R7.27E+07and R9.15E+06 respectively, while for the Single-Pass-System (SPS) they were R6.78E+07 for CAPEX and R8.43E+06 for OPEX. Once the CAPEX and OPEX were determined, they were used to calculate the Net Present Value (NPV) which was used as an indicator of economic viability. By incorporating these variables into the NPV estimation, a more robust economic model was developed which accounted for the effect of fluctuations in these variables on project investment. If energy prices are kept below 1.36 R/kWh for DPS and 1.22 R/kWh for SPS and the inflation rate is below 5.7% for SPS and 6.34% for DPS then the project is feasible. Although the breakeven point was larger than expected due to high investment costs, the NPV was found to be 1.11 billion for SPS and 1.26 billion for DPS after 20 years. The payback period was 7 years. Both the NPV and the payback period indicate that the project is economically feasible over the plant lifetime. In conclusion, this study significantly contributes to two fields. Firstly, the development of a TFN membrane for heavy metal removal from AMD is proposed and secondly the development of a novel techno-economic model for a membrane plant based on the TFN membrane.

PRESENTATIONS

S.K. Ramokgopa, K.S. Maphutha, K. Moothi. (2017)

A comparative analysis of the feasibility of using Carbon Nanotube (CNT)-reinforced membrane for Acid Mine Drainage (AMD) treatment: Proposal Defence at School of Mining Metallurgy and Chemical Engineering at University of Johannesburg.

S.K. Ramokgopa, K.S. Maphutha, K. Moothi. (2017)

A comparative analysis of the feasibility of using Carbon Nanotube (CNT)-reinforced membrane for Acid Mine Drainage (AMD) treatment: Top 20 finalist to participate in the presentation of Masters Proposal, hosted by Technology Innovation Agency (TIA) and South African Technology Network (SATN).

S.K. Ramokgopa, R. Moutloali, K. Sikhwivhilu, K. Moothi. (2018)

Carbon Nanotube-infused Thin Film Composite membrane for Acid Mine Drainage (AMD) Treatment: Oral presentation at the University of Johannesburg Annual Postgraduate Research Conference.

S.K. Ramokgopa, K. Sikhwivhilu, R. Moutloali, K. Moothi. (2019)

Thin film nanocomposite membrane for heavy metal rejection from Acid Mine Drainage (AMD): Poster presented at 20th WaterNet/ WARFSA/ GWPSA Symposium.

S.K. Ramokgopa, K. Sikhwivhilu, R. Moutloali, K. Moothi. (2019)

Thin film nanocomposite membrane for heavy metal rejection from Acid Mine Drainage (AMD): Poster presented at Nanoscience's Young Researcher's Symposium.

S.K. Ramokgopa, K. Sikhwivhilu, R. Moutloali, K. Moothi. (2019)

Thin Film Nanocomposite (TFN) membrane evaluation for Acid mine Drainage (AMD) treatment: Oral presentation at Polymer Processing Society (PPS) Europe-Africa Regional Conference.

PUBLICATIONS

S.K. Ramokgopa, K. Sikhwivhilu, R. Moutloali, K. Moothi. (2020)

Process optimization through Response Surface Methodology for treatment of acid mine drainage using carbon nanotubes-infused thin film nanocomposite membranes. Submitted to Journal of Physics and Chemistry of the Earth.

S.K. Ramokgopa, K. Sikhwivhilu, R. Moutloali, K. Moothi. (2020)

Techno-economic evaluation of carbon nanotubes-infused thin film nanocomposite membranes using time series forecasting and Monte Carlo simulation.

Manuscript in preparation.

TABLE OF CONTENT

LIST OF FIGURES

LIST OF TABLES

LIST OF ABBREVIATIONS

AFM	Atomic Force Microscopy
Al	Aluminium
AMD	Acid mine Drainage
BSA	Bovine Serum Albumin
CAPE-OPEN	Computer Aided Process Engineering Open Source
CNT	Carbon Nanotube
COFE	CAPE-OPEN Flowsheet Environment
CVD	Chemical Vapour Deposition
FB	Fluidised Bed
Fe	Iron
FTIR	Fourier Transform Infrared Spectroscopy
GDP	Gross Domestic Profit
PA	Polyamide
PAN	Polyacrylonitrile
PES	Polyether sulphone
PIP	Piperizine
PFD	Process Flow Diagram
PVDF	Poly vinylidene fluoride
IRR	Internal Rate of Return
MPD	M-phenylene diamine

Mg	Magnesium
MRR	Minimum Rate of Return
MWCNT	Multi-walled Carbon Nanotube
MWCO	Molecular Weight Cut-off
MF	Microfiltration
NF	Nanofiltration
NPBT	Net Profit Before Tax
NPAT	Net Profit After Tax
NPV	Net Present Value
RO	Reverse Osmosis
ROI	Return on Investment
SA	South Africa
SEM	Scanning Electron Microscopy
SRB	Sulphate Reducing Bacteria
SWCNT	Single-walled Carbon Nanotube
TEC	Total Equipment Cost
TEM	Transmittion Electron Microscopy
TMC	Trimesoyl Chloride
UF	Ultra Filtration
VLS	Vapour Liquid Solid
VSS	Vapour Solid Solid

LIST OF NOMENCLATURE

A_f	Cross-sectional area for feed flow	m^2
AIC	Akaike's Information Criterion	(-)
A_m	Cross-sectional area for membrane envelope	m^2
A_p	Membrane area for permeation	m^2
A_t	Cross-sectional area for membrane element	m^2
BIC	Schwarz Bayesian Information Criterion	(-)
C_{admin}	Administration costs	R
C_b	Concentration in the bulk solution	mol/L
$C_{capital}$	Capital costs	R
$C_{chemical}$	Chemical costs	R
C_{civil}	Civil engineering costs	R
$C_{deprec}(t)$	Cost of depreciation over time	R
C_{direct}	Direct costs	R
$C_{electro}$	Electrochemical costs	R
C_F	Feed concentration	mol/L
C_{fix}	Fixed costs	R
$C_{installation}$	Cost of installation	R
C_{maint}	Maintenance costs	R
C_{mech}	Mechanical costs	R
$C_{membrane}$	Membrane costs	R
C_p	Permeate concentration	mol/L
C_{lab}	Laboratory costs	R
$C_{quality\ control}$	Cost of quality control	R
C_R	Retentate concentration	mol/L
C_{raw}	Cost of raw material	R
C_{sup}	Supply cost	R
C_W	Concentration at membrane wall	mol/L
C_{util}	Utility cost	R
D	Outer diameter of the spiral	m

DB	Durbin Watson statistic	(-)
Dx	Diffusivity	m^2/s
d	diameter of pipe	m
dh	height of the feed channel	m
$\varepsilon(t)$	Stochastic variable for electricity prices	R/kWh
I_{cap}	Capital investment cost	R
I_{equip}	Equipment cost	R
I_{ncap}	Non-capital equipment cost	R
I_{start}	Start-up cost	R
I_{total}	Total investment cost	R
I_{wcap}	Working capital cost	R
J	Flux through membrane	m/s
JB	Jarque-Bera statistic	(-)
J_S	Solute flux	m/s
k	Cost component of membrane area	(-)
K_m	Mass transfer coefficient	m/s
k_S	Boundary layer coefficient	psi
k_W	Water permeability	m/s/MPa
Pr	Retentate permeate	m^2/s
Pf	Feed permeate	m^2/s
ΔP	Pressure difference	(-)
L	Length	m
Lf	Lang factor	(-)
m	Number of years within plant lifetime	years
MAE	Mean absolute error	same as y_t
MAPE	Mean absolute percentage error	same as y_t
NDP	Net driving pressure	psi
n_i	Number of envelopes	(-)
Q_F	Feed flowrate	m^3/h
Q_P	Permeate flowrate	m^3/h

Q_R	Retentate flowrate	m^3/h
R	Rejection	%
Re	Reynolds number	(-)
RMSE	Root mean square error	same as y_t
$r_f(t)$	Stochastic variable for inflation prices	(-)
$r_i(t)$	Stochastic variable for interest rates	(-)
S_C	Schmidt number	m^2/s
Sh	Sherwood number	(-)
T	Temperature	K
tm	Overall thickness of spiral envelope	m
ts	Thickness of the feed channel	m
w	Membrane width	m
W_R /rec	Water recovery	(-)
π	Osmotic pressure	psi
πf	Osmotic pressure of the feed	psi
πp	Osmotic pressure of the permeate	psi
θ	Correlation coefficient	(-)
$f_x(X_1, X_2, \dots X_d)$	Probability density function	$1/X_d$
h	Time lag in correlation matrix	year
$\sum h$	Correlation matrix at lag h	(-)
$\sum X$	Covariance matrix	(-}
pij	Correlation symmetric matrix	(-)
$\rho(X(t), Y(t+h))$	Lag correlation between X and Y	(-)
σ_{ij}	Variance of variables	(-)
δ	Factor used to update cost index	(-)
y_t	Actual value * depend on data	
$\widehat{y_t}$	Predicted value * depend on data	

CHAPTER 1

1.1 INTRODUCTION AND BACKGROUND

Acid Mine Drainage (AMD) is the acidic runoff generated from mining activities by the oxidation of sulphide to sulphuric acid through the exposure of sulphide-bearing ore to water and oxygen (Aguiar et al., 2016; Akcil and Koldas, 2006; Mthetwa, 2014; Simate and Ndlovu, 2014). Heavy metals are leached out in the process and are carried into rivers, seas and other bodies of water even contaminating soil and underground water (Alloway, 2013; Durand, 2012; McCarthy, 2011). According to Duruibe et al. (2007) mining activities account for most of the environmental pollution by heavy metals, especially the pollution of natural water sources Due to the excessive volumes of AMD that are formed, it is considered as an interminable process that is difficult to control and has high treatment costs (Aguiar *et al*., 2016; Jiwan and Kalamdhad, 2011; Simate and Ndlovu, 2014). The high concentration of metals and metalloids present in AMD compromise the ecological balance (Aguiar *et al*., 2016). As heavy metals are not biodegradable, they can accumulate in living organisms (Al-Rashdi *et al*., 2013; Lofrano *et al*., 2016; Qin and Deng, 2017). Research has shown that heavy metals can adversely affect the growth and reproductive system of animals and fish (Jiwan and Kalamdhad, 2011). In human beings, heavy metals can prevent the effective adsorption of vital minerals (Simate and Ndlovu, 2014). In addition, global water scarcity has created an opportunity for the treatment of AMD water for re-use (da Silveira *et al*., 2009; Martins *et al*., 2010; Wadekar *et al*., 2017). The treatment of AMD is of great importance to scientists and engineers all over the world, and conventional remediation techniques including ion exchange, biological treatment and neutralisation have been implemented (Mthetwa, 2014). However, these methods are either expensive, produce toxic by-products or cannot remove heavy metals to the standards required by the World Health Organisation (WHO) (Mthetwa, 2014). The use of membrane technology is rivalling current remediation techniques as it is more cost effective compared to conventional methods, and it is also easier to scale-up and modify the technology for different applications (Masebinu, *et al*., 2014; Vatanpour *et al*., 2011).

Membrane separation technology has emerged as an attractive option for wastewater treatment including the treatment of AMD (Aguiar *et al*., 2016; Al-Zoubi *et al*., 2010). Inorganic and

polymeric membranes have been used for separation (Goh and Ismail, 2017; Jhaveri and Murthy, 2016; Wang *et al*., 2015). Even so, polymeric membranes are preferred for industrial application due to their low cost (Al Aani *et al*., 2017). Moreover, they are chemically and thermally stable (Mthetwa, 2014; Wang *et al*., 2014) and their pore size and surface properties are easy to manipulate (Hua *et al*., 2012). Membranes are classified according to pore size, which determines their application (Brandhuber and Amy, 1998; Sarbolouki, 1982). Microfiltration (MF) membranes have the largest pore size and can reject suspended solids and bacteria (Liang *et al*., 2014; Mehwish *et al*., 2014). Ultrafiltration (UF) membranes have smaller pore sizes than MF and reject colloids and macromolecules in addition to the substances that MF can reject (Zhao and Yu, 2015). Nanofiltration (NF) and reverse osmosis (RO) membranes provide an advantage over the other two technologies, as they are capable of ion rejection due to their smaller pore size (Davis *et al*., 2010; Srivastava *et al*., 2013).

NF/RO polymeric membranes have been widely used in wastewater treatment applications (Blöcher *et al*., 2012; Ellouze *et al*., 2012; Lau *et al*., 2013; Wang *et al*., 2015). NF membranes have an advantage over RO membranes as they have a higher flux and lower operating pressure. The typical pore size for NF membranes ranges between 1 to 10 nm and a molecular cut of 200 to 1000 Dalton (Da) which enables a lower rejection of monovalent ions, and a higher rejection of multivalent ions (Gohil and Ray, 2017; Khulbe and Matsuura, 2017). The charge on the membrane influences ion rejection. A negative charge, which is typical of most polymeric NF membranes, allows high rejection of anions but positively charged membranes also exist (Mohammad *et al*., 2015). Donnan, steric and di-electric mechanisms govern the rejection of ions. NF and RO membranes are effective in the rejection of heavy metals in AMD (Al-Zoubi *et al*., 2010; Drioli, and Giorno, 2016; Vatanpour *et al*., 2011). Membranes with pore sizes within the NF/RO range are collectively applied as thin film composite (TFC) membranes where UF or MF membranes form the support layer (Paul and Jons, 2016). TFC membrane(s) have proven to be suitable for AMD treatment, (Al-Rashdi *et al*., 2013; Al-Zoubi *et al*., 2010), hence they were chosen in this study. Research findings to date focus on the use of TFC membranes for AMD treatment (Aguiar *et al*., 2016; Wadekar *et al*., 2017) while few studies on the capability of CNT-infused membranes for the treatment of AMD exist (Mthetwa, 2014; Vatanpour *et al*., 2011).

However, membrane fouling and concentration polarisation threatens further evolution and use of membrane technology on a commercial scale. (Jhaveri and Murthy, 2016; Li *et al*., 2013; Vatanpour *et al*., 2011). Concentration polarisation occurs when there is increase in ion concentration on the surface of the feed side of the membrane, which causes an increase in osmotic pressure and a decrease in trans-membrane pressure (Andrade *et al*., 2017). As organic, inorganic, colloidal or biological matter deposits on the membrane, it hinders the adsorption of ions by the membrane active layer that leads to a loss in selectivity (Mohammad *et al*., 2015). The pores of the membrane also become clogged leading to a decline in flux and permeability (Kim and Van der Bruggen, 2010). The membranes constantly need to be cleaned or replaced and this decreases the operability of the membrane (Kim and Van der Bruggen, 2010; Mohammad *et al*., 2015). Andrade et al. (2017) used a commercial NF 90 membrane to treat mining effluent and noticed that fouling and concentration polarisation led to an 80% decrease in flux (Andrade *et al*., 2017). Concentration polarisation can be minimised by increasing fluid velocity near the surface of the membrane such that accumulation of solutes on the membrane is reduced (Maphutha *et al*., 2013) Membrane fouling can be reduced by increasing the hydrophilicity of the membrane using various methods such as incorporating hydrophilic nanoparticles into the membrane (Baghbanzadeh *et al*., 2016) Another advantage is that the addition of hydrophilic nanoparticles is potentially beneficial in the formation of TFC membranes as they can enhance the wet zone of the top active layer, speed up diffusion of monomers to the interface and prevent the rapid change of pH in reaction by acting as a buffering agent (Zarrabi *et al*., 2016).

Carbon nanotubes (CNTs) have been perceived as the epitome of materials to be incorporated into polymers for AMD treatment (Rashid and Ralph, 2017; Vatanpour *et al*., 2011; Wang *et al*., 2015; Yengejeh *et al*., 2017). CNTs can be considered as cylindrical, seamless sheets of graphene (Ma *et al*., 2010; Mittal *et al*., 2015; Moothi *et al*., 2012). Single-walled carbon nanotubes (SWCNTs) are formed from rolling a single sheet of graphene while multi-walled carbon nanotubes (MWCNTs) are concentrically rolled sheets of graphene (Herrera-Herrera *et al*., 2012; Hussain *et al*., 2011; Maphutha *et al*., 2013; Pal and Kumar, 2016). They have been produced using arc discharge, laser ablation and chemical vapour deposition (Herrera-Herrera *et al*., 2012; Purohit *et al*., 2014; Shah and Tali, 2016). CNTs have exceptional chemical,

thermal and electrical properties owing to their cyclic structure and high aspect ratio of length to diameter (Dimpe and Nomngongo, 2017; Jourdain and Bichara, 2013).

CNTs have been used effectively as adsorbents in wastewater treatment (Dimpe and Nomngongo, 2017; Gautam and Chattopadhyaya, 2016; Jourdain and Bichara, 2013; Sakar *et al*., 2018). Due to their lightweight and high strength they have been assimilated into polymer matrixes for wastewater treatment application (Mthetwa, 2014; Shawky *et al*., 2011; Maphutha *et al*., 2013; Manawi *et al*., 2016), including the removal of heavy metals (Pyrzyńska and Bystrzejewski, 2010; Sakar *et al*., 2018; Salehi et al., 2012; Vatanpour *et al*., 2011). Not only do they deter foulants, but they can also increase flux, permeability, salt rejection and mechanical stability in membranes (Celik *et al*., 2011; de Lannoy *et al*., 2013; Liu *et al*., 2013; Yengejeh *et al*., 2017) making them ideal for use in AMD treatment. There is growing interest in the enhancement polymer membranes through the integration of numerous adsorbents including CNTs in the polymer matrix (Mittal *et al*., 2015; Sakar *et al*., 2018). Al-Hobaib *et al*. (2017) prepared a TFC membrane with different CNT loadings and found that membrane permeation, flux and salt rejection were higher for the prepared membrane compared to the unmodified membrane. Research is ongoing as to how to impart polymer-based membranes with antifouling properties, improve hydrophilicity and increase permeate flux (Li *et al*., 2013; Shawky *et al*., 2011), while increasing affinity for heavy metal rejection (Carolin *et al*., 2017; Vatanpour *et al*., 2011). As such, polymer membranes have been imbedded with nano-adsorbents such as CNTs for the removal of heavy metal ions (Mthetwa, 2014; Vatanpour *et al*., 2011).

1.2 PROBLEM STATEMENT

AMD poses a huge risk to the environment. Therefore, treatment of AMD is of primary concern. If left untreated, metal contaminants can seep into the food chain and have detrimental effects on plants, animals and human beings. Membrane technology is popular for water treatment and has even been applied in wastewater treatment. TFC membrane(s) are favoured for the treatment of AMD. However, the performance of TFC membranes can still be improved by the addition of CNTs which have been shown to improve flux, rejection, antifouling and hydrophilicity in

wastewater treatment. A superior membrane can be synthesized by incorporating CNTs in TFC membrane(s) for AMD treatment.

1.3 AIM

The aim of this study was to explore the possibility of using CNT reinforced TFN membrane(s) for application in AMD treatment. In particular, the potential of MWCNTs to enhance the flux and heavy metal rejection ability of the TFN active layer was investigated. This study establishes the effectiveness of using TFN membrane(s) embedded with different loadings of oxidised CNTs for the removal of heavy metals from AMD. Experimental the data was modelled and a simulation was developed using computer software for chemical engineering application. Furthermore, an economic evaluation of the simulated membrane plant was conducted.

1.4 RESEARCH OBJECTIVE(S)

- Synthesise and characterise TFN membranes
- Investigate the efficiency of TFN membranes in the rejection of heavy metal ions from AMD
- Develop a predictive model for the rejection of heavy metals in AMD relative to CNT loading in TFN membranes
- Simulate a TFN membrane treatment plant and evaluate the economic feasibility of the plant.

1.5 HYPOTHESIS

The inclusion of CNTs in TFN membranes will improve the flux and ion rejection of MWCNT-modified TFN membrane(s) for application in AMD treatment. Modelling and simulation will help to predict and improve factors that could hinder technology development and implementation.

1.6 SIGNIFICANCE OF RESEARCH

The research is significant, as it determines whether the infusion of MWCNTs improves membrane performance. Additionally, the research helps to determine whether MWCNT-modified TFN polymer membranes can be used for the rejection of heavy metal ions from AMD. Although, TFN membranes have been used in wastewater treatment application, TFN membranes infused with MWCNTs have not been used on a commercial scale and their operability, scalability and economic feasibility has not been investigated. This study is also significant in adding something new to the pool of knowledge that exists on the performance of CNT-TFN membranes by going beyond the lab scale tests and exploring the commercial viability of the process for AMD treatment.

1.7 THESIS OUTLINE

Chapter 1: An introduction to AMD formation is given. The effects of AMD and why treatment is important are briefly mentioned. Membrane technology is proposed as a treatment option for the removal of heavy metals from AMD. The benefits of using modified membranes for the treatment of AMD are discussed. The problem statement aims and objectives of the study are outlined.

Chapter 2: The formation of AMD is discussed in detail. A literature review of current treatment methods for AMD including membrane filtration is provided. The membrane types, characteristics, configuration, synthesis methods and applications are discussed with focus on the application of TFC membrane(s) for heavy metal rejection. The effect of modified TFC membranes on membrane performance, particularly with CNTs, is reviewed

Chapter 3: This chapter details the methodology used in the study. The type of equipment, materials and experimental procedure are given.

Chapter 4: The results obtained from modified TFN membranes for the removal of heavy metals from AMD are discussed. All parameters i.e., effect of pressure, effect of concentration, and effect of CNT loading are discussed. The results from Transmission Electron Microscopy, Raman, Fourier-transform infrared spectroscopy, and contact angle are given.

Chapter 5: The modelling and simulation of TFN membranes for heavy metal rejection is discussed. The model equations, parameters, assumptions, simulation software and simulation results and procedure are explained.

Chapter 6: An economic evaluation was performed on the plant based on optimum conditions from modelling and simulation.

Chapter 7: Conclusions and recommendations for the study are given in this chapter.

1.8 REFERENCES

Aguiar, A.O., Andrade, L.H., Ricci, B.C., Pires, W.L., Miranda, G.A., Amaral, M.C.S. (2016). Gold acid mine drainage treatment by membrane separation processes: An evaluation of the main operational conditions. *Separation and Purification Technology*, 170:360-369.

Akcil, A. and Koldas, S. (2006). Acid mine drainage (AMD): Causes, treatment and case studies. *Journal of Cleaner Production*, 14(12–13):1139-1145.

Al Aani, S., Wright, C.J., Atieh, M.A., Hilal, N. (2017). Engineering nanocomposite membranes: Addressing current challenges and future opportunities. *Desalination*, 40:11-15.

Al-Hobaib, A.S., Al-Sheetan, K.M., Shaik, M.R. and Al-Suhybani, M.S. (2017). Modification of thin-film polyamide membrane with multi-walled carbon nanotubes by interfacial polymerization. *Applied Water Science*, 7(8):4341-4350.

Alloway, B.J., (2013), 'Sources of heavy metals and metalloids in soils' in *Heavy metals in soils*. Springer: Dordrecht. pp. 11-50.

Al-Rashdi, B., Johnson, D.J., Hilal, N. (2013). Removal of heavy metal ions by nanofiltration. *Desalination*, 315:2-17.

Al-Zoubi, H., Rieger, A., Steinberger, P., Pelz, W., Haseneder, R., Hartel, G. (2010). Optimisation study for treatment of Acid Mine Drainage using membrane technology. *Separation and Technology*, 14 (14): 2004-2016.

Andrade, L.H., Ricci, B.C., Grossi, L.B., Pires, W.L., Aguiar, A.O., Amaral, M.C.S. (2017). Nanofiltration applied in gold mining effluent treatment: Evaluation of chemical cleaning and membrane stability. *Chemical Engineering Journal*, 323:545-556.

Baghbanzadeh, M., Rana, D., Lan, C.Q. and Matsuura, T. (2016). Effects of inorganic nano-additives on properties and performance of polymeric membranes in water treatment. *Separation and Purification Reviews*, 45(2):141-167.

Blöcher, C., Niewersch, C. and Melin, T. (2012). Phosphorus recovery from sewage sludge with a hybrid process of low pressure wet oxidation and nanofiltration. *Water Research*,46(6):2009-2019.

Brandhuber, P. and Amy, G. (1998). Alternative methods for membrane filtration of arsenic from drinking water. *Desalination*, 117(1-3):1-10.

Carolin, C.F., Kumar, P.S., Saravanan, A., Joshiba, G.J. and Naushad, M. Efficient techniques for the removal of toxic heavy metals from aquatic environment: A review. *Journal of Environmental Chemical Engineering*, 5:2782-2799.

Celik, E., Park, H., Choi, H. and Choi, H. (2011). Carbon nanotube blended polyethersulfone membranes for fouling control in water treatment. *Water Research*, 45(1):274-282.

Davis, M.L. (2010), 'Reverse osmosis and nanofiltration' in *Water and Wastewater Engineering: Design Principles and Practice*. McGraw-Hill:New York. pp1097h-1097c.

da Silveira, A.N., Silva, R. and Rubio, J. (2009). Treatment of acid mine drainage (AMD) in south brazil: Comparative active processes and water reuse. *International Journal of Mineral Processing*, 93(2):103-109.

de Lannoy, C., Soyer, E. and Wiesner, M.R. (2013). Optimizing carbon nanotube-reinforced polysulfone ultrafiltration membranes through carboxylic acid functionalization. *Journal of Membrane Science*, 447:395-402.

Dimpe, K.M. and Nomngongo, P.N. (2017). A review on the efficacy of the application of myriad carbonaceous materials for the removal of toxic trace elements in the environment. *Trends in Environmental Analytical Chemistry*, 16:24-31.

Durand, J.F. (2012). The impact of gold mining on the Witwatersrand on the rivers and karst system of Gauteng and North West province, South Africa. *Journal of African Earth Sciences*, 68:24-43.

Duruibe, J.O., Ogwuegbu, M. and Egwurugwu, J.N. (2007). Heavy metal pollution and human biotoxic effects. *International Journal of Physical Sciences*, 2(5):112-118.

Ellouze, E., Tahri, N. and Amar, R.B. (2012). Enhancement of textile wastewater treatment process using nanofiltration. *Desalination*, 286:16-23.

Gautam, R.K. and Chattopadhyaya, M.C., (2016). *Advanced Nanomaterials for Wastewater Remediation*. CRC Press:New York. pp 203-214.

Gohil, J.M. and Ray, P. (2017). A review on semi-aromatic polyamide TFC membranes prepared by interfacial polymerization: Potential for water treatment and desalination. *Separation and Purification Technology*, 181:159-182.

Goh, P.S. and Ismail, A.F. (2017). A review on inorganic membranes for desalination and wastewater treatment. *Desalination*, 434:60-80.

Herrera-Herrera, A.V., González-Curbelo, M.Á, Hernández-Borges, J. and Rodríguez-Delgado, M.Á. (2012). Carbon nanotubes applications in separation science: A review. *Analytica Chimica Acta*, 73:41-30.

Hua, M., Zhang, S., Pan, B., Zhang, W., Lv, L., Zhang, Q. (2012). Heavy metal removal from water/wastewater by nanosized metal oxides: A review. *Journal of Hazardous Materials*, 211:317-331.

Hussain, S., Jha, P., Chouksey, A., Raman, R., Islam, S.S., Islam, T., Choudhary, P.K. (2011). Spectroscopic investigation of modified single wall carbon nanotube (SWCNT). *Journal of Modern Physics*, 2(6):538-543.

Jhaveri, J.H. and Murthy, Z. (2016). A comprehensive review on anti-fouling nanocomposite membranes for pressure driven membrane separation processes. *Desalination*, 379:137-154.

Jiwan, S. and Kalamdhad, A.S. (2011). Effects of heavy metals on soil, plants, human health and aquatic life. *International Journal of Research in Chemistry and Environment*, (2):15-21.

Jourdain, V. and Bichara, C. (2013). Current understanding of the growth of carbon nanotubes in catalytic chemical vapour deposition. *Carbon*, 58:2-39.

Kim, J. and Van der Bruggen, B. (2010). The use of nanoparticles in polymeric and ceramic membrane structures: Review of manufacturing procedures and performance improvement for water treatment. *Environmental Pollution*, 158(7):2335-2349.

Khulbe, K.C. and Matsuura, T. (2017). Synthetic membrane characterisation–a review: Part I. *Membrane Technology*, 2017(7):7-12.

Lau, W.J., Ismail, A.F. and Firdaus, S. (2013). Car wash industry in malaysia: Treatment of car wash effluent using ultrafiltration and nanofiltration membranes. *Separation and Purification Technology*, 104:26-31.

Li, J., Shao, X., Zhou, Q., Li, M. and Zhang, Q. (2013). The double effects of silver nanoparticles on the PVDF membrane: Surface hydrophilicity and antifouling performance. *Applied Surface Science*, 265:663-670.

Liang, R., Hatat-Fraile, M., Hu, A. and Zhou, N. (2014) 'Fundamentals on Adsorption, Membrane Filtration and Advanced Oxidation Processes for Water Treatment' in *Nanotechnology for Water Treatment and Purification*. Eds. A. Hu and A. Apblett. Springer: Cham. pp. 1-45.

Liu, X., Wang, M., Zhang, S. and Pan, B. (2013). Application potential of carbon nanotubes in water treatment: A review. *Journal of Environmental Sciences*, 25(7):1263-1280.

Lofrano, G., Carotenuto, M., Libralato, G., Domingos, R.F., Markus, A., Dini, L., Gautam, R.K., Baldantoni, D., Rossi, M. and Sharma, S.K. (2016). Polymer functionalized nanocomposites for metals removal from water and wastewater: An overview. *Water Research*, 92:22-37.

Ma, P., Siddiqui, N.A., Marom, G. and Kim, J. (2010). Dispersion and functionalization of carbon nanotubes for polymer-based nanocomposites: A review. Composites part A: *Applied Science and Manufacturing*, 41(10):1345-1367.

Manawi, Y., Kochkodan, V., Hussein, M.A., Khaleel, M.A., Khraisheh, M., Hilal, N. (2016). Can carbon-based nanomaterials revolutionize membrane fabrication for water treatment and desalination? *Desalination*, 391:69-88.

Maphutha, S., Moothi, K., Meyyappan, M. and Iyuke, S.E. (2013). A carbon nanotube-infused polysulfone membrane with polyvinyl alcohol layer for treating oil-containing waste water. *Scientific Reports*, 3: 1509-1515.

Martins, M., Santos, E.S., Pires, C., Barros, R.J. and Costa, M.C. (2010). Production of irrigation water from bioremediation of acid mine drainage: Comparing the performance of two representative systems. *Journal of Cleaner Production*, 18(3):248-253.

Masebinu, S.O., Aboyade, A.O. and Muzenda, E., (2014). 'Parametric Study of Single and Double Stage Membrane Configuration in Methane Enrichment Process'. in *Proceedings of the World Congress on Engineering and Computer Science.* San Francisco, CA, USA pp. 22-24.

McCarthy, T.S. (2011). The impact of acid mine drainage in South Africa. *South African Journal of Science*, 107(5-6):1.

Mehwish, N., Kausar, A. and Siddiq, M. (2014). Advances in polymer-based nanostructured membranes for water treatment. *Polymer-Plastics Technology and Engineering*, 53(12):1290-1316.

Mittal, G., Dhand, V., Rhee, K.Y., Park, S., Lee, W.R. (2015). A review on carbon nanotubes and graphene as fillers in reinforced polymer nanocomposites. *Journal of Industrial and Engineering Chemistry*, 21:11-25.

Mohammad, A.W., Teow, Y.H., Ang, W.L., Chung, Y.T., Oatley-Radcliffe, D.L. and Hilal, N. (2015). Nanofiltration membranes review: Recent advances and future prospects. *Desalination*, 356:226-254.

Mthetwa, V. (2014). *Investigation of polyether sulfone (PES) hollow fibre membranes for the treatment of acid mine drainage*. Doctoral thesis, University of Witwatersrand, Johannesburg.

Moothi, K., Iyuke, S.E., Meyyappan, M., Falcon, R. (2012). Coal as a carbon source for carbon nanotube synthesis. *Carbon*, 50(8):2679-2690.

Pal, G. and Kumar, S. (2016). Modelling of carbon nanotubes and carbon nanotube–polymer composites. *Progress in Aerospace Sciences*, 80:33-58.

Paul, M., Jons, S.D. (2016). Chemistry and fabrication of polymeric nanofiltration membranes: A review. *Polymer,* 103:417-456.

Purohit, R., Purohit, K., Rana, S., Rana, R.S. and Patel, V. (2014). Carbon nanotubes and their growth methods. *Procedia Materials Science,* 6:716-728.

Pyrzyńska, K. and Bystrzejewski, M. (2010). Comparative study of heavy metal ions sorption onto activated carbon, carbon nanotubes, and carbon-encapsulated magnetic nanoparticles. Colloids and surfaces A: *Physicochemical and Engineering Aspects,* 362(1):102-109.

Qin, L., Ge, Y., Deng, B., Li, Z. (2017). Poly (ethylene imine) anchored lignin composite for heavy metals capturing in water. *Journal of The Taiwan Institute of Chemical Engineers*, 71:84-90.

Rashid, M.H., Ralph, S.F. (2017). Carbon nanotube membranes: Synthesis, properties, and future filtration applications. *Nanomaterials,* 7(5):99.

Salehi, E., Madaeni, S.S., Rajabi, L., Vatanpour, V., Derakhshan, A.A., Zinadini, S., Ghorabi, S. and Monfared, H.A. (2012). Novel chitosan/poly (vinyl) alcohol thin adsorptive membranes modified with amino functionalized multi-walled carbon nanotubes for cu (II) removal from water: Preparation, characterization, adsorption kinetics and thermodynamics. *Separation and Purification Technology,* 89:309-319.

Sarbolouki, M.N. (1982). A general diagram for estimating pore size of ultrafiltration and reverse osmosis membranes. *Separation Science and Technology*, 17(2):381-386.

Sarkar, B., Mandal, S., Tsang, Y.F., Kumar, P., Kim, K. and Ok, Y.S. (2018). Designer carbon nanotubes for contaminant removal in water and wastewater: a critical review. *Science of the Total Environment,* 612:561-581.

Shah, K.A., Tali, B.A. (2016). Synthesis of carbon nanotubes by catalytic chemical vapour deposition: A review on carbon sources, catalysts and substrates. *Materials Science in Semiconductor Processing*, 41:67-82.

Shawky, H.A., Chae, S., Lin, S. and Wiesner, M.R. (2011). Synthesis and characterization of a carbon nanotube/polymer nanocomposite membrane for water treatment. *Desalination*, 272(1):46-50.

Simate, G.S. and Ndlovu, S. (2014). Acid mine drainage: Challenges and opportunities. *Journal of Environmental Chemical Engineering*, 2(3):1785-1803.

Srivastava, A., Srivastava, S. and Kalaga, K. (2013), 'Carbon nanotube membrane filters' in *Handbook of Nanomaterials.* Vajtai R. (Eds). Springer: Berlin. pp. 1099-1116.

Vatanpour, V., Madaeni, S.S., Moradian, R., Zinadini, S., Astinchap, B. (2011). Fabrication and characterization of novel antifouling nanofiltration membrane prepared from oxidized multiwalled carbon nanotube/polyethersulfone nanocomposite. *Journal of Membrane Science*, 375(1):284-294.

Wadekar, S.S., Hayes, T., Lokare, O.R., Mittal, D. and Vidic, R.D. (2017). Laboratory and pilot-scale nanofiltration treatment of abandoned mine drainage for the recovery of products suitable for industrial reuse. *Industrial and Engineering Chemistry Research*, 56(25):7355-7364.

Wang, X., Yang, W.D., Yang, S. (2014). Dynamic stability of carbon nanotubes reinforced composites. *Applied Mathematical Modelling*, 38(11–12):2934-2945.

Wang, L., Song, X., Wang, T., Wang, S., Wang, Z., Gao, C. (2015). Fabrication and characterization of polyethersulfone/carbon nanotubes (PES/CNTs) based mixed matrix membranes (MMMs) for nanofiltration application. *Applied Surface Science*, 330:118-125.

Yengejeh, S.I., Kazemi, S.A., Chsner, A. (2017). Carbon nanotubes as reinforcement in composites: A review of the analytical, numerical and experimental approaches. *Computational Materials Science*, 136:85-101.

Zarrabi, H., Yekavalangi, M.E., Vatanpour, V., Shockravi, A. and Safarpour, M. (2016). Improvement in desalination performance of thin film nanocomposite nanofiltration membrane using amine-functionalized multiwalled carbon nanotube. *Desalination*, 394:83-90.

CHAPTER 2: LITERATURE REVIEW

2.1 INTRODUCTION

In South Africa (SA), the mining industry has been a source of economic growth since the 19th century. Despite a decline in mining activity, the mining industry still contributed ~8.3% to the South African GDP in 2013 (Davies, 2015; Masinidi *et al*., 2016). Mining operations utilize a large amount of water especially in mineral processing, dust suppression and slurry transportation (Vella, 2013). Gold mining is rated as a high water consuming activity compared to other mining operations (copper, coal, zinc, platinum, diamond, nickel and bauxite) (Mudd, 2007). According to Davies (2015), the average consumption of water per ton of gold produced is 716 kL. However, utilisation of water in mining is detrimental to the environment as discharge effluent contains toxic metals (Grande *et al*., 2010; Masinidi *et al*., 2016). In addition to wastewater from mining activities large amounts of acidic water has been discharged from abandoned underground mines throughout the country (Simate and Ndlovu, 2014; Tutu *et al*., 2008). Pumping in these mines has been discontinued so once these cavities are exposed to rainwater the water levels rise (Mthetwa, 2014) This leads to the outflow of highly acidic wastewater with dissolved metal species known as Acid Mine Drainage (AMD) (Durand, 2012; Lopez *et al*., 2018). Likewise, the exposure of surface mine residues to rainwater can also lead to the release of AMD through the formation of acidic rainwater run-off with mineral deposits (Naicker *et al*., 2002; Mthetwa, 2014). The release of AMD poses a threat to the environment and human beings therefore remediation and treatment of AMD is essential (Aguiar *et al*., 2016; Gautam and Chattopadhyaya, 2016; Qin and Deng, 2017).

Acidic mine drainage (AMD) is generated when sulphide-bearing minerals encounter water and oxygen. Sulphide is oxidised to form sulphate that is further oxidised to sulphuric acid (Simate and Ndlovu, 2014). The most common source of sulphide is pyrite (FeS_2) (Johnson and Hallberg, 2005), although other sulphide containing minerals can produce AMD. The oxidation of pyrite to sulphuric acid is the main reaction that occurs in the formation of AMD (Rios,

Williams and Roberts, 2008). The first reaction (equation (2.1)) is the oxidation of the sulphide mineral into dissolved iron, sulphate and hydrogen:

$$FeS_2 + \frac{7}{2}O_2 + H_2O \rightarrow Fe^{2+} + 2SO_4^{2-} + 2H^+ \quad (2.1)$$

The dissolved Fe^{2+}, $SO4^{2-}$ and H^+ represent an increase in the total dissolved solids and cause a decrease in pH (Simate and Ndlovu, 2014). If the environment is favourable ferrous iron will oxidize to ferric iron according to reaction 2.2:

$$Fe^{2+} + \frac{1}{4}O_2 + H^+ \rightarrow Fe^{3+} + \frac{1}{2}H_2O \quad (2.2)$$

At pH values between 2.3 and 3.5, ferric iron is converted to $Fe(OH)_3$ and Fe^{3+} (equation (2.3)):

$$Fe^{3+} + 3H_2O \rightarrow Fe(OH)_{3SOLID} + 3H^+ \quad (2.3)$$

Additional Fe^{3+} from equation (2) that remains after precipitation (equation (2.3)) may be used to oxidize additional pyrite (Akil and Koldas, 2006), according to equation (2.4):

$$FeS_2 + 14Fe^{3+} + 8H_2O \rightarrow 15Fe^{2+} + 2SO_4^{2-} + 16H^+ \quad (2.4)$$

Iron precipitates as $Fe(OH)_3$ may be represented by a combination of equation ((2.5)):

$$FeS_2 + \frac{15}{4}O_2 + \frac{7}{2}H_2O \rightarrow Fe(OH)_3 + 2SO_4^{2-} + 4H^+ \quad (2.5)$$

On the other hand, the overall equation for the oxidization of additional pyrite by ferric iron (Akil and Koldas, 2006).(combinations of equations 2.1-2.3) is equation (2.6):

$$FeS_2 + \frac{15}{8}O_2 + \frac{13}{2}Fe^{3+} + \frac{17}{4}H_2O \rightarrow \frac{15}{2}Fe^{2+} + 2SO_4^{2+} + \frac{17}{2}H^+ \quad (2.6)$$

As the water becomes increasingly acidic, the heavy metals in the ores become more soluble and are leached out of the ores into the acidic water (Akil and Koldas, 2006). High concentrations of heavy metals are released as sulphide is oxidized. Acid mine drainage water contains iron, sulphates, lead, aluminium, cadmium, mercury and other minerals commonly

found in mines (Mthetwa, 2014). Naicker *et al*. (2002) conducted an analysis of AMD from gold mining in the Wits basin, focusing on the Nelspruit region, and they found that sediments from the Wits basin contained 3% pyrite. Ground water contained high concentrations of sulphates (1400-1750 mg/l), iron (379-453 mg/l) and other heavy metals at a pH of 3.76-3.78. Seepage water had a lower pH than ground water due to oxidation as the groundwater rose to the surface. A study conducted by Tutu *et al*. (2008) confirmed earlier findings revealed by Naicker *et al*. (2002) that the amount of acidic run-off from the surface increased after the rainy season, increasing the amount of heavy metal pollution. According to the study conducted by Durand (2010), various water sources including the Vaal River and Limpopo River have been contaminated by the acidic run off from the abandoned mines in the Wits basin area since pumping was stopped in 1998.

All these AMD constituents have a negative impact on ecosystems and the health of human beings. AMD can lead to biological dead zones (Johnson and Hallberg, 2005). The polluted water seriously harms fish and other aquatic life (Jiwan and Kalamdhad, 2011). When iron oxides and hydroxides precipitate in AMD, they change the colour of the drainage water from clear to orange. The precipitate known as ochre can deposit on river (Figure 2-1) and ocean beds (Fripp, Ziemkiewicz and Charkavorki, 2000). Organisms that live off food from the bottom of oceans and rivers can no longer survive and this affects the aquatic food chain (Simate and Ndlovu, 2014). In addition, heavy metals affect the growth and reproductive cycle of fish. In some cases, they can lead to the death of aquatic life (Lewis and Clark, 1997). AMD causes oxidative stress to plants which interrupts their physiology and morphology (Simate and Ndlovu, 2014). The treatment of AMD to remove sulphates and other heavy metals is crucial as the latter is non-biodegradable (Qin *et al.*, 2017), thus can accumulate in the human body when ingested (Al-Rashdi *et al*., 2013), causing damage to the heart, liver, lungs, kidney and brain (Singh *et al*., 2011). They also prevent vital minerals from being properly absorbed in the body. The treatment of acidic mine water is essential in order to eliminate these harmful substances (Simate and Ndlovu, 2014).

Figure 2-1: Acid mine deposits in river (Water Legacy, 2009)

Various remediation techniques have been developed in an effort to treat AMD for water reuse and recovery of precious metals with conventional technologies (chemical precipitation, adsorption, coagulation-flocculation, flotation and electrochemical methods) and emerging membrane technologies (ion-exchange membranes, membrane distillation, membrane filtration) (Lopez *et al*., 2018).

2.1.1 Biological Treatment

Biological sulphate removal through sulphate reducing bacteria (SRB) is one of the methods used for AMD treatment (Clyde *et al*., 2016). Substrates for growth of bacteria are H_2, fatty acids or alcohol. Nutrients such as phosphate, potassium and nitrogen are added to the bioreactor to stimulate bacterial growth (Hu and Apblett, 2014). During the process, sulphides are oxidized to form sulphur (Oakes *et al*., 2014). According to Li *et al* (2017), SRB has been used effectively in the precipitation of heavy metals from AMD and the reduction process of sulphate to sulphide. Nonetheless, the carbon source used during the reaction is depleted over time and the effectiveness of the process is decreased (Mthetwa, 2014).

2.1.2 Neutralisation

AMD is also treated by neutralization using limestone, hydrated lime, soda ash, caustic soda, ammonia, calcium peroxide, metal hydroxides, kiln dust and fly ash (Maree, 2004; Ntwampe *et al*., 2015, 2016). During the process, AMD reacts with the neutralising agent to adjust the pH in order to reduce solubility of heavy metals. When the concentration of ferrous iron is low, (<50mg/L), the solution is treated at a pH range of 6.5 to 8.0 in order to precipitate ferrous hydroxide from the bulk solution. On the other hand, when the concentration of ferrous iron is high, the solution is treated at a pH range of 8.0 to 10.0 and ferrous hydroxide precipitate is aerated to form ferric hydroxide before heavy metals settle in a settling tank (Durand, 2012). Similar to biological treatment, the sludge produced during the reaction contains harmful substances, and hygienic and environmentally friendly disposal of it is difficult to achieve (Oakes *et al*., 2014).

2.2 MEMBRANE FILTRATION FOR AMD TREATMENT

Of the various remediation techniques employed in AMD treatment, membrane filtration is the most favourable (Aguiar *et al*., 2016). There is ongoing research with respect to the use of membranes, specifically polymeric membranes for wastewater and AMD treatment (Mthetwa, 2014; Maphutha, 2013). NF emerged as an ideal technology for AMD treatment as the pores are small for ion rejection (Zhang *et al*., 2015) but operate at a lower pressure than RO. MF and UF are other technologies that have been employed in water treatment, however they are not suitable for AMD treatment due to large pore sizes (Kefeni *et al*., 2017; Wang *et al*., 2015).

Clogging of the pores of the membrane is predominant with polymeric membranes and NF due to fouling and concentration polarisation (Al-Rashdi *et al*., 2013). In addition, membranes have a limited lifespan. Blending CNTs with polymeric membranes is done to improve membrane functioning (Herrera-Hererra *et al*., 2012). Studies have shown that CNTs can enhance the mechanical stability of the membranes (De Volder *et al*., 2013; Spitalsky *et al*., 2010; Wang *et al*., 2014) while improving the hydrophilic and anti-fouling properties of the membrane and

increase the solute rejection capability of the membrane (Lee *et al*., 2014). CNTs can be envisioned as sheets of graphene that have been rolled into a cylinder to form SWCNTs or MWCNTs (Lee *et al*., 2016). MWCNTs are a group of SWCNTs arranged in concentric tubes (Mattia *et al*., 2015). CNTs have superior mechanical, electrical and chemical properties (Ma *et al*., 2010). CNTs are naturally hydrophobic and have low solubility in solvents (Mehwish *et al*., 2014; Vatanpour *et al*, 2011), however, functionalization improves hydrophilicity and solubility in of the polymer matrix to reduce fouling tendency of the membrane (Drioli, and Giorno, 2016; Manawi *et al*., 2016). Membrane filtration is a technique that uses membranes to separate the solute from the bulk solution. A membrane is a physical barrier that permits the selective permeation of certain species in contact with it (Baker, 2012a; Drioli, and Giorno, 2016). Permeate passes through the membrane during filtration while impermeable substances are rejected as retentate. There is a higher amount of unwanted species in the retentate compared to the permeate (Crittenden *et al*., 2012). Dead end or cross-flow filtration operation can be used (Drioli, and Giorno, 2016). In dead end filtration, feed water flows perpendicular to the membrane (Hu and Apblett, 2014). Solids are retained on the surface of the membrane and build up leading to lower flux. In cross flow filtration, the feed water flows parallel to the membrane surface (Hu and Apblett, 2014). In this mode of operation, the shear force generated by the fluid velocity reduces the solids that accumulate on the surface of the membrane. A decline in flux is postponed since solids that would otherwise accumulate on the membrane surface are passed with the retentate. (Liang *et al*., 2014).

2.2.1Membrane separation capacities

In addition to membrane morphology, some other factors that determine membrane performance include surface roughness, surface charge, hydrophobicity, surface chemistry, mechanical durability, biological stability, chemical and thermal stability chlorine/oxidant tolerance and porosity (Martín, 2016). Membrane porosity is a crucial factor in distinguishing membrane separation processes and can be determined using bubble point analysis, microscopic analysis or porosimetery (Hu and Apblett, 2014). The molecular weight cut off (MWCO) has also been utilised to characterize pore size (Homayoonfal *et al*., 2014; Liang *et al*., 2014). Figure 2-2 shows the separation ability of different membranes based on pore size. Membranes can function by two different mechanisms. The pore flow mechanism or the solution diffusion

mechanism (Baker, 2015). As previously mentioned in chapter 1, membrane processes include MF, UF, RO) and NF (Srivastava *et al*., 2013). As MF and UF rejection mechanisms depend on size exclusion, they are able to reject substances of a larger pore size than that of the membrane regardless of the operating pressure or concentration of the solution. They function by the pore flow mechanism. RO and NF membranes rejection depends on pressure gradient and concentration gradient (Davis *et al*., 2010).

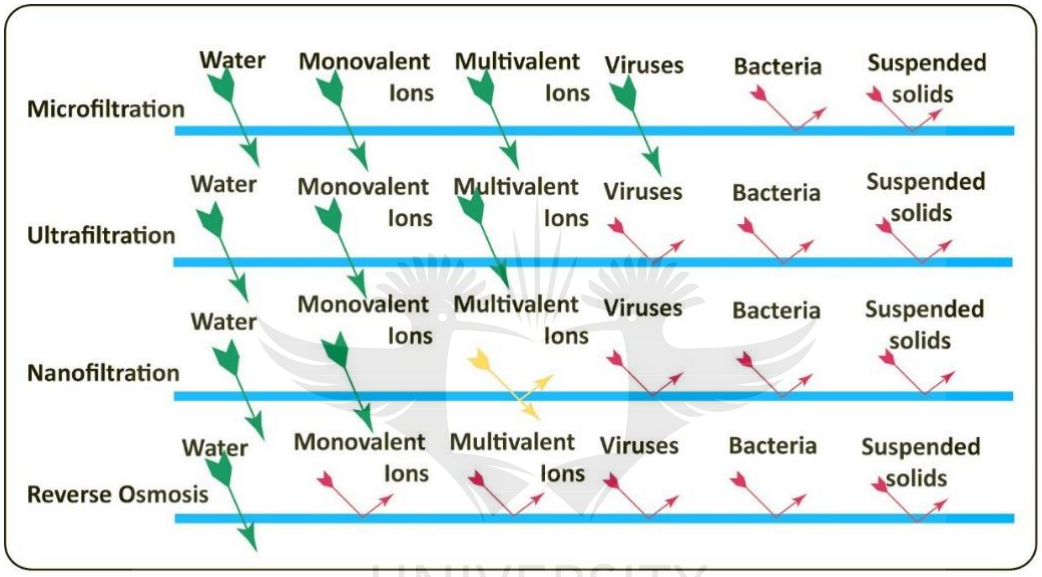

Figure 2-2: Illustration of different membrane technologies (Aquafield Water Services, 2017)

MF membranes, with the largest pore sizes in membrane separation technology have pore sizes larger than 50 nm that enable the rejection of suspended solids and bacteria (Khulbe and Matsuura, 2017). UF membranes have smaller pores than MF with pore sizes ranging between 2 and 50 nm (Khulbe and Matsuura, 2017; Srivastava *et al*., 2013; Zhao and Yu; 2015) and MWCO of 3000 to 500 000 Da. Colloids and macromolecules are primarily rejected by these membranes. RO membranes are mostly used in salt-water desalination. However, they have been used for pharmaceutical applications and industrial wastewater treatment (Singh, 2014). Since the pore sizes are smaller, high pressure is required for separation. NF membranes are preferred as a treatment option relative to RO membranes in cases where effective separation can be achieved at a lower pressure than that required for RO membranes. NF membranes have a pore size of 1 to 10 nm which relates to a MWCO of 300 to 500 Da making them ideal for ion

removal (Mohammad *et al*., 2015; Mullet, 2014). Additionally, NF membranes have a surface charge due to the dissociation of charged groups (Hu and Apblett, 2014). Carboxylic groups and sulphonic groups that are contained in polymeric membranes are ionised in feed solution. The dissociation of these groups is influenced by the pH of the feed solution (Mohammad *et al*., 2015). NF membranes follow a combination of pore flow and solution diffusion mechanisms (Geise *et al*., 2010). Donnan exclusion determines the exclusion of ions based on the surface charge of membranes (Wu *et al*., 2016). The rejection of divalent ions is higher than that of monovalent ions due to a charge on the surface of NF membranes (Mohammad *et al*., 2015; Srivastava *et al*., 2013). Neutral species are rejected based on steric effects (size exclusion) (Nicolini *et al*., 2016). Due to these qualities, NF membranes have been utilized for the treatment of wastewater in the pharmaceutical and dairy industries as well as for desalination and the removal of heavy metals (Mohammad *et al*., 2015).

2.2.2 Types of Membranes

Depending on their crystal morphology, membranes can be isotropic or anisotropic (Srivastava *et al*., 2013). Isotropic membranes have a homogenous composition and structure and may be microporous membranes, dense non-porous membranes or electrically charged membranes (Baker, 2012a). Anisotropic membranes have a heterogeneous porous or layered structure and may be phase inversion membranes or thin film composite (TFC) membranes (Figure 2-3).

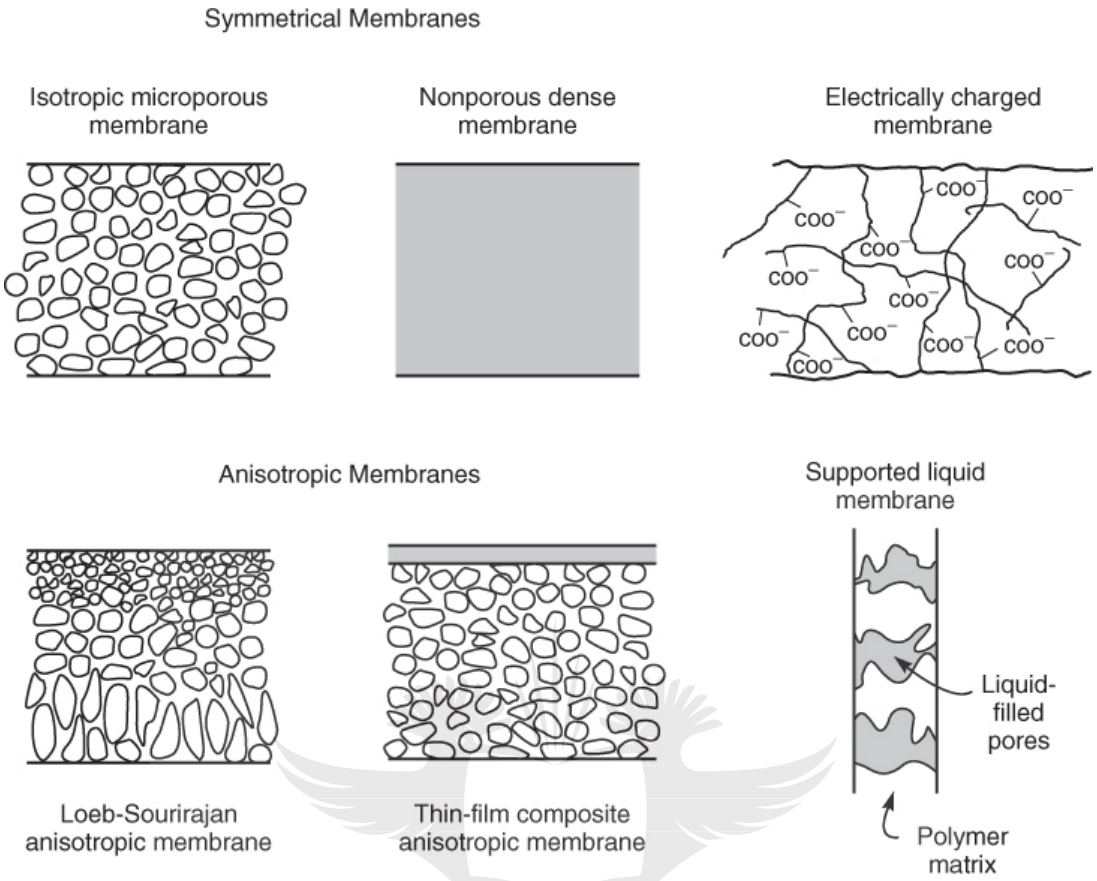

Figure 2-3: Schematic diagram showing different types of membranes (Baker, 2012a)

2.2.2.1 Isotropic membranes

Isotropic membranes may be classified as microporous, non-porous and electrically charged (Mark, 2013). Microporous membranes have pore sizes of 0.01 to 10 µm in diameter. Solute rejection follows the pore size distribution of the membrane such that particles smaller than the smallest pores of the membrane permeate through the membrane while larger particles are retained (Baker, 2012a). In the case of dense non-porous membranes, particles diffuse through the membrane based on pressure gradient, concentration gradient or electrical potential gradient (Drioli, and Giorno, 2016). The solubility and diffusivity of various components in the membrane determines their transport rate within the membrane. (Baker, 2012a). Electrically charged membranes have a positive or negative charge and can comprise of a dense or microporous structure. Rejection of ions depends on the charge of the membrane with ions that have the same charge as the membrane being retained (Baker, 2012a.)

2.2.2.2 Anisotropic membranes

There are two types of anisotropic membranes: phase inversion membranes and TFC membranes (Baker, 2015). The phase inversion method is a liquid-liquid de-mixing process that was developed by Loeb and Sourirajan to produce ultrathin cellulose acetate RO membranes (Zhou *et al*., 2008). It is a method used in both laboratory and commercial formation of NF membranes through which a polymeric solution is separated into a polymer-rich and a polymer-lean phase (Khansary *et al*., 2017; Rahimpour *et al*., 2010). During the separation process, the polymer is converted from homogenous liquid phase to solid phase (Le *et al*., 2017). The polymer-rich phase forms the polymer matrix while the polymer-lean phase forms the membrane pores. (Holda *et al*., 2013). Phase separation can be induced by evaporation of solvent from the polymer, which increases the concentration of the polymer and causes precipitation or precipitation/de-mixing (Paul and Jons, 2016). Cooling of the solution containing the polymer and solvent so that the polymer becomes less soluble in the solvent can also cause separation (Baker, 2015). Extraction, evaporation or freeze-drying may also be used in the removal of the solvent (Paul and Jons, 2016). Vapour induced phase separation is obtained by exposing a cast film consisting of polymer and solvent to a vapour atmosphere containing the non-solvent. Diffusion of the non-solvent into the cast film causes the formation of a porous membrane. Phase inversion can also be brought about by immersion precipitation which is often preferred for the formation of NF membranes as a dense top layer with small pores can be formed using this method (Nunes, 2010). To form the membrane a polymer is mixed with a solvent and cast onto a suitable support before being immersed in a coagulation bath containing the non-solvent (Drioli, and Giorno, 2016; Holda *et al*., 2013). The solvent and non-solvent are miscible and the solvent surrounding the polymer moves into the non-solvent and causes phase separation (Paul and Jons, 2016) as shown in Figure 2-4.

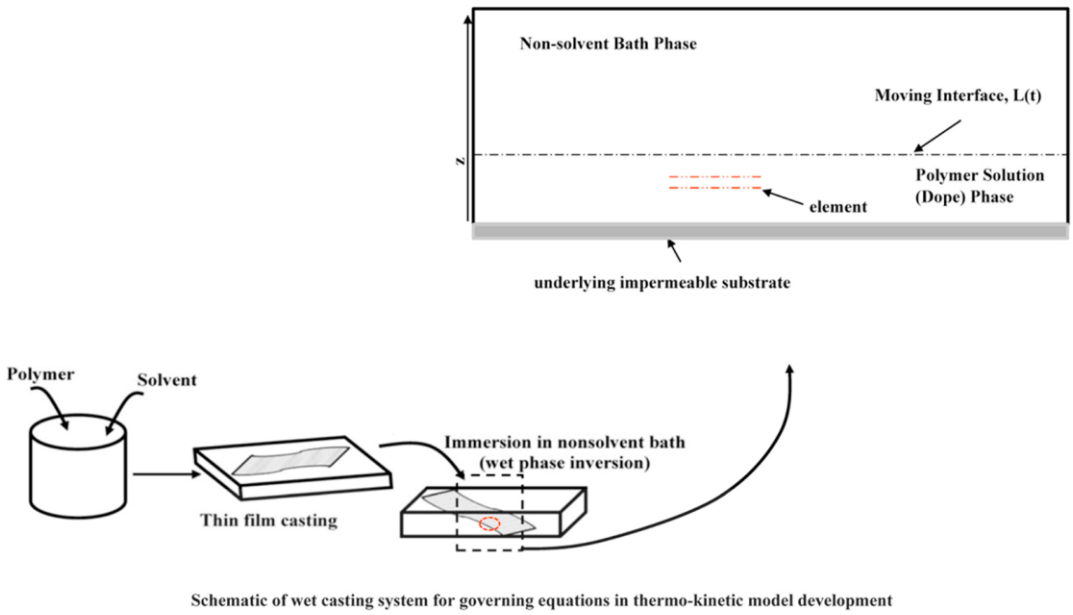

Figure 2-4: Illustration of wet phase inversion process (Khansay *et al*., 2017)

Interfacial polymerisation is a method used to produce TFC membranes (Mohammad *et al*., 2015). The membranes are formed by the reaction between two monomers at the interface of two immersible solvents (Singh, 2014). An ultrathin selective top layer that is responsible for separation and flux through the membrane is formed (Nunes, 2010; Rezania *et al*., 2019). According to Abidin *et al*. (2017) the formation of this layer is due to rapid phase inversion, which reduces the degree of polymer nucleation. The TFC layer regulates the solubility, permeability and efficiency of the membrane (Yin and Deng, 2014). Figure 2-5 shows the thin film layer that was formed by the addition of a thin polyamide selective layer on a polyacrylonitrile ultrafiltration support. Interfacial polymerisation membranes are often produced by reacting polyamides at high temperature and pressure (Paul and Jons, 2016). M-phenylene diamine (MPD) and trimesoyl chloride (TMC) are often used (Paul and Jons, 2016). Maphutha *et al.* (2013), synthesised a TFC membrane with a thin polyvinyl amide layer and a polysulfone support layer for the removal of oil from wastewater.

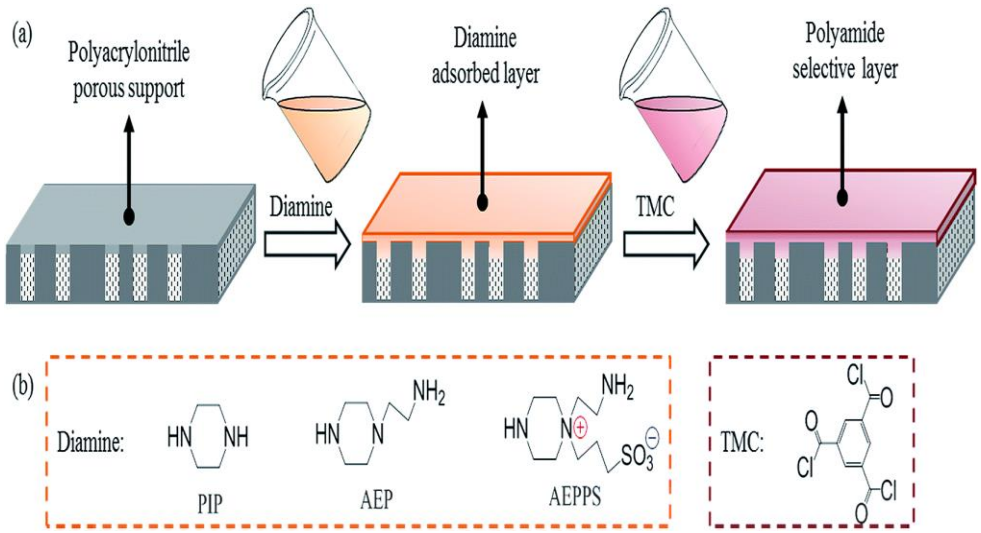

Figure 2-5: A schematic diagram of the preparation of TFC membranes (Weng *et al*., 2015)

2.2.3 Membrane configurations

Due to differences in pore size and application, different membrane equipment, flow regimes, operating modes and configurations are used for NF and RO membranes compared to MF and UF (Crittenden *et al*., 2012). There are four types of membrane configurations: Flat sheet, plate and frame, tubular, hollow fiber and spiral wound (Hu and Apblett, 2014). Flat sheet and plate and frame configurations are often used in laboratory experiments but are difficult to scale up for industrial use. Tubular configurations are preferred for ceramic membranes with low packing densities. Hollow fiber and spiral wound membranes configurations are often used in NF and RO (Hu and Apblett, 2014; Liang *et al.*, 2014). Spiral wound RO and NF membranes have been used commercially to treat AMD (Oakes *et al*., 2014).

2.2.3.1 Spiral wound modules

Spiral wound modules are easy to scale up and can be connected in series inside a single pressure vessel. Membrane material is enveloped in feed spacers and wrapped around a central perforated tube which collects permeate fluid (Baker, 2012b). Multiple envelopes may be used to reduce the pressure drop of the permeate fluid as it travels to the central pipe (Figure 2-6). Karabelas *et*

al. (2015), found that membrane performance increased with an increasing number of envelopes for a constant membrane area. However, the number of envelopes that could be used was limited by the tube diameter and the thickness of the membrane. Due to the compact design of the multi-envelope arrangement, membrane fouling and scaling poses a problem.

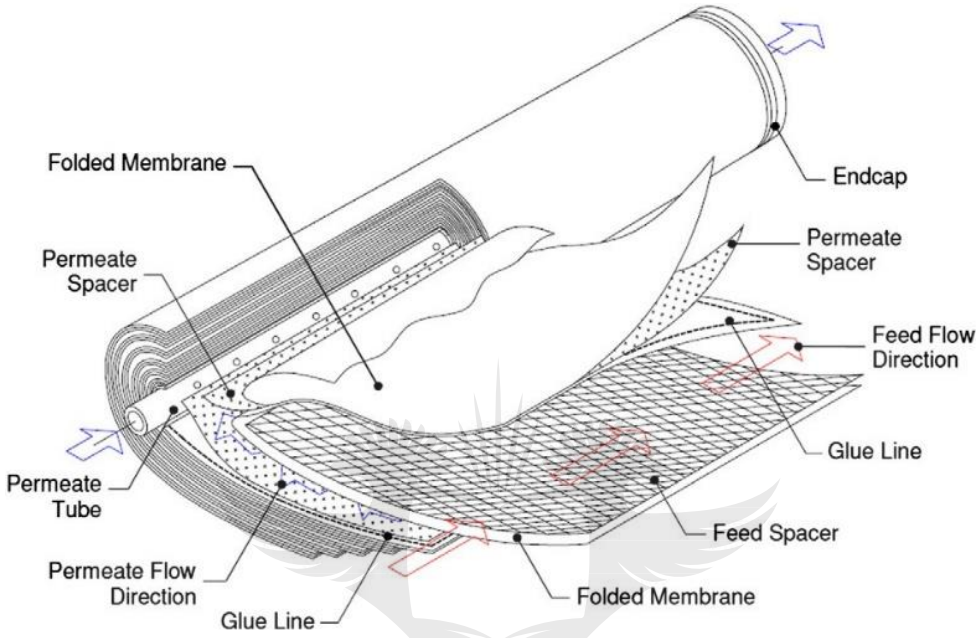

Figure 2-6: Schematic representation of spiral wound membrane module (Johnson *et al*., 2010)

Membrane modules contain membranes synthesised from various materials depending on application. Membranes have been synthesised using materials such as glass, ceramics and polymers (Wang *et al*., 2015). Membranes made from glass ceramics or metal are classified as inorganic and offer high mechanical strength and chemical resistance (Mulder, 2012). However, these membranes are not desirable for water treatment applications due to their high production costs (Al Aani *et al*., 2017). Polymer-based membranes are classified as organic (Mulder, 2012). Common polymers that are used include polyether sulfone (PES), polyvinylidene fluoride (PVDF), polyacrylonitrile (PAN) and polyamide (PA) (Le and Nunes, 2017; Wang *et al*., 2015). Polymer membranes are adaptable to a range of membrane structures, easy to prepare, inexpensive and yield high separation efficiency (Al Aani *et al*., 2017). Despite these advantages

fouling and concentration polarisation remain factors that limit the application of this technology (Mittal *et al*., 2015; Ji *et al*, 2017).

2.3 Membrane fouling and concentration polarisation

Polymer membranes are prone to clogging of the pores due to fouling which decreases operability of the membrane, increases maintenance and cleaning costs and decreases, the lifespan of the membrane resulting in the membrane needing to be frequently replaced (Mohammad *et al*., 2015). According to Van der Bruggen *et al*. (2008), membrane fouling has been linked to a decrease in membrane lifespan and stability in addition to a decrease in permeability. Organic fouling, scaling, colloidal fouling and biofouling affect the operability of membranes (Le *et al*., 2017). Organic compounds such as proteins and humic acid cause irreversible membrane fouling.

Concentration polarisation diminishes membrane performance and is caused by the accumulation of solutes on the feed side of the membrane that can lead to the formation of a gel layer on the membrane surface (Kumar *et al*., 2013). There is an increase in the concentration of the solutes on the membrane surface compared to solutes in the bulk solution (Mohammad *et al*., 2015). Concentration polarisation leads to decreasing trans-membrane pressure and an increase in osmotic pressure of the solution, where permeate flux is also reduced (Mohammad *et al*., 2015). Maphutha *et al*. (2013) found that by incorporating twisted tape into the membrane module this induces turbulence and decreases concentration polarisation.

2.4 CARBON NANOTUBES IN WATER TREATMENT

2.4.1 Chemistry of CNTs

CNTs consist of carbon atoms, which are non-metallic with four valent electrons that are available for covalent bonding (Hussain *et al*., 2011; Szab *et al*., 2010). Carbon atoms can bind together with other atoms to form different allotropes such as diamond and graphite (Hirsch, 2010; Tan *et al*., 2013). Diamond is a type of carbon with electron configuration of sp^3, which

indicates that each carbon atom is attached to four other carbon atoms (Ma *et al*., 2010; Pal and Kumar, 2016). On the other hand, graphite is formed by each carbon atom bonded to three other carbon atoms and one of them with double bonding (Katsnelson, 2007; Tan *et al*., 2013). A single atomic layer of graphite is termed graphene (Dhakate *et al*., 2011; Koziol *et al*., 2007). The carbon bonds in graphene are sp^2 hybridised (Dresselhaus *et al*., 1995). Like in graphene, CNTs have three of the valence shell electrons chemically bonded to other carbons and the free electron forms a π bond with a free electron from another carbon atom (Iyuke and Mahalik, 2006; Rahmandoust and Ayatollahi, 2016). The structure of CNTs is comparable to that of grapheme except that graphene sheets are rolled to form CNTs (Hirsch, 2010; Iyuke and Mahalik, 2006). SWCNTs are formed by rolling a single graphene sheet into a seamless cylinder, whereas multiple graphene cylinders are rolled concentrically to form MWCNTs (Dhakate *et al*., 2011; Maphutha *et al*., 2013). The nanotubes are formed by rolling up the carbon lattice in one axis of symmetry or in a direction that is different from the axis of symmetry to form zigzag, chiral or armchair tubes (Ma *et al*., 2010; Moothi *et al*., 2012) (Figure2-7).

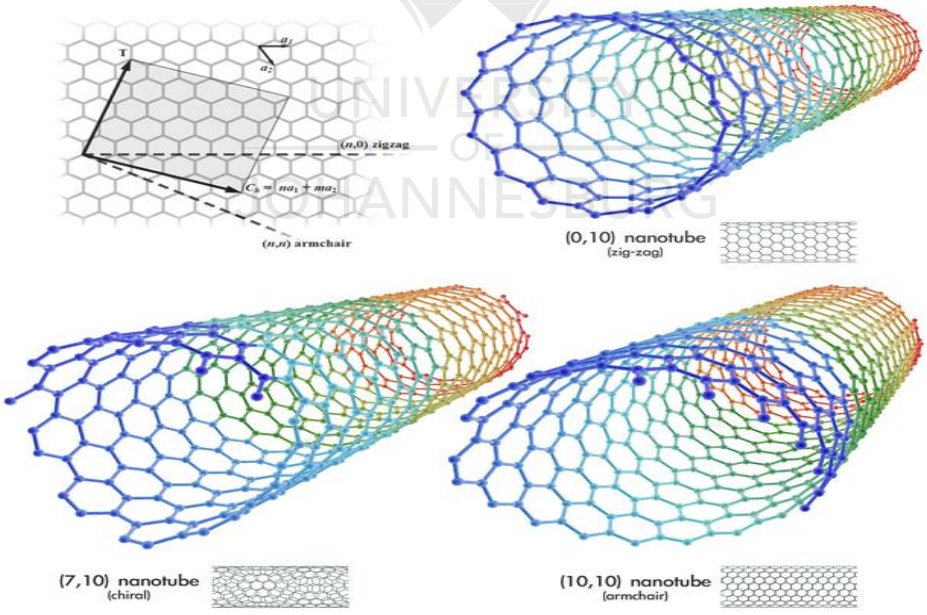

Figure 2-7: Types of CNTS i.e., zig-zag, chiral and armchair (Mittal *et al*., 2015)

The integers, *m* and *n* denote the vectors along the crystal lattice of graphene. When *m* = 0, a zigzag CNT is formed, if *m* = *n* an armchair nanotube is formed, otherwise the nanotube is chiral (Ma *et al*., 2010; Meo and Rossi, 2006). The value of *n* and *m* determines the metallic or semiconducting properties of the CNTs (De Volder *et al*., 2013; O'Connell *et al*., 2005). If (2n+m) is a multiple of 3, then the CNT is metallic, otherwise it is semiconducting (Ma *et al*., 2010). Availability of electrons and strong c-c bonds result in superior mechanical and electrical properties of the CNTs (Iyuke and Mahalik, 2006; Pal and Kumar, 2016; Thomas *et al*., 2019). MWCNTs comprise of multiple graphene sheets each with different chiralities, making it more difficult to predict their physical properties (Li and Chou, 2003; Ma *et al*., 2010)

CNT tend to form agglomerated tube bundles due to strong van der Waals forces between them (Al Aani *et al*., 2016). Ultasonication is an effective method to reduce agglomeration and facilitate dispersion of CNTs. In order to separate the CNTs, an ultrasound is applied to a solution consisting of CNTs and solvent (water, ethanol, or acetone) which causes the disentanglement of individual CNTs from the tube bundle (Ma *et al*., 2010). In addition to sonication, the addition of functional groups to the surface of CNTs can also enhance dispersion. By sonicating the CNTs in acidic medium, functional groups can be attached to the ends and walls of the CNTs or by using chemical agents. Vatanpour *et al*. (2011) sonicated MWCNTs in acidic solution containing 3M HNO_3/HSO_4 and found that carboyl groups were introduced to the surface of the CNTs. The addition of the functional groups improved the dispersion of CNTs and also improved their hydrophilicity.

2.5 CNT/POLYMER COMPOSITES

CNTs have been incorporated in polymeric matrixes for numerous uses (Mittal *et al*., 2015). The addition of CNTs to polymers improved the functioning of the polymers during water treatment. CNTs can increase flux, permeability, salt rejection, hydrophilicity and anti-fouling properties of polymeric membranes (Wang *et al*., 2015). However, the blending of polymers and CNTs to assimilate the properties of the CNTs into the matrix poses a challenge. The carbon atoms on the walls of the CNTs are chemically stable and inert, making it difficult to interact

with the surrounding polymeric matrix (Akram *et al*., 2016). Goh and Ismail, (2017) propose that the CNTs should be uniformly distributed throughout the matrix in order to achieve optimal functioning of the CNT membrane. According to Ma *et al*. (2010), the surface properties of CNTs need to be modified in order to ameliorate load transfer across the polymer/CNT composite. CNTs have been functionalised so as to improve the interfacial interactions with the polymer (Rashid and Ralph, 2017).

Research studies have also shown that the physio-chemical functionalisation of CNTs prior to incorporation in polymeric membranes decreases membrane fouling (Vatanpour *et al*., 2011). Covalent bonds can be chemically connected to the sidewalls and ends of CNTs provided the tubes are open ended (Rashid and Ralph, 2017). The functionalisation is linked with the breaking of μ bonds to form sp^3 hybrids (Ma *et al*., 2010). The formation of oxygenated groups on sidewalls and open end of CNTs has also been observed (Rashid and Ralph, 2017). Strong acids such as HNO_3, H_2SO_4 or a combination of the two have been used (Vatanpour *et al*., 2011) As the CNTs are chemically oxidised by the strong acids, hydrophilic carboxylic groups and hydroxyl groups are attached to the ends and side walls of the CNTs. The attachment of these polar groups changes the CNTs from hydrophobic to hydrophilic, thereby reducing fouling. The functional groups also produce strong interfacial bonds between the polymeric matrix and CNTs, providing an infused polymer with superior mechanical and functional properties (Ma *et al*., 2010). Some of the challenges associated with covalent bonding include the damage and fragmentation of CNTs, which reduces the mechanical properties of CNTs and destructs the μ bonds, which diminishes the transport properties of CNTs. Non-covalent functionalisation is an alternative method that preserves the nanotube structure whereby, surfactants or polymer molecules are adsorbed onto the CNT surface (Rashid and Ralph, 2017).

2.5.1 Ion removal by CNT-TFN membranes

NF membranes are capable of selective ion removal during water treatment. Gerhism and Mikulášek (2014), investigated the ability of a NF membrane AFC80 in the removal of Pb ions from aqueous solution. The study found that the membrane successfully removed 98% of lead ions. Al-Rashdi *et al*., (2013), studied the ability of NF membrane, NF270 for the rejection of

heavy metals ions which showed that Cu ions had the highest rejection rate of 92% compared to all the other ions viz. Cd, Pb, Cu, Mn. Previous studies have shown that ion rejection happens through steric, Donnan and di-electric exclusion (Kumar *et al*., 2013; Wu *et al*., 2016; Pages *et al*., 2017). The efficiency of CNT-embedded NF membranes in the removal of divalent ions has also been investigated. Wang *et al*. (2014) prepared polyethersulfone (PES)/CNT NF membranes with different CNT loadings and diameters for water treatment to investigate rejection of Na_2SO_4, $MgSO_4$ and NaCl. Since the membrane was negatively charged, ion rejection followed the Donnan exclusion mechanism.

2.5.2 Enhancement of mechanical strength of Polymeric membranes by CNTs

CNTs have a tensile strength of 63 GPa and a Young's modulus of 1 TPa (Yengejeh *et al*., 2017). Since CNTs have superior mechanical properties, incorporation with ceramics, metals and polymers has been done so as to improve their structural integrity by enhancing the mechanical strength of the polymeric matrix (Shawky *et al*., 2011). According to Fenner and Daniel (2016), CNTs improve the fracture toughness, fatigue, shear strength and influence damage tolerance of the composite membrane; which is attributed to the energy absorbing property of the CNTs. A challenge that is often encountered in the preparation of CNT/polymer composites is the agglomeration of CNTs in the polymeric matrix (Yengejeh *et al*., 2017). Agglomeration tends to occur if more than 10 wt% CNTs is added (Shulte, 2010). In order to avoid this problem, some form of shear mixing, usually ultrasonication is applied to break the van der Waals forces that bind the CNTs together and allow the dispersion to transpire (Hariss, 2009).

2.5.3 Anti-fouling ability of CNTs in polymer matrix

A study by Wang *et al*. (2014) revealed that the addition of hydrophilic CNTs decreases fouling and improves permeate flux. Vatanpour *et al*. (2011) investigated the performance and anti-fouling efficiency of PES MWCNT-embedded NF membranes. It was found that anti-fouling performance of the membrane improved after the addition of functionalised MWCNTs to the polymeric matrix while the percentage of permeate flux was increased from ~30% to ~ 88%.

Similar results were found in a study conducted by Celik (20111), using a similar PES membrane. Park *et al*. (2013) found that the addition of CNTs to the membrane structure improved the membrane surface charge and reduced fouling. The CNTs were functionalised using graft polymerisation and showed similar rejection compared to commercial UF membranes.

A study conducted by Andrade *et al*. (2017) showed that the main foulant in gold AMD sample (that was sampled from Brazil) was inorganic substances and calcium sulphate ($CaSO_4.0.5H_2O$). While the addition of functionalised CNTs to polymeric membranes has been proven to reduce fouling, in most studies humic acid or bovine serum albumin (BSA) are used as model foulants (Gautam and Chattopadhyaya, 2016). While these demonstrate the effects of organic fouling on polymer membranes, they do not provide an accurate representation of fouling due to AMD.

2.6 EFFECT OF OPERATING PARAMETERS ON MEMBRANE PERFORMANCE

Al Zoubi *et al*. (2010) investigated operating conditions, (temperature, pressure, pH, flow rate) required to achieve optimal results in AMD treatment using two commercial NF membranes (NF99 and DK) and one RO membrane. The results showed that heavy metal ion rejection remained constant with increasing pressure using NF membranes while the permeate flux increased with increasing pressure. Nicolini *et al.* (2016) tested the rejection of Na^+, Cl^-, SO_4^{2-}, K^{2+}, Ca^{2+} and Mg^{2+} ions. Similar to the results obtained by Al Zoubi *et al*. (2010) the ion rejection did not increase as the pressure increased but remained constant. As the temperature of the AMD increased, activation energy also increased. In addition, the viscosity of the AMD decreased causing flux increase with increasing temperature. The ion rejection decreased with increasing temperature because the charge on the active layer of the NF membranes changed with a changing temperature. The effect of pH on AMD was studied using the NF99 membrane, and the results showed a significant decrease in sulphate ions rejection with decreasing pH because surface charge on the membrane decreased with decreasing pH. This is attributed to increasing electrostatic repulsion between the sulphate ion and the NF membrane. As the pH decreased, so did the rejection of all ions except sulphate, and permeate flux increased with an increasing feed flow rate to both low and high concentration of the AMD sample.

In a study done by, Aguiar *et al*. (2016), comparing the main operating conditions of RO and NF membranes during gold AMD treatment, it was found that NF membranes (NF 90 and NF 270) were more effective than RO membranes in terms of flux but had higher rejection. The RO membranes had lower permeate fluxes. In addition, NF90 had the highest retention efficiency of all NF membranes studied whereas NF270 the highest permeate flux.

2.7 BARRIERS TO INDUSTRIAL APPLICATION OF CNT-TFN MEMBRANES FOR AMD TREATMENT

CNT-TFN membranes have been shown to be effective in wastewater treatment on a lab scale. However, bridging the gap between research studies and commercial application remains a challenge (Barr *et al*., 2009; Roco *et al*., 2011). As TFN-CNT technology is relatively new (Goh and Ismail, 2015), and there are very few long-term or pilot scale studies done on its application for AMD treatment. Much time, effort and money might be spent on pilot or full-scale studies only to realise that the process is not feasible at large scale. To overcome this many engineering firms and research companies prefer to simulate membrane processes based on experimental data prior to adaptation of the process for pilot or full scale. (Bobák *et al*., 2015; Corredor *et al*, 2016; Darvishmanesh *et al*, 2011) Simulation allows for the plant design to be optimised while also investigating the effect of process conditions on production (Park *et al*., 2012; Phuntsho *et al*., 2014). Another barrier is that investors are hesitant to invest in new technology without an indication of how fluctuations in CAPEX and OPEX may affect the viability of the process over time (Park *et al*., 2010; Roefs *et al*, 2017). For this reason, economic models may be modified to account for uncertainty (Huang *et al*, 2019; Tesfasgiorgis *et al*., 2015). Computer aided design has been used in combination with data driven approaches such as time-sereies forcasting to improve decision making and create frame works for not only process optimisation but also for the improvement of economic evaluation strategies. By accounting for economic risk factors, decision makers have a clearer understanding of how economic feasibility is affected over the plant's lifetime (Wang *et al*., 2019).

Research findings to date focus on the use of commercially available TFN membranes for AMD treatment while few studies on the capability of CNT-infused membranes for the treatment of AMD exist. Additionally, no studies currently incorporate process modelling and economic feasibility the study of TFN membranes for AMD treatment.

2.8 REFERENCES

Aguiar, A.O., Andrade, L.H., Ricci, B.C., Pires, W.L., Miranda, G.A., Amaral, M.C.S. (2016). Gold acid mine drainage treatment by membrane separation processes: An evaluation of the main operational conditions. *Separation and Purification Technology*, 170:360-369.

Akcil, A. and Koldas, S. (2006). Acid mine drainage (AMD): Causes, treatment and case studies. *Journal of Cleaner Production*, 14(12–13):1139-1145.

Akram, Z., Kausar, A. and Siddiq, M. (2016). Review on polymer/carbon nanotube composite focusing polystyrene microsphere and polystyrene microsphere/modified CNT composite: Preparation, properties, and significance. *Polymer-Plastics Technology and Engineering*, 55(6):582-603.

Al-Rashdi, B., Johnson, D.J., Hilal, N. (2013). Removal of heavy metal ions by nanofiltration. *Desalination*, 315:2-17.

Al-Zoubi, H., Rieger, A., Steinberger, P., Pelz, W., Haseneder, R., Hartel, G. (2010). Optimisation study for treatment of Acid Mine Drainage using membrane technology. *Separation and Technology*, 14 (14): 2004-2016.

Andrade, L.H., Ricci, B.C., Grossi, L.B., Pires, W.L., Aguiar, A.O., Amaral, M.C.S. (2017). Nanofiltration applied in gold mining effluent treatment: Evaluation of chemical cleaning and membrane stability. *Chemical Engineering Journal*, 323:545-556.

Aquafield water technology. [Online] Available at: http://www.aquafieldservices.com/index.php/technologies/membrane-filtration [Accessed 29 June 2017].

Baker, R.W. (2012a), 'Overview of membrane science and technology' in. *Membrane Technology and Applications.* John Wiley and Sons ltd: New Jersey. pp. 1-13.

Baker, R.W. (2012b), 'Membranes and modules' in. *Membrane technology and Applications.* John Wiley and Sons ltd: New Jersey. pp. 157-170.

Baker, R.W. and Low, B.T. (2015), 'Membrane Separation' in *Reference Module in Chemistry, Molecular Sciences and Chemical Engineering*. Elsevier.

Balasubramanian, K., Burghard, M. (2005). Chemically functionalized carbon nanotubes. *Small,* 1(2):180-192.

Barr, S.H., Baker, T., Markham, S.K. and Kingon, A.I. (2009). Bridging the valley of death: Lessons learned from 14 years of commercialization of technology education. *Academy of Management Learning & Education,* 8(3):370-388.

Bobák, M., Šnita, D., Hrdlička, J., Pelc, V. and Kotala, T. (2015). Innovative process simulation software not only for electromembrane processes. *Desalination and Water Treatment,* 56(12):3141-3145.

Camacho, L.M., Dume, L., Zhang, J., Li, J., Duke, M., Gomez, J., Gray, S. (2013). Advances in membrane distillation for water desalination and purification applications. *Water,* 5(1):94-196.

Celik, E., Park, H., Choi, H. and Choi, H. (2011). Carbon nanotube blended polyethersulfone membranes for fouling control in water treatment. *Water Research,* 45(1):274-282.

Corredor, E.C., Chitta, P. and Deo, M. (2016). Membrane reactor system model for gas conversion to benzene. *Fuel,* 179:202-209.

Crittenden, J.C., Trussell, R.R., Hand, D.W., Howe, K.J., Tchobanoglous, G. (2012), 'Membrane filtration' in *MWH's Water Treatment: Principles and Design, Third Edition.* John Wiley and Sons. New Jersey. pp. 819-902.

Clyde, E.J., Champagne, P., Jamieson, H.E., Gorman, C. and Sourial, J. (2016). The use of a passive treatment system for the mitigation of acid mine drainage at the Williams brothers mine (California): Pilot-scale study. *Journal of Cleaner Production,* 130:116-125.

Darvishmanesh, S., Firoozpour, L., Vanneste, J., Luis, P., Degrève, J. and Van der Bruggen, B. (2011). Performance of solvent resistant nanofiltration membranes for purification of residual solvent in the pharmaceutical industry: Experiments and simulation. *Green Chemistry*, 13(12):3476-3483.

Datsyuk, V., Kalyva, M., Papagelis, K., Parthenios, J., Tasis, D., Siokou, A., Kallitsis, I. and Galiotis, C. (2008). Chemical oxidation of multiwalled carbon nanotubes. *Carbon*, 46(6):833-840.

Davis, M.L. (2010), 'Reverse osmosis and nanofiltration' in *Water and Wastewater Engineering: Design Principles and Practice*. McGraw-Hill: New York. pp. 1097h-1097c.

Davies, R. (2015). Mines have a chance to manage water better. *Mail and Guardian* [Online] Available at :*https://mg.co.za/article/2015-08-28-00-mines-have-a-chance-to-manage-water-better* [Accessed 29 January 2017].

De Volder, M.F., Tawfick, S.H., Baughman, R.H. and Hart, A.J. (2013). Carbon nanotubes: Present and future commercial applications. *Science*, 339(6119):535-539.

Dhakate, S.R., Chauhan, N., Sharma, S., Tawale, J., Singh, S., Sahare, P.D. and Mathur, R.B. (2011). An approach to produce single and double layer graphene from re-exfoliation of expanded graphite. *Carbon*, 49(6):1946-1954.

Dresselhaus, M.S., Dresselhaus, G. and Saito, R. (1995). Physics of carbon nanotubes. *Carbon*, 33(7):883-891.

Drioli, E. and Giorno, L. Eds., (2016). *Encyclopedia of Membranes*. Springer: Berlin.

Durand, J.F. (2012). The impact of gold mining on the Witwatersrand on the rivers and karst system of Gauteng and North West province, South Africa. *Journal of African Earth Sciences*, 68:24-43.

Favvas, E.P., Nitodas, S.F., Stefopoulos, A.A., Papageorgiou, S.K., Stefanopoulos, K.L. and Mitropoulos, A.C. (2014). High purity multi-walled carbon nanotubes: Preparation, characterization and performance as filler materials in co-polyimide hollow fiber membranes. *Separation and Purification Technology,* 122:262-269.

Fenner, J.S., Daniel, I.M. (2016), 'Fracture Toughness and Impact Damage Resistance of Nanoreinforced Carbon/Epoxy Composites' in *Fracture. Fatigue, Failure and Damage Evolution.* Springer: Cham. pp. 213-224.

Gautam,R.K. and Chattopadhyaya,M.C. (2016). *Advanced nanomaterials for wastewater remediation,* CRC Press.

Geise, G.M., Lee, H., Miller, D.J., Freeman, B.D., McGrath, J.E. and Paul, D.R. (2010). Water purification by membranes: The role of polymer science. *Journal of Polymer Science Part B: Polymer Physics,* 48(15):1685-1718.

Gherasim, C., Mikulek, P. (2014). Influence of operating variables on the removal of heavy metal ions from aqueous solutions by nanofiltration. *Desalination,* 343:67-74.

Goh, P.S. and Ismail, A.F. (2015). Is interplay between nanomaterial and membrane technology the way forward for desalination? *Journal of Chemical Technology and Biotechnology,* 90(6):971-980.

Goh, P.S. and Ismail, A.F. (2017). A review on inorganic membranes for desalination and wastewater treatment. *Desalination.* 434:.60-80.

Grande, J.A., Jiménez, A., Romero, S., de la Torre, María Luisa and Gómez-Olivera, T. (2010). Quantification of heavy metals from AMD discharged into a public water supply dam in the Iberian pyrite belt (SW Spain) using centered moving average. *Water, Air, and Soil Pollution,* 212(1-4):299-307

Gu, B., Kim, D.Y., Kim, J.H. and Yang, D.R. (2011). Mathematical model of flat sheet membrane modules for FO process: Plate-and-frame module and spiral-wound module. *Journal of Membrane Science*, 379(1):403-415.

Harris, P.J.F. (2009), 'Synthesis catalytic chemical vapour deposition and related methods' in *Carbon Nanotube Science Synthesis Properties and Applications*. Ed. P. Harris. Cambridge University Press. pp. 44-72.

Hirsch, A. (2010). The era of carbon allotropes. *Nature Materials*, 9(11):868-871.

Homayoonfal, M., Mehrnia, M.R., Shariaty-Niassar, M., Akbari, A., Ismail, A.F. and Matsuura, T. (2014). A comparison between blending and surface deposition methods for the preparation of iron oxide/polysulfone nanocomposite membranes. *Desalination*, 354:125-142.

Hu, A. and Apblett, A. (2014). *Nanotechnology for water treatment and purification.* Springer. Switzerland. pp. 307-361.

Huang, L., Wang, D., He, C., Pan, M., Zhang, B., Chen, Q. and Ren, J. (2019). Industrial wastewater desalination under uncertainty in coal-chemical eco-industrial parks. *Resources, Conservation and Recycling*, 145:370-378

Hołda, A.K., Aernouts, B., Saeys, W. and Vankelecom, I.F. (2013). Study of polymer concentration and evaporation time as phase inversion parameters for polysulfone-based SRNF membranes. *Journal of Membrane Science*, 442:196-205.

Ji, Y., Qian, W., Yu, Y., An, Q., Liu, L., Zhou, Y. and Gao, C. (2017). Recent developments in nanofiltration membranes based on nanomaterials. *Chinese Journal of Chemical Engineering*, *25*(11):1639-1652.

Jiwan, S. and Kalamdhad, A.S. (2011). Effects of heavy metals on soil, plants, human health and aquatic life. *International Journal of Research in Chemistry and Environment*, (2):15-21.

Johnson, J. and Busch, M. (2010). Engineering aspects of reverse osmosis module design. *Desalination and Water Treatment,* 15(1-3):236-248.

Johnson, D.B. and Hallberg, K.B. (2005). Acid mine drainage remediation options: A review. *Science of the Total Environment,* 338(1–2):3-14.

Karabelas, A.J., Kostoglou, M., Koutsou, C.P. (2015). Modelling of spiral wound membrane desalination modules and plants–review and research priorities. *Desalination,* 356:165-186.

Kefeni, K.K., Msagati, T.A.M. and Mamba, B.B. (2017). Acid mine drainage: Prevention, treatment options, and resource recovery: A review. *Journal of Cleaner Production,* 151:475-493.

Iyuke S. E., Mahalik, N. P. (2006). 'Carbon Nanotube Production and Applications: Basis of Nanotechnology' in *Micromanufacturing and Nanotechnology,* Springer: Berlin. pp. 219-245.

Kaksonen, A.H. and Puhakka, J.A. (2007). Sulfate reduction based bioprocesses for the treatment of acid mine drainage and the recovery of metals. *Engineering in Life Sciences,* 7(6):541-564.

Katsnelson, M.I. (2007). Graphene: Carbon in two dimensions. *Materials Today,* 10(1-2):20-27.

Khansary, M.A., Marjani, A. and Shirazian, S. (2017). On the search of rigorous thermo-kinetic model for wet phase inversion technique. *Journal of Membrane Science,* 538:18-33.

Khulbe, K.C. and Matsuura, T. (2017). Synthetic membrane characterisation–a review: Part I. *Membrane Technology,* 2017(7):7-12.

Kochkodan, V. and Hilal, N. (2015). A comprehensive review on surface modified polymer membranes for biofouling mitigation. *Desalination,* 356187-207.

Koziol, K., Vilatela, J., Moisala, A., Motta, M., Cunniff, P., Sennett, M., Windle, A. (2007). High-performance carbon nanotube fiber. *Science,* 318(5858):1892-1895.

Kumar, V.S., Hariharan, K.S., Mayya, K.S., Han, S. (2013). Volume averaged reduced order donnan steric pore model for nanofiltration membranes. *Desalination*, 322:21-28.

Le, N.L., Duong, P.H.H. and Nunes, S.P. (2017), 'Advanced Polymeric and Organic–Inorganic Membranes for Pressure-Driven Processes' in *Comprehensive Membrane Science and Engineering (Second Edition)*. Eds. E. Drioli, L. Giorno, and E. Fontananova. Elsevier: Oxford, pp. 120-136.

Lee, J., Chae, H., Won, Y.J., Lee, K., Lee, C., Lee, H.H., Kim, I. and Lee, J. (2013). Graphene oxide nanoplatelets composite membrane with hydrophilic and antifouling properties for wastewater treatment. *Journal of Membrane Science*, 448:223-230.

Lee, H.D., Kim, H.W., Cho, Y.H. and Park, H.B. (2014). Experimental evidence of rapid water transport through carbon nanotubes embedded in polymeric desalination membranes. *Small*, 10(13):2653-2660.

Lee, J., Jeong, S. and Liu, Z. (2016). Progress and challenges of carbon nanotube membrane in water treatment. *Critical Reviews in Environmental Science and Technology*, 46(11-12):999-1046.

Lewis, M.E. and Clark, M.L. (1997). How does streamflow affect metals in the upper Arkansas river. *Washington: Government Printing Office.*

Li, X., Mo, Y., Li, J., Guo, W. and Ngo, H.H. (2017). In-situ monitoring techniques for membrane fouling and local filtration characteristics in hollow fiber membrane processes: A critical review. *Journal of Membrane Science*, 528:187-200.

Liang, R., Hatat-Fraile, M., Hu, A. and Zhou, N. (2014) 'Fundamentals on Adsorption, Membrane Filtration and Advanced Oxidation Processes for Water Treatment' in *Nanotechnology for Water Treatment and Purification*. Eds. A. Hu and A. Apblett. Springer: Cham. pp. 1-45.

Lin, H., He, Z., Sun, Z., Vu, J., Ng, A., Mohammed, M., Kniep, J., Merkel, T.C., Wu, T. and Lambrecht, R.C. (2014). CO 2-selective membranes for hydrogen production and CO 2 capture–Part I: Membrane development. *Journal of Membrane Science*, 457:149-161.

Liu, W., Chai, S., Mohamed, A.R. and Hashim, U. (2014). Synthesis and characterization of graphene and carbon nanotubes: A review on the past and recent developments. *Journal of Industrial and Engineering Chemistry,* 20(4):1171-1185.

Lopez, J., Reig, M., Gibert, O., Valderrama, C. and Cortina, J.L. (2018). Evaluation of NF membranes as treatment technology of acid mine drainage: Metals and sulphate removal. *Desalination,* 440122-134.

Naicker, K., Cukrowska, E. and McCarthy, T.S. (2003). Acid mine drainage arising from gold mining activity in Johannesburg, South Africa and environs. *Environmental Pollution,* 122(1):29-40.

Nicolini, J.V., Borges, C.P., Ferraz, H.C. (2016). Selective rejection of ions and correlation with surface properties of nanofiltration membranes. *Separation and Purification Technology,* 171:238-247.

Ntwampe, I.O., Waanders, F.B., Fosso-Kankeu, E. and Bunt, J.R. (2015). Turbidity removal efficiencies of clay and af-PFCl polymer of magnesium hydroxide in AMD treatment. *International Journal of Science and Research,* 4:38-55.

Ntwampe, I.O., Waanders, F.B. and Bunt, J.R. (2016). Destabilization dynamics of clay and acid-free polymers of ferric and magnesium salts in AMD without pH adjustment. *Water Science and Technology,* 74(4):861-875.

Nunes, S.P., Sougrat, R., Hooghan, B., Anjum, D.H., Behzad, A.R., Zhao, L., Pradeep, N., Pinnau, I., Vainio, U. and Peinemann, K. (2010). Ultraporous films with uniform nanochannels by block copolymer micelles assembly. *Macromolecules,* 43(19):8079-8085.

Oakes, K., Shan, Z., Kaliaperumal, R., Zhang, S.X. and Mkandawire, M. (2014), 'Nanotechnology in Contemporary Mine Water Issues' in *Nanotechnology for Water Treatment and Purification.* Springer: Cham. pp. 307-361.

Ma, P., Siddiqui, N.A., Marom, G. and Kim, J. (2010). Dispersion and functionalization of carbon nanotubes for polymer-based nanocomposites: A review. *Composites part A: Applied Science and Manufacturing,* 41(10):1345-1367.

Manikandan, D., Mangalaraja, R.V., Avila, R.E., Siddheswaran, R. and Anathakumar, S. (2013). Montmorillonite–carbon nanotube nanofillers by acetylene decomposition using catalytic CVD. *Applied Clay Science*, 71:37-41.

Martín, M.M. (2016).'Water' in *Industrial Chemical Process Analysis and Design.* Elsevier: Boston. pp 125-197.

Meo, M. and Rossi, M. (2006). Prediction of young's modulus of single wall carbon nanotubes by molecular-mechanics based finite element modelling. *Composites Science and Technology,* 66(11-12):1597-1605.

Mubarak,N.M., Abdullah,E.C., Jayakumar,N.S., Sahu,J.N. (2014). An overview on methods for the production of carbon nanotubes. *Journal of Industrial and Engineering Chemistry, 20*(4), pp.1186-1197.

Manawi, Y., Kochkodan, V., Hussein, M.A., Khaleel, M.A., Khraisheh, M., Hilal, N. (2016). Can carbon-based nanomaterials revolutionize membrane fabrication for water treatment and desalination? *Desalination,* 391:69-88.

Maphutha, S., Moothi, K., Meyyappan, M. and Iyuke, S.E. (2013). A carbon nanotube-infused polysulfone membrane with polyvinyl alcohol layer for treating oil-containing wastewater. *Scientific Reports,* 3: 1509-1515.

Maree, J.P., Hlabela, P., Nengovhela, R., Geldenhuys, A.J., Mbhele, N., Nevhulaudzi, T. and Waanders, F.B. (2004). Treatment of mine water for sulphate and metal removal using barium sulphide. *Mine Water and The Environment,* 23(4):195-203.

Mark, H.F. (2013), *Encyclopedia of Polymer Science and Technology, concise* John Wiley and Sons.

Mattia, D., Leese, H. and Lee, K.P. (2015). Carbon nanotube membranes: From flow enhancement to permeability. *Journal of Membrane Science,* 475:266-272.

McCarthy, T.S. (2011). The impact of acid mine drainage in South Africa. *South African Journal of Science,* 107(5-6):1

Meyyappan, M., Srivastava, D. (2003), 'Carbon nanotubes' in *Handbook of Nanoscience Engineering and Technology*. CRC Press: Florida. pp. 14

Mohammad, A.W., Teow, Y.H., Ang, W.L., Chung, Y.T., Oatley-Radcliffe, D.L. and Hilal, N. (2015). Nanofiltration membranes review: Recent advances and future prospects. *Desalination,* 356:226-254.

Moothi, K., Iyuke, S.E., Meyyappan, M. and Falcon, R. (2012). Coal as a carbon source for carbon nanotube synthesis. *Carbon,* 50(8):2679-2690.

Mthetwa, V. (2014). *Investigation of polyether sulfone (PES) hollow fibre membranes for the treatment of acid mine drainage*. Doctoral thesis, University of Witwatersrand, Johannesburg.

Mudd, G.M. (2007). February. Resource consumption intensity and the sustainability of gold mining. In *Proceedings of the 2nd International Conference on Sustainability Engineering and Science*.

Mullett, M., Fornarelli, R., Ralph, D. (2014). Nanofiltration of mine water: Impact of feed pH and membrane charge on resource recovery and water discharge, *Membranes,* 4(2):163–180.

Mulder, J. (2012), *Basic principles of Membrane Technology* Springer Science and Business Media: Germany. pp. 297-303.

O'Connell, M.J., Eibergen, E.E. and Doorn, S.K. (2005). Chiral selectivity in the charge-transfer bleaching of single-walled carbon-nanotube spectra. *Nature Materials,* 4(5):412-418.

Pagès, N., Reig, M., Gibert, O., Cortina, J.L. (2017). Trace ions rejection tunning in NF by selecting solution composition: Ion permeances estimation. *Chemical Engineering Journal*, 308:126-134.

Pal, G. and Kumar, S. (2016). Modelling of carbon nanotubes and carbon nanotube–polymer composites. *Progress in Aerospace Sciences*, 80:33-58.

Park, C., Park, P., Mane, P.P., Hyung, H., Gandhi, V., Kim, S. and Kim, J. (2010). Stochastic cost estimation approach for full-scale reverse osmosis desalination plants. *Journal of Membrane Science*, 364(1-2):52-64.

Park, P., Lee, S., Cho, J. and Kim, J. (2012). Full-scale simulation of seawater reverse osmosis desalination processes for boron removal: Effect of membrane fouling. *Water Research*, 46(12):3796-3804.

Park, S., Jung, J., Lee, S., Baek, Y., Yoon, J., Seo, D.K. and Kim, Y.H. (2014). Fouling and rejection behaviour of carbon nanotube membranes. *Desalination*, 343:180-186.

Paul, M., Jons, S.D. (2016). Chemistry and fabrication of polymeric nanofiltration membranes: A review. *Polymer*, 103:417-456.

Phuntsho, S., Hong, S., Elimelech, M. and Shon, H.K. (2014). Osmotic equilibrium in the forward osmosis process: Modelling, experiments and implications for process performance. *Journal of Membrane Science*, 453:240-252.

Purohit, R., Purohit, K., Rana, S., Rana, R.S. and Patel, V. (2014). Carbon nanotubes and their growth methods. *Procedia Materials Science*, 6:716-728.

Qin, L., Ge, Y., Deng, B., Li, Z. (2017). Poly (ethylene imine) anchored lignin composite for heavy metals capturing in water. *Journal of the Taiwan Institute of Chemical Engineers*, 71:84-90.

Rahmandoust M., Ayatollahi M.R. (2016) 'Carbon Nanotubes' in *Characterization of Carbon Nanotube Based Composites under Consideration of Defects. Advanced Structured Materials*, vol. 39. Springer: Cham. pp. 5-63.

Rahimpour, A., Jahanshahi, M., Mortazavian, N., Madaeni, S.S. and Mansourpanah, Y. (2010). Preparation and characterization of asymmetric polyethersulfone and thin-film composite polyamide nanofiltration membranes for water softening. *Applied Surface Science,* 256(6):1657-1663.

Rashid, M.H., Ralph, S.F. (2017). Carbon nanotube membranes: Synthesis, properties, and future filtration applications. *Nanomaterials,* 7(5):99.

Rezania, H.J., Vatanpour, V., Shockravi, A. and Ehsani, M. (2019). Study of synergetic effect and comparison of novel sulfonated and carboxylated bulky diamine-diol and piperazine in preparation of negative charge NF membrane. *Separation and Purification Technology,* 222:284-296.

Rios, C.A., Williams, C.D. and Roberts, C.L. (2008). Removal of heavy metals from acid mine drainage (AMD) using coal fly ash, natural clinker and synthetic zeolites. *Journal of Hazardous Materials,* 156(1):23-35.

Roco, M.C., Mirkin, C.A. and Hersam, M.C. (2011). Nanotechnology research directions for societal needs in 2020*:* Summary of international study *Journal of Nanoparticle Research,* 13: 897-919.

Roefs, I., Meulman, B., Vreeburg, J.H. and Spiller, M. (2017). Centralised, decentralised or hybrid sanitation systems? Economic evaluation under urban development uncertainty and phased expansion. *Water Research,* 109:274-286.

Schulz, M.J., Ruff, B., Johnson, A., Vemaganti, K., Li, W., Sundaram, M.M., Hou, G., Krishnaswamy, A., Li, G., Fialkova, S., Yarmolenko, S., (2013). 'New Applications and Techniques for Nanotube Superfiber Development' in Nanotube *Superfiber Materials*. William Andrew Publishing. pp. 33-59.

Shawky, H.A., Chae, S., Lin, S. and Wiesner, M.R. (2011). Synthesis and characterization of a carbon nanotube/polymer nanocomposite membrane for water treatment. *Desalination*, 272(1):46-50.

Simate, G.S. and Ndlovu, S. (2014). Acid mine drainage: Challenges and opportunities. *Journal of Environmental Chemical Engineering*, 2(3):1785-1803.

Singh, R., Gautam, N., Mishra, A. and Gupta, R. (2011). Heavy metals and living systems: An overview. *Indian Journal of Pharmacology*, 43(3):246.

Singh, R. (2014), 'Introduction to membrane technology' in *Membrane Technology and Engineering for Water Purification: Application, Systems Design and Operation*. Butterworth-Heinemann. pp. 1-78.

Srivastava, A., Srivastava, S. and Kalaga, K. (2013), 'Carbon nanotube membrane filters' in *Handbook of Nanomaterials.* Vajtai R. (Eds). Springer: Berlin. pp. 1099-1116.

Spitalsky, Z., Tasis, D., Papagelis, K., Galiotis, C. (2010). Carbon nanotube–polymer composites: Chemistry, processing, mechanical and electrical properties. *Progress in Polymer Science*, 35(3):357-401.

Szab, A., Perri, C., Csat, A., Giordano, G., Vuono, D. and Nagy, J.B. (2010). Synthesis methods of carbon nanotubes and related materials. *Materials*, 3(5):3092-3140.

Tan, S.M., Poh, H.L., Sofer, Z. and Pumera, M. (2013). Boron-doped graphene and boron-doped diamond electrodes: Detection of biomarkers and resistance to fouling. *Analyst*, 138(17):4885-4891.

Tesfasgiorgis, H., Sebola, M., and Muzenda, E. (2015). Economic evaluation of anaerobic digestion technology. *South African Journal of Chemical Engineering*, 20(2):80-90.

Thembrsite, (2016). [Online]. Available at: http://www.thembrsite.com/news/cut-membrane-technology-demonstrates-successful-landfill-leachate-water-treatment-using-their-t-cut-tubular-modules-as-part-of-a-sidestream-mbr/ [Accessed 30 October 2017].

Thomas, S., Mishra, R.K. and Asiri, A.M. (2019). *Sustainable polymer composites and nanocomposites.* Springer.

Tutu, H., McCarthy, T.S., Cukrowska, E. (2008). The chemical characteristics of acid mine drainage with particular reference to sources, distribution and remediation: The Witwatersrand basin, South Africa as a case study. *Applied Geochemistry,* 23(12):3666-3684.

Van der Bruggen, B., Mänttäri, M. and Nyström, M. (2008). Drawbacks of applying nanofiltration and how to avoid them: A review. *Separation and Purification Technology,* 63(2):251-263.

Vatanpour, V., Madaeni, S.S., Moradian, R., Zinadini, S., Astinchap, B. (2011). Fabrication and characterization of novel antifouling nanofiltration membrane prepared from oxidized multiwalled carbon nanotube/polyethersulfone nanocomposite. *Journal of Membrane Science,* 375(1):284-294.

Vella, H. (2013). Managing water consumption in mining. [Online]. Available at: http://www.mining-technology.com/features/feature-managing-water-consumption-mining-global-shortage/ [Accessed 29 January 2017].

Wang, X., Yang, W.D., Yang, S. (2014). Dynamic stability of carbon nanotubes reinforced composites. *Applied Mathematical Modelling,* 38(11–12):2934-2945.

Wang, L., Song, X., Wang, T., Wang, S., Wang, Z., Gao, C. (2015). Fabrication and characterization of polyethersulfone/carbon nanotubes (PES/CNTs) based mixed matrix membranes (MMMs) for nanofiltration application. *Applied Surface Science,* 330:118-125.

Wang, Z., Wang, Y., Xu, G. and Ren, J. (2019). Sustainable desalination process selection: Decision support framework under hybrid information. *Desalination,* 465:44-57.

Wu, C., Liu, S., Wang, Z., Zhang, J., Wang, X., Lu, X., Jia, Y., Hung, W., Lee, K. (2016). Nanofiltration membranes with dually charged composite layer exhibiting super-high multivalent-salt rejection. *Journal of Membrane Science,* 517:64-72.

Yengejeh, S.I., Kazemi, S.A., Chsner, A. (2017). Carbon nanotubes as reinforcement in composites: A review of the analytical, numerical and experimental approaches. *Computational Materials Science,* 136:85-101

Yin, J. and Deng, B. (2015). Polymer-matrix nanocomposite membranes for water treatment. *Journal of Membrane Science,* 479:256-275.

Zhang, T.C., Surampalli, R.Y., Vigneswaran, S., Tyagi, R.D., Leong Ong, S. and Kao, C.M. eds., (2012). 'Membrane Technology and Environmental Applications'. *In American Society of Civil Engineers*.

Zhang, Y., Zhang, S. and Chung, T. (2015). Nanometric graphene oxide framework membranes with enhanced heavy metal removal via nanofiltration. *Environmental Science and Technology,* 49(16):10235-10242.

Zhao, D. and Yu, S. (2015). A review of recent advance in fouling mitigation of NF/RO membranes in water treatment: Pretreatment, membrane modification, and chemical cleaning. *Desalination and Water Treatment,* 55(4):870-891.

Zhou, J., Ren, J., Lin, L., Deng, M. (2008). Morphology evolution of thickness-gradient membranes prepared by wet phase-inversion process. *Separation and Purification Technology,* 63(2):484-486.

CHAPTER3: METHODOLOGY

The development and application of membrane technology for wastewater treatment offers an opportunity to design membranes that are more cost effective and energy efficient for treating water for reuse or safe disposal (Adnan *et al*., 2010; Lau *et al*., 2012; Lee *et al*., 2016). Researchers have focused on the addition of nanomaterials to thin film composite (TFC) membranes (Fathizadeh *et al*., 2011; Rajaeian *et al*., 2013) Among the various studied nanomaterials are CNTs (Wu *et al*., 2010; Zarrabi *et al*., 2016). As mentioned in Chapter 2, CNTs have desirable mechanical, chemical, and thermal properties that can be used to enhance the performance of TFC compared with that of pristine membranes. CNTs can also alter the physio-chemical properties of the membrane. Provided CNTs contain carboxylic groups mentioned in Chapter 2, they can be embedded in the polyamide layer of TFC membranes. CNTs also have a high specific surface area, unique adsorption properties and wide distributions of reactive surface sites which makes them ideal for incorporation in membranes to improve rejection and flux (Vatanpour *et al*., 2011; Sakar *et al*., 2018). Chapter 3 deals with the methods and materials used to oxidise CNTs as well as the characterisation techniques used to confirm oxidation. TFN membranes are suitable for AMD treatment, (Aguiar *et al*., 2016; Al-Rashdi *et al*., 2013; Al-Zoubi *et al*., 2010) hence they were chosen as the focus in this study. The preparation of TFN membranes is also detailed along with the characterisation methods for the prepared membranes.

3.1 DESIGN OF EXPERIMENTS

Traditionally, experimental methodology used to perform experiments involves changing one parameter at a time while keeping other parameters constant (Aghaei *et al*., 2017; Khayet *et al*., 2011). This approach is expensive, time consuming and requires many runs (Gholami *et al*., 2012; Shojaeimehr *et al*., 2014). It also neglects the influence of other interacting parameters which are kept constant, thereby, making it difficult to optimise a process (Kirmizakis *et al*., 2014; Myers *et al*., 2016). Design of experiments (DOE) is used when input variables of an experiment can be varied to optimise the output (Danmaliki *et al*., 2017; Myers *et al*., 2016;

Varala *et al*., 2016). DOE was done using JMP statistical software version 14. The design method was based on the central composite design with fractional factorials (Alidokht *et al*., 2011; Ghasemi *et al*., 2011; Jadhav *et al*., 2016). There are other methods for DoE, however this method is useful when the factors that need to be studied are 5 or greater (Myers *et al*., 2016). For the experiments done in this study the 5 factors studied were pressure, CNT loading, and feed concentrations of the synthetic AMD namely, iron, magnesium, and aluminium. The factors were used to determine 4 responses which were flux, iron rejection, magnesium rejection and aluminium rejection. The factors and levels studied are shown in Table 3.1 where factor levels are coded from low level (-1) to high level (+1) and centre points at 0. Surface response models were generated and a quadratic approximation was considered to explain the behaviour as shown in Equation (3.1):

$$Y = b_0 + \sum_{i=1}^{n} b_i x_i + \sum_{i=1}^{n} b_{ii} x_i^2 + \sum_{i=1}^{n-1} \sum_{j=i}^{n} b_{ij} x_i x_j \qquad (3.1)$$

where Y is the predicted response, b_0 is the constant coefficient, b_i the linear coefficients, b_{ij} the interaction coefficients and x_i, x_j are the coded levels of the process factors studied (Aghaei and Yengejeh, 2017; Myers *et al*., 2016). The validity of the model was tested with an analysis of variance (ANOVA) with the confidence level used as 95% (Auta and Hameed, 2011; Chabbi *et al*., 2017).

Table 3-1: Levels of factors

Factors	**Units**	**Level**		
		Low (-1)	**Centre (0)**	**High (+1)**
Pressure	Bar	10	15	20
CNT loading	mg/ml	0,2	0,3	0,4
Mg conc.	Ppm	100	150	200
Fe conc.	Ppm	1000	1500	2000
Al conc.	Ppm	100	150	200

3.2 MATERIALS AND REAGENTS

MWCNTs with an outer diameter of 6 to 13 nm and length from 2.5 to 20µm, with purity >98%, were purchased from Sigma Aldrich. Nitric acid (65%) and sulphuric acid (98%) were supplied by Ace Chemicals. Commercial LY ultrafiltration UF PES membranes with a MWCO of 100,000Da were purchased from Synder Filtration (USA). For the preparation of polyamide TFC n-hexane (anhydrous ≥99%) and the monomers Piperazine (PIP) and Trimesoyl chloride (TMC, 98%) were used as received from Sigma Aldrich. Sodium dodecyl sulfate (SDS) (98.5%) was purchased from Sigma Aldrich. $Fe_2(SO_4)_3.7H_2O$, $Al_2(SO_4)_3.18H_2O$ and $MgSO_4$ salts for synthetic AMD synthesis were supplied by Rochelle Chemicals. Deionized (DI) water with a conductivity of 5.5 µS/m at 25ºC was produced by a Milli-Q vacuum purification system.

3.3 PREPARATION AND CHARACTERISATION OF CNTS

3.3.1 Oxidation of CNTS

CNTs were oxidised using a mixture of 35% HNO_3 and 98% H_2SO_4 (3:1) (Vatanpour *et al*., 2017). An amount of 2 g of CNTs was added to 200 ml of the solution. CNTs were oxidised by acid treatment with the acid mixture using a microwave digester. The reaction was carried out at 150 W for 1 hr at 70˚C (Lui *et al*, 2008). The CNTs were then washed until pH 7 and dried in a vacuum oven at 60˚C for 12 hr (Shawky *et al*., 2011).

3.3.2 Characterization of CNTs

A JEOL-JEM 2100F high-resolution transmission electron microscopy (HR-TEM) was used to characterise the CNTs before and after oxidation. The CNT samples were sonicated in acetone in preparation for analysis. A few drops of the solution were placed on a carbon coated copper grid before viewing under 200kV. Low voltage is required to avoid damage to the nanotubes due to the electron beam (Vatanpour *et al*., 2017). Perkin Elmer Raman Station 400 equipped with a CCD detector was used to determine the graphitic structure of CNTs. Raman spectroscopy is a quick non-destructive method that can be used to analyse carbon samples (Lui *et al*., 2014). Samples were characterised using a 1.96 eV excitation energy. Total Reflectance Fourier Transform Infrared Spectroscopy (ATR-FTIR) was used to study functional groups of

the pristine and *f*-MWCNTs (García *et al*., 2018). The Perkin Elmer model number L1280026 FTIR-ATR was used in the range 400-4000cm^{-1}.

3.4 PREPARATION AND CHARACTERISATION OF TFN MEMBRANES

3.4.1 Preparation of TFN membranes

Thin film composite membranes were prepared using a modified interfacial polymerisation process. It was recommended by the manufacturer that the membranes be stored in a solution of glycerol and water to preserve membrane pores (Synder Filtration) In order to remove the glycerol on the surface the membranes were immersed in an aqueous solution of 0.6 mol/L HCl for 40 min. The excess acid was neutralised by 0.5 mol/L NaOH solution (Shen *et al*., 2013). Commercial UF-PES support membranes were pre-treated by soaking them in 0.50% of SDS overnight. SDS is an anionic surfactant and was used to clean the membranes before use (Ang *et al*., 2011). The membranes were then washed with distilled water for 1 hr and allowed to dry in the fume hood for 2 hr. The pre-treated membranes were immobilised onto glass plates using double sided tapes and paper tapes. The paper tapes kept the double-sided tapes in place. The PES flat sheet membranes were immersed in the organic solution of 0.40% w/v TMC in hexane for 30 min, before immersion in the aqueous solution of DI water and PIP for 30 min. The membranes were then immersed in the organic solution again for 30 min for further polymerisation and formation of the skin layer (Wu *et al*., 2010; Wu *et al*., 2013). It is important to note that in order to maintain a uniform layer on the membrane surface, a rubber roller was used to remove residual droplets of aqueous solution on the top surface before immersing the membrane in the organic solution. PIP is an aliphatic diamine that is commonly used in the preparation of TFC membranes. PIP and TMC are polymerised on the membrane support to form the active layer of the membrane (Misdan *et al*., 2014). The reaction of the amine with the acyl halide to form a polyamide thin layer is shown in Figure 3-1. Weighted amounts of CNTs (0-0.6 mg/ml) were added to the TFC membrane to form TFN membranes. The CNTs and 0.05mg/ml SDS and were added to the aqueous solution with ultrasonication for at least 60 min until a well dispersed solution was obtained. Ultrasonic agitation was used to avoid agglomeration of CNTs in the aqueous solution. SDS was found to help with the dispersion of

CNTs in aqueous solution (Lee *et al*., 2014; Wu *et al*., 2013). The membrane was dried in an oven at 60˚C after being washed with DI water. Finally, the prepared membrane was stored in DI water in the freezer at 20°C until testing. Figure 3-2 shows an overview of the method used for CNT-TFN membranes.

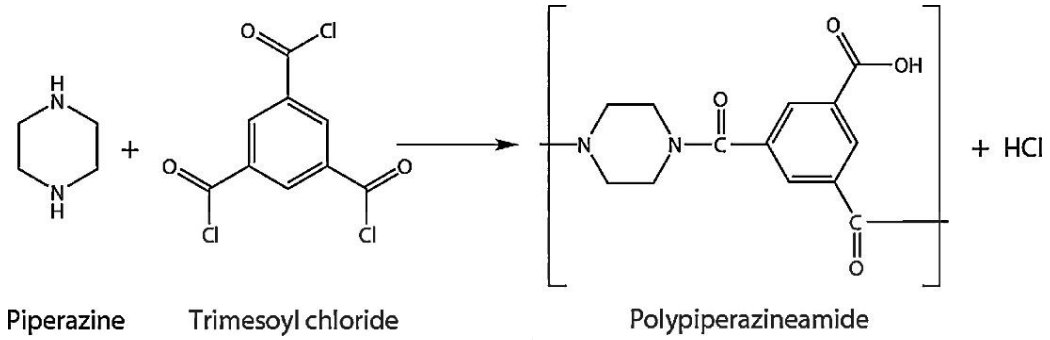

Figure 3-1**:** A scheme of cross-linking reaction between piperazine and trimesoyl chloride (Dalwani *et al*., 2011)

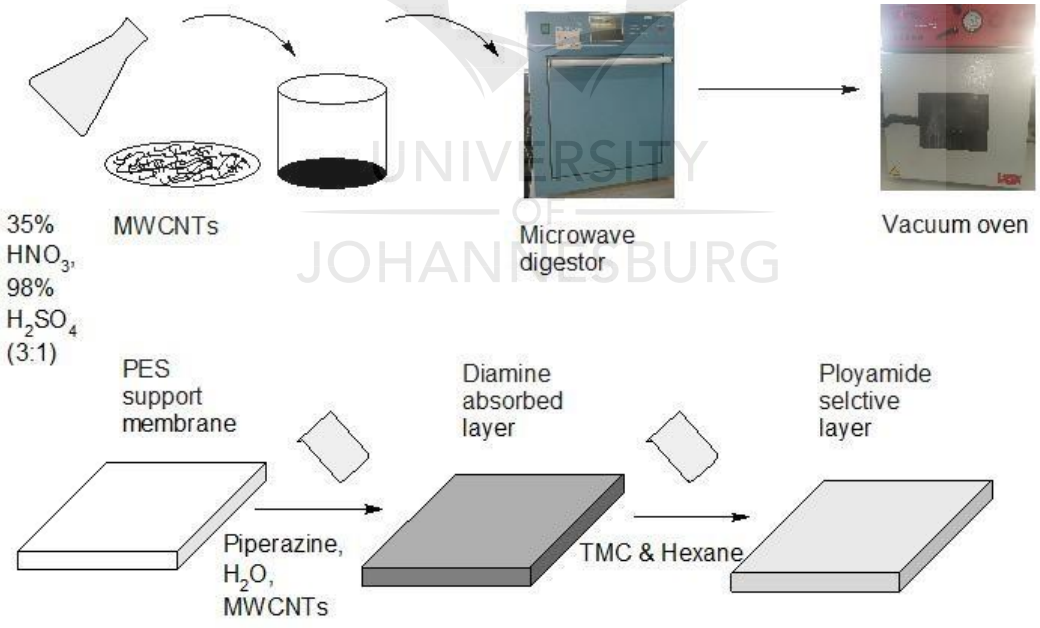

Figure 3-2: Preparation of CNT-TFN membranes

3.4.2 Characterisation of TFN membranes

The Scanning Electron Microscopy (SEM) was used to characterise the membrane structure. A 20 kV electron acceleration voltage was used. Membrane samples were freeze fractured in liquid nitrogen in order to prepare them for analysis. Also, membrane samples were carbon-coated before analysis to prevent charging. Atomic Force Microscopy (AFM) was used to measure the surface roughness. Membrane hydrophilicity was quantified using a contact angle analyser and a sessile drop method (Vatanpour *et al*., 2011). Deionized water (2µL) was dropped onto a dry membrane using a syringe, and the contact angle was measured. Readings were taken from different locations on the membrane and the average values were reported.

3.5 PREPARATION OF SYNTHETIC AMD SOLUTION

Synthetic AMD solution was prepared based on heavy metals commonly found in gold AMD in South Africa (Tutu *et al*., 2008). Required amounts of $Fe_2(SO4)_3.7H_2O$, $Al_2(SO4)_3.18H_2O$ and $MgSO_4$ were weighed and dissolved in deionised water to give solution of 1000 ml with 2000 mg/L Fe^{3+}, 200 mg/L Al^{3+} and 200 mg/L Mg^{2+}. H_2SO_4 was added to ensure that the pH was below 3 and to bring the SO_4^{2-} concentration to 6000 mg/L (Masindi *et al*., 2015).

3.6 PERFORMANCE OF TFN MEMBRANES

3.6.1 Pure water permeation

Membrane pure water permeability was determined using a crossflow filtration rig with a membrane area of 42 cm^2 (Figure 3-4). The filtration rig consisted of a feed tank with a temperature controller, two pressure gauges (0-1500 psi) at the inlet and outlet of the membrane module, a flow meter on the retentate side, a low-pressure peristaltic pump and valves (Yokwana, 2014). Membrane samples were compacted at 5-25 bar before analysis in order to obtain steady flow (Gumbi, 2015; Wang *et al*., 2017). Flux was measured every 15 minutes for an hour. Flux was calculated using Equation (3.2):

$$J_W = V/At \quad (3.2)$$

where; J_W (L/m^{2}h) is flux, V (L) is permeate volume, A (m^2) is the membrane effective area and t (h) is the filtration time (Mahdavi *et al*., 2017).

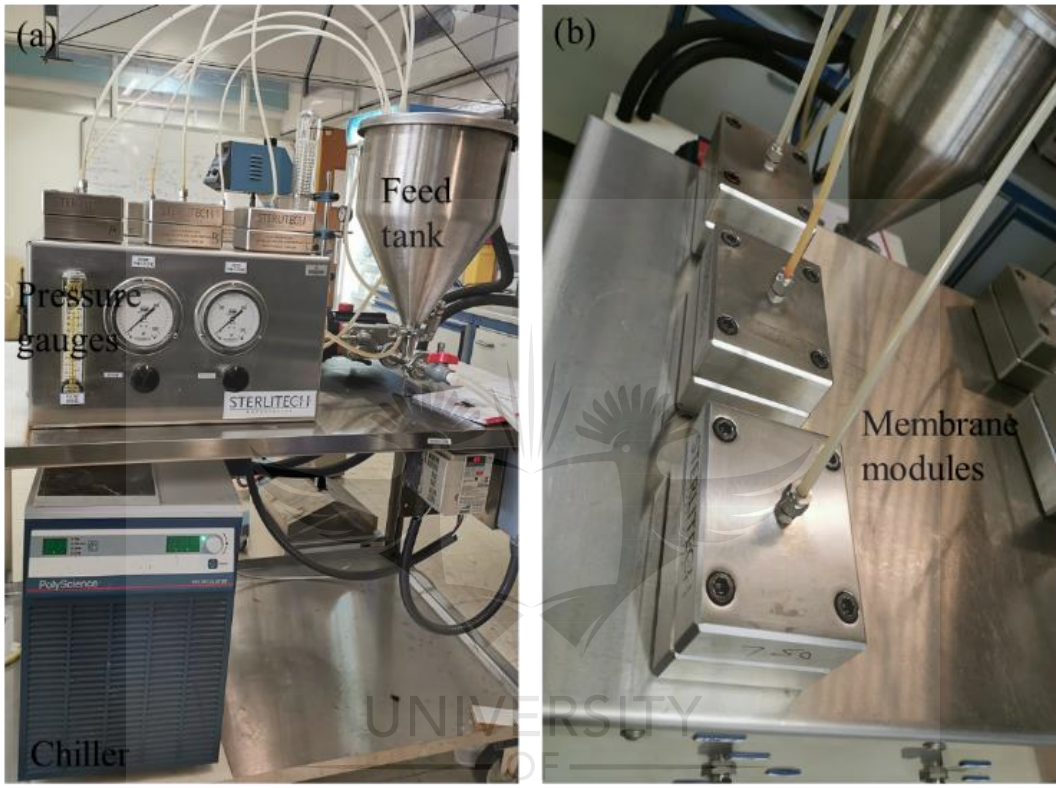

Figure 3-3: Photo of (a) Crossflow filtration rig, (b) membrane modules

Ion rejection rates and flux tests were conducted. Membrane permeability was determined by measuring the flux of single, binary and tertiary salt solutions of the $Fe_2(SO4)_3.7H_2O$, $Al_2(SO4)_3.18H_2O$ and $MgSO_4$ heavy metal salts. Ion rejection was determined by measuring the salt concentration in the feed and permeate streams using a conductivity meter. The ion rejection was calculated using equation (3.3):

$$R(\%) = 1 - \left(\frac{C_p}{C_f}\right) * 100 \quad (3.3)$$

where; R is the percentage of ion rejection and C_p and C_f are the conductivity of the feed and permeate respectively (Mahdavi *et al*., 2017).

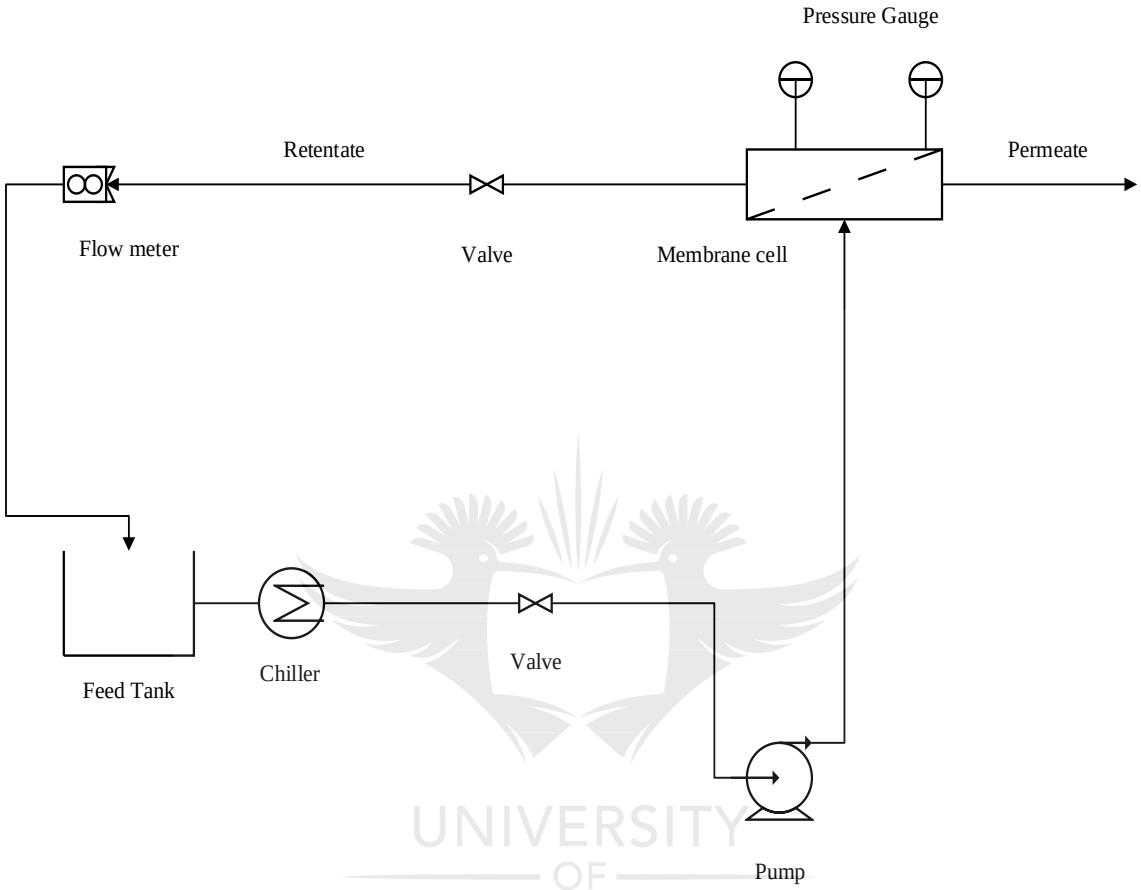

Figure 3-4: Experimental crossflow filtration rig

3.7 REFERENCES

Adnan, S., Hoang, M., Wang, H., Bolto, B. and Xie, Z. (2010). Recent trends in research, development and application of membrane technology in the pulp and paper industry. *Appita: Technology, Innovation, Manufacturing, Environment,* 63(3):235.

Aghaei, F. and Jalilzadeh Yengejeh, R. (2017). Investigation of effective parameters on the performance of NF membrane in simultaneous removal of Cr (VI) and Cu from contaminated water. *Pollution,* 3(3):383-394.

Alidokht, L., Khataee, A.R., Reyhanitabar, A. and Oustan, S. (2011). Cr (VI) immobilization process in a Cr-spiked soil by zerovalent iron nanoparticles: Optimization using response surface methodology. *Clean Soil, Air, Water,* 39(7):633-640.

Ang, W.S., Tiraferri, A., Chen, K.L. and Elimelech, M. (2011). Fouling and cleaning of RO membranes fouled by mixtures of organic foulants simulating wastewater effluent. *Journal of Membrane Science,* 376(1-2):196-206.

Auta, M. and Hameed, B.H. (2011). Optimized waste tea activated carbon for adsorption of methylene blue and acid blue 29 dyes using response surface methodology. *Chemical Engineering Journal,* 175:233-243

Chabbi, A., Yallese, M.A., Meddour, I., Nouioua, M., Mabrouki, T. and Girardin, F. (2017). Predictive modeling and multi-response optimization of technological parameters in turning of polyoxymethylene polymer (POM C) using RSM and desirability function. *Measurement,* 95:99-115.

Dalwani, M., Benes, N.E., Bargeman, G., Stamatialis, D. and Wessling, M. (2011). Effect of pH on the performance of polyamide/polyacrylonitrile based thin film composite membranes. *Journal of Membrane Science,* 372(1-2):228-238.

Danmaliki, G.I., Saleh, T.A. and Shamsuddeen, A.A. (2017). Response surface methodology optimization of adsorptive desulfurization on nickel/activated carbon. *Chemical Engineering Journal,* 313:993-1003.

Fathizadeh, M., Aroujalian, A. and Raisi, A. (2011). Effect of added NaX nano-zeolite into polyamide as a top thin layer of membrane on water flux and salt rejection in a reverse osmosis process. *Journal of Membrane Science,* 375(1-2):88-95.

García, A., Rodríguez, B., Oztürk, D., Rosales, M., Diaz, D.I. and Mautner, A. (2018). Incorporation of CuO nanoparticles into thin-film composite reverse osmosis membranes (TFC-RO) for antibiofouling properties. *Polymer Bulletin*, 75(5):2053-2069.

Gholami, R.M., Mousavi, S.M. and Borghei, S.M. (2012). Process optimization and modeling of heavy metals extraction from a molybdenum rich spent catalyst by aspergillus Niger using response surface methodology. *Journal of Industrial and Engineering Chemistry,* 18(1):218-224.

Gumbi, N. (2015). *Fabrication of nanosilver/ carbon nanotubes polyamide thin-film composite membranes for water treatment*. MSc. Dissertation, University of Johannesburg, Johannesburg.

Khayet, M., Cojocaru, C. and Essalhi, M. (2011). Artificial neural network modeling and response surface methodology of desalination by reverse osmosis. *Journal of Membrane Science,* 368(1-2):202-214.

Kirmizakis, P., Tsamoutsoglou, C., Kayan, B. and Kalderis, D. (2014). Subcritical water treatment of landfill leachate: Application of response surface methodology. *Journal of Environmental Management,* 1469-15.

Lau, W.J., Ismail, A.F., Misdan, N, and Kassim, M.A. (2012). A recent progress in thin film composite membrane: A review. *Desalination,* 287:190-199.

Lee, H.D., Kim, H.W., Cho, Y.H. and Park, H.B. (2014). Experimental evidence of rapid water transport through carbon nanotubes embedded in polymeric desalination membranes. *Small,* 10(13):2653-2660.

Liu, Y., Li, Y. and Yan, X. (2008). Preparation, characterization, and application of l-cysteine functionalized multi-walled carbon nanotubes as a selective sorbent for separation and pre-concentration of heavy metals. *Advanced Functional Materials,* 18(10):1536-1543.

Liu, W., Chai, S., Mohamed, A.R. and Hashim, U. (2014). Synthesis and characterization of graphene and carbon nanotubes: A review on the past and recent developments. *Journal of Industrial and Engineering Chemistry*, 20(4):1171-1185.

Nan Shen, J., Chao Yu, C., Min Ruan, H., Jie Gao, C. and Van der Bruggen, B. (2013). Preparation and characterization of thin-film nanocomposite membranes embedded with poly (methyl methacrylate) hydrophobic modified multiwalled carbon nanotubes by interfacial polymerization. *Journal of Membrane Science,* 442:18-26.

Mahdavi, M.R., Delnavaz, M. and Vatanpour, V. (2017). Fabrication and water desalination performance of piperazine–polyamide nanocomposite nanofiltration membranes embedded with raw and oxidized MWCNTs. *Journal of the Taiwan Institute of Chemical Engineers*, 75:189-198.

Masindi, V., Gitari, M.W., Tutu, H. and DeBeer, M. (2015). Efficiency of ball milled south african bentonite clay for remediation of acid mine drainage. *Journal of Water Process Engineering*, 8:227-240.

Misdan, N., Lau, W.J., Ismail, A.F., Matsuura, T. and Rana, D., 2014. Study on the thin film composite poly (piperazine-amide) nanofiltration membrane: Impacts of physicochemical properties of substrate on interfacial polymerization formation. *Desalination*, *344*, pp.198-205.

Myers, R.H., Montgomery, D.C. and Anderson-Cook, C.M. (2016). *Response surface methodology: process and product optimization using designed experiments.* John Wiley and Sons. pp. 273-277.

Shojaeimehr, T., Rahimpour, F., Khadivi, M.A. and Sadeghi, M. (2014). A modeling study by response surface methodology (RSM) and artificial neural network (ANN) on Cu adsorption optimization using light expended clay aggregate (LECA). *Journal of Industrial and Engineering Chemistry,* 20(3):870-880.

Tutu, H., McCarthy, T.S., Cukrowska, E. (2008). The chemical characteristics of acid mine drainage with particular reference to sources, distribution and remediation: The Witwatersrand basin, South Africa as a case study. *Applied Geochemistry,* 23(12):3666-3684.

Yokwana, K. (2014). *Towards the synthesis of doped carbon nanotube/polysulfone nanofiltration membranes for the removal of organic pollutants from water*. MTech. Dissertation, University of Johannesburg, Johannesburg.

Varala, S., Dharanija, B., Satyavathi, B., Rao, V.B. and Parthasarathy, R. (2016). New biosorbent based on deoiled karanja seed cake in biosorption studies of Zr (IV): Optimization using Box–Behnken method in response surface methodology with desirability approach. *Chemical Engineering Journal,* 302:786-800.

Vatanpour, V., Madaeni, S.S., Moradian, R., Zinadini, S., Astinchap, B. (2011). Fabrication and characterization of novel antifouling nanofiltration membrane prepared from oxidized multiwalled carbon nanotube/polyethersulfone nanocomposite. *Journal of Membrane Science,* 375(1):284-294.

Wang, K., Abdalla, A.A., Khaleel, M.A., Hilal, N. and Khraisheh, M.K. (2017). Mechanical properties of water desalination and wastewater treatment membranes. *Desalination,* 401:190-205.

Wu, H., Tang, B. and Wu, P. (2010). MWNTs/polyester thin film nanocomposite membrane: An approach to overcome the trade-off effect between permeability and selectivity. *The Journal of Physical Chemistry C,* 114(39):16395-16400.

Wu, H., Tang, B. and Wu, P. (2013). Optimization, characterization and nanofiltration properties test of MWNTs/polyester thin film nanocomposite membrane. *Journal of Membrane Science,* 428:425-433.

Zarrabi, H., Yekavalangi, M.E., Vatanpour, V., Shockravi, A. and Safarpour, M. (2016). Improvement in desalination performance of thin film nanocomposite nanofiltration membrane using amine-functionalized multiwalled carbon nanotube. *Desalination,* 394:83-90.

CHAPTER4: RESULTS AND DISSCUSSION

Mathematical models can be used for prediction, optimisation and simulation of processes and have been applied successfully in different areas of science and research (Cano-Odena *et al*., 2011; Khayet *et al*., 2011; Shojaeimehr *et al*., 2014). Mathematical models can either be (i) theoretical (or parametric) models based on fundamental knowledge (mechanism) of the process, also known as the knowledge based approach, or (ii) empirical (or non-parametric) models which do not involve the knowing of fundamental principles governing the process (Khayet, *et al*., 2011). In membrane technology, methods of mathematical modelling include Design of Experiments (DOE), and Response surface methodology (RSM) (Garg and Joshi, 2014; Khayet, *et al*., 2011) and Machine Learning Models such as ANN (Solemani *et al*., 2013).

According to Solemani *et al*. (2013) machine learning techniques are able to model and analyse complex problems that were previously difficult or impossible to solve (Qin *et al*.,2012; Torregrossa *et al*., 2018). Maphutha (2013) determined the effects of membrane filtration on oily wastewater and modelled the results using Artificial Neural Networks (ANN) while Solemani *et al*. (2013) used ANN to predict the permeation flux and optimize operating conditions for separation of oil from industry wastewater using membrane filtration. However, ANN models require large data sets for training and testing of the network. DOE and RSM have been used to tune machine learning hyper parameters (Lujan-Moreno *et al*., 2018). Still, they can be used for prediction and process optimisation in the same way as ANN with fewer number of experiments required for modelling.

Linear and non-linear multi-variate regression problems are solved using RSM models by finding a solution to an objective function that needs to be optimised (Chauhan *et al*., 2013; Khayet, *et al*., 2011; Varala *et al*., 2016). Explicit expressions of the system or process under study are not needed for prediction and optimisation therefore, RSM belongs to modelling tools dealing with development of non-parametric simulative models also known as ‘’black-box models’’. A predetermined number of experimental runs is set and the resulting data is modelled to develop the design variables and optimise the response (Cheng *et al*., 2014; Danmaliki *et al*., 2017).

In this chapter, RSM models are used in order to predict behaviour based on experiments and determine an empirical objective function that can give the optimum conditions for process simulation. The parameters to be optimised are flux and rejection and the parameters to be varied are CNT loading, pressure and the heavy metal concentrations. Before RSM could be carried out different experiments were carried out in order to determine the design constraints and feasible region. This included the functionalisation and characterisation of CNTs as well as the testing and characterisation of the TFN membranes. DOE was conducted using methods described in Chapter 3.

4.1 STRUCTURAL STUDIES OF MWCNTS

4.1.1 TEM of pristine and oxidised MWCNTS

Pristine CNTs were oxidised using methods described in Chapter 3. Figure 4.1 shows the TEM images of pristine and microwave oxidised CNTs at different magnifications. The amount of amorphous carbon and metal catalyst (red arrows) in and around the pristine CNTs (Figure 4-1(a)) was reduced compared to the oxidised CNTs (Figure 4-1(b)). The agglomeration of CNTs was also reduced for microwave-assisted oxidation (Figure 4-1 (e)) compared to the pristine CNTs (Figure 4-1(d)). Figure 4-1 (c) shows the CNTs after microwave oxidation at higher magnification. From Figure 4-1(c) the walls of the CNTs are visible and no damage or defects on the tube walls was observed. Therefore, the CNTs stayed intact after oxidation making microwave oxidation a viable method for CNT oxidation. According to Xin and Li (2011), defects on the CNT walls may cause the electrical conductivity of the CNTs to decrease which could affect their performance in the membrane composite.

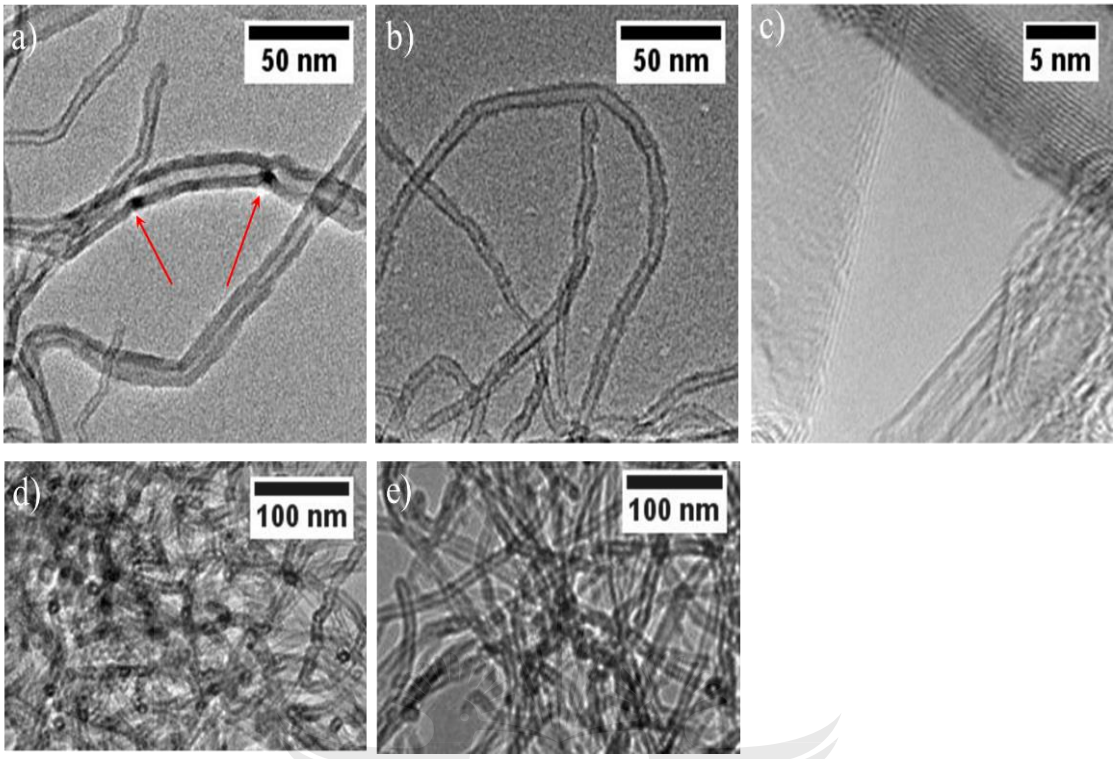

Figure 4-1: TEM of (a), (d) pristine and (b), (c), (e) microwave oxidised CNTs

4.1.2 Raman of Pristine and Oxidised MWCNTs

The results of the Raman Spectroscopy for microwave-oxidised (*f*-CNT) and pristine CNTs are shown in Figure 4-2. The first peak occurs at 1320 cm^{-1} which is known as the D band which arises due to the sp^3 hybridized carbons in the nanotube walls and is an indication of the disordered carbons in the walls. The second peak occurs at 1580 cm^{-1} which is known as the G band and is related to the tangential stretching of the sp^2 bonded carbons in the graphene sheets (Sigh *et al*., 2013). The ID/IG ratio shown in Table 4-1 indicates that the intensity of the D band to G band increases after oxidation which is an indication that the tubes became less graphitic and crystalline and more disordered. The ID/IG ratio is a good indication of the defects on a CNT sample (Lui *et al*., 2013). Therefore, the more defects on the CNT surface, the higher the ID/IG ratio. In the case of chemical oxidation, the surface defects are from the attachment of -COOH groups to the CNT walls.

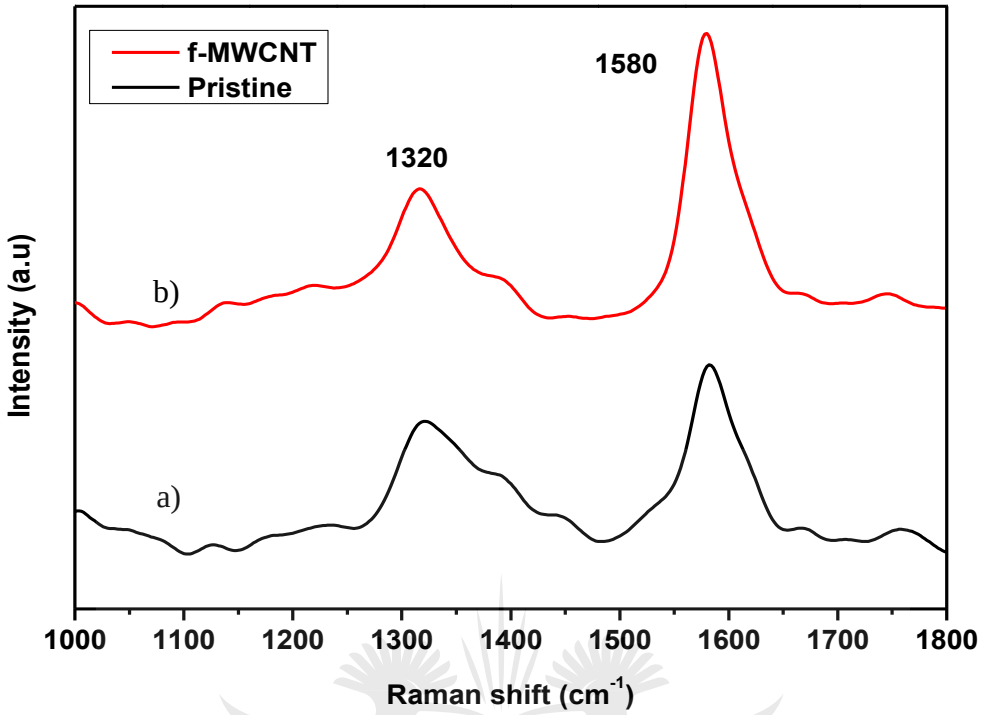

Figure 4-2: Raman spectra of pristine (a) and oxidised (b) CNTs

Table 4-1: Raman of pristine and oxidised CNTs

	G	D	I G	I D	ID/IG
Pristine	1580	1320	365	200	0.54
f-MWCNT	1580	1320	372	320	0.86

4.1.3 FTIR of pristine and oxidised MWCNTS

The ATR-FTIR of pristine and oxidised CNTs is shown in Figure 4-3. The broad peak observed at for the microwave oxidised CNTs 3288 cm^{-1} is associated with the O-H stretch stretching of the functional groups on the tube walls. The peak observed at 1642cm^{-1} is associated with the C=O of the carboxylic group. The peak at 1308 cm^{-1} may be due to the asymmetric stretching of the C=C-OH bonds on the CNTs backbone. The ATR-FTIR confirmed that there were changes to the pristine CNT structure, mainly the appearance of carboxylic groups which confirm the functionalization of the CNTs.

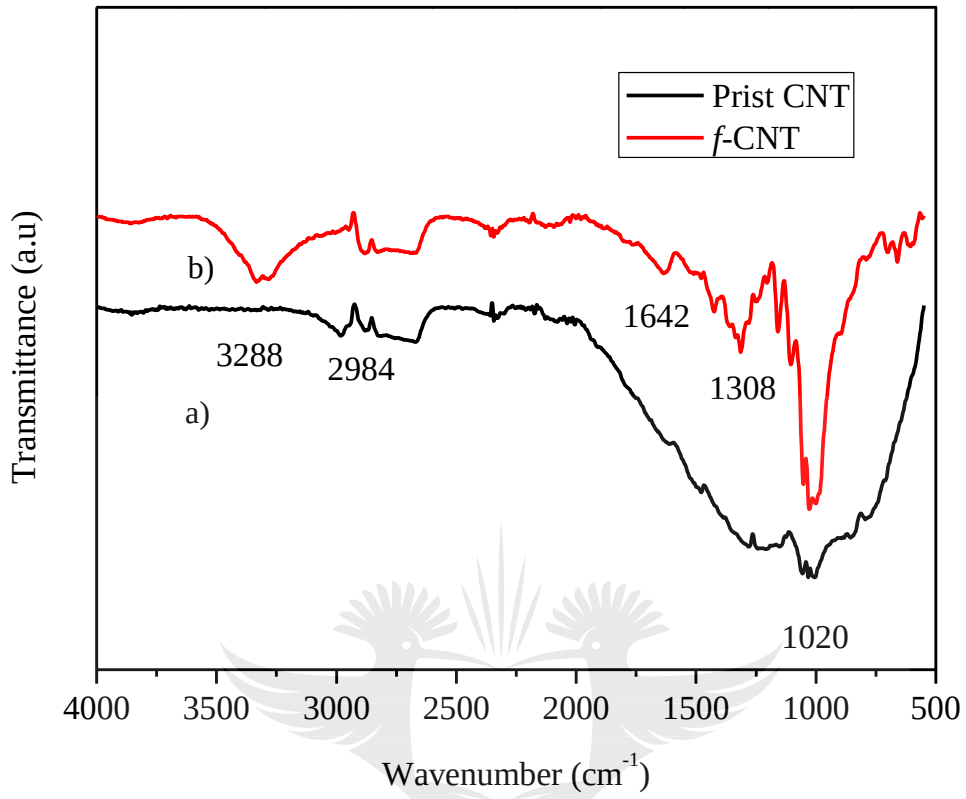

Figure 4-3: FTIR spectra of pristine (a) and oxidised (b) CNTs

4.2 STRUCTURAL STUDIES OF POLYAMIDE TFN MEMBRANES

4.2.1 Contact angle measurements

Incorporation of CNTS on the TFN surface improves hydrophilicity of the membranes leading to an increase in permeate flux (Ma *et al*., 2019). According to Zhao et al (2014) the hydrophilicity of TFN can be attributed to an introduction of carboxyl functionalized CNTs which equipped the membrane with more carboxyl groups. As shown in Figure 4-4, at 0.3% CNT loading the lowest contact angle 38.4° was observed, which indicated the hydrophilicity of membranes was increased with an increase in CNT. Upon further addition of CNTs the contact angle increased and was highest at 0.6% CNT loading with a water contact angle of 74.8°.

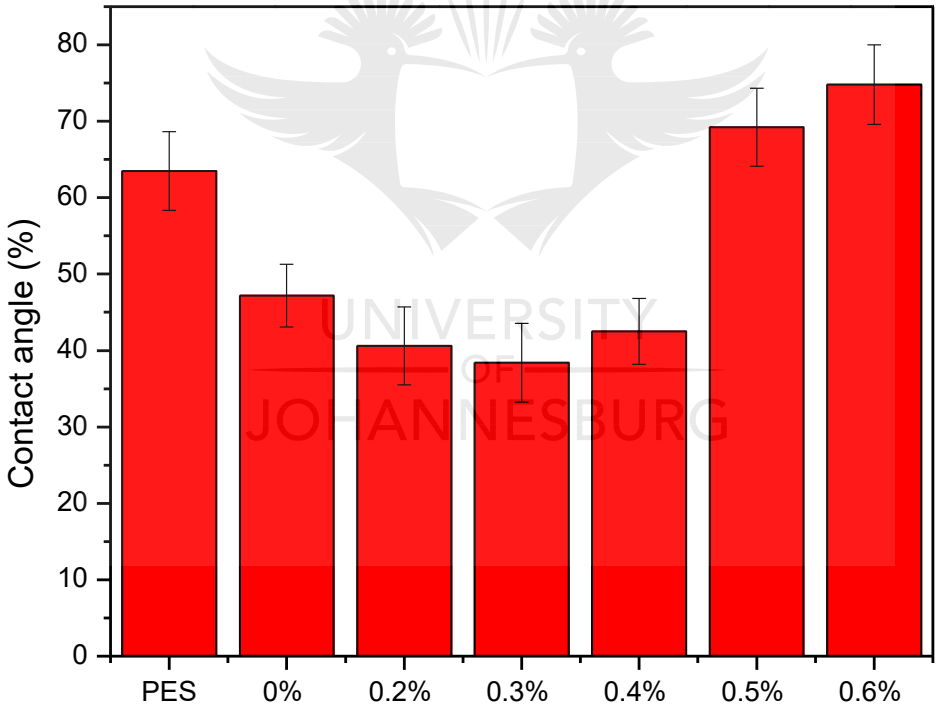

Figure 4-4: Contact angle measurement of PES support and TFN with 0%-0.6% MWCNT loading

4.2.2 SEM analysis

Figure 4-5 shows the SEM imaging of the PES support (Figure 4-5 (a)) in which macro voids can be seen on the membrane surface (Vatanpour *et al*., 2011). After the reaction of TMC and piperazine, a smooth uniform thin polyamide layer can be seen on the TFN membrane surface (Figure4-5 (b)) (Parsamanesh *et al*., 2020) TFN membrane with different CNT loadings are shown in Figure 4-5 (c) and (d). At lower loading of 0.3% CNT (Figure 4-5 (c)) layer is observed on the membrane. However, at higher loadings of 0.5% (Figure 4-5 (d)) there was agglomeration of CNTs on the membrane surface which affected the diffusion of monomers and inhibited the formation of the active layer (Ding *et al*., 2018).

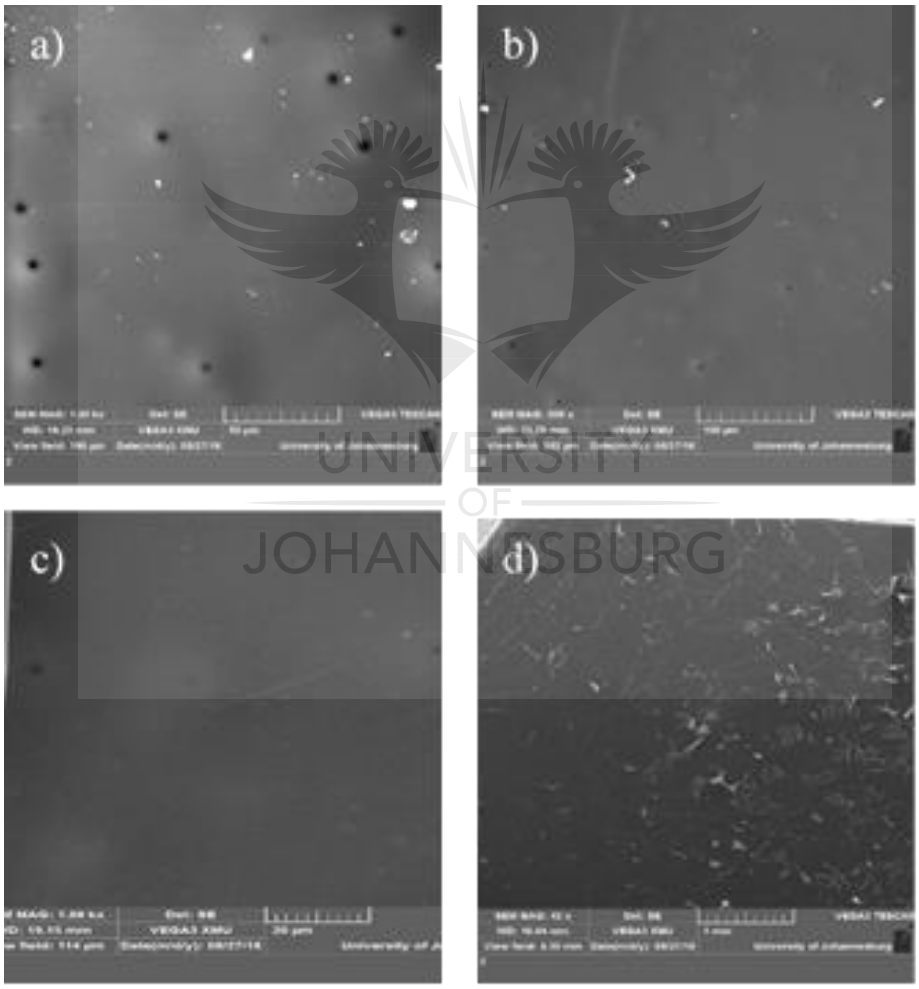

Figure 4-5: SEM of a) pristine, b) 0% c)0.3% and d)0.5% TFFN membrane with CNT

4.2.3AFM analysis

Figure 4-6 shows the surface roughness and 3-D AFM images of a) pristine PES membranes, b) TFN with 0% CNT membranes and c) TFN membranes modified with 0.3% CNTs. As can be seen from the images the shaded parts of the membrane are the valleys in the membrane and the bright points constitute the peaks of the membrane. The membrane surface morphology changed in comparison with the neat PES support, TFN and further with the addition of CNTs to the TFN. Table 4-2 outlines the surface roughness of the membranes. Ra is the mean roughness while Rq is the root mean square roughness. The surface roughness of the TFN membrane increased compared to PES and further increase was observe at 0.3% CNT loading. This was contrary to findings by Vatanpour *et al*. (2011) and Rameetse *et al*. (2020) where surface roughness decreased upon addition of CNT to the thin film membrane. The effect of CNT loading on membrane hydrophilicity was investigated further by doing pure water flux studies.

Table 4-2: Surface roughness of membranes

Type	***Rq***	***Ra***
PES	2,62 nm	1,79 nm
TFN 0%	139,83 nm	113,95 nm
TFN 0.3%	289,8 nm	223,08 nm

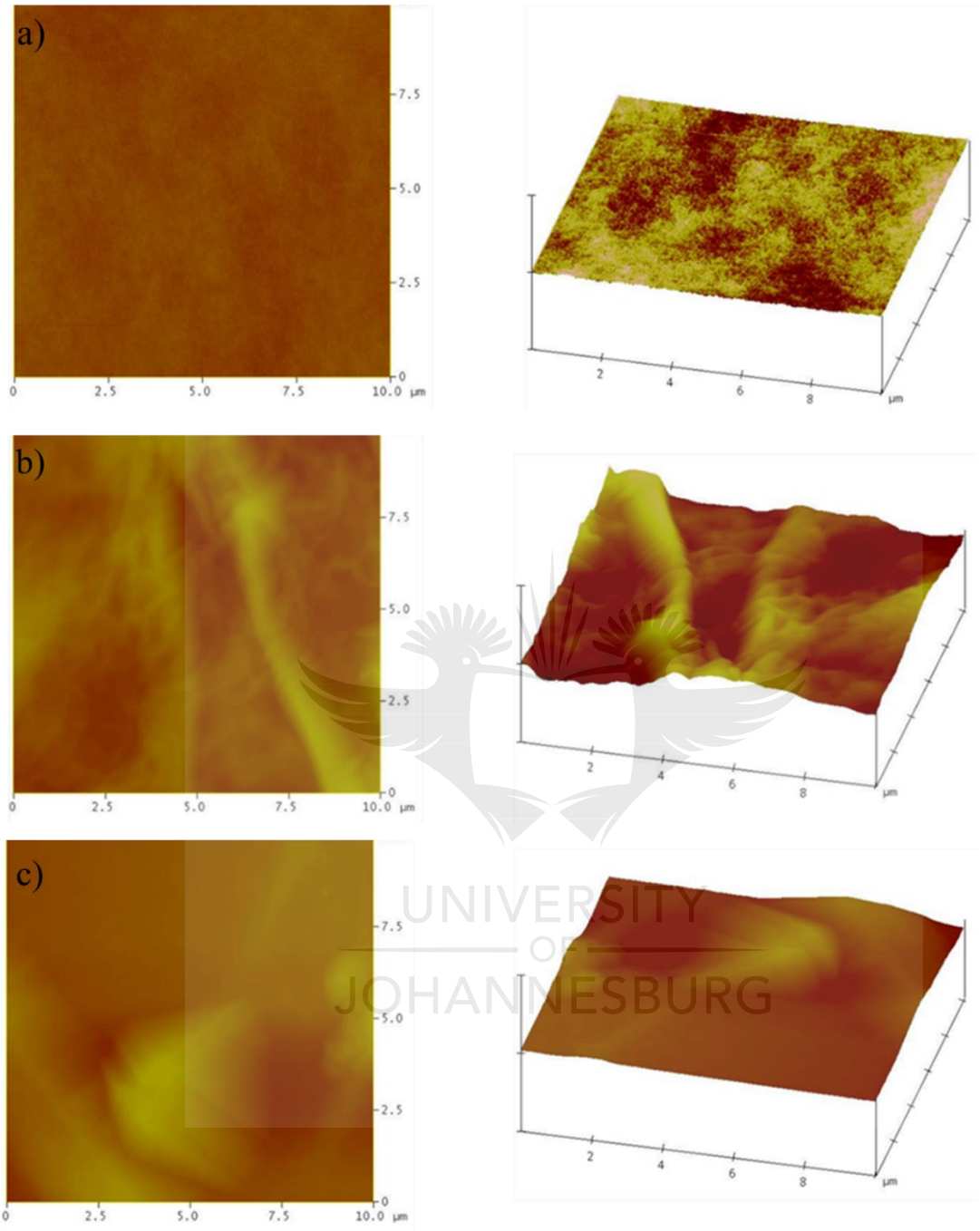

Figure 4-6: AFM images of (a) PES support (b) and TFN membranes (c) TFN modified with 0.3% CNTs

4.2.4 ATR-FTIR analysis of membrane

Figure 4-7 shows ATR-FTIR peaks of PES support membrane, pristine TFN membrane without MWCNT loading. The PES support consists of benzene rings, ether and sulfone group. ATR-

FTIR spectra over wave 1800-800cm $^{-1}$ show the support layer and the polyamide layers due to the penetration depth of >300nm which gives the chemical information of both the polyamide layer and the polyethersulfone layer (Tang *et al*., 2009). The strong sharp band at 1095 cm^{-1} and 1245 cm^{-1} shows the symmetric and asymmetric stretching of the S=O bonds. For the TFC membrane there was a shift to 1083 cm^{-1} and 1236 cm^{-1}, respectively. The shift to lower wave numbers indicates that the mass of the molecules was increased. The frequency of vibration is inversely proportional to the mass of the vibrating molecule. The peak at 1715cm^{-1} shows the free carboxyl group. The bands at 1419 cm^{-1} and 2963 cm^{-1} correspond to C-H stretching, (Rezania *et al*., 2018) At wave numbers of 4000-2600 cm^{-1} the penetration depth for the ATR-FTIR is <~200 nm which is ideal for analysing chemical properties of TFC polyamide layer (Tang *et al*., 2009).The TFC membrane peaks between 3000 cm^{-1} and 2800 cm^{-1} indicates the stretching of the $-CH_3$ and $-CH_2$ stretching vibrations (El-Arnaouty *et al*., 2015).

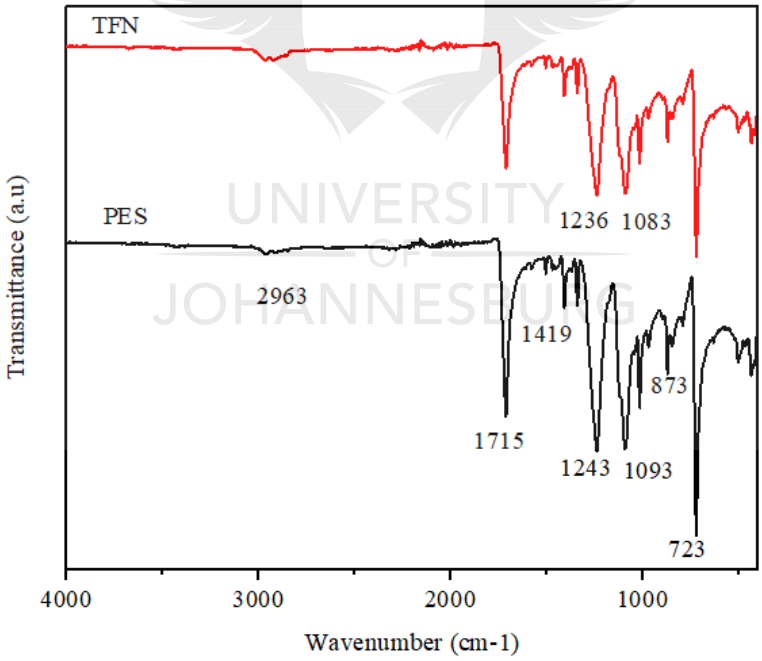

Figure 4-7: FTIR of PES and TFN membrane

4.3 MEMBRANE FILTRATION PERFORMANCE

4.3.1 Pure water flux

Pure water flux measurements as a function of pressure were carried out as shown in Figure 4-8. As expected, flux increases with an increase in transmembrane pressure (TMP) (Rahimpour *et al*., 2010). Flux increased for 0% to 0.3% CNT loading across all pressures studied of 5 to 20 bar. This can possibly be because incorporated CNTs can hinder the formation of a densely cross-linked polymer structure, contributing to the enhancement of pure water flux compared to the pristine TFC membrane (Wu *et al*., 2013). Upon further increase of CNT loading from 0.4% to 0.6% the flux declined across pressures of 5 to 20 bar. When the amount of CNTS is higher > 0.3%, the distribution of CNTs across the membrane surface is not uniform and CNTs are not well dispersed leading to agglomeration of CNTs in solution, and consequently on the membrane surface (Xin and Li, 2011). The clustered CNT bundles have a smaller specific surface area and lower adsorption activity with the membrane surface (Rahimpour *et al*., 2010). Therefore, over high concentrations of CNTs in the aqueous phase there is a decrease in TFN water permeation rate (Xin and Li, 2011).

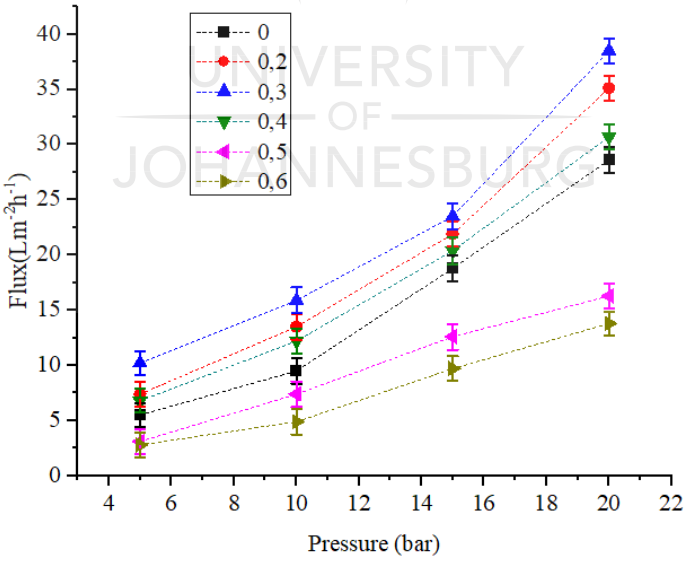

Figure 4-8: Pure water permeability of TFN membranes with different MWCNT loading

4.3.2 Effect of single, binary and tertiary solutions

Figures 4-9 (a)-(f) shows the permeate flux and rejection during the performance testing of the TFN membranes for single salt solutions. The flux increased with an increase in pressure due to the increase in applied force on the membrane up to a concentration of 0.3% MWCNT loading after which the flux began to drop. This may be due to the agglomeration of CNTs at higher concentrations (0.4-0.6%) which leads to pore blockage in the membrane and therefore a decline in flux. The rejection of the salt solutions increased with an increase in CNT loading up to 0.3% MWCNT after which the rejection began to drop, which is similar to what was observed with the flux measurements for single salt solutions. At lower loadings <0.3% MWCNT loading there was a slight variation in the permeate flux between the three salt solutions. However, for higher concentrations the permeate flux did not vary much across all three heavy metal ions which is a strong indicator that flux was more dependent on CNT loading and pressure than type of heavy metals for higher MWCNT loadings, whereas lower MWCNT loadings had a slight effect in increasing the flux. Again, at lower concentrations the MWCNTs are better dispersed on the membrane surface, thereby creating channels for the permeate to flow through the inside of the tube wall on the membrane surface. At higher concentrations, in this case <0.3% MWCNT loading, the tubes tend to agglomerate, and the channels are blocked.

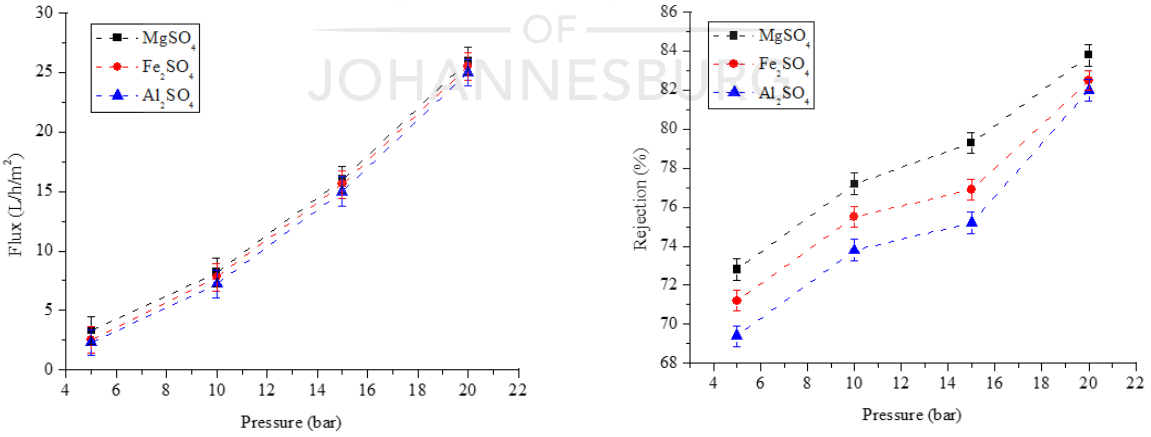

a)

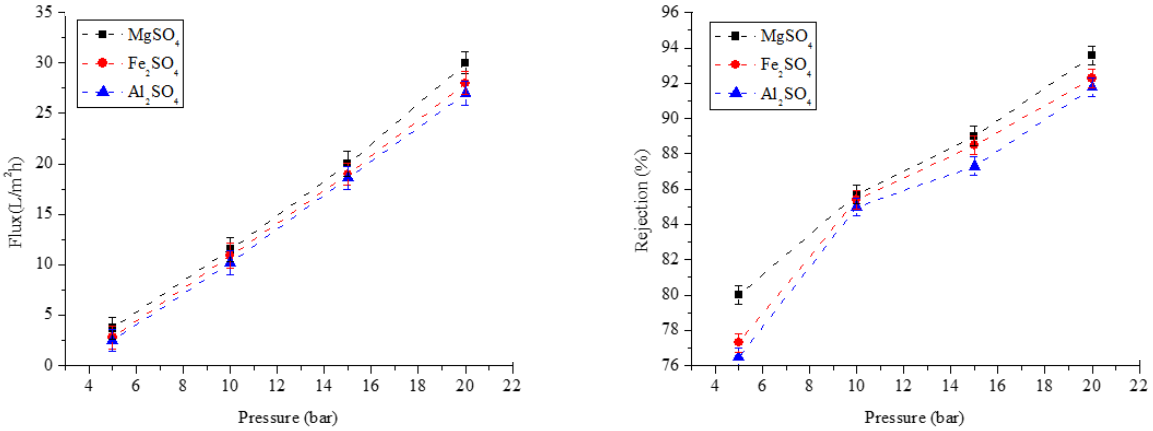

b)

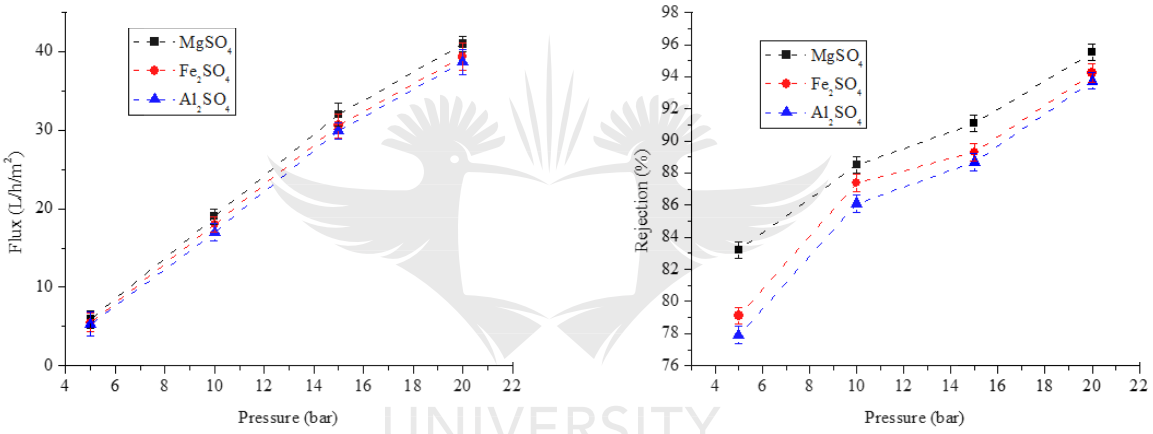

c)

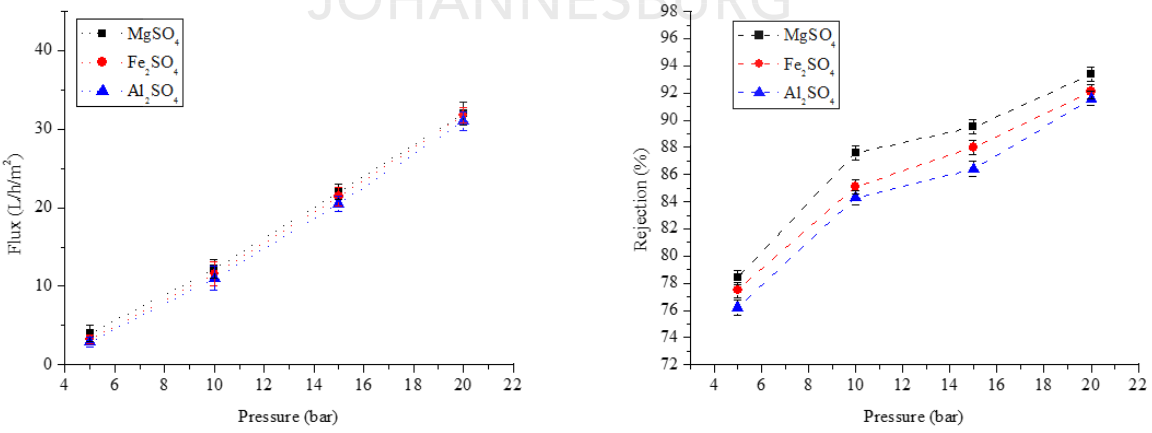

d)

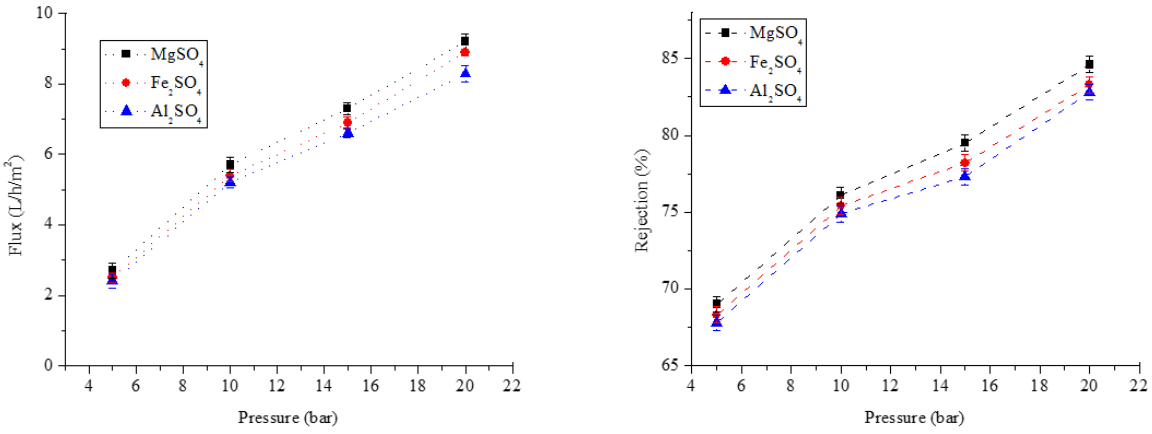

e)

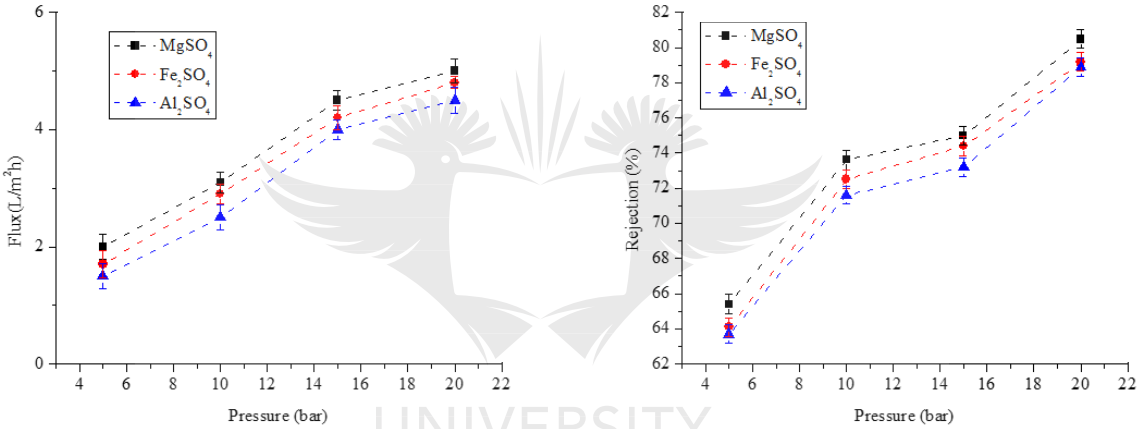

f)

Figure 4-9: Flux and rejection of single salt solutions of 2000 ppm Fe_2SO_4, $MgSO_4$ and $Al_2(SO_4)_3$ for TFN with (a) 0% CNT loading, (b) 0.2% CNT loading, (c) 0.3% CNT loading, (d) 0.4% CNT loading, (e) 0.5% CNT loading, (f) 0.6% CNT loading

Figure 4-10 (a)-(f) shows the permeate flux and rejection during the performance testing of the TFN membranes for binary salt solutions. Like with the single salt solutions there was an increase in permeate flux with an increase in pressure. However, there is was no significant difference between flux of single salt ions and binary salt ions which is an indication again that pressure and CNT loading had a greater effect on permeate flux. For the binary salt solutions, the Fe_2SO_4 and $MgSO_4$ solution had a slightly higher flux followed by the Fe_2SO_4 and $Al_2(SO_4)_3$ solution for all CNT loadings.

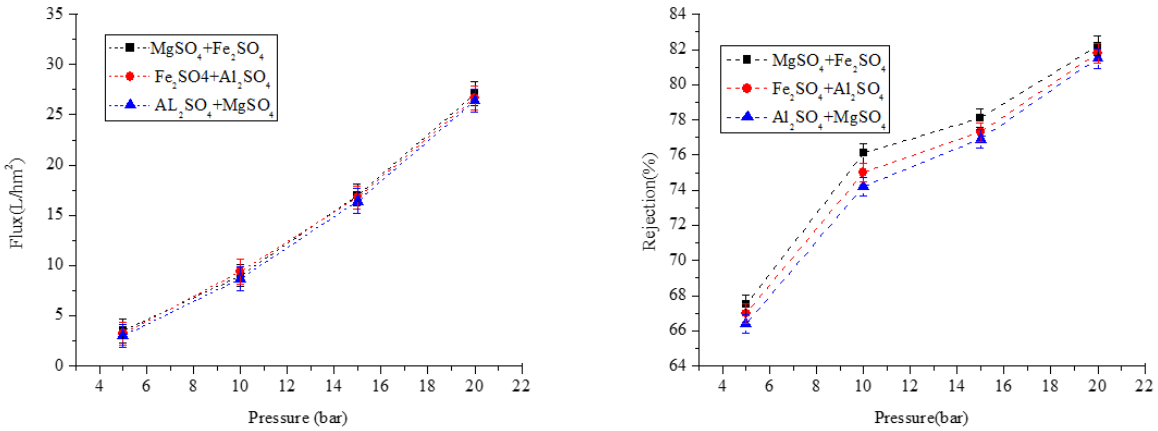

a)

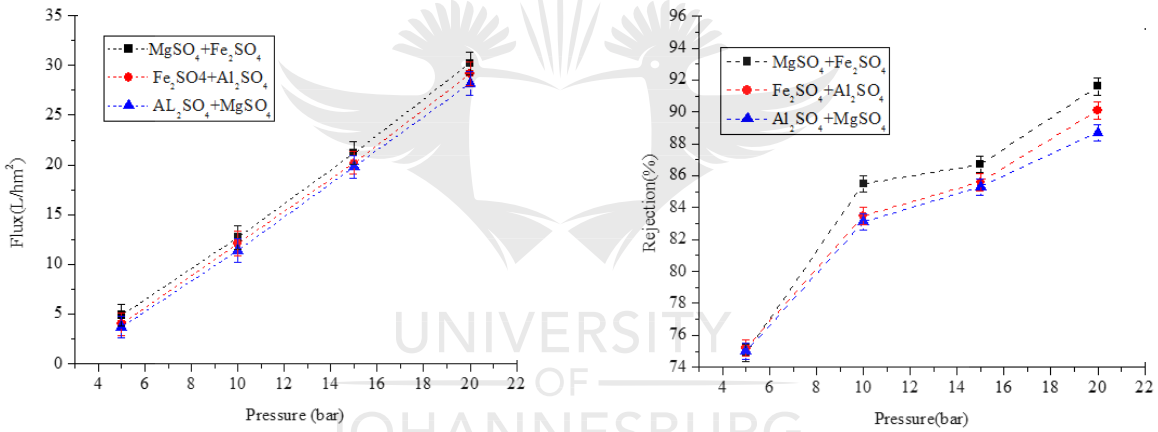

b)

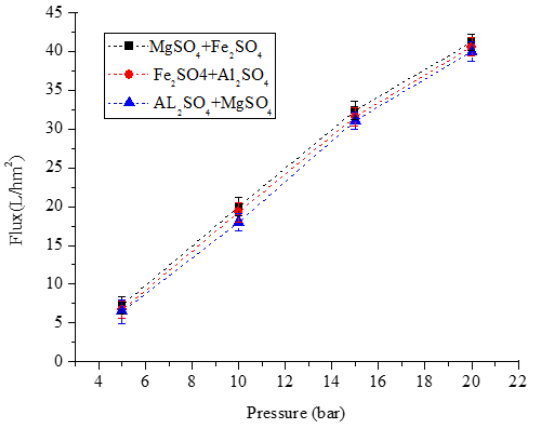

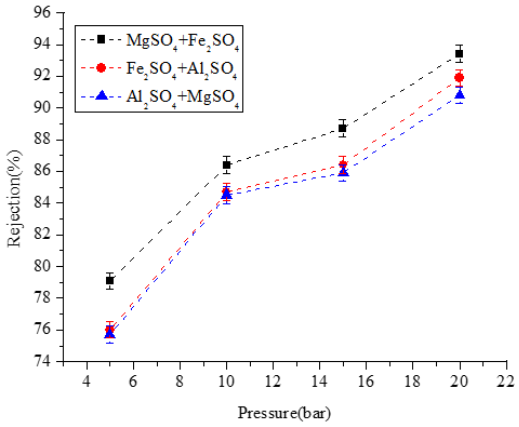

c)

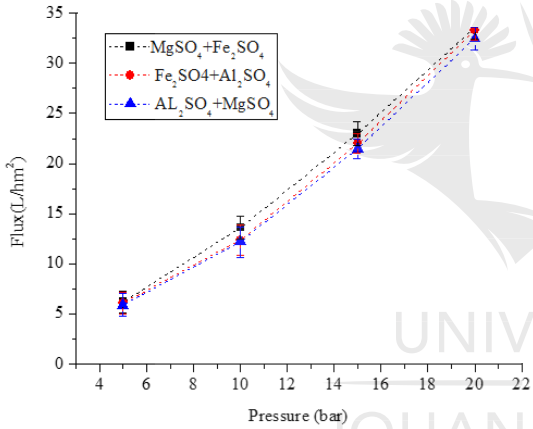

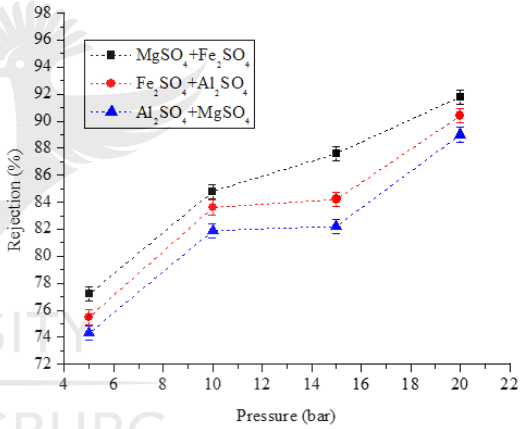

d)

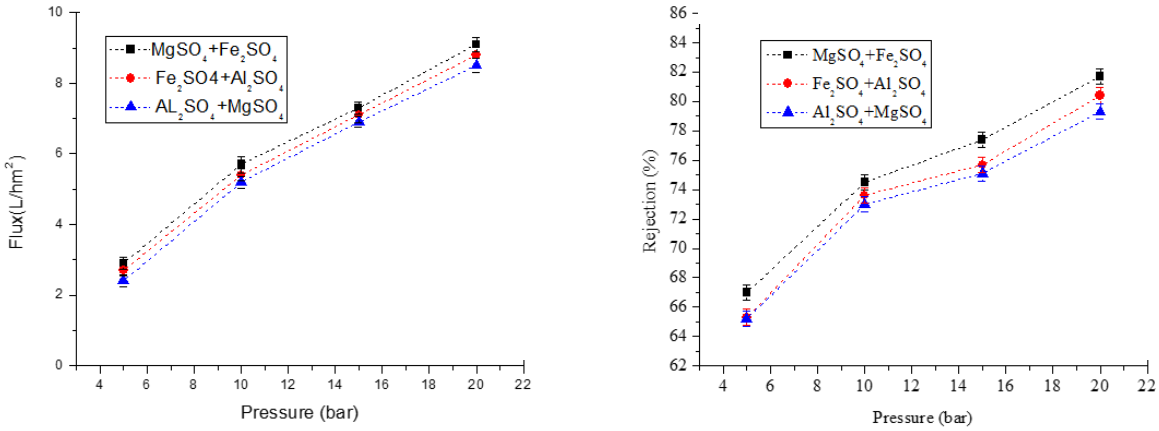

e)

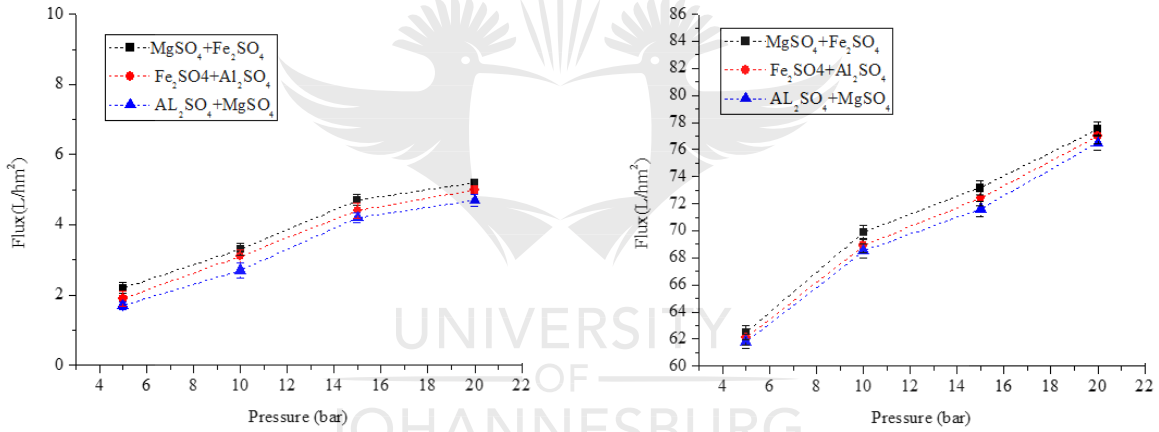

f)

Figure 4-10: Flux and rejection of binary salt solutions of 2000ppm Fe_2SO_4, $MgSO_4$ and $Al_2(SO_4)_3$ for TFN with (a) 0% CNT loading, (b) 0.2% CNT loading, (c) 0.3% CNT loading, (d) 0.4% CNT loading, (e) 0.5% CNT loading, (f) 0.6% CNT loading

Figure 4-11 shows the a) rejection and b) flux of the tertiary synthetic AMD solution for a loading of 0 to 0.6% CNTs. As with single and binary solutions, a similar trend was observed in terms of flux and rejection at different pressures (5 to 20 bar) for the CNT loadings studied. CNT loading had an effect on flux and rejection. Rejection and flux were highest at 0.3% CNT

loading. However, rejection for tertiary solution was 85% and flux was 38 L/m^{2}h at 0.3% CNT loading and 20 bar.

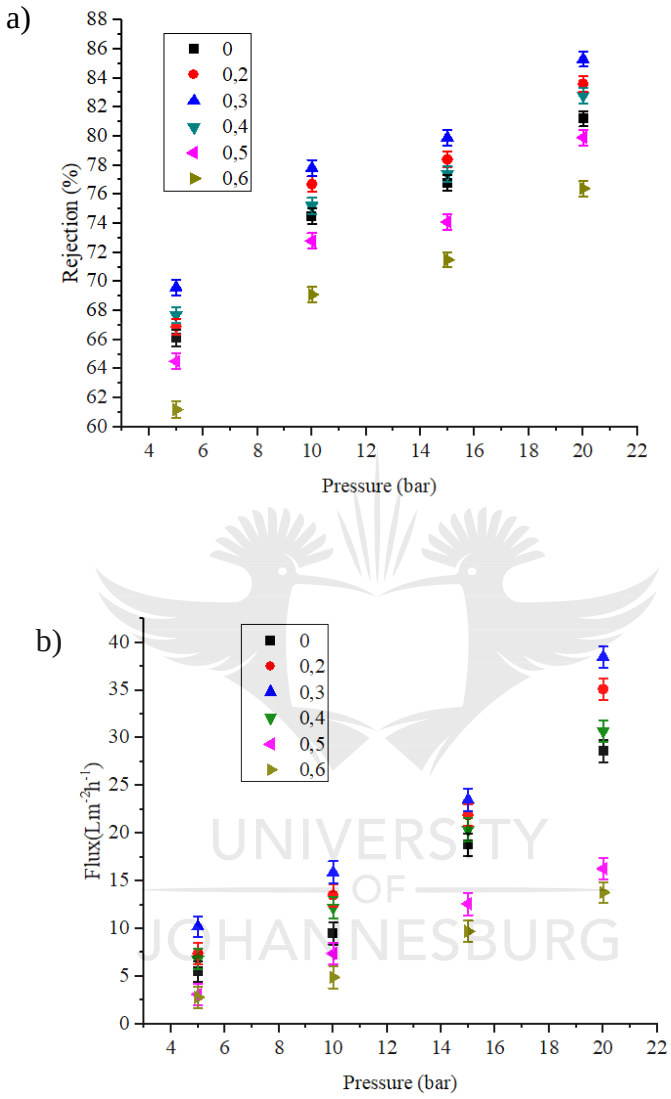

Figure 4-11: Flux and rejection of tertiary salt solutions of 2000ppm Fe_2SO_4, 200 ppm$MgSO_4$ and 200 ppm $Al_2(SO_4)_3$ for TFN with 0% - 0.6% MWCNT

Figure 4-12 shows the shows the flux and rejection of for single, binary and tertiary solutions at maximum pressure of 20 bar. Rejection of heavy metal ions followed the sequence $MgSO_4$ > $Fe_2(SO_4)_3$ > $Al_2(SO_4)_3$ The ionic size for Fe^{3+} was 73 Radius/pm, while for Mg^{2+} it was 79 Radius/pm and for Al^{3+} it was 57 Radius/pm. According to Tansel *et al* 2006, ionic permeability and the ionic size are inversely correlated therefore ions with a larger ionic size are expected to

be less permeable through the membrane. The larger the positive charge of a cation, the smaller its radius because there are less electrons in its outer shell. Also, according to Al-Rashdi *et al* 2013, water molecules are more tightly held to smaller cations and therefore have a larger hydration radius. For larger unhydrated ions, since the charge is more dispersed, the hydration water is held less strongly (Rivas, *et al*., 2011; Tansel *et al* 2006). Magnesium has a large hydration radius as it is a small cation with a valence of 2. As a result, magnesium is closely bound to the water molecules around it as it approaches the membrane surface. The hydration shell around the magnesium ion prevents it from closely approaching the membrane surface therefore it is unable to pass through the membrane pores. Similarly, iron has a lower rejection than magnesium but higher than aluminium which correlates with the ionic size of the ions.

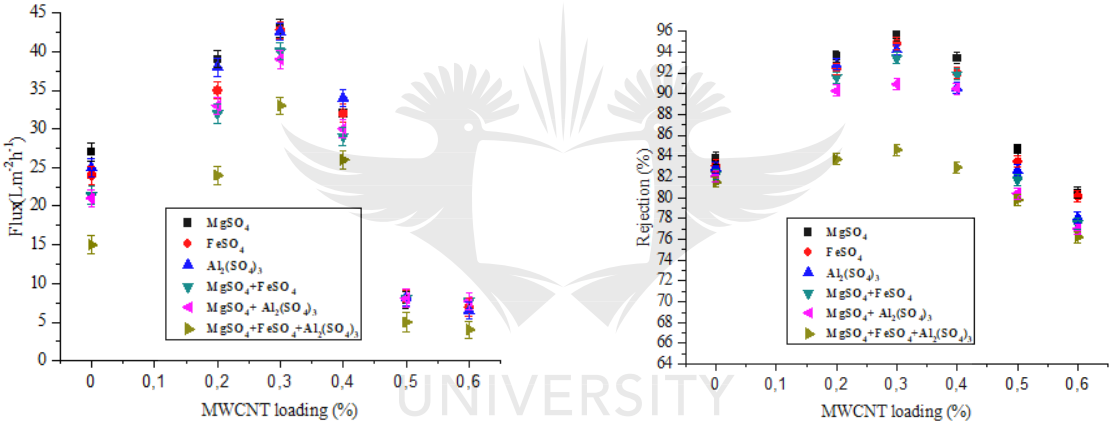

a) b)

Figure 4-12: Flux and rejection of single, binary and tertiary solutions Fe_2SO_4, $MgSO_4$ and $Al_2(SO_4)_3$ for different MWCNT loadings at 20 bar

4.3.3 Effect of operating time

Figure 4-13 shows the normalised flux plotted against time after filtration with a tertiary solution of heavy metal ions. This was done in order to determine if there was any decline in flux over time caused by filtration for the AMD solution. The normalised flux was determined as current flux of a membrane divided by its corresponding initial flux. It can be seen from Figure4.13(a) that there was a decline in flux after about 4 hrs after which flux for 0.3%, 0.2%, and 0.4% CNT

loading stabilised for about 20 hrs. The result indicates that flux performance of TFN-CNT membrane is also 5% higher than that of TFN membrane without CNTs. It suggests the incorporation of CNTs improves the anti-fouling ability of membrane, which may be ascribed to the higher hydrophilicity brought by the hydrophilic groups of CNTs. However, flux for all the other CNT loadings continued to decline by up to 23% after 20 hrs which might be an indication of pore blocking by the heavy metal solution. Similarly, for Figure 4.13(b) the flux decreased over time however flux declined more rapidly by 27% and was less stable throughout the filtration period for the bare PES membrane.

a)

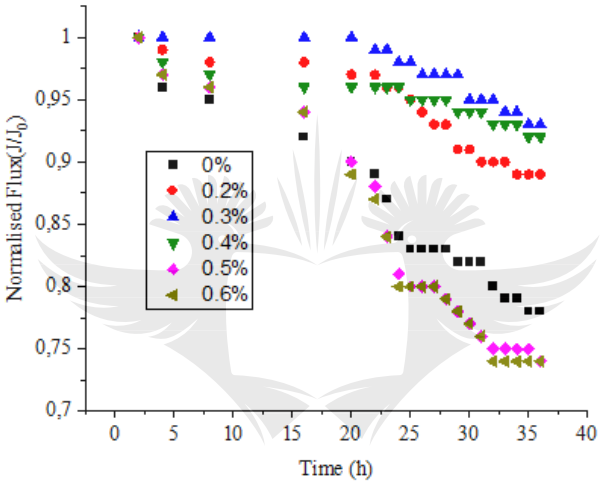

b)

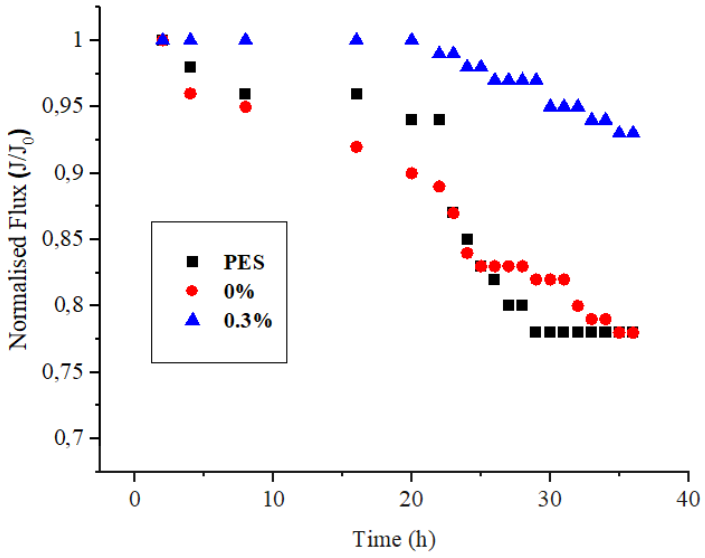

Figure 4-13: Normalized flux of TFN membranes for a) TFN at different MWCNT loadings and b) TFN at 0% and 3% loading compared to PES filtration with tertiary solution of 2000 ppm $FeSO_4$, 200 ppm $MgSO_4$, 200 ppm $Al_2(SO_4)_3$

4.4 PREDICTIVE MODELLING USING RSM

RSM modelling was used to facilitate process optimisation through the development of an empirical model to describe the TFN membrane performance over a range of process conditions using DOE methodology described in Chapter 3 (Khayet *et al.*, 2011). Mathematical computation and statistical analysis generated a graphical interpretation of the models in RSM applications.

The central composite design (CCD) method was used to investigate the effect of factors on the performance of TFN membranes for the removal of heavy metal ions from AMD. The experimental design for the factors including coded and actual values is shown in Table 4-3. The application of DOE and RSM leads to the development of response matrixes for the prediction of TFN membrane performance (Auta and Hameed, 2011; Khayet *et al.*, 2011). Through simulation, the TFN-model can be used for determining the main and mutual effects of parameters for the range of factors that were studied (Danmaliki *et al.*, 2017).

Table 4-3: Experimental design with actual and coded values

Pattern	A	B	C	D	E	Pressure (bar)	MWCNT (%)	$Fe_2(SO_4)_3$ (ppm)	$MgSO_4$ (ppm)	$Al_2(SO4)_3$ (ppm)
—–++	-1	-1	-1	1	1	10	0,2	1000	100	150
+++–+	1	1	1	-1	1	15	0,3	1500	150	150
A0000	1	0	0	0	0	10	0,2	1500	150	100
—+–+	-1	-1	1	-1	1	10	0,4	2000	100	100
000A0	0	0	0	1	0	15	0,2	1500	150	200
–++––	-1	1	1	-1	-1	20	0,4	1500	200	100
0000a	0	0	0	0	-1	10	0,4	2000	200	200
0A000	0	1	0	0	0	20	0,4	2000	150	150
0a000	0	-1	0	0	0	15	0,3	2000	200	100
++—–	1	1	-1	-1	-1	20	0,4	1000	200	200
00A00	0	0	1	0	0	10	0,4	1000	200	100
——–	-1	-1	-1	-1	-1	15	0,4	1000	100	100
+–+––	1	-1	-1	1	-1	10	0,2	1000	200	200
–+–+–	-1	1	-1	1	-1	10	0,2	2000	200	150
000a0	0	0	0	-1	0	10	0,3	1500	150	150
+–+++	1	-1	1	1	1	15	0,3	1500	100	150
a0000	-1	0	0	0	0	15	0,2	1000	200	100
0	0	0	0	0	0	15	0,4	1000	150	150
+–+––	1	-1	1	-1	-1	15	0,3	1500	100	150
00a00	0	0	-1	0	0	20	0,2	1500	200	150
+++––	1	1	1	1	-1	10	0,2	2000	100	200
–+++	-1	1	1	1	1	20	0,3	1000	150	100
0000A	0	0	0	0	1	15	0,3	1500	150	150
0	0	0	0	0	0	10	0,4	1000	100	200
+—+	1	-1	-1	-1	1	20	0,2	2000	100	100
—+––	-1	-1	1	1	-1	20	0,2	1000	100	200
++–++	1	1	-1	1	1	20	0,3	2000	200	200
–+—+	-1	1	-1	-1	1	20	0,4	1500	100	200

Figure 4-14 (a-d) shows the response surface plots given by the TFN-model as a function of different variables. The response surface model was able to give a prediction of optimum conditions of 20 bar and 0.3% CNT loading for the factors studied (pressure, CNT loading, iron concentration, magnesium concentration and aluminium concentration with fewer number of experiments. The response surface indicates that increasing both pressure and CNT loading will enhance the flux and rejection of the membrane as indicated by the optimum region (red). It is worth noting that the optimum loading for all three cases where both flux and rejection were optimised at a CNT loading of 0.3% and a pressure of 20 bar. A permeate flux of 83%, 94% $MgSO_4$ rejection, 92% $Fe_2(SO_4)_3$ rejection, and 89% $Al_2(SO_4)_3$ rejection was observed. The rejection of heavy metal ions follows the same trend as was observed from experiments, however values from the model were lower than experimental values. This is due to the second-degree interactions between process variables that cannot be accounted for in the preliminary experiments.

a)

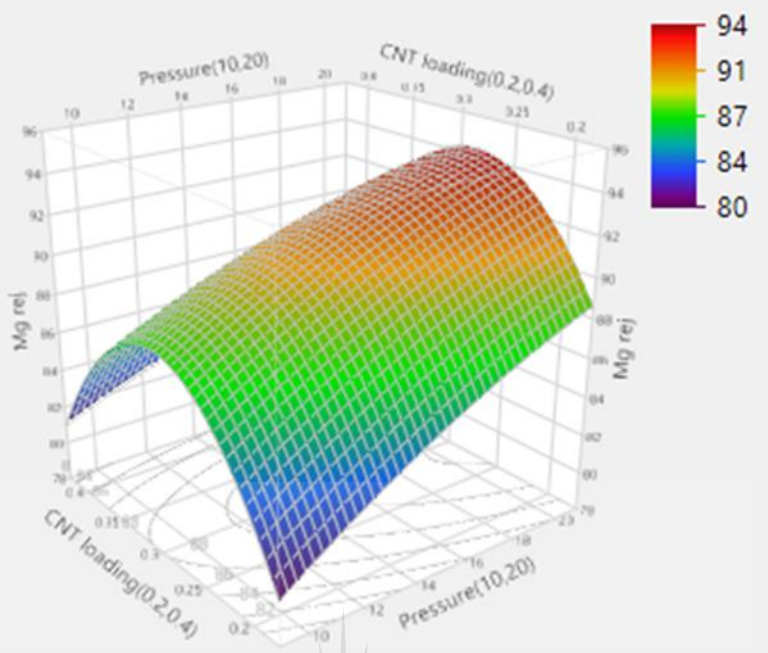

b)

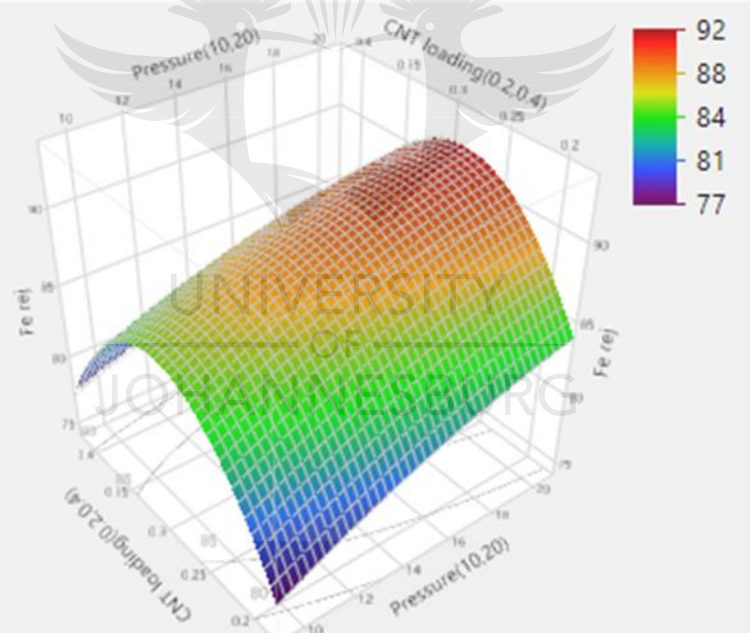

c)

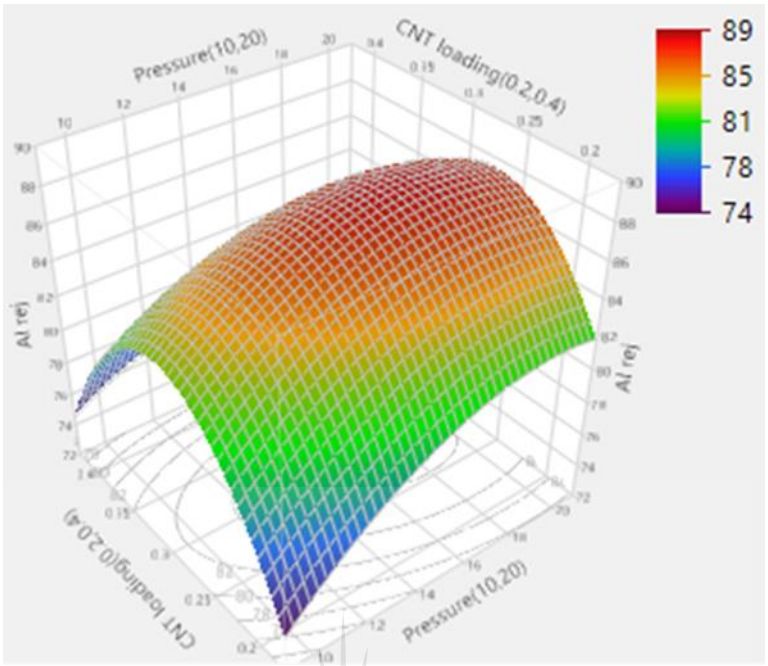

d)

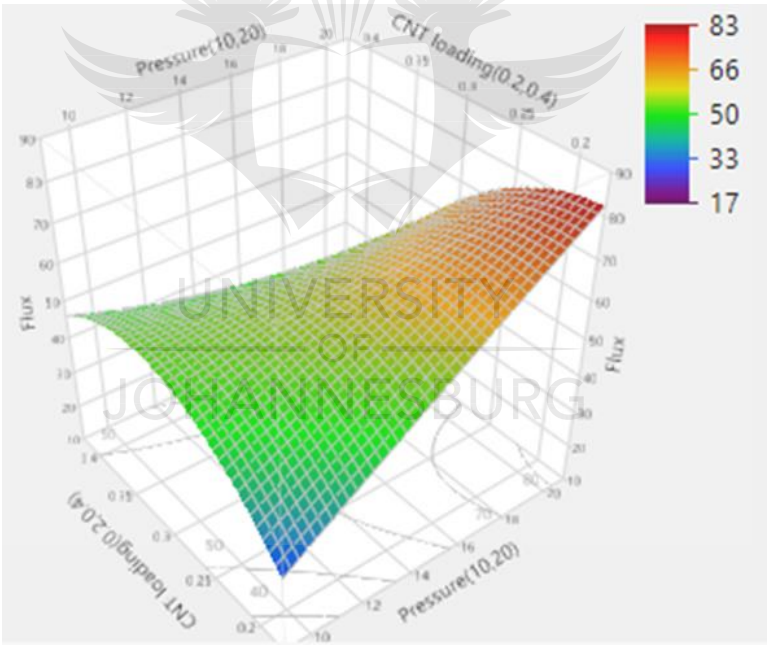

Figure 4-14: Response surface plots of the predicted performance of tertiary solution for a) $MgSO_4$ rejection, b) $Fe_2(SO_4)_3$ rejection, c) $Al_2(SO_4)_3$ rejection and d) permeate flux of TFN membranes at a pressure of 10 to 20 bar, (0.2-0.4%) CNT loading and feed salt concentrations of 100-200 ppm MgSO4, 1000-2000 ppm Fe_2SO4, 100-200 ppm $Al_2(SO_4)_3$.

In addition, the effects of each interaction were determined (Table 4-4) and effects with a PV value <0.05 were considered to be significant (Behera *et al*., 2018). Effects with a higher logWorth were considered to have a greater effect on the model (Skinner *et al*., 2019). Therefore, iron concentration, pressure and CNT loading were found to be the main factors that affect optimisation of the process.

Table 4-4: Effects of interactions of studied factors

Source	LogWorth	PValue	
Fe conc(1000,2000)	3.899	0.00013	
Pressure*CNT loading	3.630	0.00023	
CNT loading(0.2,0.4)	3.579	0.00026	^
Fe conc*Fe conc	3.391	0.00041	
CNT loading*Mg conc	3.362	0.00043	
Pressure*Fe conc	3.297	0.00051	
CNT loading*Al conc	3.295	0.00051	
Pressure*Mg conc	3.174	0.00067	
Al conc(100,200)	3.014	0.00097	^
Al conc*Al conc	2.968	0.00108	
Pressure(10,20)	2.918	0.00121	^
CNT loading*CNT loading	2.892	0.00128	
Mg conc*Al conc	2.874	0.00134	
Mg conc*Mg conc	2.387	0.00410	
Fe conc*Al conc	2.332	0.00466	
Mg conc(100,200)	1.947	0.01129	^
Fe conc*Mg conc	1.936	0.01159	
Pressure*Al conc	1.296	0.05056	
Pressure*Pressure	1.163	0.06868	
CNT loading*Fe conc	0.558	0.27649	

The adequacy of the model was tested by means of ANOVA and the results are shown in (Table 4-5). According to ANOVA, the *F*-value which measures whether there is significant variance in the means of the data was determined (Khayet *et al*., 2011). An *F*-value of 1 indicates that variances are equal. Thus, the further away the *F*-value is from unity, the more statistically significant the variation in the mean of the data. Based on *F*-value and the degrees of freedom, the *P*-value is then calculated. To validate a RS model from a statistical standpoint, the *F*-value should be as high as possible whereas the *P*-value should be as low as possible. Most RS models are validated for prediction if the *P*-value is less than 0.05 (Khayet *et al*., 2011). However, values less than 0.1 are also accepted depending on the process. All interactions were shown to be statistically significant based on Prob> F apart from (Pressure *Al conc, Pressure*Pressure, CNT loading *Fe conc) these effects were shown not to significantly affect the model.

Table 4-5: Effects of input parameters for RSM

Effect Tests

Source	Nparm	DF	Sum of Squares	F Ratio	Prob > F
Pressure(10,20)	1	1	275.2600	825.7799	0.0012*
CNT loading(0.2,0.4)	1	1	1263.6208	3790.862	0.0003*
Fe conc(1000,2000)	1	1	2639.2381	7917.714	0.0001*
Mg conc(100,200)	1	1	29.0364	87.1091	0.0113*
Al conc(100,200)	1	1	344.0474	1032.142	0.0010*
Pressure*Pressure	1	1	0.7259	2.1777	0.2780
Pressure*CNT loading	1	1	1421.6799	4265.040	0.0002*
CNT loading*CNT loading	1	1	259.3669	778.1006	0.0013*
Pressure*Fe conc	1	1	659.3521	1978.056	0.0005*
CNT loading*Fe conc	1	1	0.3852	1.1556	0.3949
Fe conc*Fe conc	1	1	819.0145	2457.044	0.0004*
Pressure*Mg conc	1	1	497.2206	1491.662	0.0007*
CNT loading*Mg conc	1	1	766.0339	2298.102	0.0004*
Fe conc*Mg conc	1	1	28.2527	84.7582	0.0116*
Mg conc*Mg conc	1	1	80.7486	242.2457	0.0041*
Pressure*Al conc	1	1	1.1229	3.3688	0.2079
CNT loading*Al conc	1	1	656.5204	1969.561	0.0005*
Fe conc*Al conc	1	1	71.0517	213.1551	0.0047*
Mg conc*Al conc	1	1	249.0413	747.1238	0.0013*
Al conc*Al conc	1	1	309.2775	927.8326	0.0011*

4.5 REFERENCES

Al-Hobaib, A.S., Al-Sheetan, K.M., Shaik, M.R. and Al-Suhybani, M.S. (2017). Modification of thin-film polyamide membrane with multi-walled carbon nanotubes by interfacial polymerization. *Applied Water Science,* 7(8):4341-4350.

Andrade, L.H., Aguiar, A.O., Pires, W.L., Grossi, L.B. and Amaral, M. (2017). Comprehensive bench-and pilot-scale investigation of NF for gold mining effluent treatment: Membrane performance and fouling control strategies. *Separation and Purification Technology,* 174:44-56.

Behera, S.K., Meena, H., Chakraborty, S. and Meikap, B.C. (2018). Application of response surface methodology (RSM) for optimization of leaching parameters for ash reduction from low-grade coal. *International Journal of Mining Science and Technology,* 28(4):621-629.

Chauhan, G., Pant, K.K. and Nigam, K.D. (2013). Development of green technology for extraction of nickel from spent catalyst and its optimization using response surface methodology. *Green Processing and Synthesis,* 2(3):259-271.

Cheng, R., Li, G., Cheng, C., Liu, P., Shi, L., Ma, Z. and Zheng, X. (2014). Removal of bacteriophage f2 in water by nanoscale zero-valent iron and parameters optimization using response surface methodology. *Chemical Engineering Journal,* 252:150-158.

Danmaliki, G.I., Saleh, T.A. and Shamsuddeen, A.A. (2017). Response surface methodology optimization of adsorptive desulfurization on nickel/activated carbon. *Chemical Engineering Journal,* 313:993-1003.

Ding, J., Yang, S., Pan, J., Zheng, Y., Sotto, A. and Shen, J. (2018). A novel nanofiltration membrane inspired by an asymmetric porous membrane for selective fractionation of monovalent anions in electrodialysis. *Royal Society of Chemistry Advances,* 8(53):30502-30511

Du Preez, R., Clarke, K.G., Callanan, L.H. and Burton, S.G. (2015). Modelling of immobilised enzyme biocatalytic membrane reactor performance. *Journal of Molecular Catalysis B: Enzymatic*, 119:48-53.

El-Arnaouty, M.B., Eid, M. and Abdel Ghaffar, A.M. (2015). Radiation synthesis of stimuli responsive micro-porous hydrogels for controlled drug release of aspirin. *Polymer-Plastics Technology and Engineering*, 54(12):1215-1222.

Elumalai, V., Brindha, K. and Lakshmanan, E. (2017). Human exposure risk assessment due to heavy metals in groundwater by pollution index and multivariate statistical methods: A case study from South Africa. *Water*, 9(4):234.

Feng, S., Yu, G., Cai, X., Eulade, M., Lin, H., Chen, J., Liu, Y. and Liao, B. (2017). Effects of fractal roughness of membrane surfaces on interfacial interactions associated with membrane fouling in a membrane bioreactor. *Bioresource Technology*, 244:560-568.

Garg, M.C. and Joshi, H. (2014). A new approach for optimization of small-scale RO membrane using artificial groundwater. *Environmental Technology*, 35(23):2988-2999.

Gohil, J.M. and Ray, P. (2017). A review on semi-aromatic polyamide TFC membranes prepared by interfacial polymerization: Potential for water treatment and desalination. *Separation and Purification Technology*, 181:159-182.

Hilal, N., Al-Zoubi, H., Darwish, N.A. and Mohammad, A.W. (2005). Characterisation of nanofiltration membranes using atomic force microscopy. *Desalination*, 177(1-3):187-199.

Khayet, M., Cojocaru, C. and Essalhi, M. (2011). Artificial neural network modeling and response surface methodology of desalination by reverse osmosis. *Journal of Membrane Science*, 368(1-2):202-214.

Khorshidi, B., Thundat, T., Pernitsky, D. and Sadrzadeh, M. (2017). A parametric study on the synergistic impacts of chemical additives on permeation properties of thin film composite polyamide membrane. *Journal of Membrane Science,* 535:248-257

Kusworo, T.J., Busairi, A., Ismail, A.F., Mustafa, A. and Budiyono, A. (2012). Purification of biogas using carbon nanotubes mixed matrix membrane: Effect of functionalization of carbon nanotubes using silane agent. *Sustainable Membrane Technology for Energy, Water, And Environment,* 267.

Lee, J. 2019, "Carbon Nanotube-Based Membranes for Water Purification" in *Nanoscale Materials in Water Purification* Elsevier, , pp. 309-331.

Lujan-Moreno, G.A., Howard, P.R., Rojas, O.G. and Montgomery, D.C. (2018). Design of experiments and response surface methodology to tune machine learning hyper parameters, with a random forest case-study. *Expert Systems with Applications,* 109:195-205.

Ma, X., Guo, H., Yang, Z., Yao, Z., Qing, W., Chen, Y., Xu, Z. and Tang, C.Y. (2019). Carbon nanotubes enhance permeability of ultrathin polyamide rejection layers. *Journal of Membrane Science,* 570:139-145.

Mäkelä, M. (2017). Experimental design and response surface methodology in energy applications: A tutorial review. *Energy Conversion and Management,* 151:630-640.

Masindi, V., Gitari, M.W., Tutu, H. and DeBeer, M. (2015). Efficiency of ball milled South African bentonite clay for remediation of acid mine drainage. *Journal of Water Process Engineering,* 8:227-240.

Masindi, V., Gitari, M.W., Tutu, H. and De Beer, M. (2016). Fate of inorganic contaminants post treatment of acid mine drainage by cryptocrystalline magnesite: Complimenting experimental results with a geochemical model. *Journal of Environmental Chemical Engineering,* 4(4):4846-4856.

Mthetwa, V. (2014). *Investigation of polyether sulfone (PES) hollow fibre membranes for the treatment of acid mine drainage*. Doctoral thesis, University of Witwatersrand, Johannesburg.

Parsamanesh, M., Mansourpanah, Y. and Tehrani, A.D. (2020). Improving the efficacy of PES-based mixed matrix membranes incorporated with citric acid–amylose-modified MWCNTs for HA removal from water. *Polymer Bulletin,* 1-19.

Qin, X., Gao, F. and Chen, G. (2012). Wastewater quality monitoring system using sensor fusion and machine learning techniques. *Water Research,* 46(4):1133-1144.

Rahimpour, A., Jahanshahi, M., Mortazavian, N., Madaeni, S.S. and Mansourpanah, Y. (2010). Preparation and characterization of asymmetric polyethersulfone and thin-film composite polyamide nanofiltration membranes for water softening. *Applied Surface Science,* 256(6):1657-1663.

Rameetse, M.S., Aberefa, O. and Daramola, M.O. (2020). Effect of loading and functionalization of carbon nanotube on the performance of blended polysulfone/polyethersulfone membrane during treatment of wastewater containing phenol and benzene. *Membranes,* 10(3):54.

Rezania, H.J., Vatanpour, V., Shockravi, A. and Ehsani, M. (2019). Study of synergetic effect and comparison of novel sulfonated and carboxylated bulky diamine-diol and piperazine in preparation of negative charge NF membrane. *Separation and Purification Technology,* 222:284-296.

Rivas, B.L., Pereira, E.D., Palencia, M. and Sánchez, J. (2011). Water-soluble functional polymers in conjunction with membranes to remove pollutant ions from aqueous solutions. *Progress in Polymer Science,* 36(2):294-322

Sabbaghi, S., Maleki, R., Shariaty-Niassar, M., Zerafat, M.M. and Nematollahi, M.M. (2012). Modeling of chloride ion separation by nanofiltration using machine learning techniques. *International Journal of Nanoscience and Nanotechnology,* 8(4):185-190.

Selvamuthu, D. and Das, D. (2018). *Introduction to Statistical Methods, Design of Experiments and Statistical Quality Control,* Springer. Singapore. pp. 315-351.

Shawky, H.A., Chae, S., Lin, S. and Wiesner, M.R. (2011). Synthesis and characterization of a carbon nanotube/polymer nanocomposite membrane for water treatment. *Desalination,* 272(1):46-50.

Shojaeimehr, T., Rahimpour, F., Khadivi, M.A. and Sadeghi, M. (2014). A modeling study by response surface methodology (RSM) and artificial neural network (ANN) on Cu2 adsorption optimization using light expended clay aggregate (LECA). *Journal of Industrial and Engineering Chemistry,* 20(3):870-880

Singh, C., Srivastava, S., Ali, M.A., Gupta, T.K., Sumana, G., Srivastava, A., Mathur, R.B. and Malhotra, B.D., (2013). Carboxylated multiwalled carbon nanotubes based biosensor for aflatoxin detection. *Sensors and Actuators B: Chemical*, 185:258-264.

Simate, G.S., Iyuke, S.E., Ndlovu, S. and Heydenrych, M. (2012). The heterogeneous coagulation and flocculation of brewery wastewater using carbon nanotubes. *Water Research,* 46(4):1185-1197.

Skinner, D.Z., Cuevas, C. and Bellinger, B.S. (2019). Cytoplasmic and nuclear genetic components of membrane stability of winter wheat plants exposed to sub-zero temperatures. *Journal of Agronomy and Crop Science,* 205(3):334-340.

Soleimani, R., Shoushtari, N.A., Mirza, B. and Salahi, A. (2013). Experimental investigation, modeling and optimization of membrane separation using artificial neural network and multi-objective optimization using genetic algorithm. *Chemical Engineering Research and Design,* 91(5):883-903.

Tang, C.Y., Kwon, Y. and Leckie, J.O. (2009). Effect of membrane chemistry and coating layer on physiochemical properties of thin film composite polyamide RO and NF membranes: I. FTIR and XPS characterization of polyamide and coating layer chemistry. *Desalination,* 242(1-3):149-167.

Tansel, B., Sager, J., Rector, T., Garland, J., Strayer, R.F., Levine, L., Roberts, M., Hummerick, M. and Bauer, J. (2006). Significance of hydrated radius and hydration shells on ionic permeability during nanofiltration in dead end and cross flow modes. *Separation and Purification Technology,* 51(1):40-4.

Torregrossa, D., Leopold, U., Hernández-Sancho, F. and Hansen, J. (2018). Machine learning for energy cost modelling in wastewater treatment plants. *Journal of Environmental Management,* 223:1061-1067.

Varala, S., Dharanija, B., Satyavathi, B., Rao, V.B. and Parthasarathy, R. (2016). New biosorbent based on deoiled Karanja seed cake in biosorption studies of Zr (IV): Optimization using Box–Behnken method in response surface methodology with desirability approach. *Chemical Engineering Journal,* 302:786-800.

Wu, H., Tang, B. and Wu, P. (2013). Optimization, characterization and nanofiltration properties test of MWNTs/polyester thin film nanocomposite membrane. *Journal of Membrane Science*, 428:425-433.

Xin, F. and Li, L. (2011). Decoration of carbon nanotubes with silver nanoparticles for advanced CNT/polymer nanocomposites. *Composites Part A: Applied Science and Manufacturing*, 42(8):961-967.

Zhou, C., Shi, Y., Sun, C., Yu, S., Liu, M. and Gao, C. (2014). Thin-film composite membranes formed by interfacial polymerization with natural material sericin and trimesoyl chloride for nanofiltration. *Journal of Membrane Science*, 471:381-391.

Zhao, H., Qiu, S., Wu, L., Zhang, L., Chen, H. and Gao, C. (2014). Improving the performance of polyamide reverse osmosis membrane by incorporation of modified multi-walled carbon nanotubes. *Journal of Membrane Science*, 450:249-256.

CHAPTER 5: MODELLING AND SIMULATION

Chemical process simulation and design enables engineers to design and test plant performance before the actual plant is built (Tolksdorf *et al*., 2019; van Baten and Pons, 2014). Unique insights into plant behaviour can be garnered from the development and simulation based on mass and energy balances (Shaalan *et al*., 2001). Mass and energy balance equations can be generated based on laboratory scale data (Costa, 2006). In this chapter a membrane-based process was designed and simulated for flux and rejection of heavy metal ions from AMD in order to test the operational feasibility of the process on a commercial scale. Open-source chemical engineering software was used for the simulation where overall algorithms and modelling equations across the membrane were derived from mass and energy balances.

5.1 PROCESS FLOW DIAGRAMS

Before the plant was modelled and simulated the arrangement of components within the plant had to be determined. The proposed process scheme for the treatment of AMD using membrane filtration is shown using a Process Flow Diagram (PFD). PFDs are a two-dimensional representation of process piping and equipment in a plant (Casavant and Coˆté, 2004). PFDs show how unit operations are connected by material, energy and information streams (Peshev and Livingston, 2013). Figure 5-1 shows the PFD for the membrane plant. The feed stream contains water and heavy metal ion concentrations that were tested at lab scale.

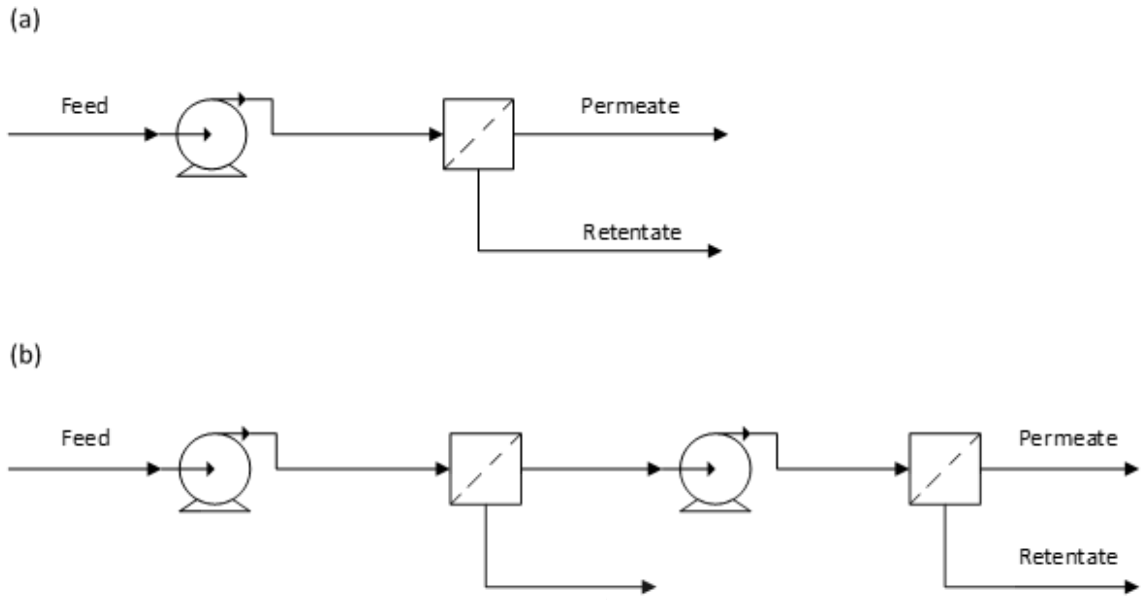

Figure 5-1: PFD of membrane plant for (a) single pass system and (b) double pass system AMD treatment

In order to simulate the plant, input streams must be specified (Valentínyi and Mizsey, 2014). Information for the input streams of the model were generated from experimental data. When running the plant simulation, the information from the input material streams is physically and chemically transformed through the unit operation (Casavant and Coˆté, 2004). Common examples of unit operations include pumps, heat exchangers, mixers, separators etc. Most process modelling software such as Chemcad, Aspen Plus, Aspen HYSYS, DWSIM, and Prosim Plus have built-in models for unit operations that perform the necessary calculations by performing mass and energy balances between the input information streams, and the interacting units to generate the output streams (Peshev and Livingston, 2013;. Tolksdorf *et al*., 2016; Tolksdorf *et al*., 2019).

The afore-mentioned process simulators have embedded tools for the development of custom unit operations using basic programming languages such as Java, C^{++}, Python, Fortan and Visual Basic (van Baten and Pons, 2014). Alternately, software such as Matlab, Scilab and Excel can be used to define unit operations that are supported by the process simulators. These software

have their own programming facilities which allow the user to develop a custom unit operation that will be compatible with any CAPE (Computer-Aided Process Engineering- Open source) compliant simulator (Corredor *et al*., 2016).

CAPE-OPEN was developed for the design and operation of chemical processes. The CAPE-OPEN programme is a computer aided process engineering software tool that allows for the plug-in or export of 3rd party unit operations or thermodynamic models (Barrett Jr *et al*., 2011). The CAPE-OPEN environment has unit operations, property packages and thermodynamic packages included. It also allows for interpretability between unit operations developed in other software, hence it was chosen for this study. CAPE-OPEN uses an iterative process to solve unit operation and thermodynamic models for simulation in the flowsheet environment. Thus, CAPE-OPEN allows for the engineer to use user defined unit operations with CAPE-OPENs embedded thermodynamic models or to even modify thermodynamic models based on application within the flowsheet (Barrett Jr *et al*, 2011).

For this study Scilab was used. Scilab is an open source programming language that allows the scientific computing of Matrixes, Polynomials, Linear Equations, Signal Processing, Ordinary Differential Equations and statistics (Salleh, 2012). Scilab is also CAPE-OPEN compliant and allows for development of models and customisation of unit operations in CAPE OPEN.

5.2 MODELING EQUATIONS

Modelling of the membrane was done through iteration of the overall mass balance and developing the specific flux equation which were coupled by the compositions. As shown in Figure 5.2, the overall flows are depicted as discretising the membrane into sequential, differential area elements along the length of the membrane. A steady-state approach was considered for a given point x. Q is the flow in the feed channel of water and the solute that permeates the membrane; and C is the change in concentration across the membrane. The model

considers a spiral wound membrane rather than a flat sheet membrane because as previously mentioned in Chapter 2, flat sheet membranes are difficult to scale-up for industrial use.

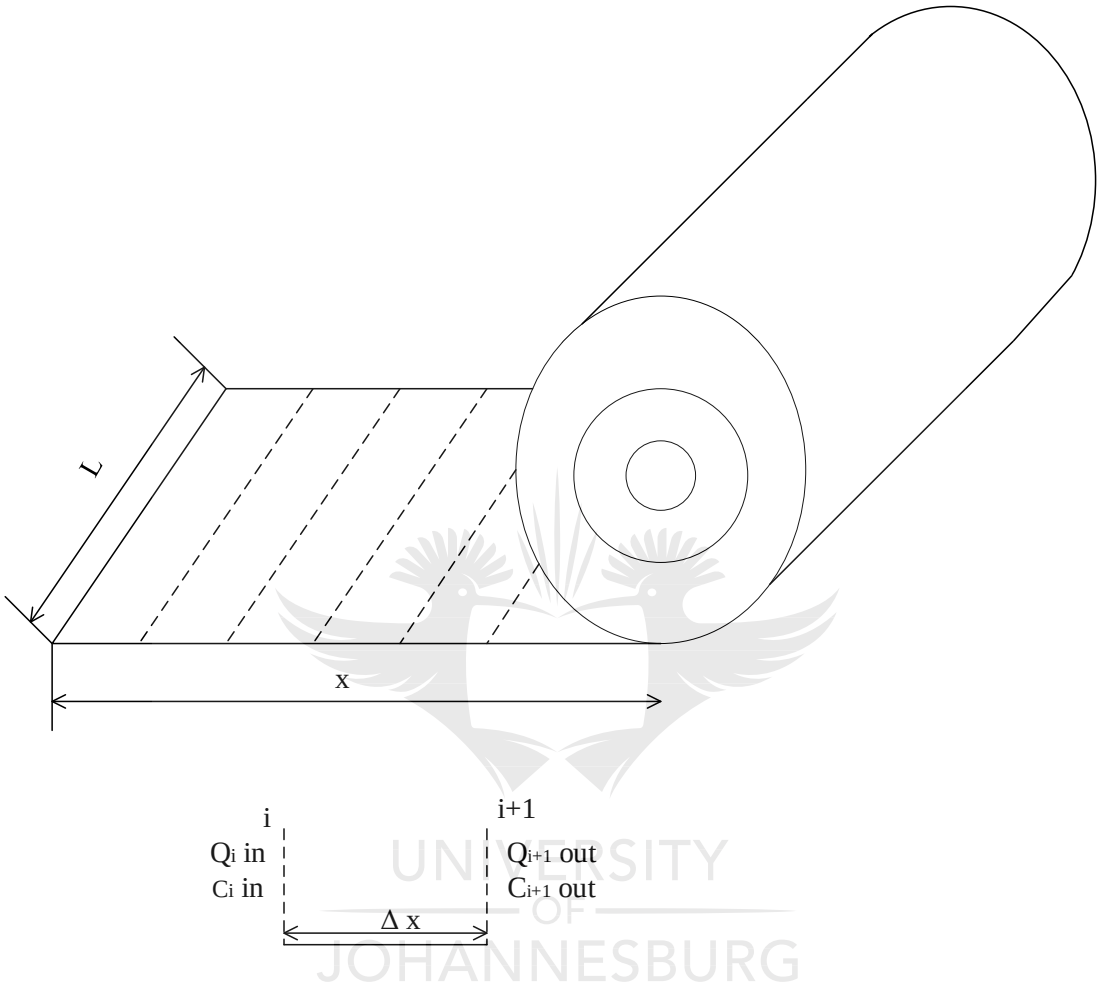

Figure 5-2: Spiral wound membrane divided into sections along membrane flow channel

The Reynolds number (Re) was calculated using Equation 5.1. using the fluid density (ρ) viscosity (μ) and superficial velocity (u). The superficial velocity was found by dividing the flowrate by the cross-sectional area. The cross-sectional area for flow was dependant on the height of the feed channel which was determined by the spacer thickness. (Pellegrino and Phu, 2006).

$$Re = \frac{\rho u L}{\mu} \tag{5.1}$$

Secondly the net driving pressure (NDP) was used to calculate permeate fluxes across the differential membrane area by subtracting the pressure head, osmotic pressure and outgoing feed pressure from the incoming feed pressure (Pellegrino and Phu, 2006).

$$NDP = Pf + \pi p - Pb - \pi f \quad (5.2)$$

The solute concentration (C) in moles per litre, temperature (T) in Kelvin, and the ideal gas constant (R) and the molar mass of the solute (m) in grams per mole were used to determine osmotic pressure (Pellegrino and Phu, 2006). The osmotic pressure was calculated in pascals and converted to bar.

$$\pi = \frac{CRT}{M} \quad (5.3)$$

deCosta (1993) used the statistical relationship between the Reynolds (Re), Shimdt (Sc) and Sherwood (Sh) numbers to calculate the mass transfer coefficients in channels (Km) i.e. the rate of mass transfer per unit area per unit concentration and the frictional pressure losses of the system.

$$K_m = \frac{m}{Am(C_i - C_{i+1})} \quad (5.4)$$

$$Sh = \frac{kdh}{D} \quad (5.5)$$

$$S_C = \frac{\mu}{\rho.D} \quad (5.6)$$

$$W_R = \frac{Q_P}{Q_F} \quad (5.7)$$

$$Q_R = Q_F - Q_P \quad (5.8)$$

$$C_p = C_F(1 - R_r) \quad (5.9)$$

$$C_R = \frac{Q_F.C_F - Q_P.C_P}{Q_R} \quad (5.10)$$

$$C_b = \frac{C_R + C_F}{2} \quad (5.11)$$

$$ks = \frac{D}{dh}.a.Re^{b}.Sc^{0.33} \quad (5.12)$$

$$C_W = C_b.\frac{exp\frac{J_v}{k}}{R_R+(1-R_R)} \quad (5.13)$$

Equations ((5.1) -(5.13)) were used as inputs to the membrane filtration model that was developed. The membrane filtration model was first coded in Scilab and then interfaced with CAPE-OPEN Flowsheet environment (COFE) as a CAPE-OPEN user Model. The model consists of continuous plug flow filtration equations describing the rejection and flux in the membrane module. Dimensionless mass balance equations ((Eq5.14-5.26)) including the Van't Hoff equation for osmotic pressure (Foley, 2013).

$$\frac{dQ}{dA} = -J \quad (5.14)$$

$$\frac{dQ_C}{dA} = -J_S \quad (5.15)$$

where dQ is change in flow rate, dA is change in area

$$\frac{dC}{dA} = \frac{1}{Q}(cJ - J_S) = \frac{J}{Q}(c - cp) \quad (5.16)$$

$$J = k_W(\Delta P - \Delta\pi) \quad (5.17)$$

$$J_S = k_S(c_W - c_P) \quad (5.18)$$

$$J_S = c_P J \quad (5.19)$$

Where c_W is wall concentration and c_P is permeate concertation

Differentiating at constant ΔP

$$dJ = -k_W\frac{d\pi_W}{dc_W}dc_W + k_W\frac{d\pi_P}{dc_P}dc_P \quad (5.20)$$

$$dJ_S = k_S dc_W - k_S dc_P \quad (5.21)$$

$$dJ_S = c_P dJ + J dc_P \quad (5.22)$$

Where $\pi_w$and π_P are osmotic pressure expressed as functions of c_W and c_P respectively. Combining these three equations and dividing by dA gives after some algebra.

$$\frac{\partial c_P}{dA} = \theta \frac{dc_W}{dA} \tag{5.23}$$

$$\text{Where } \theta = \frac{k_s + c_p k_w \frac{d\pi_w}{dc_w}}{k_W(\Delta P - \Delta\pi) + k_s c_P k_w \frac{d\pi_P}{dc_P}} \tag{5.24}$$

The Van't Hoff equation was used for osmotic pressure at higher molecules pressure as dilute species. When the Van't Hoff equation applies, this is simplified by:

$$\frac{d\pi_w}{dc_w} = \frac{d\pi_P}{dc_P} = iRT \tag{5.25}$$

Now the basic flux model can be written:

$$K\ ln\frac{c_w - c_p}{c - c_p} - k_w(\Delta P - \Delta\pi) = 0 \tag{5.26}$$

The model considers change in flow rate and concentration across the membrane, therefore a set of differential equations were developed and solved using Euler's method in Scilab. An equation that involves one or more derivatives of the unknown function is called an Ordinary Differential Equation (ODE). An ODE contains an independent variable, a dependant variable and derivatives of the dependant variable. ODE's are used for mathematical computation of equations in science and engineering (Wouwer *et al*., 2014). The order of the ODE equation is determined by the order of the highest derivative. For example, if the first derivative is the only derivative the equation is called a first order ODE (Salleh, 2012).

Euler's methods are simple methods for solving First Order ODEs, particularly suitable for quick computing because of their great simplicity. Euler's method also called the tangent line method uses a fixed step size h and generates the approximate solution. Euler's can be derived from Taylor series expansion (Salleh, 2012).

5.3 MODELLING APPROACH

As previously mentioned, unit operations are embedded in various process simulation software including CAPE-OPEN. However, in the case of membrane filtration of heavy metal ions, there is no existing unit operation that offers an accurate description of the process. Therefore, the membrane unit operation was developed through user added models. An approach similar to that used by Bobák *et al*. (2015) was developed to model a process simulator for membrane filtration. Scilab scripting language was used to solve a set of ordinary differential equations (ODEs) which were incorporated into the Scilab Unit Operation in CAPE-OPEN. The chemical compounds and thermodynamic properties were imported from ChemSep at http://www.chemsep.org/ for use in the CAPE-OPEN Flowsheet Environment.

Figure 5-3 shows how the mass transfer models were developed for solution of the ODEs in Scilab. The input variables were used to calculate the variables for the mass balance which were used to solve the ODEs and determine Qi and Ci across the membrane. Once Qi and Ci were close to the values determined experimentally then they could be used to calculate flux and rejection.

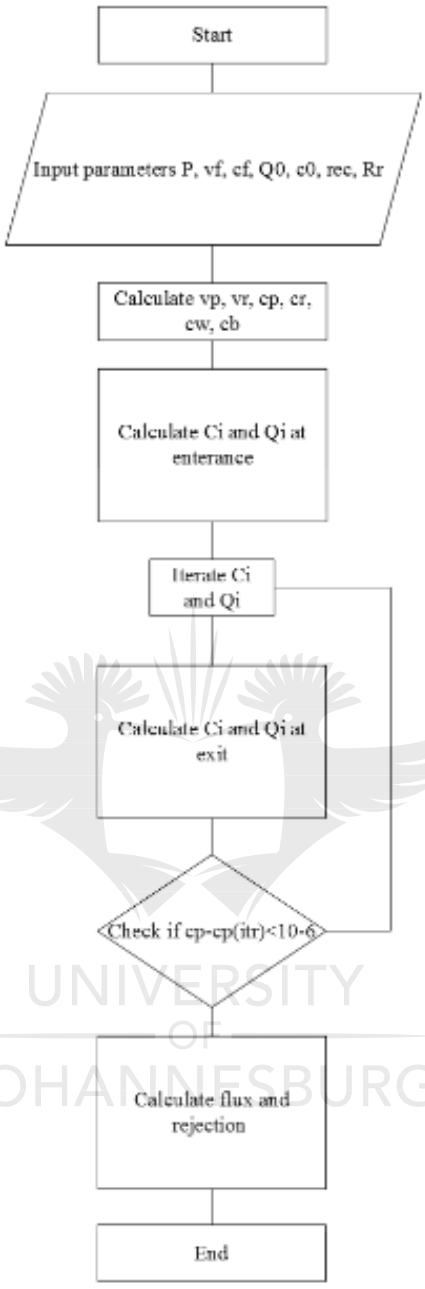

Figure 5-3: Algorithm for solution of mass transfer models

Figure 5-4 shows the Scilab CAPE-OPEN Unit operation interface. It allows the user to edit information specific to the unit operation such as the feed and product ports, parameters specific to the unit operation, Scilab code and any additional files needed by the unit operation for calculation.

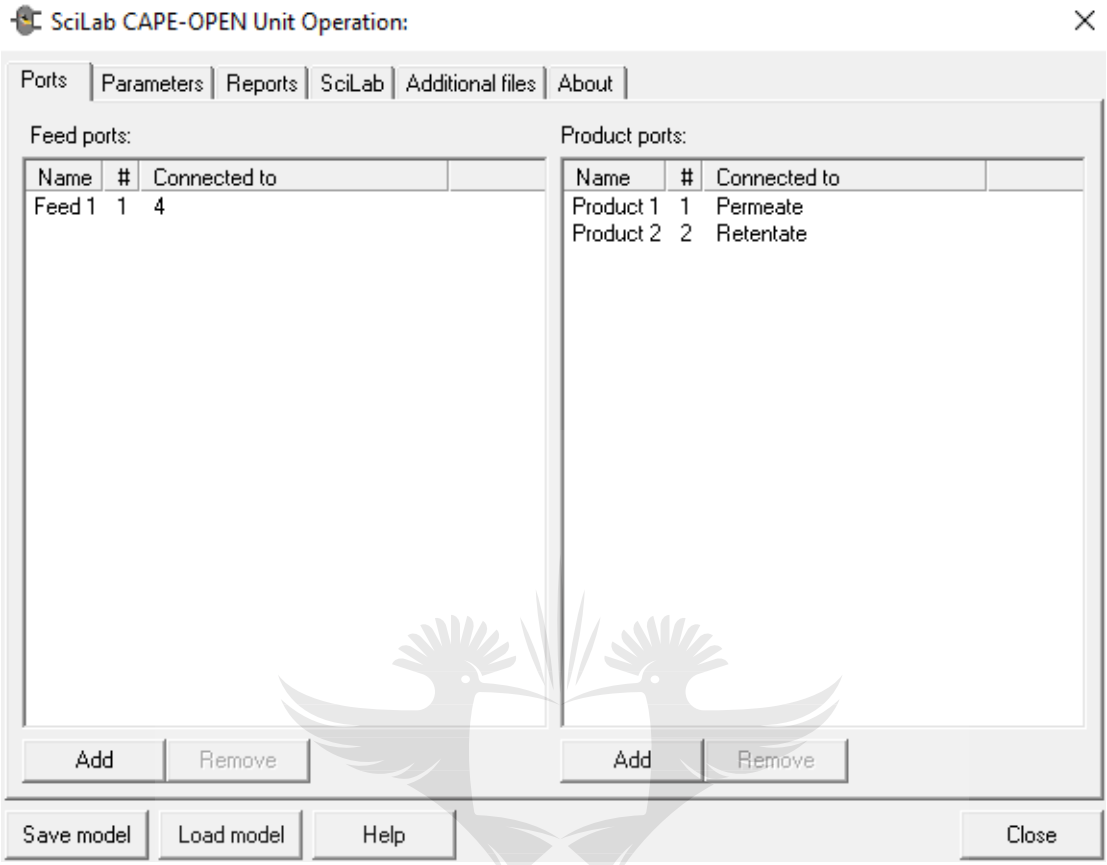

Figure 5-4: Scilab unit operation editor

Inputs into the model are the feed composition and flow rate, operating pressure, membrane area, length and number of membrane units (Corredor *et al*., 2016). Figure 5-5 shows the code specified under the 'Scilab' tab of the unit operation which was used to get the properties of the feed stream and specify the product stream.

calc - Notepad

File Edit Format View Help

```
// Enter your SciLab calculations here

Pf=getFeedProp(1,"pressure");
Tf=getFeedProp(1,"temperature");
Ff=getFeedProp(1,"totalFlow");
xf=getFeedProp(1,"fraction")

A=getParameter("Membrane area");
L=getParameter("Length");
th=0.2


exec('membraneode1.sci');

Fp=(1-th)*Ff;
Pp=Pf;

Fr=th*Ff;
Pr=Pf;

setProduct(1,Fp,xp,"temperature",Tf,"pressure",Pp);
setProduct(2,Fr,xr,"temperature",Tf,"pressure",Pr);
```


Figure 5-5: Scilab code for ports connected to unit operation to obtain feed and product stream properties

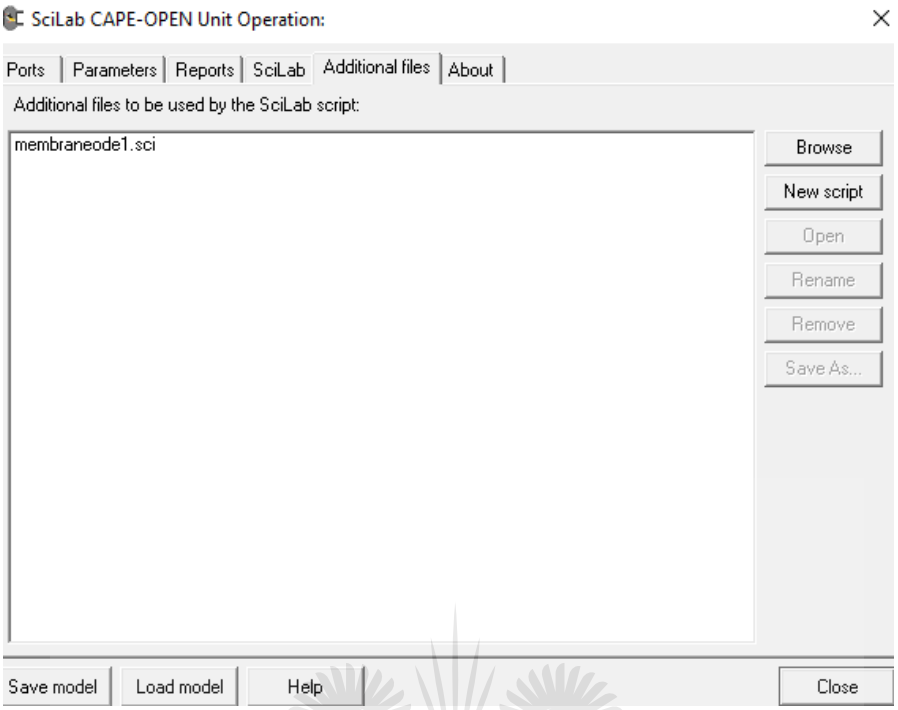

Figure 5-6: File containing additional Scilab code to be executed by Scilab Unit operation

Figure 5-7 shows the file containing Scilab code that was used to perform calculations for the unit operation. The file contains the code for equations discussed in section 5.3.

```
a=cw-cp;
b=c-cp;
s=1/b';
d=a*s';
v=[1;0;0;0;0];
e=d*v;


//ODES
Qi=Q0+l*log(exp(e))*x-Kw(deltap-delta0);
Ci=C0-l*cp*x;

rl=[Qi'];
r2=[Ci'];
rx=[rl,r2];
```

```
    //Euler integration
    h=0.1;
    x=[0:h:100];
    nout=200;
    xk=0;
    rout=[Qi]';
    zout=[Ci]';
    for i=1:nout
        [rx]=membrane_ode(xk,r0);
        ri=rx*h;
        xk=xk+h;
    end

    //Feed
    m=[0.76;0.02;0.02;0.2];
    xf=m;

    //Permeate
    alpha=0.95
    xp2=m(2)*(1-alpha);
    xp3=m(3)*(1-alpha);
    xp4=m(4)*(1-alpha);
    wp=[xp2;xp3;xp4];
    gp=sum(wp);
    xp1=1-gp;
    xp=[xp1;xp2;xp3;xp4];

    //Retentate
    xr2=m(2)*alpha;
    xr3=m(3)*alpha;
    xr4=m(4)*alpha;
    wr=[xr2;xr3;xr4];
    gr=sum(wr);
    xr1=1-gr;
    xr=[xr1;xr2;xr3;xr4];


        //Plot
        subplot(2,1,1)
        plot(x',rout(:,1));
        ylabel('Q(x)');
        xlabel('(x)');

        subplot(2,1,2)
        plot(x',zout(:,2));
        ylabel('C(x)');
        xlabel('(x)');
```


Figure 5-7: Scilab code run in Scilab unit operation

5.4 MODEL INTEGRATION

Figure 5-8 shows the overall method used for development of the membrane simulation. It is important for the Scilab membrane model to be integrated into the user interface, in this case CAPE-OPEN so that the simulation can run. Once the simulation was run, information for equipment sizing was obtained from the CAPE-OPEN process Flowsheet Environment (COFE). Once the equipment has been sized an economic evaluation can be performed on the process.

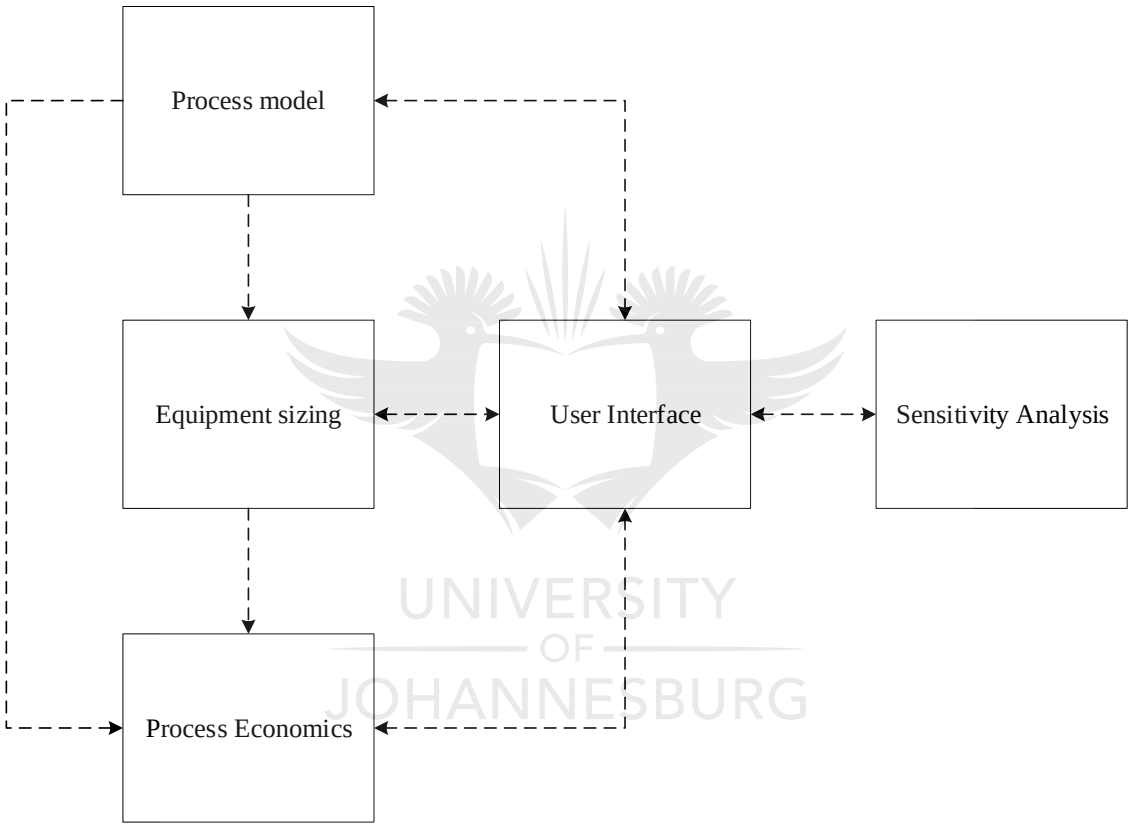

Figure 5-8: Flowchart for development of techno-economic model (Burk, 2018)

Once the mathematical model has been included in the unit operation and integrated in the simulation environment, the required physical, chemical and thermodynamic information of material streams for simulation of the unit operation can be obtained from the property package (Peshev and Livingston, 2013). The user can specify the set of components, physical properties and thermodynamic properties needed to develop the property package (van Baten and Pons, 2014). COFE allows for property packages to be developed from Chemsep. Chemsep is an open-source chemical database which contains the physical, chemical and thermodynamic properties

of over six hundred compounds (Kooijman and Taylor, 2006). However, in many cases databanks of pure components are not readily available in the simulation environment, or a compound of interest is missing (Peshev and Livingston, 2013).

A new compound can be defined by the user by adding it to the Pure Components Database (PCD) (Kooijman and Taylor, 2006). Thus, heavy metal ions of interest (Fe^{2+}, AL^{2+}, Mg) were added to Chemsep through the PCD. Figure 5-9 shows Chempsep's PCD database with the user-defined components added. Equation orientated optimisation techniques applied iteratively to simplified models of the flowsheet (Kisala *et al*, 1987).

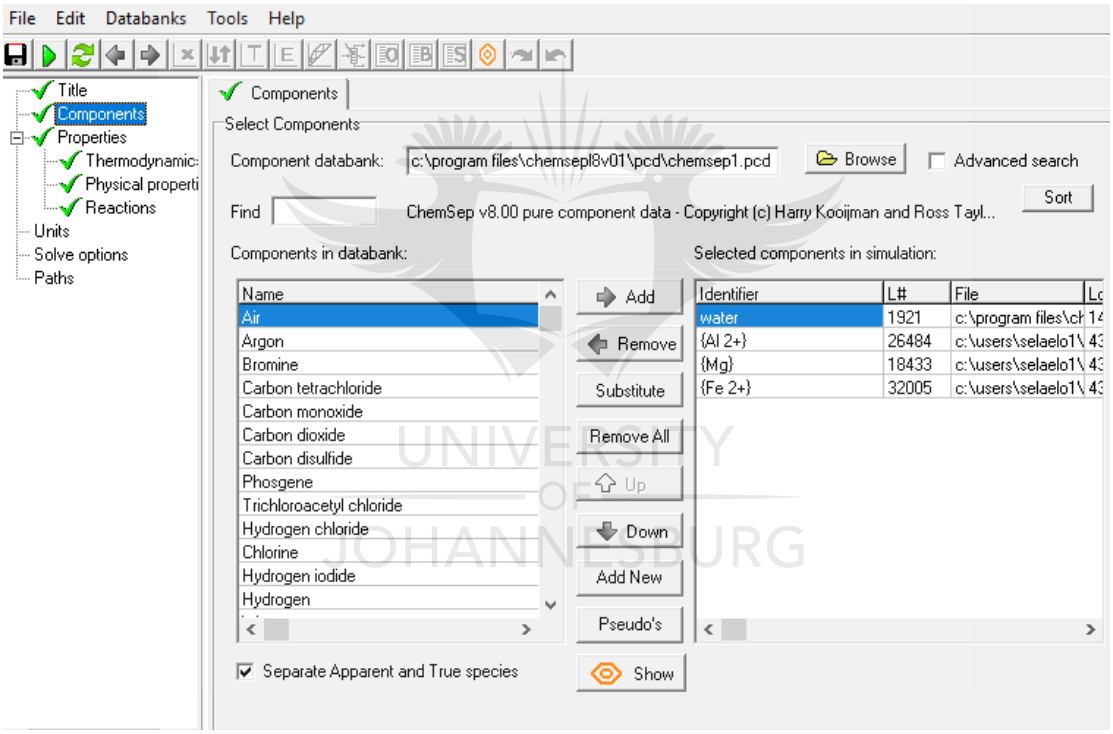

Figure 5-9: Pure Component database in Chemsep

Parameter	Value	Units
R	95	%
Rr = R/100	0.95	
rec = 0.8	0.8	

Qf = 1000;	1000	m^3/h
Qp = Qf*rec;	800	m^3/h
Qr = 1000-Qp;	200	m^3/h
vf = Qf/3600;	0.277778	m^3/s
vp = vf*rec;	0.222222	m^3/s
vr = vf-vp;	0.055556	m^3/s
cfMg = 0.02;	0.02	mol/L
cfAl = 0.02;	0.02	mol/L
cfFe = 0.2;	0.2	mol/L
cfH2O = 1-(cfMg+cfAl+cfFe);	0.76	mol/L
cpMg = Rr*cfMg;	0.019	mol/L
cpAl = Rr*cfAl;	0,019	mol/L
cpFe = Rr*cfFe;	0.19	mol/L
cpH2O = Rr*cfH2O;	0.722	mol/L
crMg = cfMg - cpMg;	0.001	mol/L
crAl = cfAl - cpAl;	0.001	mol/L
crFe = cfFe - cpFe;	0.01	mol/L
crH2O = cfH2O - cpH2O;	0.038	mol/L
cbMg = (cfMg+crMg)/2;	0.0105	mol/L
cbAl = (cfAl+crAl)/2;	0.0105	mol/L
cbFe = (cfFe+crFe)/2;	0.105	mol/L
cbH2O = (cfH2O+crH2O)/2;	0.399	mol/L
D = 0.061;	0.061	M
dx = 0.0191;	0.091	M

A = 0.5334;	0.5334	M	
c = 0.0305;	0.0305	M	
w = 0.4572;	0.4572	M	
ni = 1;	1		number of envelopes, each envelope has 2 membranes
L = 1.2195;	1.2195	M	
tm = 0.001450512;	0.001451	M	
ts = 0.0007112;	0.000711	M	
At = (%pi*(D^2)-(d^2))/4;	0.00962	m^2	
Am = L*tm;	0.001769	m^2	
Af = At-Am;	0.007851	m^2	
Ap = L*w;	0.557555	m^2	
v = ((vf+vr)/2)*(1/Af);	21.22948	m/s	
dh = ts;	0.000711	M	assume density and viscosity of water
ρ = 1000;	1000	kg/m^3	
μ = 0.000891;	0.000891	kg/ms	
Re = (v*dh*rho)/mu;	16945.46		
Dx = 0.0000000008;	8E-10		
Sc = mu/(rho*Dx);	1113.75	m^2/s	
ax = 0.5;	0.5		
bx = 0.54;	0.54		
ks = (Dx/dh)*(Re^b)*(Sc^0.33);	0.002189	m/s	(Erricson, 1999)
jv = vp/Ap;	0.398565	m/s	
jvk = jv/ks;	182.0843	m/s	

cwMg = cbMg*exp(jvk)/(Rr+(1-Rr)*exp(jvk);		0.050065	mol/L
cwAl = cbAe*exp(jvk)/(Rr+(1-Rr)*exp(jvk);		0.050065	mol/L
cwFe = cbFe*exp(jvk)/(Rr+(1-Rr)*exp(jvk);		0.500648	mol/L
cwH2O = cbH2O*exp(jvk)/(Rr+(1-Rr)*exp(jvk);		0.399222	mol/L
deltap = 5.514;		5.514	MPa
deltao = 2.399;		2.399	MPa
kw = jv/(deltap-deltao);		0.12795	m/Mpa/s

5.5 RESULTS AND DISCUSSION

The model was built in Scilab and imported to the Scilab Unit Operation for simulation in COFE. In order for the Scilab Unit Operation block run in the simulation, the appropriate thermodynamic package was added from Chemsep including user defined components. Figure 5-10 shows the result after the simulation was run. Process simulation was carried out for the membrane filtration system. The permeate and retentate yield were calculated using dimensionless mass balances. The performance of the proposed unit operation was estimated by the simulation model. By assuming a feed of 1000 m^3/day, a flux recovery of 80% could be simulated. From the simulated data there was a 95% reduction of ions in the permeate stream which is consistent with experimental data.

(a)

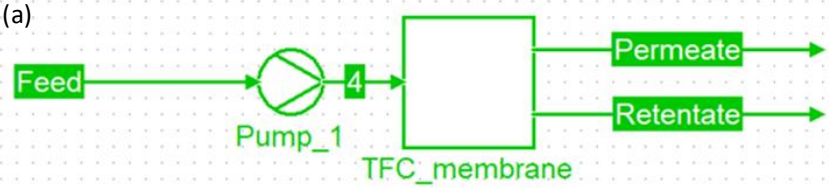

Stream	Feed	Permeate	Retentate	Unit
Pressure	101325	131325	131325	Pa
Temperature	300	300.011	300.011	K
Volume	1000	800.005	200.001	m³ / day
Mole frac water	0.76	0.988	0.772	
Mole frac {Al 2+}	0.02	0.001	0.019	
Mole frac {Mg}	0.02	0.001	0.019	
Mole frac {Fe 2+}	0.2	0.01	0.19	

(b)

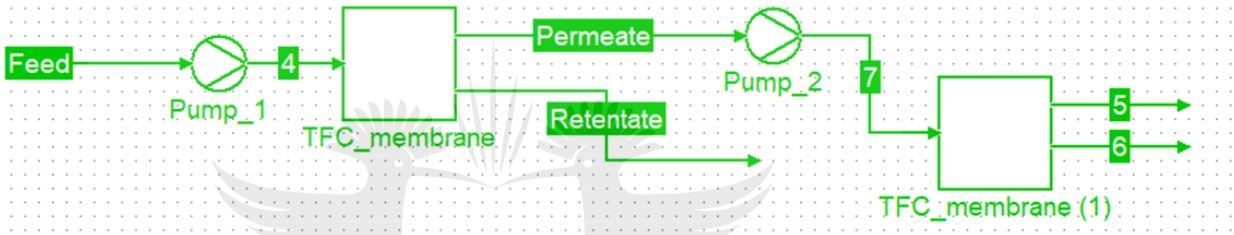

Stream	Feed	Permeate	Retentate	Unit
Pressure	1.01325	10.0132	10.0132	bar
Temperature	25	25.3315	25.3315	°C
Volume	1000	800.166	200.042	m³ / day
Mole frac water	0.76	0.9688	0.7912	
Mole frac {Al 2+}	0.02	0.0026	0.0174	
Mole frac {Mg}	0.02	0.0026	0.0174	
Mole frac {Fe 2+}	0.2	0.026	0.174	

Stream	7	5	6	Unit
Pressure	20.0132	20.0132	20.0132	bar
Temperature	25.6565	25.6565	25.6565	°C
Volume	800.326	640.26	160.065	m³ / day
Mole frac water	0.9688	0.98674	0.74806	
Mole frac {Al 2+}	0.0026	0.00013	0.00247	
Mole frac {Mg}	0.0026	0.00013	0.00247	
Mole frac {Fe 2+}	0.026	0.013	0.247	

Figure 5-10: Membrane filtration plant in COFE

The experimental rejection at pressures of 5 bar to 20 bar was previously determined and compared to the predicted rejection generated from the mass balance. The rejection increased with an increase in pressure and the predicted rejection showed a similar trend as shown in Table 5-1.

Table 5-1: Experimental and predicted rejection for TFN membrane

Pressure (bar)	Experimental Rejection (%)	Predicted Rejection (%)
5	76	79
10	85	86
15	90	90
20	93	94
5	76	78
10	85	86
15	90	90
20	96	95
5	75	77
10	82	84
15	88	88
20	95	93
5	78	80
10	87	88
15	90	92
20	93	95
5	75	78
10	87	88
15	90	91
20	94	95

A regression line was fitted to experimental vs predicted values with a 95% confidence interval as shown in Figure 5-11. Although the plot showed a good fit, statistical analysis was conducted to check if this was the case.

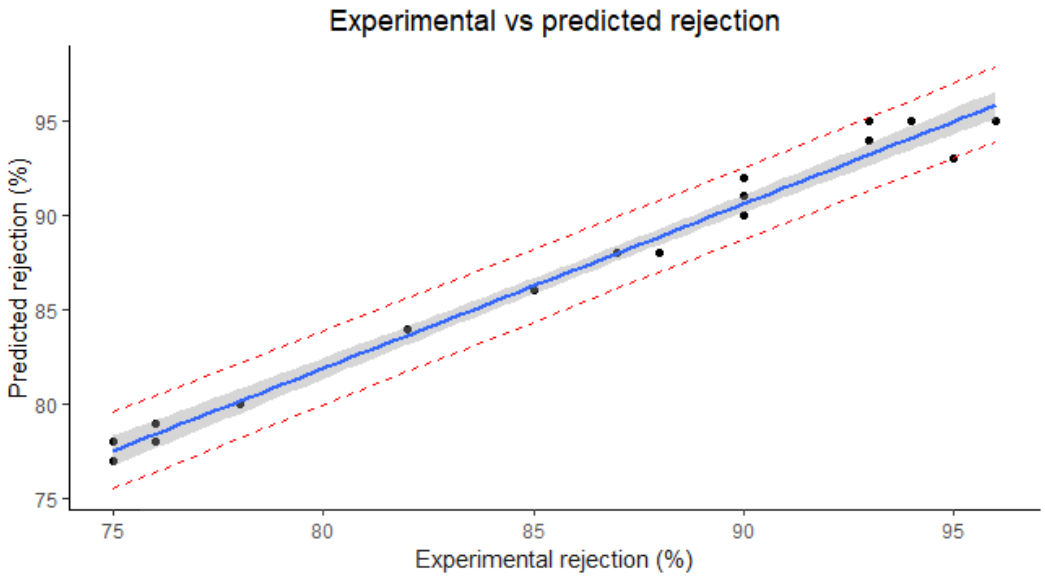

Figure 5-11: Plot of experimental vs predicted rejection

Table 5-2 gave the summary statistics and lack of fit test for the rejection model. The RSE was 0.833 which indicated that the error between the actual and predicted results was not significant. The R-squared of 0.981 was close to 1 which indicated that the model adequately explained the variance between experimental and predicted values (Aghaei and Jalilzadeh, 2017; Nair *et al.*, 2014). The adjusted R-squared also accounted for the number of variables and is almost equal to R-squared indicating that the variance in the model is completely explained by R-squared. The p-value of < 2.2E-16 was < 0.05 and therefore the model was statistically significant (Nair *et al.*, 2014). From the coefficients the regression equation for rejection was given by: Predicted rejection = 0.870* Experimental rejection + 12.299 + error. The equation can be used for prediction of future values from experiments if conducted under pressures of 5 to 20 bar.

Table 5-2: Statistical analysis of rejection

	Residuals:			
Min	-1.964			
Q1	-0.574			
Median	-0.087			
Q3	0.472			
Max	1.776			
Coefficients:				
	Estimate	**Std. Error**	**t-value**	**Pr(>|t|)**
Intercept	12.299	2.497	4.926	0.000109 ***
Experimental rejection	0.870	0.029	30.156	< 2E-16 ***
Signif. codes: 0 '***' 0.001 '**' 0.01 '*' 0.05 '.' 0.1 ' ' 1				
Fit statistics				
R-squared	0.981			
Adjusted R-squared	0.980			
DF	18.000			
F-statistic	909.400			
p-value	< 2.2E-16			
RSE	0.883			

In addition to the stats summary the residuals were further examined to determine if the model was a good fit of the data (Aghaei, and Jalilzadeh, 2017). The mean of the residuals was zero and the sum of the residuals was zero as shown in Figure 5-14(a). Also, from the normal Q-Q plot in Figure 5-14(b) most of the points fall on the 45° line indicating that the residuals were normally distributed (Nair *et al*., 2014). The homoscedasticity was checked by studentized test to examine the residuals for obvious outliers. The variance of errors was found to be constant as shown in Figure 5-14(c).

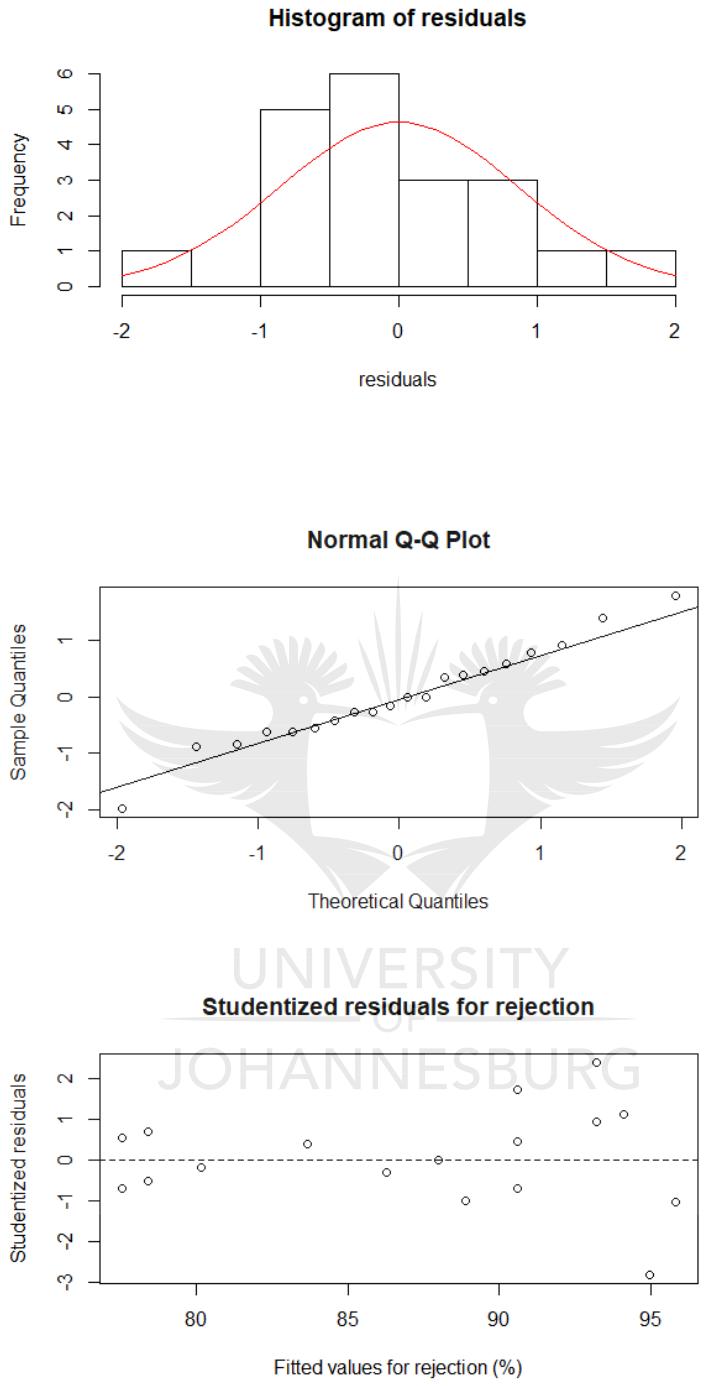

Figure 5-12: Check for goodness of fit for rejection model using a) Histogram plot, b) Normal Q-Q plot and c) Studentized plot

Table 5-3 shows the experimental flux at pressures of 5 bar to 20 bar was previously determined and compared to the predicted flux generated from the mass balance. Similar to rejection, flux increased with an increase in pressure.

Table 5-3: Experimental and predicted flux for TFN membrane

Pressure (bar)	**Actual Flux**	**Predicted Flux**
5	11.04	12.70
10	17.07	19.62
15	23.14	24.19
20	38.00	40.92
5	10.19	12.40
10	18.79	19.78
15	24.83	25.19
20	40.55	40.08
5	11.14	12.75
10	17.60	18.59
15	23.18	24.33
20	39.10	40.40
5	11.87	13.02
10	17.98	17.95
15	23.27	24.49
20	39.38	39.20
5	10.27	11.05
10	18.50	19.06
15	23.90	24.22
20	40.95	40.42

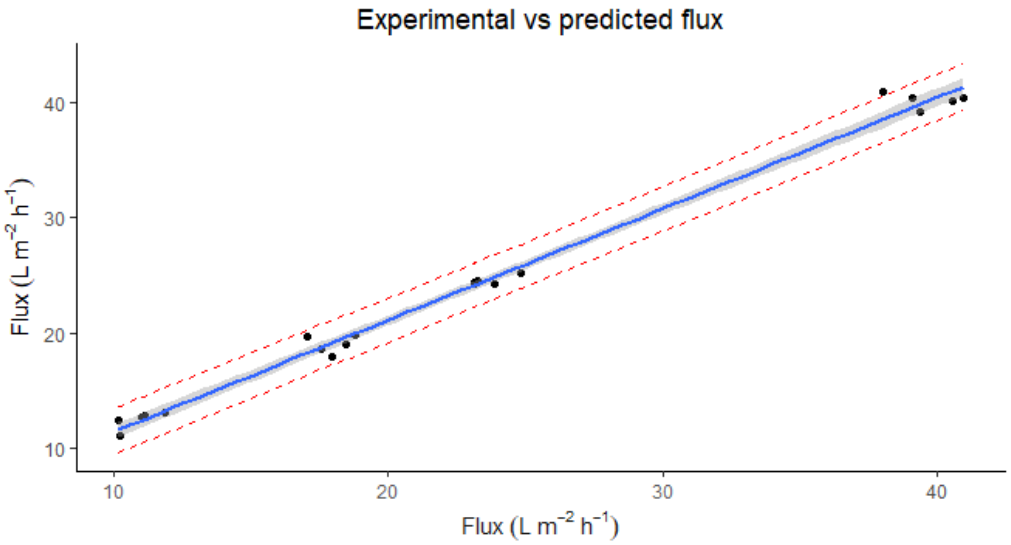

Figure 5-13: Experimental and predicted flux for TFN membrane

Table 5-4 gave the summary statistics and lack of fit test for the flux model. Like rejection the RSE of 0.891 was not significant. R-squared of 0.993 was close to 1 and the adjusted R-squared was equal to R-squared. The p-value of < 2.2E-16 was < 0.05 and therefore the model was statistically significant (Aslantas *et al.*, 2020). From the coefficients the regression equation for flux was given by: Predicted flux = 0.968* Experimental flux + 1.719 + error. Similar to rejection, the equation can be used for prediction of future values under the same process conditions.

Table 5-4: Statistical analysis of rejection

	Residuals:			
Min	-1.173			
Q1	-0.616			
Median	-0.146			
Q3	0.260			
Max	2.419			
Coefficients:				
	Estimate	Std. Error	t-value	Pr(>|t|)
Intercept	1.719	0.477	3.606	0.00202 **
Experimental flux	0.968	0.019	51.496	< 2E-16 ***
Signif. codes: 0 '***' 0.001 '**' 0.01 '*' 0.05 '.' 0.1 ' ' 1				
R-squared	0.993			
Adjusted R-squared	0.993			
DF	18			
F-statistic	2652			
p-value	< 2,2E-16			
RSE	0.891			

The residuals of the flux model were examined for goodness of fit. From Figure 5-15(a) the residuals were normally distributed with an average of zero and a sum of zero. The Q-Q plot in Figure 5-15b) confirmed normal distribution. The residuals were checked for outliers using the studentized test to as shown in Figure 5-14(c).

a)

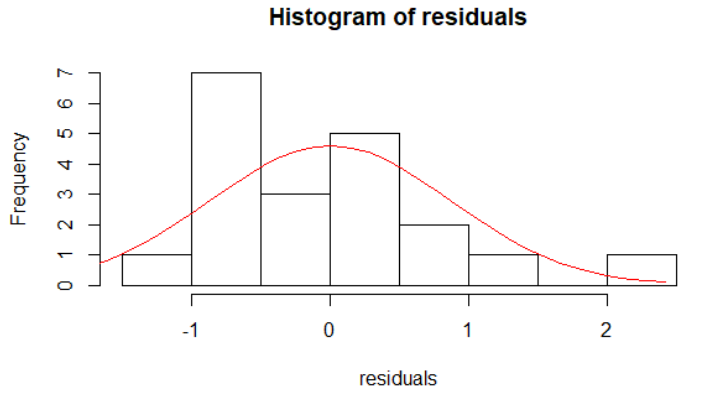

b)

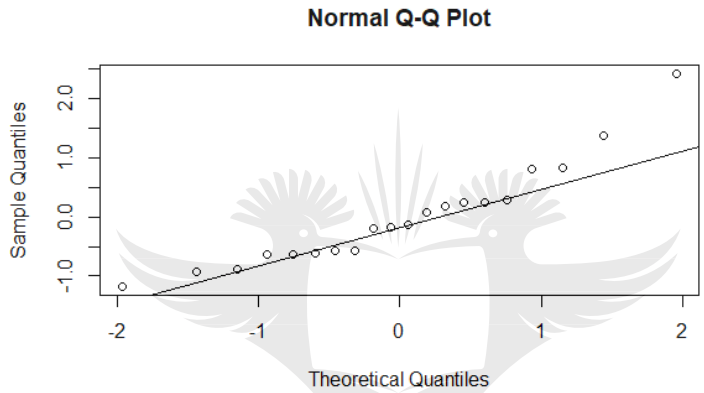

c)

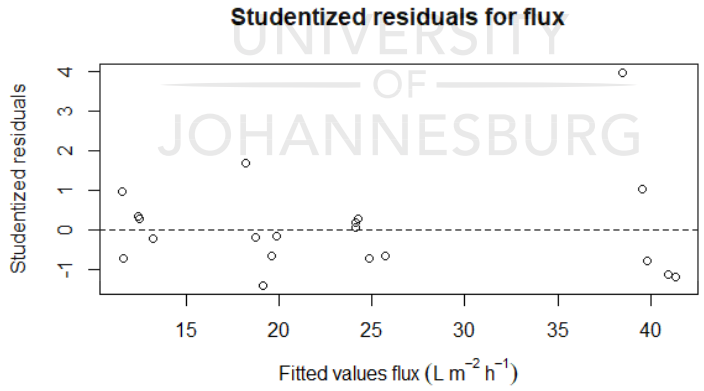

Figure 5-14: Check for goodness of fit for flux model using a) Histogram plot, b) Normal Q-Q plot and c) Studentized plot

5.6 CONCLUSION

A filtration scheme for the removal of heavy metal ions from AMD was simulated in Scilab. The system consisted of a SPS or DPS filtration process. The model could closely approximate flux and rejection based on experimental values. High total recoveries of up to 95% and can be achieved for both systems. The suggested scheme is based on a user-based model that links the applied models to the simulation environment for customisation of the process, in this case the removal of heavy metal ions from AMD. The models were based on mass balance equations. However, the principals of process design are set so that the proposed scheme can be adjusted to include other parameters or modified for different processes. The models was 99% accurate in predicting rejection and 98% accurate in predicting flux for pressures of 5 to 20 bar.

5.7 REFERENCES

Aghaei, F. and Jalilzadeh, Y.R. (2017). Investigation of effective parameters on the performance of NF membrane in simultaneous removal of Cr (VI) and Cu from contaminated water.

Aslantas, K., Danish, M., Hasçelik, A., Mia, M., Gupta, M., Ginta, T. and Ijaz, H. (2020). Investigations on surface roughness and tool wear characteristics in micro-turning of TI-6Al-4V alloy. *Materials,* 13(13):2998.

Barrett Jr, W.M., van Baten, J. and Martin, T. (2011). Implementation of the waste reduction (WAR) algorithm utilizing flowsheet monitoring. *Computers and Chemical Engineering,* 35(12):2680-2686.

Bobák, M., Šnita, D., Hrdlička, J., Pelc, V. and Kotala, T. (2015). Innovative process simulation software not only for electromembrane processes. *Desalination and Water Treatment,* 56(12):3141-3145.

Casavant, T.E. and Coˆté, R.P. (2004). Using chemical process simulation to design industrial ecosystems. *Journal of Cleaner Production,* 12(8-10):901-908.

Corredor, E.C., Chitta, P. and Deo, M. (2016). Membrane reactor system model for gas conversion to benzene. *Fuel,* 179:202-209.

Costa, A.R. and De Pinho, M.N. (2006). Performance and cost estimation of nanofiltration for surface water treatment in drinking water production. *Desalination,* 196(1-3):55-65.

Foley, G. (2013). *Membrane filtration: a problem solving approach with MATLAB* Cambridge University Press. New York. pp. 310-312.

Kisala, T.P., Trevino-Lozano, R.A., Boston, J.F., Britt, H.I. and Evans, L.B. (1987). Sequential modular and simultaneous modular strategies for process flowsheet optimization. *Computers and Chemical Engineering,* 11(6):567-579.

Kooijman, H.A. and Taylor, R. (2006). The ChemSep book. *Technical documentation.*

Nair, A.T., Makwana, A.R. and Ahammed, M.M. (2014). The use of response surface methodology for modelling and analysis of water and wastewater treatment processes: A review. *Water Science and Technology,* 69(3):464-478.

Omar, M.N., Shaidan, M.N.H. and Hussain, S., (2018) February. Simulation Comparison on PRICO LNG Process Using Open and Proprietary Sources. In *Proceedings of the 2018 7th International Conference on Software and Computer Applications* pp. 36-39.

Peshev, D. and Livingston, A.G. (2013). OSN designer, a tool for predicting organic solvent nanofiltration technology performance using aspen one, MATLAB and CAPE OPEN. *Chemical Engineering Science,* 104:975-987.

Salleh, Z. (2012). Ordinary differential equations (ODE) using euler's technique and SCILAB programming. *Mathematical Models and Methods in Modern Science,* 20(4):264-269.

Shaalan, H.F., Sorour, M.H. and Tewfik, S.R. (2001). Simulation and optimization of a membrane system for chromium recovery from tanning wastes. *Desalination,* 141(3):315-324.

Tolksdorf, G., Esche, E., van Baten, J. and Wozny, G. (2016). Taylor-Made Modeling and Solution of Novel Process Units by Modular CAPE-OPEN-based Flowsheeting *Computer Aided Chemical Engineering,* 38:787-792.

Tolksdorf, G., Esche, E., Wozny, G. and Repke, J. (2019). Customized code generation based on user specifications for simulation and optimization. *Computers and Chemical Engineering,* 121:670-684.

Van Baten, J. and Pons, M. (2014). CAPE-OPEN: Interoperability in industrial flowsheet simulation software. *Chemie Ingenieur Technik,* 86(7):1052-1064

Valentínyi, N. and Mizsey, P. (2014). Comparison of pervaporation models with simulation of hybrid separation processes. *Periodica Polytechnica Chemical Engineering,* 58(1):7-14.

Wouwer, A.V., Saucez, P. and Vilas, C., (2014), *Simulation of Ode/Pde Models with MATLAB®, OCTAVE and SCILAB: Scientific and Engineering Applications*. Springer.

CHAPTER 6: ECONOMIC EVALUATION

An era in which industrial processes are connected and automated through Information and Communication Technology (ICT), known as the fourth industrial revolution is greatly advancing (Shrouf *et al*., 2014). In the Fourth Industrial Revolution (4IR), industrial ecosystems are controlled, managed and developed through a network of devices and software so that productivity can be improved, and costs can be reduced (Petrasch, and Hentschke, 2016; Rodic 2017). In alignment with the 4IR, higher flexibility in production is necessary which requires more robust process and economic models (Zhou *et al*., 2015). Also, to cope with specified production and operation conditions, faster decision making is often required (Lasi *et al*., 2014). In order for decision makers to select the most sustainable technology for the application in the least amount of time, a decision analysis method must be followed which considers the most feasible outcome (Wang *et al*., 2019).

One of the most important decisions to be made in process engineering is whether or not to invest in certain technology (Judd, 2017; Minke and Turek, 2015). Although membrane technology has shown to be operationally feasible, investment in membrane water treatment plants requires comprehensive economic feasibility studies (Amigun *et al*., 2011; Miralles *et al*., 2017). Many such studies do not consider fluctuations in the price of electricity, inflation rate and interest rate over the plant lifetime which can have an enormous impact on the economic viability of a project (Park *et al*., 2010). In such studies the electricity, interest rate and inflation rate are modelled as deterministic or fixed variables and fail to account for economic risk (Amigun *et al*., 2011).

Park *et al*. (2010) conducted a cost analysis for design and operation of a full-scale RO desalination plant. It was found that using a deterministic model in which each of the initial cost values are kept constant, was inadequate in estimating the cost for both design configurations studied. In comparison, the stochastic model, accounted for variations in energy costs, interest rates and inflation in the plant lifetime. However, Park *et al* (2010) did not consider growth of the membrane market over time. The compound annual growth rate (CAGR) of nanofiltration and reverse osmosis markets is expected to be 5.3% and 8.7%, respectively. CAGR has been

used to estimate uncertainty in cash flows through Monte Carlo simulation (Shaffie and Jaaman, 2016).

In this chapter, stochastic variables are developed for electricity, inflation rate and interest rate and annual growth rate so that the decision-making process is more adaptable to these changes. Past records are used to generate future projections of stochastic variables using probability distributions. This stochastic cost estimation variables are incorporated into capital cost and operational cost estimations. The model was applied to the plant designed in Chapter 5. Net Present Value (NPV) was determined for SPS and DPS, and to assess profitability of the investment. The impact of predicted changes in electricity prices and inflation on energy cost and water production cost was determined through a sensitivity analysis. It is anticipated that investors and decision makers will be better informed for making investment and management decisions by using models that can respond flexibly to market needs. (Amigun *et al*., 2011; Ou *et al*., 2016).

6.1 MONTE CARLO SAMPLING FOR FINANCIAL RISK ASSESSMENT

An adequate financial model for risk assessment is able to incorporate variations in key variables that effect the investment decision and economic returns (Park *et al*., 2010). Probability distributions are generated from fluctuations in historical price data and are used to model risky parameters as stochastic variables for risk assessment (Olatunji *et al* 2018; Heo *et al*., 2019). Variables are generated from their historical likelihood of occurrence (or frequency), thereby giving a reasonable projection for future values to be modelled upon (Amigun *et al*., 2011; Platon and Constantinescu, 2014).

Monte Carlo simulation is a suitable method for risk assessment used by investors and decision makers (Olaru *et al*., 2014; Shaffie and Jaaman, 2016; Van dorp and Duffery, 1999). Sampling techniques are used to simulate the effect of fluctuations in economic parameters (Amigun *et al*., 2011; Hastings, 1970). Monte Carlo simulation has been used in economic feasibility studies and is increasingly being used for risk evaluation in engineering projects (Arnold *et al*., 2015; van Dorp and Duffey, 1999). Batan *et al*. (2016) used Monte Carlo simulation to generate a set

of varying economic risk factors (material costs and energy costs) to determine the effect of these factors on the minimum fuel selling price (MFSP). Compared to the base case in which material and energy costs were fixed, the material and energy costs generated from Monte Carlo simulation Monte Carlo simulation involves repeated sampling of random variables from their probability distributions, and computation of their statistical properties (Clarke, 1993; de Silva *et al*., 2014). A random number generator can be repeatedly run (>1000) to create the random variables (Arnold *et al*., 2015; Dehghani *et al*., 2014).

A random number generator algorithm is used to generate a multivariate distribution from which correlated variables are randomly sampled (Park *et al*., 2010; Onishi *et al*., 2017). Random variables and stochastic processes for simulation purposes are required to be well modelled and generated mathematically (Hammersley, 1960). It is important that the random variable or stochastic process generated should resemble its measured or statistical and probabilistic properties (Cai., 2018; Van dorp and Duffery, 1999). For a random variable, its probability distribution can be generated to show fluctuations in pricing data (Heo *et al*., 2019). For a stochastic process, two important properties have been used for the process: the probability distribution and the power spectral density (Cai, 2018). The probability density function for continuous random variables $(X_1, X_2, \dots X_d)$ can be expressed as Equation (6.1):

$$f_x(X_1, X_2, \dots X_d) = 1\sqrt{(2\pi)^2|\sum X|}\exp-\frac{1}{2}(X-\mu)^T \sum_x^{-1}(X-\mu) \qquad (6.1)$$

In which μ represents the dimensional vector d with expected mean (nominal) values of each random variable. $|\sum X|$ is the determinant of the dXd covariance matrix $\sum X$. While the diagonal element of the matrix $\sum X$ is a symmetric positive matrix that contains the variances σ^2 for each variable, non-diagonal elements of $\sum X$ indicates the covariance between variables σ_{ij} obtained from the correlation symmetric matrix p_{ij} (Equation (6.2)) (Onishi *et al*., 2017):

$$p_{ij} = \frac{\sigma_{ij}}{\sigma_i^2.\sigma_j^2} \qquad (6.2)$$

This symmetric matrix relates each pair of correlated random variables, wherein non-diagonal elements can assume values between -1 and +1 (Onishi *et al*., 2017).

A probability distribution is generated from the randomly chosen variables for the economic indicators and used to determine the economic viability of a project (Amigun *et al*., 2011). The distribution is able to fully account for uncertainty over the lifetime of the process. Greater probability of risk is associated with input variables that have historically been more unstable (Amigun *et al*., 2011).

6.2 ECONOMIC INDICATORS FOR FINANCIAL FEASIBILITY

Cost is a major factor that determines whether a technology is worth implementing or not (Shahmansouri and Bellona, 2015; Long *et al*., 2019). An economic analysis was performed to determine if the project is economically viable (Santiago *et al*., 2017). There are several factors that can be evaluated in an economic analysis such as NPV, IRR, ROI payback method but ROI and NPV commonly used (Himmerblau, 1978).

In order to determine the economical evaluation based on IRR, the NPV of investment is needed (Basile and Nunes, 2011). The NPV is the value obtained when the present value of cash flow is equal to the invested capital. The discount rate (DR) also influences the NPV. NPV can be calculated using Equation (6.3):

$$NPV = \sum_{m=1}^{plant\ life} \frac{NPAT}{(1+DR^{m})} - I_{total} \quad (6.3)$$

where; NPAT the net profit after income tax and I_{total} is the total investment cost. The total investment cost is found from summing the capital and non-capital investment costs, working capital costs and start costs (Equation (6.4)):

$$I_{total} = I_{cap} + I_{ncap} + I_{wcap} + I_{start} \quad (6.4)$$

where; I_{cap} is investment capital cost, I_{ncap} is non-capital investment cost, I_{wcap} is working capital costs and I_{start} is start costs.

The minimum rate of return (MRR) needed by the investor to make the project economically feasible must be set. For chemical industry projects, income tax 8%-18% (Basile and Nunes, 2011) is used. In order for the investment to be economically viable the IRR must be greater than the MRR (Mellichamp, 2013) (Equation (6.5)).

$$IRR > MRR \tag{6.5}$$

The net profit before income tax (NPBT) is found by subtracting depreciation (DP) from the gross profit (GP) The net profit after tax (NPAT) is the NPBT minus the income tax (IT) (Basile and Nunes, 2011) (Equations (6.6)-(6.9)).

$$NPAT = NPBT - IT \tag{6.6}$$

$$NPBT = GP - DP \tag{6.7}$$

$$IT = 0.25NPBT \tag{6.8}$$

The total equipment cost (TEC), is the sum of all equipment costs (Equation (6.9)).

$$TEC = \sum I_{equip} \tag{6.9}$$

where; I_{equip} is the equipment cost.

$$I_{cap} = 1.45Lf \times TEC \tag{6.10}$$

The Lang factor (Lf) depends on the type of process and equipment used (Basile and Nunes, 2011; Sinnot and Richardson, 2013) (Equations (6.11)-(6.13)).

$$I_{ncap} = 0.25I_{cap} \tag{6.11}$$

$$I_{wcap} = 0.15I_{total} \tag{6.12}$$

$$I_{start} = 0.10(I_{cap} + I_{ncap}) \tag{6.13}$$

The total revenue (TR) is calculated from gross profit minus total costs (TC) (Equation (6.14)).

$$TR = GP - TC \tag{6.14}$$

Total costs are calculated from direct costs C_{direct} and fixed costs C_{fix} (Equations (6.15)-(6.17)).

$$TC = C_{direct} + C_{fix} \tag{6.15}$$

$$C_{fix} = 0.03\left(I_{cap} + I_{ncap}\right) \tag{6.16}$$

$$C_{direct} = C_{raw} + C_{util} + C_{maint} + C_{sup} + C_{lab} + C_{admin} \tag{6.17}$$

where C_{raw} is cost of raw materials, C_{util} is utility costs, C_{sup} is supply costs, C_{lab} is labour costs and C_{admin} is administration costs and C_{maint} is maintenance costs which are calculated from total equipment costs using Equation (6.18):

$$C_{maint} = 0.04Lf \times TEC \tag{6.18}$$

Supply costs are calculated using Equation (6.19):

$$C_{sup} = 0.06\left(I_{cap} + I_{ncap}\right) \tag{6.19}$$

Labour costs are a fraction of the total costs (Equation (6.20)).

$$C_{lab} = 0.20TC \tag{6.20}$$

Administration costs are a function of labour costs (Equation (6.21)).

$$C_{admin} = 0.20C_{lab} \tag{6.21}$$

Depreciation is calculated from total investment costs (Equation (6.22)).

$$DP = 0.07I_{cap} \tag{6.22}$$

Verbene and Wouters (1993) developed a cost evaluation model for NF membrane system known as the Verbene Cost model (Ali and Mohammad, 2005). The model was based on project practical data and actual tender from suppliers. Bruggen *et al* (2001) used the Verbene Cost model to determine the impact of economic factors on wastewater treatment system (Mohammad *et al*., 2004). Assumptions for the model are presented in Table 6.1. This model was adapted and used in conjunction with the above (Equations (6.3)-(6.22)) to investigate the effect of TFN membrane process parameters on the cost of a TFN system (Ali and Mohammad, 2005). The cost model was expressed in 1993 US$ and should first be converted to 1993 ZAR and then actualised to represent current values by applying the Chemical Engineering Plant Cost index ratio which can be considered equal to 607.5/359.2 (January 2019/full year 1993) (Jenkins, 2020)

Capital cost terms:

(i) Civil investment i.e. costs associated with where installation of membrane system is to be built. Depreciation period is 30 years (Equation (6.23)) (Ali and Mohammad, 2005).

$$C_{civil} = 862\delta.(Q_f + 1239n) \quad (6.23)$$

where δ is factor used to update cost index to the current year, Q_f is the feed flowrate and n is the number of years.

(ii) Mechanical engineering costs for pumps, filters piping etc. Depreciation period is 15 years (Equation (6.24)) (Elazhar *et al*., 2013).

$$C_{mech} = 3608\delta.(Q_f^{0.85} + 908n) \quad (6.24)$$

(iii) Electrochemical costs: costs for energy supply, control engineering and all electronic components (Equation (6.25)).

$$C_{electro} = \delta(1.4 \times 10^6 + 54PQ_f) \quad (6.25)$$

(iv) Membrane investment cost: membrane installation costs for a membrane lifetime of 5 years (Elazhar *et al*., 2013). According to the model the membrane cost for installation of one module is €1000 which is converted to Rands (Equation (6.26)).

$$C_{membrane} = \delta(16146.42n) \tag{6.26}$$

Operating cost items:

(i) Depreciation costs: depreciation rate upon investment cost (Elazhar *et al*., 2013). The depreciation of investment cost is based on stochastically modelled variables for interest rate (Equation (6.27)).

$$C_{deprec}(t) = r_i(t).\left(\frac{C_{civil}}{30} + \frac{1}{15}(C_{mech} + C_{electro}) + \frac{C_{membrane}}{5}\right) \tag{6.27}$$

(ii) Cost of energy needed to pump the feed stream into membrane system (Elazhar *et al*., 2013) An electrical cost is estimated using stochastically modelled variables for energy cost (Equation (6.28)).

$$\left[\left(\left(\frac{Q_f * \Delta P}{n}\right) + \left(Q_r \frac{\Delta P}{n}\right)\right).\left(\frac{\varepsilon(t)}{1000}\right)\right] \tag{6.28}$$

(iii) Chemical cost: cost needed by a total of chemical materials which be filtered. The cost is used as 0.37 R/m^3 filtration (Equation (6.29)).

$$C_{chemical} = 0{,}37Q_f \tag{6.29}$$

(iv) Maintenance cost: 2% of the total investment costs (Equation (6.30)) (Elazhar *et al*., 2013).

$$C_{maint} = 0.02C_{capital} \tag{6.30}$$

(v) Quality control cost: 2% of total investment costs (Equation (6.31)) (Elazhar *et al*., 2013).

$$C_{quality\ control} = 0.02C_{capital} \quad (6.31)$$

(vi) Operation of installation: 2% of total investment costs (Equation (6.32)) (Elazhar *et al*., 2013).

$$C_{installation} = 0.02C_{capital} \quad (6.32)$$

Cost of the membrane module was determined in relation to membrane area required to achieve desired flux and rejection (Chapter 5) using the equation developed by Sethi and Wiesner, (2000) (Equation (6.33)).

$$C_{membrane} = kA^n \quad (6.33)$$

Where k represents the weight of the cost component and A is the membrane area

The overall investment and operating costs have been presented in Table 6.2. The economic evaluation is based on the annualised capital cost. Given the total investment in R, for a capacity of 1000 m^3/day (Peters, 2010).

6.3 ASSUMPTIONS OF MODEL

The following economic parameters were used for probabilistic modeling:

* Price of electricity
* Interest rate
* Inflation rate
* Annual growth rate

The plant was designed to treat 1000 m^3/h, with the maximum permeate flow rate set at 80% based on experimental data and RSM. The assumptions for plant operation are summarized in Table 6-1.

Table 6-1: Plant operation assumptions

NF membrane plant data		**Units**
Plant capacity	1000	m^3/h
Operating hours	20	H
Recovery rate	95	%
Feed Pressure	20	Bar
Pump efficiency	75	%
Membrane lifespan	5	Years
Amortization period	20	Years

The volatility of financial markets, lack of accessible, affordable energy and large capital investment required make it exceedingly challenging to make reliable investment predictions based on fixed cost values (Park *et al*., 2010). More so in the case of pressure driven membrane processes which have extensive energy requirements (Hu and Apblett, 2014; Phatumchina *et al*., 2018). Therefore, the cost estimation for a TFN membrane filtration plant requires stochastic variables to be modeled using statistical methods that account for fluctuations in input variables and produce predictions with quantifiable uncertainties. Changes in interest rate, electricity price and inflation rate have been shown to influence the profitability of a membrane treatment plant over the plant lifetime (Park et al., 2010). Therefore, there is a necessity to develop economic models that can accommodate uncertainty and risk.

6.4 MODEL DEVELOPMENT

Figure 6-1 outlines the method used for cost estimation in this study. First the specifications for water quality and operating conditions were obtained from Chapter 4 and Chapter 5. The NPV is calculated from the total CAPEX and OPEX based on the total volume of water produced in m^3 for an entire plant lifetime of 20 years.

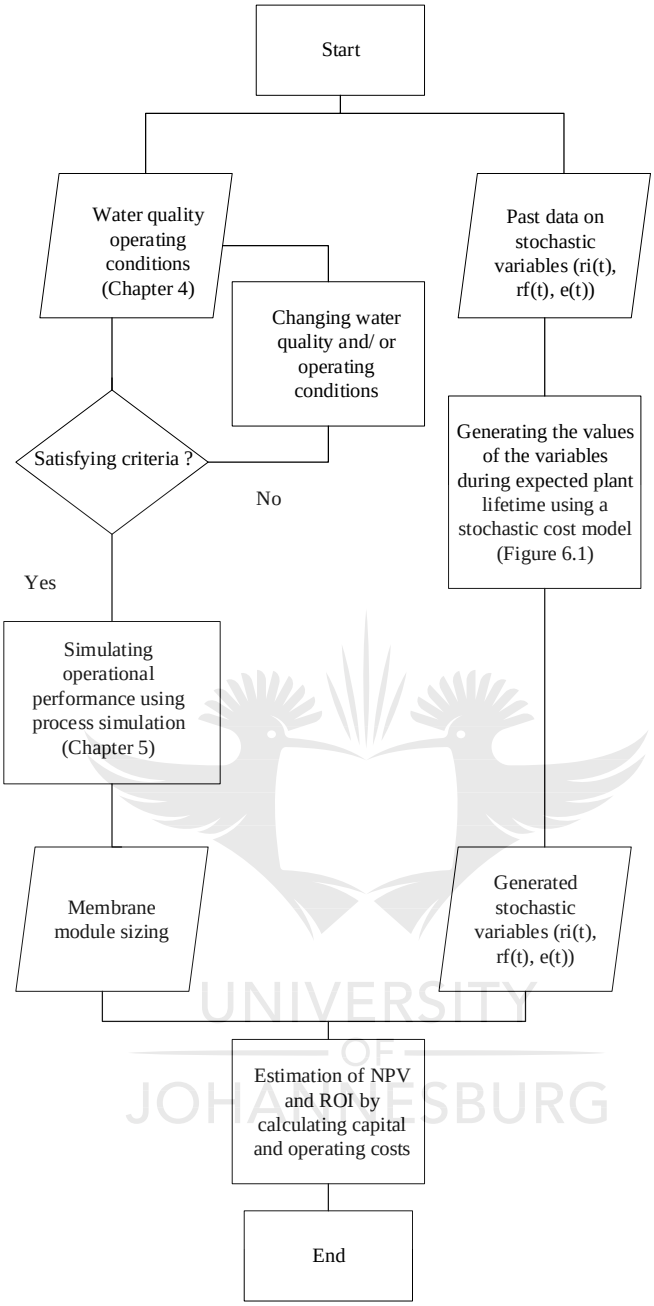

Figure 6-1: Flow chart for stochastic cost estimation of TFN plant

If a deterministic approach is used in the cost estimation, then for every input variable there will be one fixed output variable generated. However, for this study we are interested in the effect of fluctuations in inflation, interest rate and electricity. Therefore, deterministic methods cannot be used. Instead, probability distributions are generated from a set of random numbers for each year throughout the lifetime of the plant and used to generate dynamic probability distributions

as outputs which vary throughout the lifetime of the plant (Park *et al*., 2010). Probability distributions were generated for each year of operation (Section 6.5), and their average values were used for deterministic cost evaluation. Figure 6.2 shows the steps to randomly generate values of $r_i(t)$, $r_f(t)$, and $\varepsilon(t)$, during plant lifetime.

6.5 MODELING OF STOCHASTIC VARIABLES

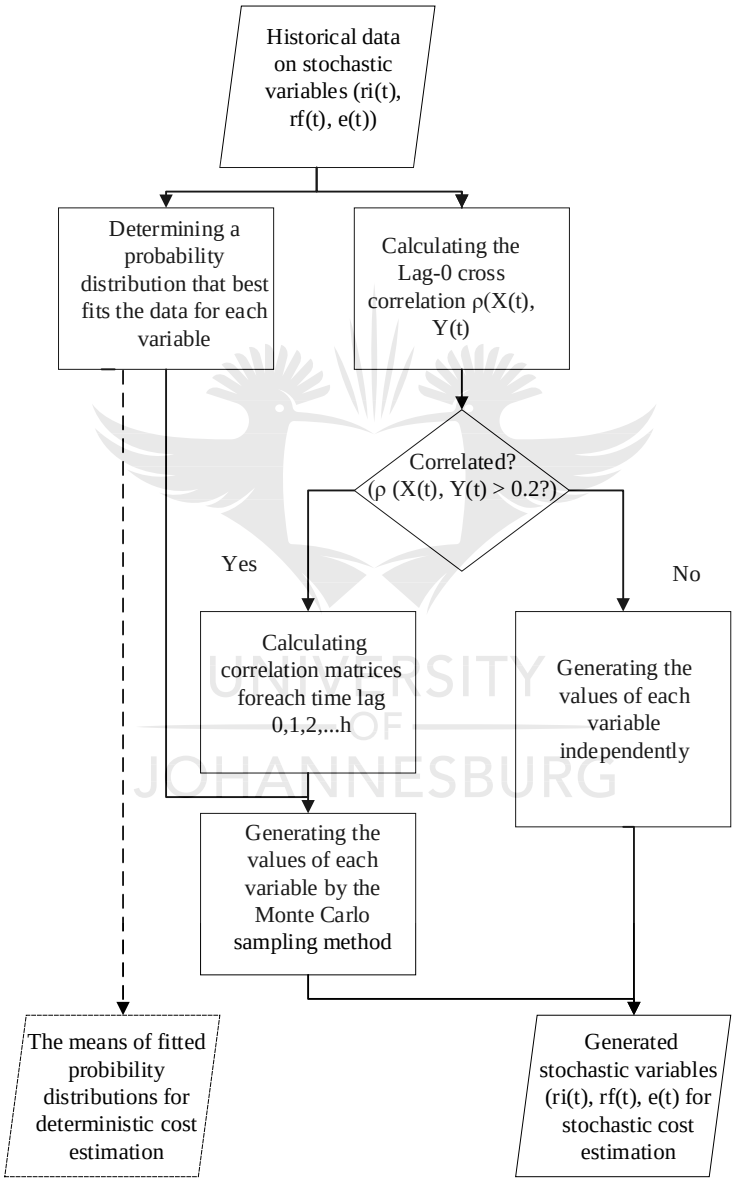

Figure 6-2: Flowchart for generating stochastic variables of interest rate (ri(t), inflation rate (rf(t)) and electricity price (e(t) at year t from past data. The deterministic cost estimation is shown by dashed lines as a base for comparison.

Historical data was collected from International Monetary Fund, 2019 for the stochastic variables of interest rate ($r_i(t)$) and inflation ($r_f(t)$), while electricity data ($\varepsilon(t)$) was collected from Eskom, 2019. The relationship of the different variables to each other (correlation) was determined. There are two types of correlation: autocorrelation and cross-correlation (Park *et al*., 2010). Cross correlation indicates the similarity between two discrete variables as a function of the lag, whereas autocorrelation measures correlations within the same variable where the lag is zero. For a time difference h and a positive increase in x leads to a positive increase in y at $h = 0$ then x and y are positively cross correlated at lag-0. Similarly, if positive increase in x leads to a positive increase in x at $h = 1$ then x has a positive autocorrelation at lag-1. Lag-h correlation between two sets of variables $X(t)$ and $Y(t + h)$ is denoted as and estimated by the following equation when the number of datapoints is n ($1<T<n$) and $h<n$-1) (Park *et al*., 2010).

$$\rho(X(t), Y(t+h)) \approx \frac{(\frac{1}{n-h})\sum_{i=1}^{n-h}(X(i)-X)(Y(t+h)-Y)}{[\frac{1}{n-1}\sum_{i=1}^{n}(X(i)-X](Y(i)-Y)]} \quad (6.34)$$

Where $\approx$ denotes 'approximately equal to' and X and Y are the sample means of each variable

The correlation is expressed in a range of values between -1 and +1. When the correlation is closer to unity, a strong positive correlation is observed and the pair of variables tend to move in the same direction. If the correlation is approaching -1, then the pair of variables have a strong inverse relationship and tend to change in the opposite direction, i.e. one variable increases as the other decreases. A correlation of 0 indicates that there is no relationship between the two variables. Lag h correlation becomes 0 as h increases, because datapoints in the present and far distant future tend to be independent.

Lag 0 cross-correlation for each pair of variables was first calculated following steps shown in Figure 6-2. A < 0.2 lag cross-correlation was not considered to be significant enough ($\rho(X(t))$, $Y(t)$) for all possible pairs. Any variable with a cross correlation below 0.2 was treated as independent and was generated separately.

A probability distribution (e.g. exponential, lognormal normal distribution etc.) and the correlation matrices of variables are needed are needed to generate cross-correlated random

variables (Figure6.2). Probability distribution fitting will be described in section 6.6. The correlation matrix at lag h for inflation, interest rate and electricity price was defined as:

$$\sum_{\mathrm{h}} = \begin{matrix} p((r_i(t), r_i(t+h)) & p((r_i(t), r_f(t+h)) & p\,((r_i(t), \varepsilon(t+h)) \\ p((r_f(t), r_i(t+h)) & p((r_f(t), r_f(t+h)) & p((r_f(t), \varepsilon(t+h)) \\ p((\varepsilon(t), r_i(t+h)) & p((\varepsilon(t), r_f(t+h)) & p((\varepsilon(t), \varepsilon(t+h)) \end{matrix} \quad (6.35)$$

The autoregressive integrated moving average (ARIMA) model combines three different processes comprising of (i) an autoregressive (AR) function regressed on past values of the process, (ii) a moving average (MA) function regressed on a purely random process and (iii) an integrated part (I) that makes the data series stationary by differencing (Brownlee 2017; Khasei and Bigari 2010). The model uses the correlation between an observation and some number of lagged observations and can be used for analysis and forecasting of time series data (Brownlee, 2017; Contreras *et al*., 2003). The ARIMA model was used to generate stochastic variables through probability distribution and correlation matrices, $\sum 0, \sum 1 \ldots \sum PLmax$ as inputs to the model. Deterministic cost results were generated from the means of the fitted probability distributions for comparison with stochastic cost results. Before the ARIMA model can be fitted, the time series data needs to be stationary meaning that the mean of the data must be constant over time. The trend must also be removed by differencing and power transformation to stabilize the trend (Khasei and Bigari 2010). Once these conditions have been met, the order of the ARIMA can be determined using the method proposed by Box and Jenkins (1976) where the autocorrelation (ACF) and partial correlation (PACF) and degree of differencing are used to identify the order of the model. The polynomial order of the model is represented by non-negative integers p,d,q (Kardakos *et al*., 2013) where p is shown by the order of the PACF, q is shown by the order of the ACF and d is the degree of differencing applied to the time series data.

Once the models have been fitted, the prediction performance of the models can be evaluated using three indices: root mean square error (RMSE), mean absolute error (MAE) and mean absolute percentage error (MAPE) that are commonly used to assess the goodness of fit of time-

series models (Lahmiri, 2016; Parmar and Bhardwaj, 2014; Zhou *et al*., 2018). The formulas are defined by the following equations:

$$RMSE = \sqrt{\frac{1}{n}\sum_{t=1}^{n}(y_t - \hat{y}_t)^2} \quad (6.34)$$

$$MAE = \frac{1}{n}\sum_{t=1}^{n}|y_t - \hat{y}_t| \quad (6.35)$$

$$MAPE = \frac{1}{n}\sum_{t=1}^{n}\frac{|y_t - \hat{y}_t|}{y_t} \quad (6.36)$$

Where y_t is the actual values over time t and $\hat{y}_t$ is the predicted values over time t for n number of observations.

Akaike's Information Criterion (AIC) for a set of models and investigate the models with lowest AIC values. The AIC equation defined by:

$$AIC = -2l(\hat{\theta}y) + 2K \quad (6.37)$$

where K is the number of estimated parameters in the model including the intercept and $l(\widehat{\theta y})$ is the log-likelihood at its maximum point of the estimated model (Pho *et al*., 2019).

When estimating model parameters using maximum likelihood estimation, it is possible to increase the likelihood by adding additional parameters, which may result in over fitting The Schwarz Bayesian Information Criterion (BIC) resolves this problem by introducing a penalty term for the number of parameters in the model and investigate the models with lowest BIC values. The BIC equation is defined as follows:

$$BIC = -2l(\widehat{\theta y}) + Kln(n) \quad (6.38)$$

where n is a sample size; K is the number of estimated parameters in the model including the intercept and $l(\widehat{\theta y})$ is the log-likelihood at its maximum point of the estimated model. Along with AIC and BIC, significance level of coefficient values is also important to decide which values affect the model (Pho *et al*., 2019).

The Durbin Watson statistic tests the residuals from a first order regression analysis for autocorrelation (Akter *et al*., 2014). The Durbin-Watson statistic ranges between 0 and 4. When the sample has a value of 2, there is no autocorrelation. Values from 0 to less than 2 indicate positive autocorrelation and values from 2 to 4 indicate negative autocorrelation (Kenton, 2019). The maximum likelihood estimation (MLE) is used to estimate the ARIMA model by trying to maximize the log-likelihood for given values of p, d, and q when finding parameter estimates so as to maximize the probability of obtaining the observed values (Aduda, *et al*., 2016). A limitation of the Durbin Watson statistic is that it cannot be used on small samples (Akter *et al*., 2014) The Durban Watson statistic is given by:

$$d = \frac{\sum_{t=2}^{T}(e_t - e_{t-1})^2}{\sum_{t=1}^{T} e_t^2} \tag{6.39}$$

Where e_t is the residuals and T is the number of observations.

The Jarque Bera (JB) statistic tests for normality of the data. If data is normally distributed, then the skewness is equal to 1 and the kurtosis is equal to 3 which is the same as kurtosis equal to zero. Therefore, the null hypothesis is that the skewness is zero and the kurtosis is zero If the p-value> 0.05 then the null hypothesis is rejected, and the data is not normally distributed (Ismail *et al*., 2016)

6.6 GENERATION OF DYNAMIC VARIABLES FROM HISTROICAL RECORDS

Stochastic variables, $r_i(t)$, $r_f(t)$, and $\varepsilon(t)$ were generated historical records from the years 1958 to 2018 (Eskom, 2019; International Monetary Fund, 2019). Cross-correlations at $\Delta t = 0$ were determined for past records. First, probability distributions of $r_i(t)$, $r_f(t)$ and $\varepsilon(t)$ were fitted to historical data as shown in Figures 6-3 by SPSS and R, resulting probability distributions as shown below. Inflation ($r_f(t)$) and electricity ($\varepsilon(t)$) had an exponential probability distribution and interest rate ($r_i(t)$) had a log normal distribution. Fitting these distributions was useful for forecasting future values which were expected to have the same probability distributions as historical values.

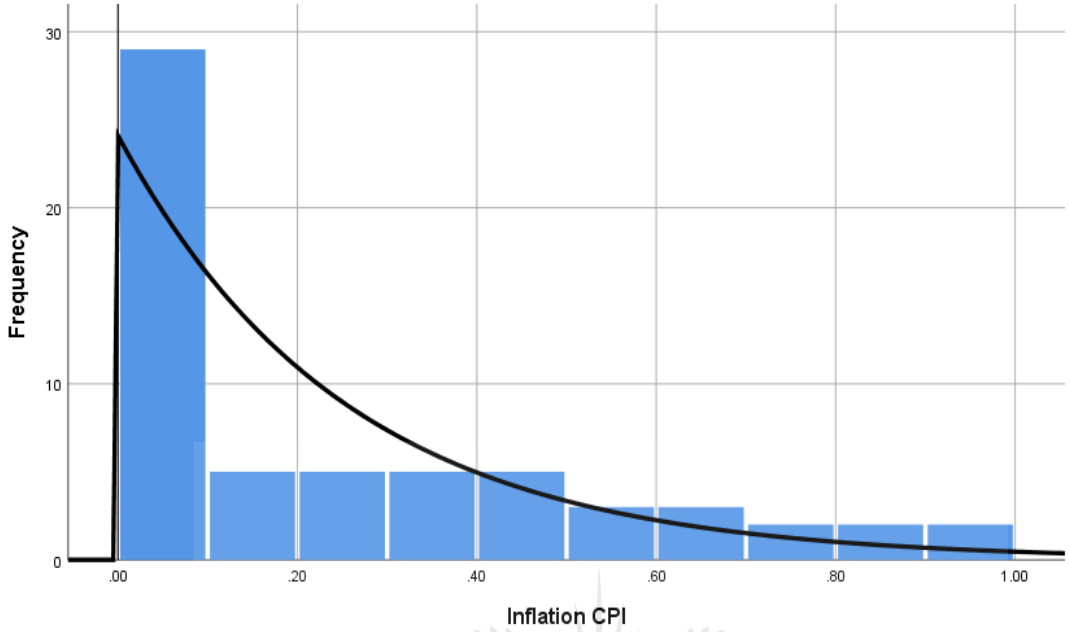

Figure 6-3: Probability distribution fitted to past data on inflation.

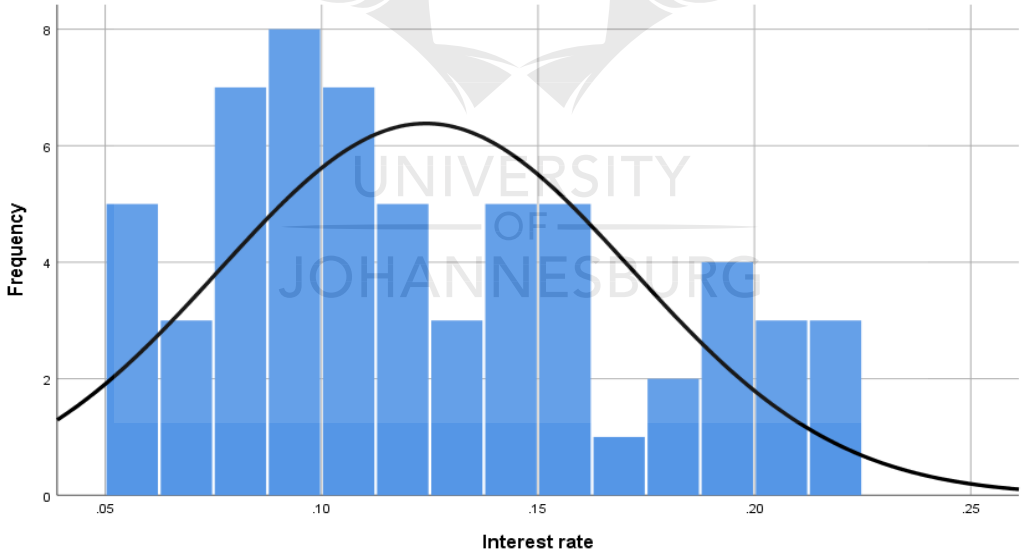

Figure 6-4: Probability distribution fitted to past data on interest rate

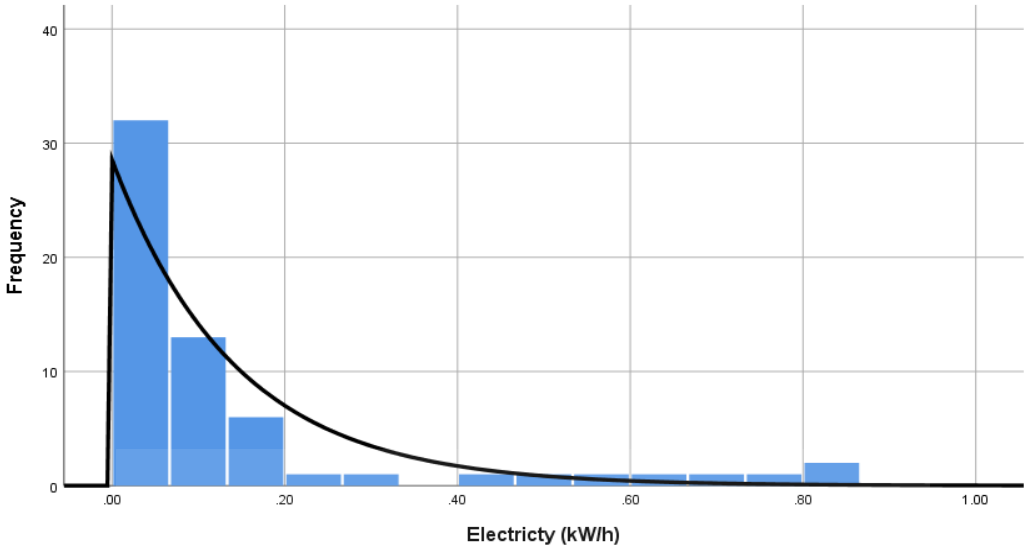

Figure 6-5: Probability distribution fitted to past data on electricity prices.

Various forecasting methods exists for forecasting of time series data. Among them are ARIMA and exponential smoothing models from innovation state space (ETS) (Panigrahi, and Behera, 2017). ETS has some advantages over ARIMA as it can deal with both linear and non-linear patterns in the data and data does not need to be stationary (Kantas, *et al*., 2009) However forecasts are made on weighted averages of past observations. The latest observations are given exponentially more weight than past observations which can influence the forecasting accuracy of the models (Panigrahi and Behera, 2017). Both models were fit to historical data and compared, before the chosen models were used for forecasting.

In order for ARIMA models to be used, the series needs to be stationary. A stationary series does not have a trend i.e. the mean and variance do not change over time. In order to test the stationarity of the historical data the Augmented Dickey Fuller (ADF) test was used with a critical threshold of 0.05, and with a null hypothesis (H0) of non-stationarity of the variable (Aduda *et al*., 2016; Ifa and Guetat, 2018). Therefore, for p-values < 0.05 the data is stationary, otherwise it is non-stationary. Table 6-2 shows the results of the ADF test for the stochastic variables. The p-value for all the variables $r_i(t)$, $r_f(t)$, and $\varepsilon(t)$ was > 0.05 therefore the null hypothesis was accepted, and the variables were not stationary.

Table 6-2: ADF to test for stationary variables

Augmented Dickey-Fuller Test	
Variable	p-value
Inflation	0.99
Interest rate	0.8385
Electricity	0.9002

The variables needed to be differenced in order to make them stationary. The natural logarithmic transformation was taken for historical values of inflation, interest rate and electricity (Jakaša *et al*., 2011). After transforming inflation and interest data were still not stationary so differencing was used (Jakaša *et al*., 2011; Loutatidou *et al*., 2014). In order to obtain the terms of the ARIMA model, p was determined from PACF plot and q was determined from ACF plot after finding d. The d term of (p,d,q) was dependent on the degree of differencing for each time series. Figure 6-6(a) showed the autocorrelation (ACF) for inflation after applying the natural log transform and differencing twice, Figure 6-6(b) showed the autocorrelation (ACF) after differencing for interest rate and log-transform for interest rate. Electricity was differenced once to make it stationary as shown in Figure 6-6(c). The q term was found from the ACF after differencing (Aduda *et al*., 2016). For inflation q=2, for interest rate and q=0, and for electricity q=1. These estimates for p, d, q were compared with other common ARIMA models.

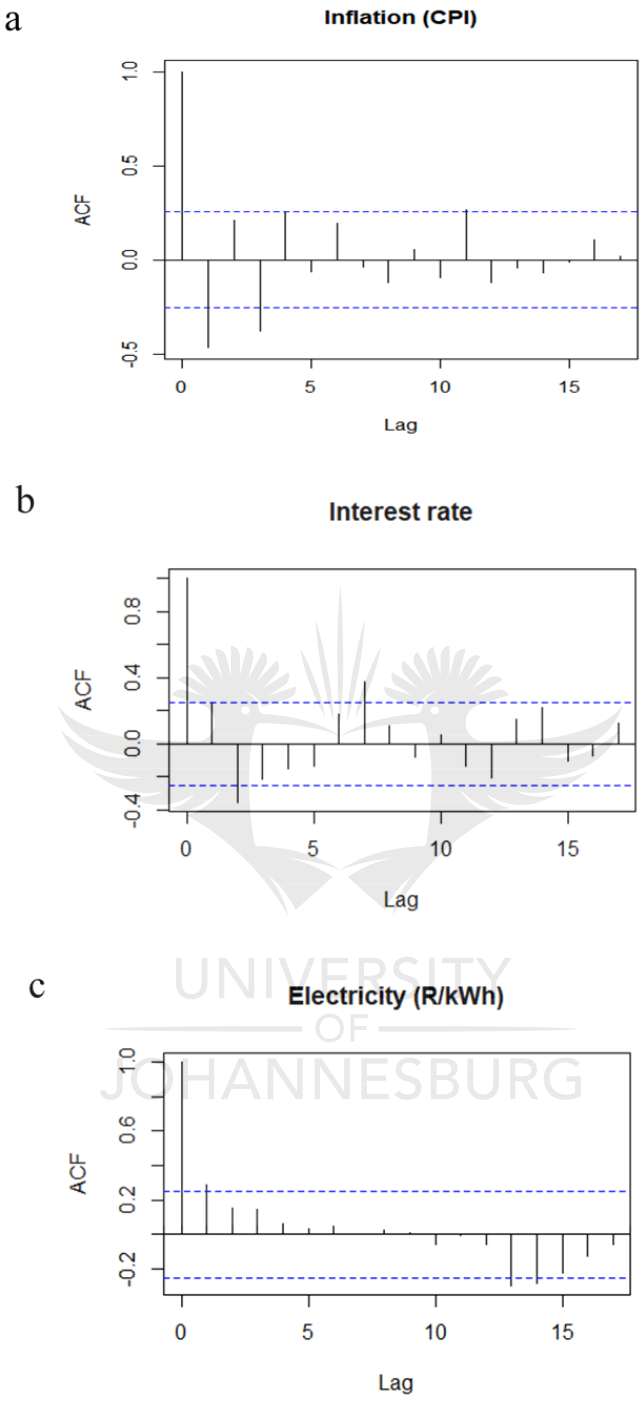

Figure 6-6: Auto correlation of (a) inflation, (b) interest rate and (c) electricity price

Once the data was made stationary by differencing, the partial autocorrelation (PACF) was used to determine the value of p. PACF significant spike at lag 0 for all stochastic variables as shown in Figure 6-7(a),(b) and(c), therefore p was set equal to 0 for ARIMA models.

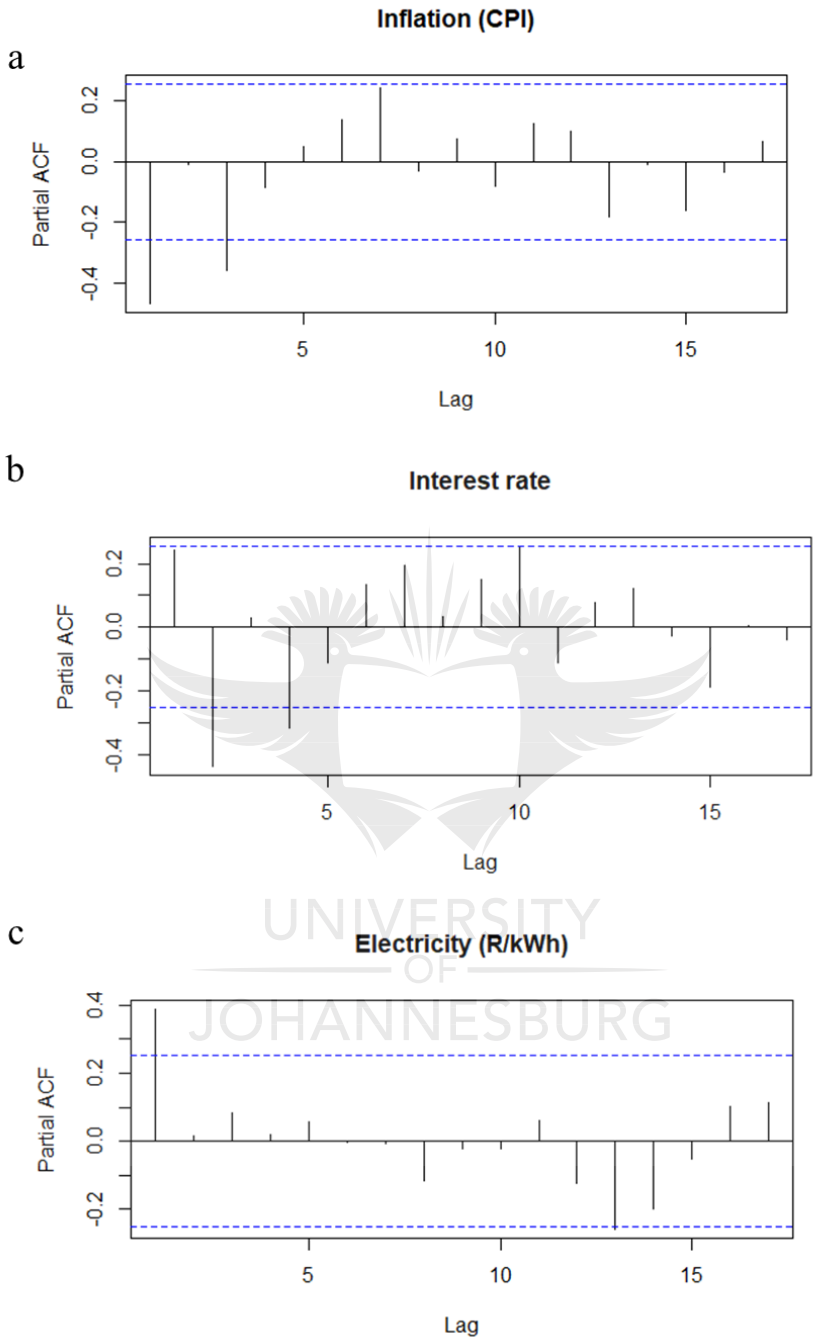

Figure 6-7: Partial auto-correlation of (a) inflation (b) interest rate and (c) electricity price

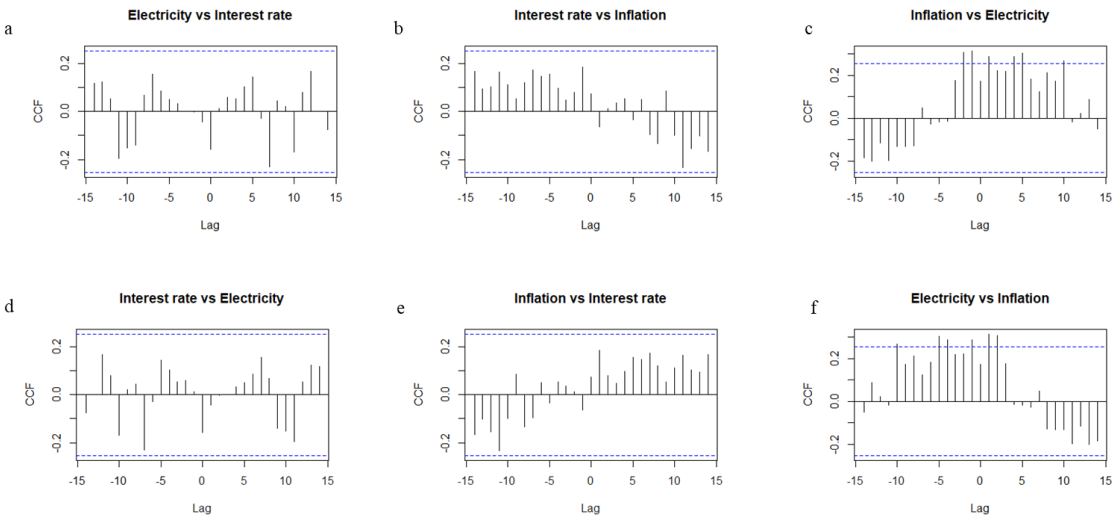

Figure 6-8: Cross-correlation of (a) electricity price and interest rate, (b) interest rate and inflation and (c) inflation and electricity price, (d), (e) and (f) are the inverse of (a), (b) and (c) respectively.

The most commonly used ARIMA models: random walk model (0,1,0), differenced 1st order model (1,1,0) (Ismail *et al*., 2016), simple exponential smoothing (0,1,1), linear exponential smoothing (0,2,1), dampened trend linear exponential smoothing (1,1,2), linear exponential smoothing without dampened trend (0,1,2) (Ismail *et al*., 2016), were compared to the ETS model as shown in Table 6-3 and the most appropriate model was selected for each variable considering the RMSE, MAPE, MAE for ARIMA and ETS.

Table 6-3: Model fit comparison for ARIMA and ETS

	Inflation			Interest rate			Electricity		
	RMSE	MAE	MAPE	RMSE	MAE	MAPE	RMSE	MAE	MAPE
ARIMA (0,1,0)	0,011	0,007	3,054	0,029	0,017	12,527	0,027	0,013	6,003
ARIMA (0,1,1)	0,011	0,007	2,994	0,016	0,009	6,237	0,019	0,010	5,453
ARIMA (1,1,0)	0,012	0,007	2,360	0,010	0,006	2,351	0,011	0,007	2,994
ARIMA (1,1,2)	0,009	0,005	1,858	0,009	0,004	0,672	0,009	0,004	0,672
ARIMA (0,2,1)	0,009	0,004	0,672	0,039	0,016	14,085	0,011	0,007	2,033
ARIMA (0,1,2)	0,010	0,006	2,351	0,011	0,007	4,808	0,016	0,009	5,372
ETS(MAN)	0,011	0,006	2,962	0,022	0,015	11,108	0,015	0,008	6,735

The ETS(MAN) and ARIMA models were used to predict values using in-sample forecasting as shown in Figure 6.9. Graphically ETS models were a better fit than ARIMA models. However, it was important to test how well the chosen ETS(MAN) models fit the data (Suleman and Sarpong, 2012). The residuals of the fitted ETS models were examined to determine lack of fit.

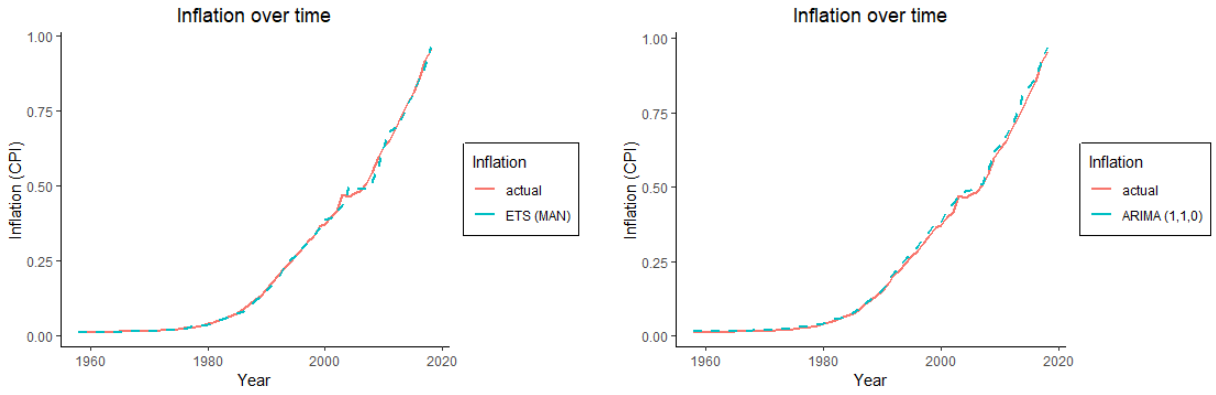

a)

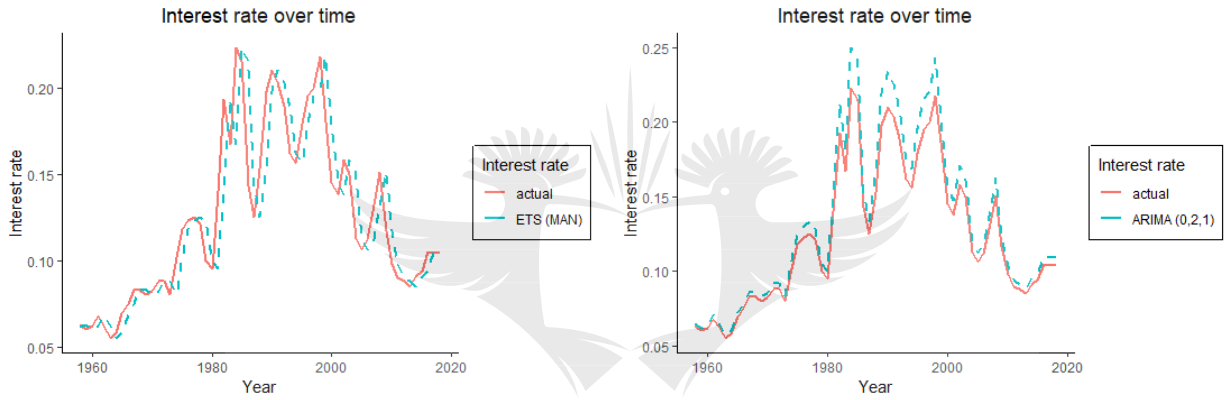

b)

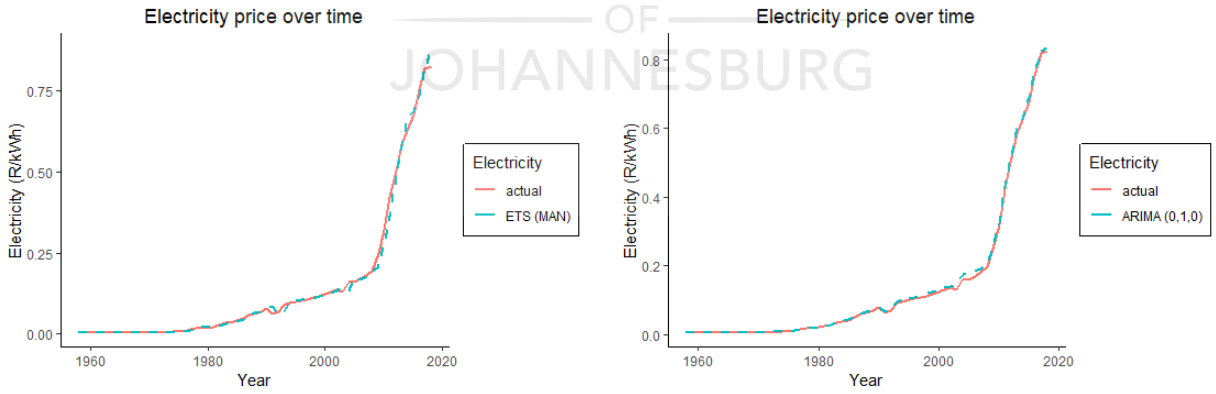

c)

Figure 6-9:Actual values and predicted values from ETS and ARIMA models for a) inflation, b) interest rate and c) electricity prices.

6.7 RESULTS AND DISCUSSION

6.7.1 Statistical analysis of ETS(MAN) time series model

Table 6-4 shows the statistical analysis of the actual values of stochastic variables compared to values predicted by the ETS(MAN) model for inflation, interest rate and electricity price. Minimum, 1st quartile, mean, median, 3rd quartile and maximum values are given for each variable. For all variables, the mean was greater than the median which indicated that values were not normally distributed, and the data was positively skewed (Zhou *et al*., 2019). From the statistical analysis, predicted values were slightly lower than actual values.

Table 6-4: Statistical analysis of economic variables

Parameters	Actual inflation	Predicted inflation	Actual interest rate	Predicted interest rate	Actual electricity price	Predicted electricity price
Min	0.001	0.0108	0.055	0.055	0.005	0.005
Q1	0.018	0.0177	0.088	0.085	0.006	0.006
Median	0.118	0.115	0.113	0.114	0.063	0.062
Mean	0.253	0.251	0.124	0.123	0.143	0.140
Q3	0.463	0.433	0.156	0.1156	0.138	0.134
Max	0.957	0.963	0.223	0.223	0.825	0.883

Before the models could be used to predict future values, the residuals of the fitted data were examined using the Ljung-Box (LB) test with lag of 15. The result of the LB test on the residuals was shown in Table 6-6. The p-value of inflation was 0.297, interest rate was 0.016 and for electricity price was 0.928. P-values for inflation and electricity were >0.05 indicating the residuals were not autocorrelated (Aduda *et al*., 2016). Results of the LB test were further supported by ACF of the residuals as shown in Figure 6-10.

Table 6-5: Box-Ljung test on residuals

Box-Ljung test	Inflation residuals	Interest rate residuals	Electricity price residuals (R/kWh)
X-squared	17.378	36.313	7.872
Df	15	15	15
p-value	0.297	0.016	0.928

a)

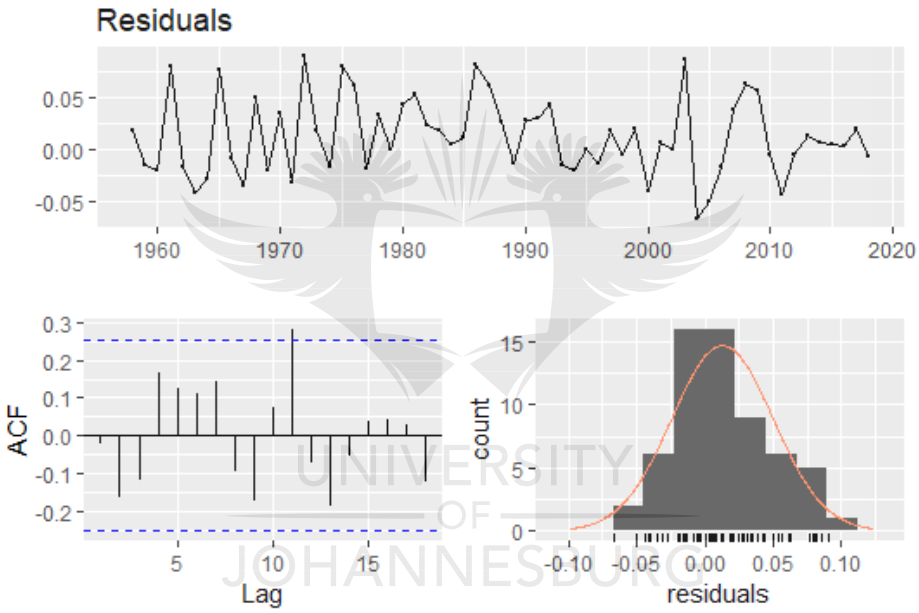

b)

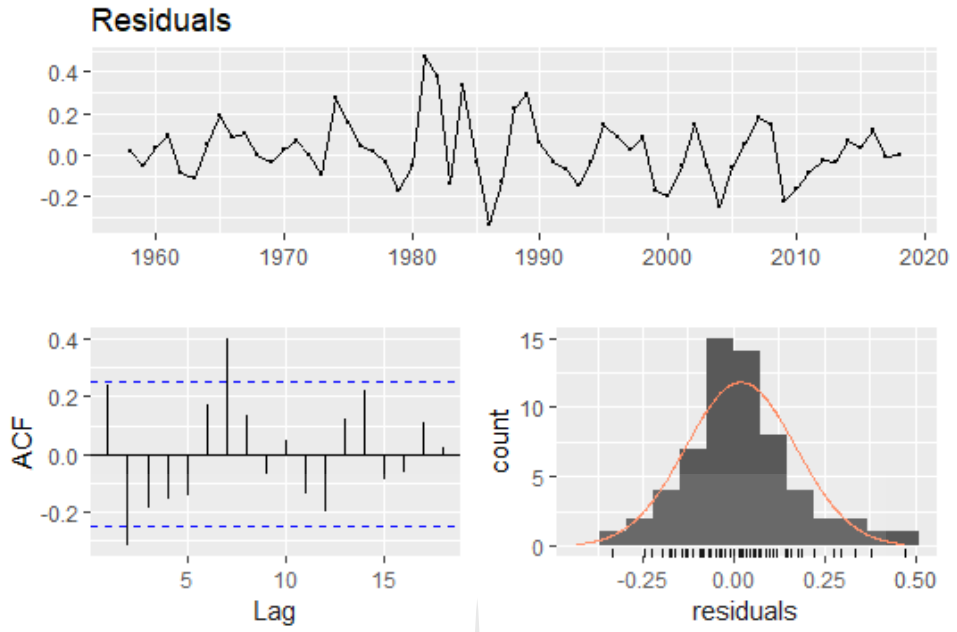

c)

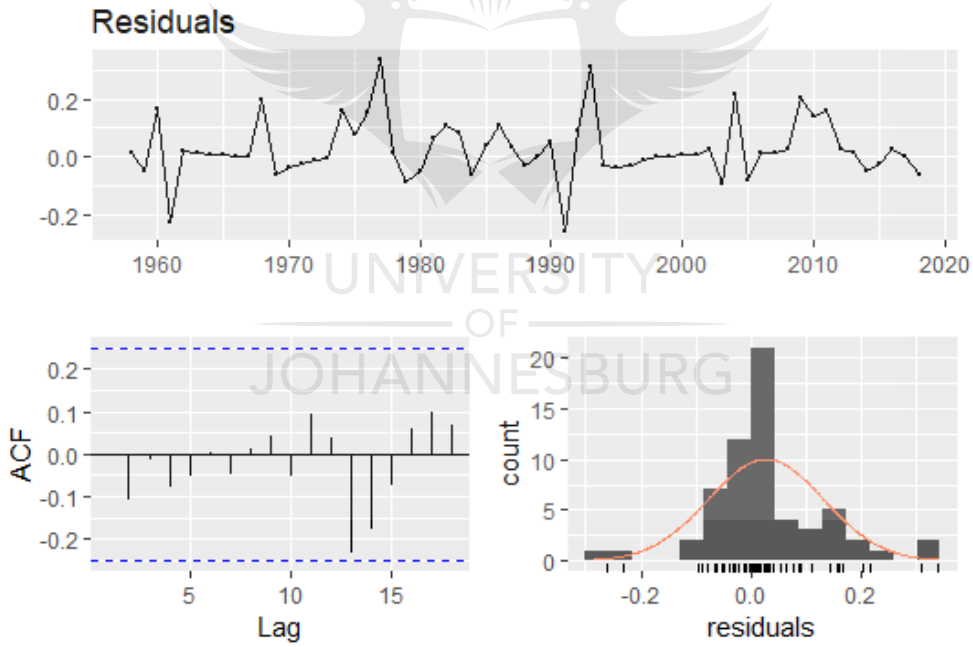

Figure 6-10: ACF, histogram and studentised plot of residuals for fitted models of a) inflation, b) interest rate and c) electricity

The interest rate p-value was <0.05 therefore the residuals were autocorrelated. For this reason, the ETS(MAN) model was not used to fit interest rate. The ARIMA models were re-examined,

since comparison was among models of the same order differencing AIC, and log likelihood was used. The lowest AIC for interest rate was chosen which was ARIMA model (0,1,2). The final fitted models were ETC(MAN) for interest rate, ARIMA (0,1,2) for interest rate and ETC(MAN) for electricity.

ARIMA models	**Inflation**		**Interest rate**		**Electricity**	
	AIC	**log likelihood**	**AIC**	**log likelihood**	**AIC**	**log likelihood**
(0,1,0)	-194.04	98.02	-204.38	98.02	-194.04	98.02
(0,1,1)	123.2	64.6	-123.5	64.6	-204.4	105.19
(0,2,1)	-80.72	43.36	-80.76	43.36	-80.72	43.36
(0,1,2)	-209.5	109.75	-219.42	116.71	-133.1	71.59

Figure 6-11 shows the historical values shown by the blue line and values predicted by the model are shown by the red dotted lines Figure 6.11 (a)-(c). It can be observed from the model that inflation and electricity price continue to increase over time as expected while interest rate follows the pattern of historical data by fluctuating over time.

a)

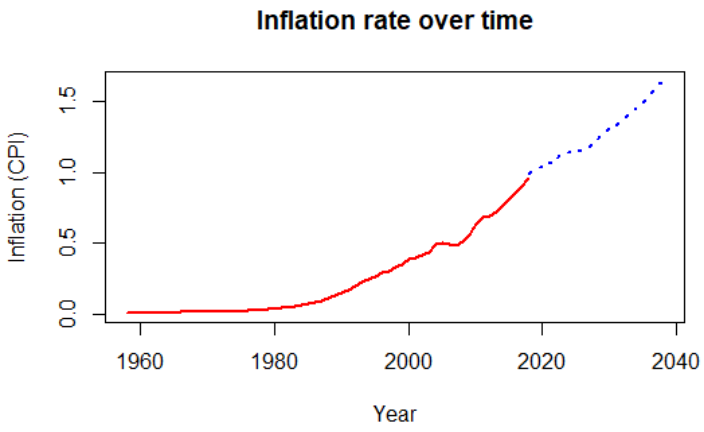

b)

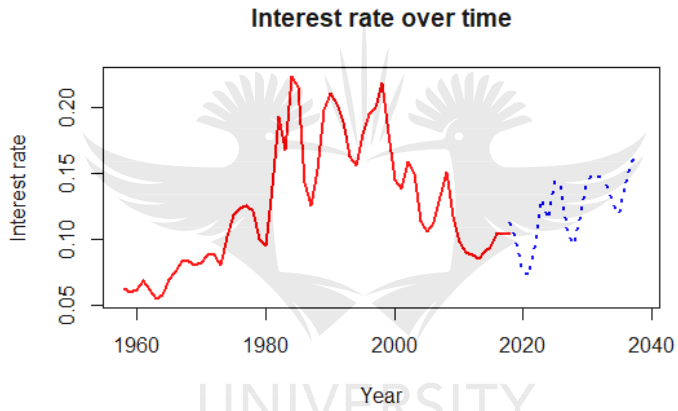

c)

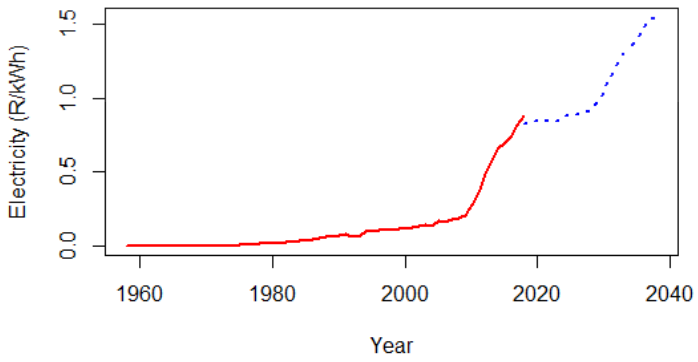

Figure 6-11: Historical values and predicted vales of (a) inflation, (b) interest rate and (c) electricity price. Predicted values are indicated by the red dotted lines and historical values by the blue solid line.

6.7.2 Cost analysis

Table 6-7 shows the cumulative NPV for SPS and DPS. The NPV was negative for SPS for the first 7 years and for the first 6 years of DPS. SPS had higher investment cost and therefore took longer to reach the break-even point.

Table 6-6: NPV for SPS and DPS

Year	CNPV SPS	CNPV DPS
1	-1.27E+08	-1.27E+08
2	-1.39E+08	-1.35E+08
3	-1.32E+08	-1.24E+08
4	-1.17E+08	-1.04E+08
5	-9.64E+07	-7.82E+07
6	-6.72E+07	-4.52E+07
7	-2.51E+07	1.97E+06
8	4.15E+07	7.63E+07
9	1.62E+08	2.11E+08
10	2.81E+08	3.43E+08
11	3.95E+08	4.70E+08
12	5.03E+08	5.90E+08
13	6.04E+08	7.03E+08
14	6.98E+08	8.07E+08
15	7.84E+08	9.02E+08
16	8.62E+08	9.89E+08
17	9.33E+08	1.07E+09
18	9.97E+08	1.14E+09
19	1.05E+09	1.20E+09
20	1.11E+09	1.26E+09

Figure 6-12 shows the cumulative NPV for the deterministic approach (i.e. the means of from the fitted probability distribution) for SPS and DPS simulated in Chapter 5. In both cases the project is only profitable after 7 years based on CNPV>0, due to the high investment costs of

R107 Million for DPS R115 Million for SPS. Also, for the DPS, the CNPV after 20 years R126 Billion is higher than for SPS 111 Billion.

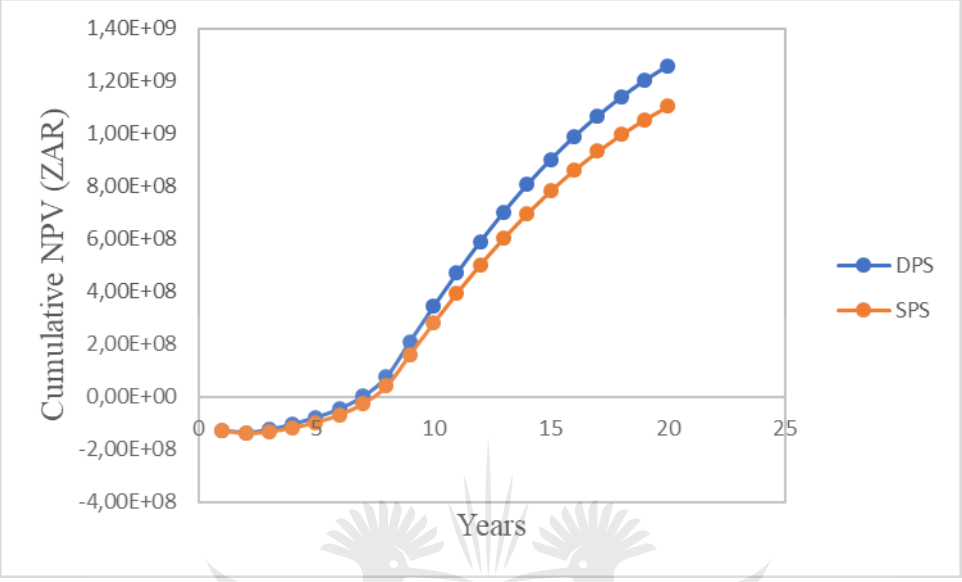

Figure 6-12: Cumulative NPV for SPS and DPS based on deterministic approach

A huge contributing factor to the difference in NPV was the energy cost. As energy requirement for pumping of the feed stream increases so does the energy cost which increases the unit production cost (UC). The unit production cost was the sum of the capital cost depreciated over the plant lifetime and operating cost per m^3 of water treated (Bhojwani *et al*., 2019). As seen in Table 6-8, for SPS, the energy requirement for P01 was estimated at 29.321 kWh for a feed of $1000m^3$/day at 20 bar, while for DPS the energy requirement was estimated at 13.889 kWh for P01 at $1000m^3$/day feed and 10 bar and 12.348 kWh at $800m^3$/day feed at 20 bar for P02. Lower operating pressures in the case of DPS also meant that pump maintenance costs are lower at R36761 than for SPS R41081.

Table 6-7: Effect of energy cost on NPV

	Units	SPS	DPS
Energy cost	R/kWh	2.05E+05	1.83E+05
Power requirement	kWh	29.321	26.237
Pump maintenance cost	R	1.45E+06	1.36E+06
Capex	R	6.78E+07	7.27E+07
Opex	R	8.43E+06	9.15E+06
Unit cost	R/100m^3	34.680	31.032
NPV	R	1.11E+09	1.26E+09

6.7.3 Sensitivity analysis

In Section 6.7.2 it was determined that the cost of energy had a major effect on UC of water. However, the electricity price is also expected to have an impact on UC since the energy cost increase with electricity price. Table 6-8 shows the estimated UC for water production for SPS and DPS with the electricity price modelled as stochastic variables for 20 years of operation of the plant. It can be seen that the UC increases over time as the electricity price increases. For SPS the UC is higher than for DPS due to previously mentioned pumping requirements. When considering the Probability density curve for Figure 6-13 (a) there is a 7.2% probability that SPS will exceed the limiting unit cost (LUC) of 26.7 (R/m^3) while for Figure 6.10 (b) there is a 6% probability that DPS will exceed the LUC. SPS exceeds the LUC in the 14th year of operation but by then the investment has been paid off and the revenue is enough to offset production costs. Similarly, with DPS the LUC is reached in the 16th year of operation but is offset by revenue.

Table 6-8: Effect of electricity on Unit cost

Year	Electricity (R/m^3)	Unit cost SPS ($R/100m^3$)	Unit cost DPS ($R/100m^3$)
1	0.821	19.637	17.572
2	0.827	17.697	15.836
3	0.834	17.847	15.970
4	0.843	18.056	16.157
5	0.835	17.875	15.995
6	0.866	18.563	16.611
7	0.866	18.557	16.606
8	0.876	18.778	16.803
9	0.886	19.014	17.014
10	0.902	19.368	17.331
11	0.959	20.640	18.469
12	1.033	22.305	19.959
13	1.141	24.767	22.162
14	1.229	26.759	23.944
15	1.316	28.768	25.743
16	1.361	29.800	26.666
17	1.411	30.984	27.725
18	1.494	32.908	29.447
19	1.562	34.504	30.875
20	1.569	34.680	31.032

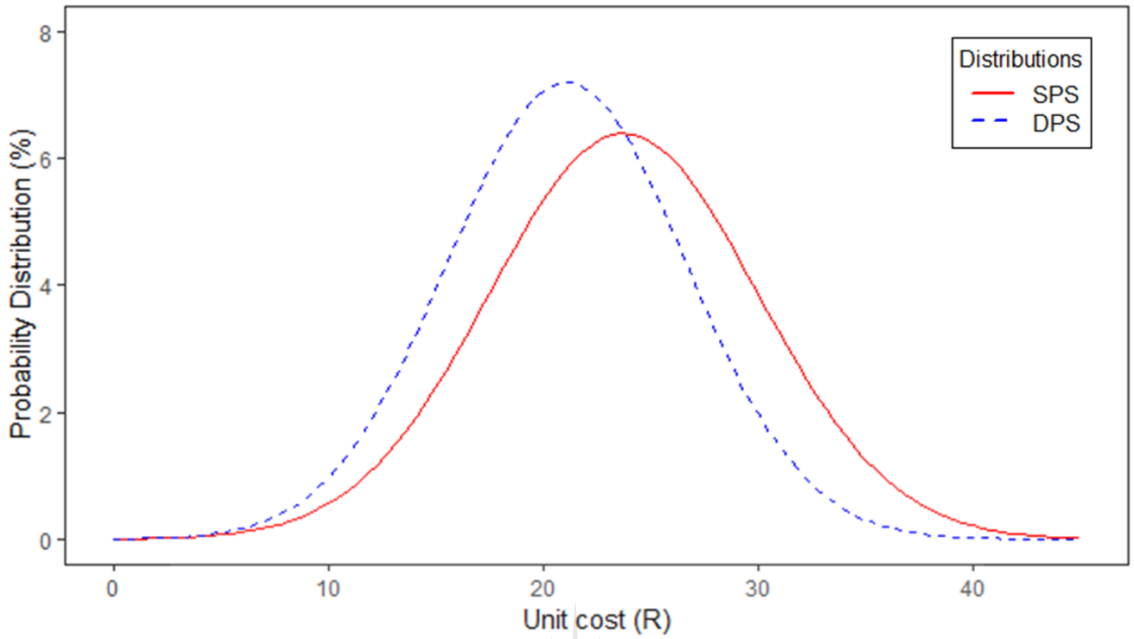

Figure 6-13: Probability of SPS and DPS system to exceed limiting unit cost

The Inflation rate affects the value of money. Inflation rate is often driven up by an increase in the price of goods and services which decreases the value of money and negatively affects profits. Table 6-4 shows the effect of increasing inflation rate on profit for SPS and DPS. As seen from the table the profit decreases year on year as the inflation rate rises. In order for the project to be viable the profit must remain above R108667747 for SPS and above R158237330 for DPS which corresponds to an inflation rate of 5.7% and 6.34% respectively. Although it was previously shown that the that the project is profitable due to positive NPV, the profitability of the project also depends on the strength of the currency (rand to dollar) especially in the case of projects with large investment costs.

Table 6-9: Effect of Inflation on Profit

Year	Profit SPS (R)	Profit DPS (R)	Inflation (%)
1	2.20E+08	2.46E+08	4.348
2	2.18E+08	2.43E+08	4.413
3	2.09E+08	2.34E+08	4.460
4	2.04E+08	2.28E+08	4.624
5	1.84E+08	2.06E+08	4.728
6	1.89E+08	2.11E+08	5.101
7	1.86E+08	2.08E+08	5.017
8	1.84E+08	2.06E+08	5.064
9	1.79E+08	2.00E+08	5.096
10	1.68E+08	1.87E+08	5.205
11	1.52E+08	1.70E+08	5.411
12	1.42E+08	1.58E+08	5.709
13	1.38E+08	1.54E+08	5.909
14	1.28E+08	1.43E+08	5.973
15	1.19E+08	1.33E+08	6.174
16	1.09E+08	1.21E+08	6.342
17	9.78E+07	1.09E+08	6.536
18	8.73E+07	9.75E+07	6.741
19	6.85E+07	7.65E+07	6.942
20	5.88E+07	6.56E+07	7.299

Table 6-11 shows the effect of pressure and the number of modules on energy cost for SPS. As the pressure increases, the number of modules decreases as less membrane area is required to achieve the required flux and rejection. The relation of membrane modules to pressure was determined by the simulation in Chapter 5. Figure 6-12 shows the energy cost in relation to the feed pressure and number of modules required. The balance between pressure and number of modules is at the intersection point of 16.3 bar and 165 modules the energy cost is R59405.

However, based on Chapter 5 the optimum feed pressure was determined to be 20 bar which corresponds to a reduction in number of modules but a higher energy cost of R104972. The difference in pressure is only 3,7 bar but the difference in cost is R45567 and a 16.7% increase in OPEX. A possible solution is to keep feed pressure at 20 bar with number of modules at 100 and consider a government subsidy to cover the cost.

Table 6-10: Pressure, number of modules and energy cost values

Pressure (bar)	**Number of modules**	**Cenergy (R)**
5	235	11167
10	193	27195
15	182	43258
20	100	104972

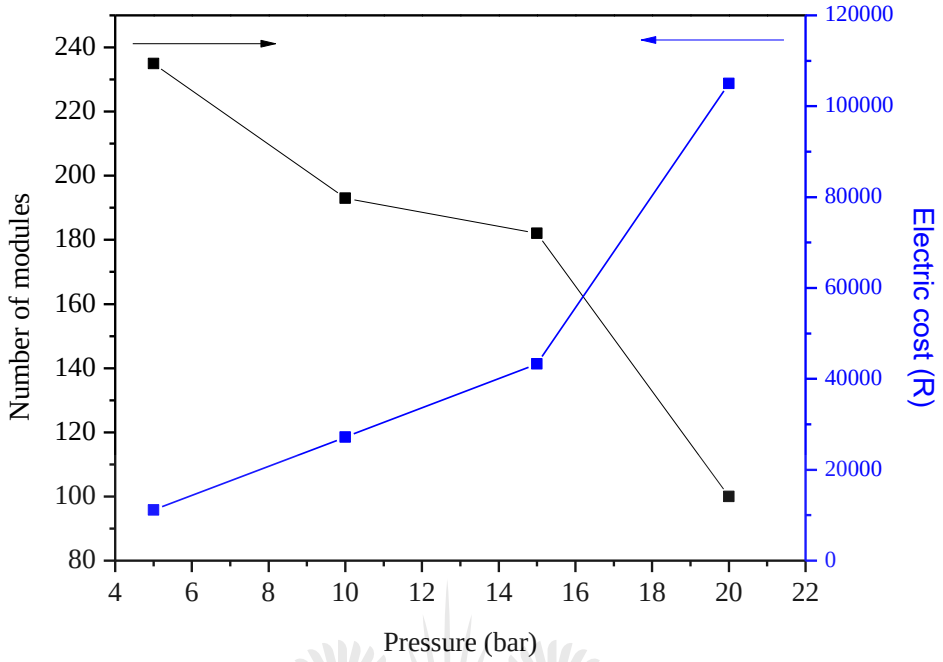

Figure 6-14: Effect of pressure on number of modules and electricity cost

Market growth rate can potentially affect NPV (Shaffie and Jaaman, 2016) According to BCC Research LLC (2014), the global market for nanofiltration membranes was set to grow by 15.6% from 2014 to 2019, while it was estimated that by 2025 the market would have grown by 5.3%. The global market for spiral wound membranes was expected to have a cumulative annual growth rate (CAGR) of 10.9% (Grand view research, 2020). Using these estimates growth rate with a maximum of 5%, mean of 3.5%, a minimum of 2% and a standard deviation of 0.55% was assumed. The growth rate was simulated using triangular distribution (da Silva Pereira *et al.*, 2014). NPV, IRR Profitability index (PI) and payback period are some of the most important capital budgeting techniques used (Hall and Millard, 2010). An IRR <10% is favorable while a profitability index <1 indicates that a project is economically viable (Abdallah *et al.*, 2018). Table 6-11 shows the results for sensitivity analysis on growth rate. As seen from the table NPV IRR Profitability index and Payback period increases with an increase in growth rate for both SPS and DPS. Growth rate had a positive effect on all indicators accept payback period which increased with an increase in growth rate although the payback period for all cases was still lower than for the deterministic approach.

Table 6-11: Simulation for 5000 iterations of min (2%), most likely (3.5%) and maximum (5%) cases of growth rate

SPS					
2%		**3.5%**		**5%**	
NPV	6.81E+08	NPV	8E+08	NPV	8.9E+09
IRR	67%	IRR	68.16%	IRR	70.13%
PI	6.89	PI	7.59	PI	8.71
Payback	0.93	Payback	1.05	Payback	1.21

DPS					
2%		**3.5%**		**5%**	
NPV	1.03E+09	NPV	9E+08	NPV	1E+09
IRR	80.20%	IRR	79%	IRR	80.05%
PI	9.89	PI	8.95	PI	10.13
Payback	0.85	Payback	0.69	Payback	0.90

CAPEX consists of civil engineering costs, mechanical costs, membrane costs and electro-technical costs as seen in Table 6-13 and are expected to be incurred at the beginning of the process. For the TFN membrane plant, the civil engineering and mechanical cost were R1.87E+07 and R17E+06 respectively. for DPS and R1.82E+07 and R6.96E+06 for SPS. DPS civil and mechanical costs were higher due to the extra space and building material, piping and connections that was needed for the DPS. OPEX for SPS (R8.43E+06**)** was compared to that of DPS (R9.15E+06**)** and OPEX of DPS were found to be higher. Due to lower operating pressure, the membranes for DPS do not need to be replaced as frequently therefore membrane costs are lower. The chemical costs for SPS were higher as the membrane needed to be cleaned more frequently than DPS assuming a membrane lifespan of 5 years. Maintenance, quality control and installation costs were taken as 2% of the total investment cost for both SPS and DPS. The NPV for both SPS (R1.11E+09) and DPS (R1.26E+09) was positive after 20 years despite the high investment cost. It was previously determined in section 6.7.3 that the price of electricity

affects the UC of water. An increase in the price of electricity over 20 years from R0.821/m^3 to R1.569/m^3 led to an increase in UC of R31.032 per 100m^3 water produced for SPS and R34.680 per 100m^3 water produced for DPS. Inflation was shown to have a negative effect on profit. Over the plant lifetime, as inflation increased from 4.348% to 7.299%, profit decreased from R2.20E+08 to R6.56E+07 for SPS and from R2.46E+08 to R5.88E+07 for DPS. When comparing the growth rate of NF/RO markets, an increase in growth rate from 2% to 5% was shown to slightly increase the payback period. However, compared to the deterministic approach, growth rate was shown have a positive impact on payback period. For a growth rate of 5% the payback period was reduced from 6 years to 0.90 years for SPS and from 7.2 years to 1.21 years for DPS.

Table 6-12: Summary of key economic indicators for over plant lifetime of 20 years

	DPS		SPS
CAPEX (R)	**7.27E+07**	**CAPEX (R)**	**6.78E+07**
Ccivil (R)	1.87E+07	Ccivil (R)	1.82E+07
Cmechanical (R)	7.17E+06	Cmechanical (R)	6.96E+06
Ctelectro (R)	4.57E+07	Ctelectro (R)	4.08E+07
Cmembrane (R)	1.84E+06	Cmembrane (R)	2.12E+06
OPEX (R)	**9.15E+06**	**OPEX**	**8.43E+06**
Depreciation (R)	4.49E+06	Depreciation (R)	4.16E+06
Cenergy (R)	6.33E+06	Cenergy (R)	6.28E+06
Cchemical (R)	4.24E+04	Cchemical (R)	4.88E+04
Cmaintainace (R)	1.45E+06	Cmaintainace (R)	1.36E+06
Cquality (R)	1.45E+06	Cquality (R)	1.36E+06
Cinstallation (R)	1.45E+06	Cinstallation (R)	1.36E+06
Total investment Cost (R)	1.15E+08	Total investment Cost (R)	1.08E+08
NPV (R)	1.26E+09	NPV (R)	1.11E+09
UC (R/100 m^3)	34.680	UC (R/100 m^3)	31.032
electricity price (R/kWh)	1.569	electricity price (R/kWh)	1.569
Inflation (%)	7.299	Inflation (%)	7.299
Profit (R)	5.88E+07	Profit (R)	6.56E+07
Growth rate (%)	5	Growth rate (%)	5
Payback period (years)	1.21	Payback period (years)	0.90

Electro technical costs (ETC) (energy supply, process control engineering and plant automation) contributed to 60% of the capital costs for SPS and 62% of the capital costs for DPS as seen in Figure 6-15 (a) and (b). The difference might seem small but it corresponds to a difference of approximately R4.98 Million for 20 years of operation. Although a large portion of the CAPEX is due to the ETC, there are a number of reasons why the cost is justifiable. Since the plant is fully automated, less people are needed in order to run the plant, hence a reduction in labour costs. Labour costs were based were 0.027€/m^3 (Moser *et al.*, 2015). Also, the process conditions can be easily monitored and controlled, and deviations form product specifications can quickly be identified and managed ensuring the quality of water. Plant automation also means that the plant can be seamlessly integrated with PCs and other smart devices so that the plant can be remotely monitored and controlled reducing the risk of work-related injuries and so that plant data is stored in a cloud location for easy access by personnel (Carlsson et al., 2016; Hegazy, and Hefeeda, 2014). Decision making will therefore be easier and more effective if decision makers and employees all have access to plant information from central, interconnected software in agreement with the 4IR (Castro, 2012). Civil chemical and membrane costs made up the other 40% of OPEX for SPS and 38% for DPS. Since these costs were based on 2% of the total investment cost, the percentage distribution for SPS was similar to DPS.

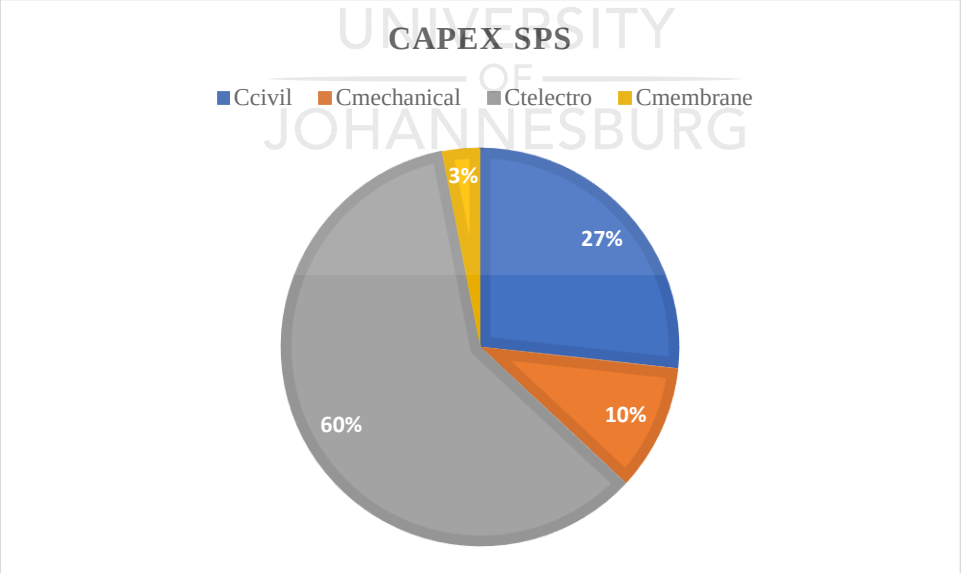

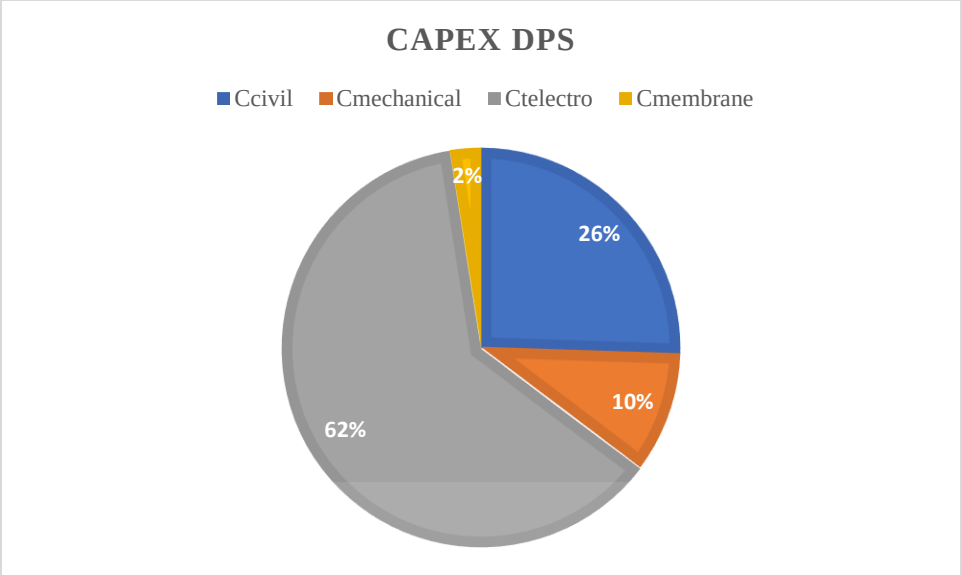

Figure 6-15: Breakdown of CAPEX for a) SPS and b) DPS for plant lifetime of 20 years

Figure 6-16 showed the influence of energy cost, depreciation, installation cost, maintenance cost and quality control costs on OPEX. Energy cost had a significant influence on the OPEX (43%) for SPS and (42%) for DPS and was dependent on both the number of modules and the pressure. In order to run the plant high pressures of up to 20 bar were needed which increased pumping costs and therefore increased energy costs. The OPEX was also largely affected by depreciation. The longer the plant is in operation the more it depreciates. The cost of installation, maintenance and quality control contributed 10% each to the OPEX although installation costs for DPS were slightly higher.

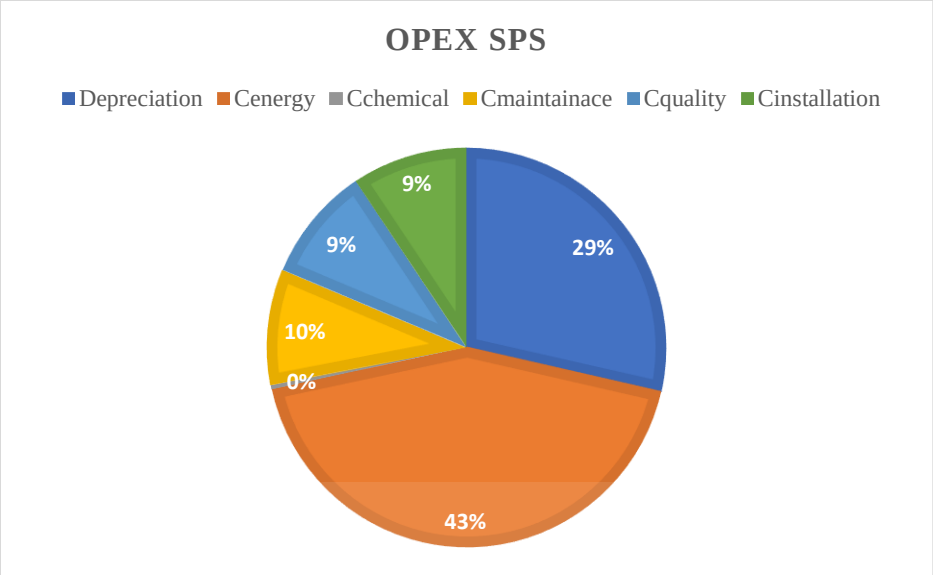

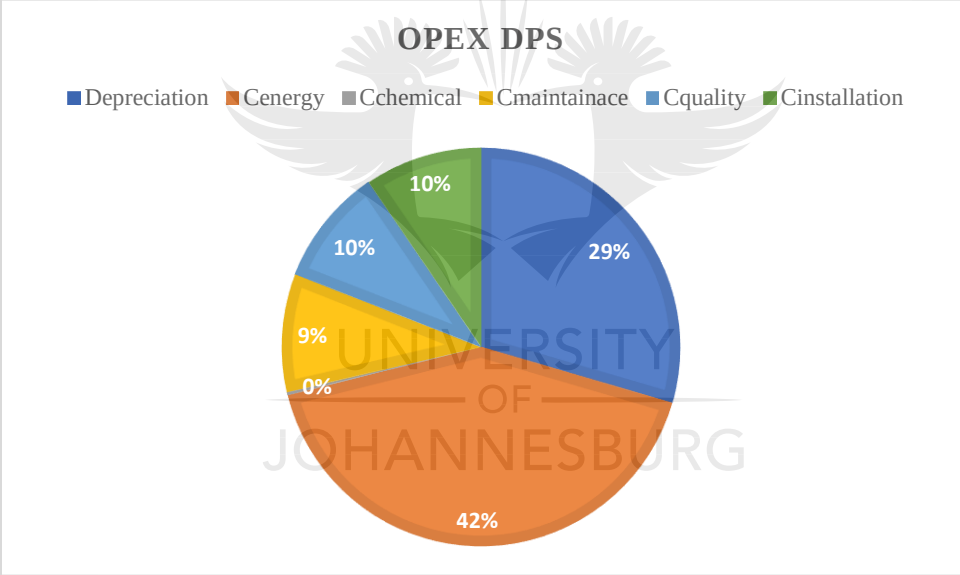

Figure 6-16: Breakdown of CAPEX for a) SPS and b) DPS for plant lifetime of 20 years

6.8 CONCLUSION

Most investment projects are expected to break-even within the 5th year however in this case the break-even point was after 7 years due to the high investment costs of plant automation. Even so, for both SPS and DPS the project was still economically viable due to positive NPV of R1.11E+09 for SPS and R1.26E+09 for DPS after 20 years. Techno-electric costs were shown to amount the bulk of the CAPEX which was found to be R6.78E+07 for SPS and R7.27E+07 for DPS while energy cost accounted for majority of OPEX which was found to be R8.43E+06 for SPS and 9.15E+06 for DPS. The stochastic approach was effective in evaluating risky economic variables such as electricity price and inflation that would have otherwise not been achievable through the deterministic approach. The water production cost per cubic meter was shown increase from R19.637 to R34.680 for SPS and from R17.572 to R31.032 for DPS as the price of electricity increased over the plant lifetime of 20 years. Similarly, inflation was shown to affect the profit of the plant over time. The profit decreased as the inflation increased from R2.2E+08 in the first year to R5.88E+07 by the 20th year for SPS and decreased from R2.46E+08 in the first year to R6.56E +07 by the 20th year for DPS. In addition, a sensitivity analysis on growth rate revealed that the payback period could be reduced by up to 6 years if this variable was included in the stochastic model. For the plant lifetime of 20 years the projected variables allow investors and decision makers to more effectively determine which parameters are most at risk based on cost and investment outcomes.

6.9 REFERENCES

Abdallah, M., Shanableh, A., Shabib, A. and Adghim, M. (2018). Financial feasibility of waste to energy strategies in the United Arab Emirates. *Waste Management,* 82:207-219.

Ali, N., Mohammad, A.W. and Ahmad, A.L. (2005). Use of nanofiltration predictive model for membrane selection and system cost assessment. *Separation and Purification Technology,* 41(1):29-37.

Amigun, B., Petrie, D. and Görgens, J. (2011). Economic risk assessment of advanced process technologies for bioethanol production in South Africa: Monte Carlo analysis. *Renewable Energy,* 36(11):3178-3186.

Arnold, U. and Yildiz, Ö (2015). Economic risk analysis of decentralized renewable energy infrastructures–A Monte Carlo simulation approach. *Renewable Energy,* 77:227-239.

Basile, A. and Nunes, S.P. (2011), 'Economic analysis of membrane use in industrial applications' in *Advanced Membrane Science and Technology for Sustainable Energy and Environmental Applications.* Woodhead Publishing. pp. 91-96.

Batan, L.Y., Graff, G.D. and Bradley, T.H. (2016). Techno-economic and Monte Carlo probabilistic analysis of microalgae biofuel production system. *Bioresource Technology,* 219:45-52.

BCC Research LLC (2014). Global NF membranes market set to reach $445.1 million by 2019. *Membrane Technology,* 2014(10):2-3.

Bhojwani, S., Topolski, K., Mukherjee, R., Sengupta, D. and El-Halwagi, M.M. (2019). Technology review and data analysis for cost assessment of water treatment systems. *Science of the Total Environment,* 651:2749-2761.

Cai, G.Q. (2018). Generation of correlated random variables and stochastic processes. *Probabilistic Engineering Mechanics*, 52:40-46.

Carlsson, O., Pereira, P.P., Eliasson, J., Delsing, J., Ahmad, B., Harrison, R. and Jansson, O., 2016, October. Configuration service in cloud based automation systems. In *IECON 2016-42nd Annual Conference of the IEEE Industrial Electronics Society* (pp. 5238-5245).

Castro, R.E., (2012). *Automation contingency plan for continuity of plant operation* (No. 2012-36-0116). SAE Technical Paper.

Clarke, R. and Low, A. (1993). Risk analysis in project planning: A simple spreadsheet application using Monte-Carlo techniques. *Project Appraisal*, 8(3):141-146.

Contreras, J., Espinola, R., Nogales, F.J. and Conejo, A.J. (2003). ARIMA models to predict next-day electricity prices. *IEEE Transactions on Power Systems*, 18(3):1014-1020.

Da Silva Pereira, Edinaldo José, Pinho, J.T., Galhardo, M.A.B. and Macêdo, W.N. (2014). Methodology of risk analysis by Monte Carlo method applied to power generation with renewable energy. *Renewable Energy*, 69:347-355.

Dehghani, M., Saghafian, B., Nasiri Saleh, F., Farokhnia, A. and Noori, R. (2014). Uncertainty analysis of streamflow drought forecast using artificial neural networks and Monte-Carlo simulation. *International Journal of Climatology*, 34(4):1169-1180.

Elazhar, F., Tahaikt, M., Zouahri, A., Taky, M., Hafsi, M. and Elmidaoui, A. (2013). Defluoridation of moroccan groundwater by nanofiltration and electrodialysis: Performances and cost comparison. *World Applied Science Journal*, 22(6):844-850.

Grand view research, (2020) Spiral Membranes Market Size, Industry Report, 2020-2027. [Accessed 30 January 2021].

Hall, J. and Millard, S. (2010). Capital budgeting practices used by selected listed South African firms. *South African Journal of Economic and Management Sciences,* 13(1):85-97.

Hammersley, J.M. (1960). Monte Carlo methods for solving multivariable problems. *Annals of the New York Academy of Sciences,* 86(3):844-874.

Hastings, W.K. (1970). Monte Carlo sampling methods using Markov chains and their applications. *Biometrika,* 57:97-109.

Hegazy, T. and Hefeeda, M. (2014). Industrial automation as a cloud service. *IEEE Transactions on Parallel and Distributed Systems,* 26(10):2750-2763.

Heo, J., Kim, S., Yeon, W., Lee, H., Lee, B. and Lim, H. (2019). Deterministic and stochastic economic analysis based on historical natural gas and CO2 allowance prices for steam reforming of methanol. *Energy Conversion and Management,* 193:140-148.

Himmelblau, D.M. (1978). *Fault detection and diagnosis in chemical and petrochemical processes.* Elsevier Science Ltd.

Hu, A. and Apblett, A. eds., (2014), *Nanotechnology for water treatment and purification*. Springer: Switzerland. pp. 1-45.

Huang, L., Wang, D., He, C., Pan, M., Zhang, B., Chen, Q. and Ren, J. (2019). Industrial wastewater desalination under uncertainty in coal-chemical eco-industrial parks. *Resources, Conservation and Recycling,* 145:370-378.

Ifa, A. and Guetat, I. (2018). Does public expenditure on education promote Tunisian and Moroccan GDP per capita? ARDL approach. *The Journal of Finance and Data Science,* 4(4):234-246.

Ismail, M.T., Audu, B. and Tumala, M.M. (2016). Comparison of forecasting performance between MODWT-GARCH (1, 1) and MODWT-EGARCH (1, 1) models: Evidence from African stock markets. *The Journal of Finance and Data Science*, 2(4):254-264.

Jakaša,T., Andročec,I. and Sprčić,P. (2011). *2011 8th International Conference on the European Energy Market (EEM).* pp. 222-225.

Jenkins, S., (2020) [Online]. 2019 Chemical Engineering Plant Cost Index. *Business and Economics*, Chemical Engineering Essentials for the CPI professional. Available at: https://www.chemengonline.com/2019-chemical-engineering-plant-cost-index-annual-average/ [Accessed 21 January 2021].

Judd, S.J. (2017). Membrane technology costs and me. *Water Research*, 12:21-9.

Kantas, N., Doucet, A., Singh, S.S. and Maciejowski, J.M. (2009). An overview of sequential Monte Carlo methods for parameter estimation in general state-space models. *IFAC Proceedings Volumes*, 42(10):774-785.

Kardakos, E.G., Alexiadis, M.C., Vagropoulos, S.I., Simoglou, C.K., Biskas, P.N. and Bakirtzis, A.G., (2013), 'Application of time series and artificial neural network models in short-term forecasting of PV power generation'. In *48th International Universities' Power Engineering Conference (UPEC)*, Dublin, Ireland. pp. 1-6. IEEE.

Karlis, A.D. and Papadopoulos, D.P. (2000). A systematic assessment of the technical feasibility and economic viability of small hydroelectric system installations. *Renewable Energy*, 20(2):253-262.

Khashei, M. and Bijari, M. (2010). An artificial neural network (p, d, q) model for timeseries forecasting. *Expert Systems with Applications*, 37(1):479-489.

Lahmiri, S. (2016). A variational mode decomposition approach for analysis and forecasting of economic and financial time series. *Expert Systems with Applications,* 55:268-273.

Lasi, H., Fettke, P., Kemper, H., Feld, T. and Hoffmann, M. (2014). Industry 4.0. *Business and Information Systems Engineering*, 6(4):239-242.

Long, S., Zhao, L., Liu, H., Li, J., Zhou, X., Liu, Y., Qiao, Z., Zhao, Y. and Yang, Y. (2019). A Monte Carlo-based integrated model to optimize the cost and pollution reduction in wastewater treatment processes in a typical comprehensive industrial park in China. *Science of the Total Environment,* 647:1-10.

Loutatidou, S., Chalermthai, B., Marpu, P.R. and Arafat, H.A. (2014). Capital cost estimation of RO plants: GCC countries versus southern Europe. *Desalination*, 347:103-111.

Mellichamp, D.A. (2013). New discounted cash flow method: Estimating plant profitability at the conceptual design level while compensating for business risk/uncertainty. *Computers and Chemical Engineering*, 48:251-263.

Minke, C. and Turek, T. (2015). Economics of vanadium redox flow battery membranes. *Journal of Power Sources*, 286:247-257.

Miralles-Cuevas, S., Oller, I., Agüera, A., Pérez, J.S. and Malato, S. (2017). Strategies for reducing cost by using solar photo-fenton treatment combined with nanofiltration to remove microcontaminants in real municipal effluents: Toxicity and economic assessment. *Chemical Engineering Journal,* 318:161-170.

Mohammad, A.W., Ahmad, A.L. and Hilal, N. (2004). Optimized nanofiltration membranes: Relevance to economic assessment and process performance. *Desalination,* 165:243-250.

Moser, M., Trieb, F., Fichter, T., Kern, J. and Hess, D. (2015). A flexible techno-economic model for the assessment of desalination plants driven by renewable energies. *Desalination and Water Treatment*, 55(11):3091-3105.

Olaru, M., Şandru, M. and Pirnea, I.C. (2014). Monte carlo method application for environmental risks impact assessment in investment projects. *Procedia-Social and Behavioral Sciences,* 109:940-943.

Olatunji, O.A., Orundami, A.O. & Ogundare, O. (2018). Causal relationship between material price fluctuation and project's outturn costs. *Built Environment Project and Asset Management,* 8(4):358-371.

Park, C., Park, P., Mane, P.P., Hyung, H., Gandhi, V., Kim, S. and Kim, J. (2010). Stochastic cost estimation approach for full-scale reverse osmosis desalination plants. *Journal of Membrane Science,* 364(1-2):52-64.

Parmar, K.S. and Bhardwaj, R. (2014). Water quality management using statistical analysis and time-series prediction model. *Applied Water Science*, 4(4):425-434.

Petrasch, R. and Hentschke, R., (2016), 'Process modeling for Industry 4.0 applications: Towards an Industry 4.0 process modeling language and method'. In *13th International Joint Conference on Computer Science and Software Engineering (JCSSE),* Khon Kaen, Thailand, pp. 1-5. IEEE.

Peters, T. (2010). Membrane technology for water treatment. *Chemical Engineering and Technology*, 33(8):1233-1240.

Phanthumchinda, N., Thitiprasert, S., Tanasupawat, S., Assabumrungrat, S. and Thongchul, N. (2018). Process and cost modeling of lactic acid recovery from fermentation broths by membrane-based process. *Process Biochemistry,* 68:205-213.

Pho, K., Ly, S., Ly, S. and Lukusa, T.M. (2019). Comparison among Akaike information criterion, Bayesian information criterion and Yuong's test in model selection: A case study of violated speed regulation in Taiwan. *Journal of Advanced Engineering and Computation,* 3(1):293-303.

Platon, V. and Constantinescu, A. (2014). Monte Carlo method in risk analysis for investment projects. *Procedia Economics and Finance,* 15:393-400.

Rodič, B. (2017). Industry 4.0 and the new simulation modelling paradigm. *Organizacija,* 50(3):193-207.

Santiago J.F.P., Lucero D.J.G., Pantoja J.G. (2017), 'Effect of the Transport Properties on the Design of a Plant and on the Economy of the Sweetening Process of Natural Gas Using Membranes'. In: *Membranes*. Springer: Cham. pp. 125-132.

Sethi, S. and Wiesner, M.R. (2000). Cost modeling and estimation of crossflow membrane filtration processes. *Environmental Engineering Science,* 17(2):61-79.

Shaffie, S.S. and Jaaman, S.H. (2016). Monte Carlo on net present value for capital investment in Malaysia. *Procedia-social and Behavioural Sciences,* 219:688-693.

Shahmansouri, A. and Bellona, C. (2015). Nanofiltration technology in water treatment and reuse: Applications and costs. *Water Science and Technology,* 71(3):309-319.

Shrouf, F., Ordieres, J. and Miragliotta, G., (2014), 'Smart factories in Industry 4.0: A review of the concept and of energy management approached in production based on the Internet of Things paradigm'. In *International Conference on Industrial Engineering and Engineering Management.* Selangor, Malaysia. pp. 697-701.

Sinnott, R., Richardson, J.F. and Coulson, J.M. (2013). *Chemical engineering: An introduction to chemical engineering design* Elsevier.

Stathopoulos, A. and Karlaftis, M.G. (2003). A multivariate state space approach for urban traffic flow modeling and prediction. *Transportation Research Part C: Emerging Technologies,* 11(2):121-135.

Suleman, N. and Sarpong, S. (2012). Empirical approach to modeling and forecasting inflation in Ghana. *Current Research Journal of Economic Theory*, 4(3):83-87.

Tesfasgiorgis, H., Sebola, M., and Muzenda, E. (2015). Economic evaluation of anaerobic digestion technology. *South African Journal of Chemical Engineering,* 20(2):80-90.

Wang, Z., Wang, Y., Xu, G. and Ren, J. (2019). Sustainable desalination process selection: Decision support framework under hybrid information. *Desalination,* 465:44-57.

Van Dorp, J.R. and Duffey, M.R. (1999). Statistical dependence in risk analysis for project networks using Monte Carlo methods. *International Journal of Production Economics,* 58(1):17-29.

Zhou, K., Liu, T. and Zhou, L., (2015), 'Industry 4.0: Towards future industrial opportunities and challenges'. In *12th International conference on fuzzy systems and knowledge discovery (FSKD).* Zhangjiajie, China. pp. 2147-2152).

Zhou, L., Zhao, P., Wu, D., Cheng, C. and Huang, H. (2018). Time series model for forecasting the number of new admission inpatients. *BMC Medical Informatics and Decision Making,* 18(1):1-11.

CONCLUSION AND RECOMMENDATIONS

6.10 CONCLUSION

Membrane based technologies have become one of the most viable solutions to overcome challenges of water demand due to population growth and industrial application. The intensive development and continuous advancement of membrane technology offers substantial improvements in energy recovery systems and cost reduction in water treatment and wastewater processes. One of the objectives of the study was to produce CNT-modified TFN membranes for the treatment of heavy metal ions from AMD. From the study, it was noted that the treatment of synthetic AMD with the TFN membrane led to a significant reduction in heavy metal concentration up to 95%, an increase in flux up to 83% and an increase in pH up to 6.7. Hence the TFN membranes were successful in treating synthetic AMD. From the data collected it was observed that rejection followed the sequence Mg^{2+}>Fe^{3+}>Al^{3+}. Moreover, problems related to the system such as agglomeration of the MWCNTs on the membrane surface were carefully monitored and controlled at lab scale so that they do not affect process optimisation. RSM was used to determine the effect of factors (heavy metal concentration, pressure and MWCNT loading) on operating parameters and to determine the conditions for process optimisation and scale-up.

In order for effective scale-up of the process to occur it was important to reproduce the success of lab scale experiments into commercial or pilot scale through modelling and simulation. Similarity of operating parameters needs to be maintained as process throughput is increased for scale-up for consistent monitoring of process performance. The optimum conditions derived from modelling simulations were for a CNT loading of 0.3% and a pressure of 20 bar for maximum flux and rejection of all three heavy metals in solution. A membrane treatment plant was successfully designed and simulated such number of units needed to achieve product specifications was determined and flux and rejection were predicted. Improvement of the system design was considered by evaluating a SPS and DPS system. The SPS system had a higher energy consumption but higher rejection. Statistical analysis was performed on predicted versus actual values of flux and rejection. The model was 99% accurate in predicting rejection and 98% accurate in predicting flux. Analysis also revealed a linear relationship between experimental

and predicted values that could be used to predict future values given experimental values provided that experiments are performed at 5 to 20 bar.

The capital investment and operating expenditure of the process was considered and parameters affecting the process were modelled as stochastic variables. It was concluded that fouling had profound impact on membrane operating cost, while energy cost and interest rates influenced the profitability of the project as a whole. The cost modelling and analysis revealed that the project would only be economically feasible if energy prices were kept below 1.36 R/kWh for DPS and 1.22R/kWh for SPS while the inflation rate needs to be below 5.7% for SPS and 6.34% for DPS. The NPV was found to be R1.11E+09 for SPS and R1.26E+09 for DPS. The CAPEX and OPEX for SPS were found to be R6.78E+07 and R8.43E+06 while for DPS the CAPEX was R7.27E+07 and OPEX was R9.15E+06.

In conclusion, various aspects of membrane technology need to be considered in order to have a viable process considering lab data, design and economic aspects. Attention should also be given to important parameters for scale-up of the process such that the process is optimised. Thus, a promising membrane-based process was developed that can potentially alleviate water demand.

6.11 RECOMMENDATIONS AND FUTURE WORK

Significant improvement in membrane research and development has made this technology economically viable and attractive for commercial application. There has been considerable focus on modification of membrane materials improvement of hydrophilicity to promote superior water permeability. In addition, factors crucial to the industrial development and application of NF/RO technology including energy efficiency, module configuration and process design, environmental considerations of waste disposal re-use are being explored. Therefore, it is recommended that these parameters be further investigated.

In terms of improving membrane hydrophilicity the developed TFN membrane can be infused with other carbon- based nanomaterials such as graphene oxide (GO), fullerenes and carbon-

based quantum dots to compare the flux, rejection and anti-fouling capabilities to the CNT-TFN membrane that was produced.

Due to their small size, nanoparticles on exposure, can easily penetrate the skin. Airborne nanoparticles can deposit in the lungs and respiratory tract. More research is needed to determine the effects of CNTs and other carbon-based nanomaterials once they enter the human body. However, CNTs have been shown to have biocidal properties. As such, they have the ability to disrupt the cell membrane of microorganisms and block metabolic pathways which leads to the deactivation of microorganisms. However, provided CNTs are well dispersed and properly embedded in the polymer matrix, no leaching of CNTs from the membrane is expected. In addition, when CNTs are treated with acid, metal impurities that are present in the pristine CNT structure are removed. Even so, it is recommended that that toxicity studies be done on the TFC-CNT membranes to ensure that it is not harmful to the end user (mining industry and wastewater treatment plants).

Efforts to mitigate the environmental impact of nanoparticles on the environment is progressing. Therefore, it is recommended that the synthesis of CNTs from green waste materials such fruit peel waste be explored. Additionally, other potential green nano-adsorbents such as the tannin-based metal oxide adsorbents can be combined with CNTs for photodegradation of heavy metal ions. Metal oxides also provide additional functional groups that can enhance membrane performance. Synthetic polymers such as PES also have a negative impact on the environment. Non-toxic and biodegradable materials such as Chitosan can be combined with polymers to develop more environmentally friendly membrane material.

In this study modelling and simulation for plant design was based on mass balances from flux and rejection experimental data. To further improve the robustness of the model it is recommended that studies be conducted over a longer period (3 months or more) after which further characterisation and testing of the membrane can be conducted including SEM to study swelling, asymmetry, void size and morphological changes on the membrane surface. and EDAX to study fouled deposits on the membrane surface. Furthermore, transport properties of the membrane also be incorporated into the model based on collected data. From similar studies

spiral wound membranes proved to have stable flux up to 3 months and only biofouling occurred in the dead-space between the element and the stainless-steel housing Non-corrosive pressure housing elements can be used to avoid this issue.

Scaling is an obstacle in treatment of AMD by membrane processes that has been found to greatly influence the capital investment and operating expenditure. Ultrafiltration is a potential method that can be considered for removal of foulants and scaling prior to treatment with the TFN system.

Process costs in this study were mainly dominated by energy and membrane replacement. The investment cost was greatly affected by equipment cost part of which was the membrane cost. Therefore, it is recommended that a metal recovery post treatment step be considered as part of the process in order to recover some of the heavy metals and reduce cost associated with the process.

Another factor that contributed significantly to membrane costs is space requirements and components used in large scale operation which increased the investment cost and resulted in higher overall cost. Larger size membrane elements are commercially available which offer an increased membrane active layer by increasing the nominal diameter of the membranes. By reducing the footprint and number of piping connections needed, the operational and maintenance costs of the plant can be reduced thereby reducing the total cost.

APPENDIX A1: TEM CHARACTERISATION

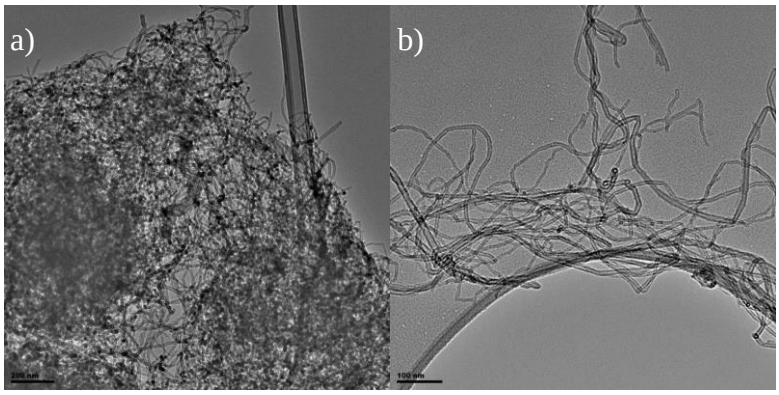

Figure A-0-1: TEM of pristine (a) and oxidised (b) CNTS

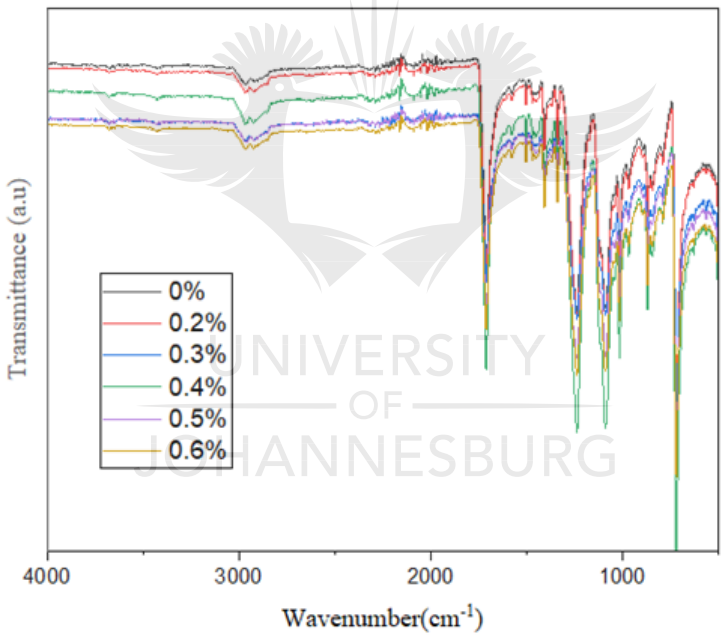

Figure A-0-2: FTIR of TFN membranes at different CNT loadings

a)

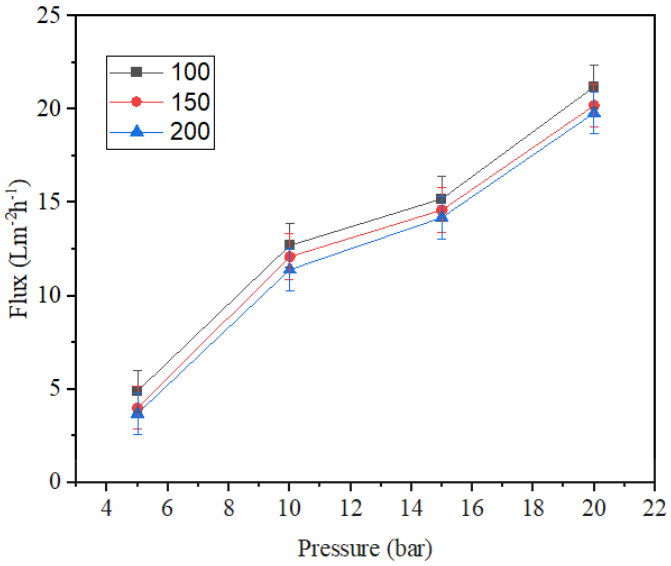

b)

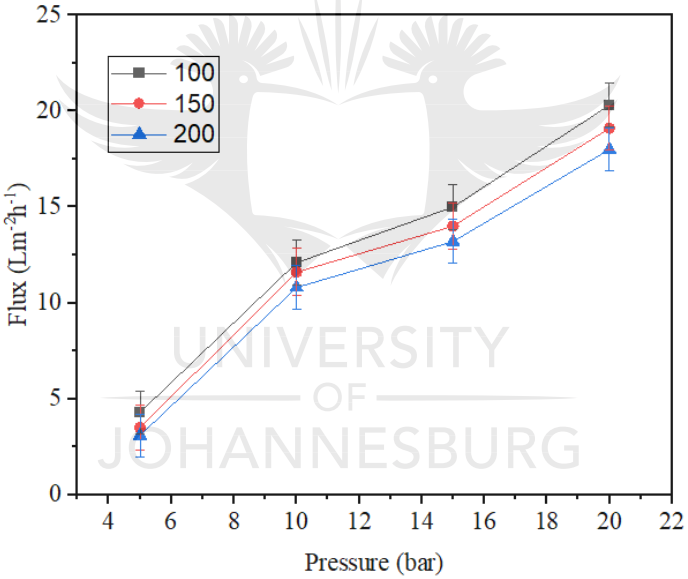

c)

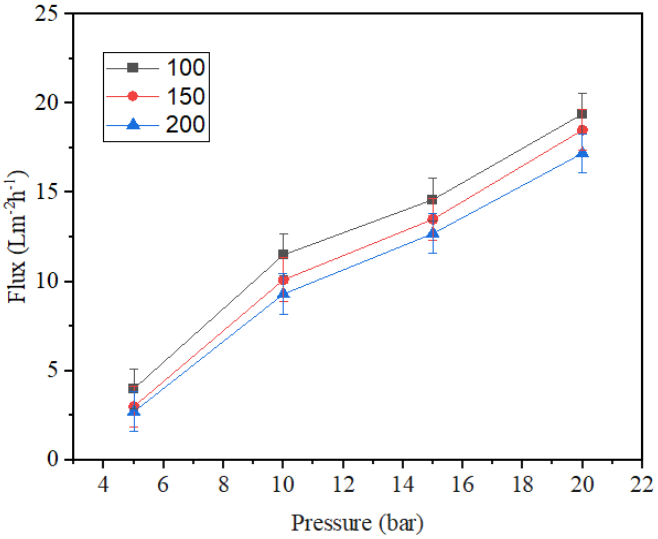

Figure A-0-3: Flux for varying feed concentration of a) $MgSO_4$, b) $Fe_2(SO_4)_3$ and c) $Al_2(SO_4)_3$

a)

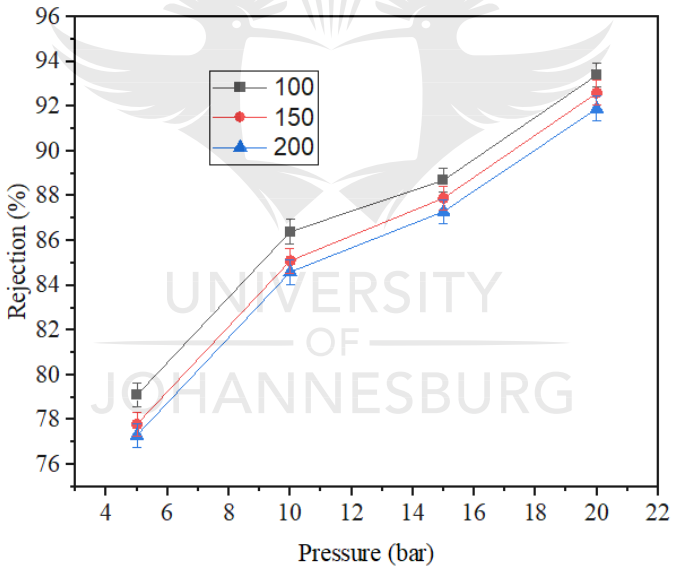

b)

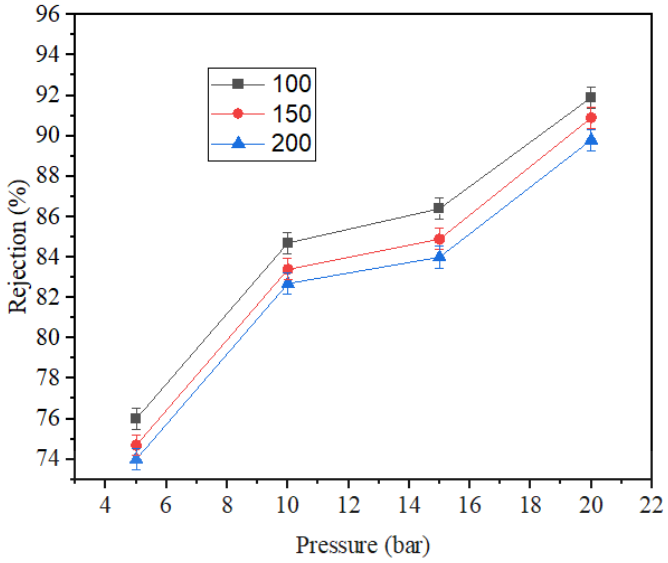

c)

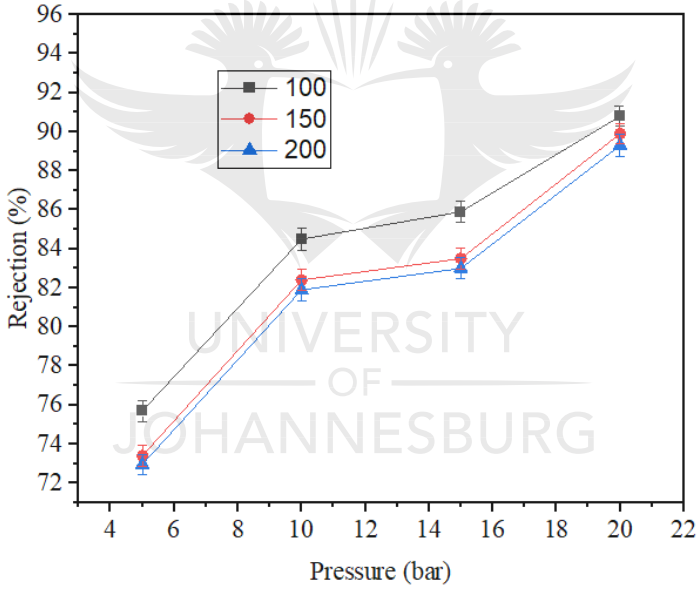

Figure A-0-4: Rejection for varying feed concentration of a) $MgSO_4$, b) $Fe_2(SO_4)_3$ and c) $Al_2(SO_4)_3$

APPENDIX B: RSM model and ANOVA tables

Table B-1: ANOVA for Response Surface Quadratic Model for effects of input parameters Analysis of Variance Table for Al^{3+} response

Source	Nparm	DF	Sum of Squares	F Ratio	Prob > F
Pressure(10,20)	1	1	31.843715	31.8437	0.0300*
CNT loading(0.2,0.4)	1	1	22.686030	22.6860	0.0414*
Fe conc(1000,2000)	1	1	2.401903	2.4019	0.2613
Mg conc(100,200)	1	1	9.703708	9.7037	0.0894
Al conc(100,200)	1	1	30.786527	30.7865	0.0310*
Pressure*Pressure	1	1	13.077516	13.0775	0.0687
Pressure*CNT loading	1	1	12.140137	12.1401	0.0734
CNT loading*CNT loading	1	1	85.766395	85.7664	0.0115*
Pressure*Fe conc	1	1	27.647154	27.6472	0.0343*
CNT loading*Fe conc	1	1	0.232903	0.2329	0.6770
Fe conc*Fe conc	1	1	0.012873	0.0129	0.9200
Pressure*Mg conc	1	1	26.880411	26.8804	0.0352*
CNT loading*Mg conc	1	1	1.288410	1.2884	0.3741
Fe conc*Mg conc	1	1	3.059401	3.0594	0.2224
Mg conc*Mg conc	1	1	7.885483	7.8855	0.1069
Pressure*Al conc	1	1	2.399871	2.3999	0.2615
CNT loading*Al conc	1	1	3.173174	3.1732	0.2168
Fe conc*Al conc	1	1	14.140718	14.1407	0.0640
Mg conc*Al conc	1	1	3.625167	3.6252	0.1972
Al conc*Al conc	1	1	45.670389	45.6704	0.0212*

a)

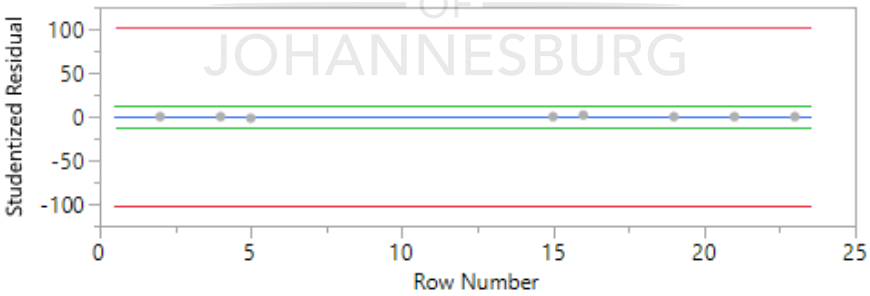

b)

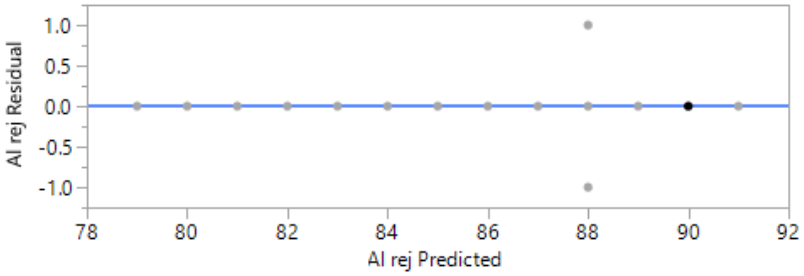

c)

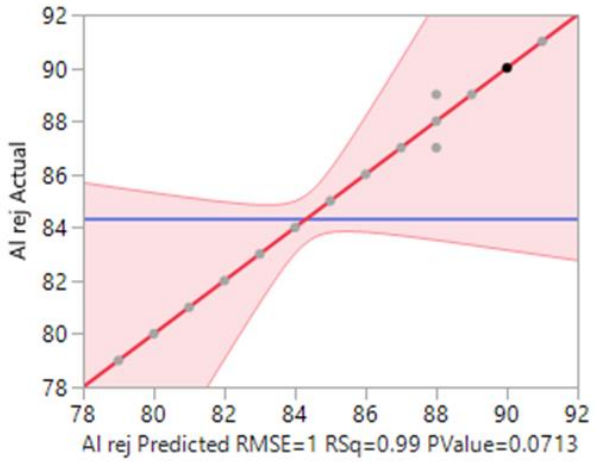

Figure B1: a) Residual, b) Studentised residual and c) Actual vs Predicted values of Al^{3+}rejection

Table B-2: ANOVA for Response Surface Quadratic Model for effects of input parameters

Analysis of Variance Table for Fe^{3+} response

Source	Nparm	DF	Sum of Squares	F Ratio	Prob > F
Pressure(10,20)	1	1	69.38919	208.1676	0.0048*
CNT loading(0.2,0.4)	1	1	2.18613	6.5584	0.1246
Fe conc(1000,2000)	1	1	10.26196	30.7859	0.0310*
Mg conc(100,200)	1	1	12.51551	37.5465	0.0256*
Al conc(100,200)	1	1	133.67024	401.0107	0.0025*
Pressure*Pressure	1	1	1.27516	3.8255	0.1896
Pressure*CNT loading	1	1	1.80173	5.4052	0.1456
CNT loading*CNT loading	1	1	84.24654	252.7396	0.0039*
Pressure*Fe conc	1	1	27.35781	82.0734	0.0120*
CNT loading*Fe conc	1	1	0.73232	2.1970	0.2765
Fe conc*Fe conc	1	1	2.28862	6.8658	0.1200
Pressure*Mg conc	1	1	12.37315	37.1194	0.0259*
CNT loading*Mg conc	1	1	0.07761	0.2328	0.6771
Fe conc*Mg conc	1	1	16.33876	49.0163	0.0198*
Mg conc*Mg conc	1	1	2.31765	6.9529	0.1187
Pressure*Al conc	1	1	6.09680	18.2904	0.0506
CNT loading*Al conc	1	1	0.76166	2.2850	0.2698
Fe conc*Al conc	1	1	8.75800	26.2740	0.0360*
Mg conc*Al conc	1	1	1.52791	4.5837	0.1656
Al conc*Al conc	1	1	18.60847	55.8254	0.0174*

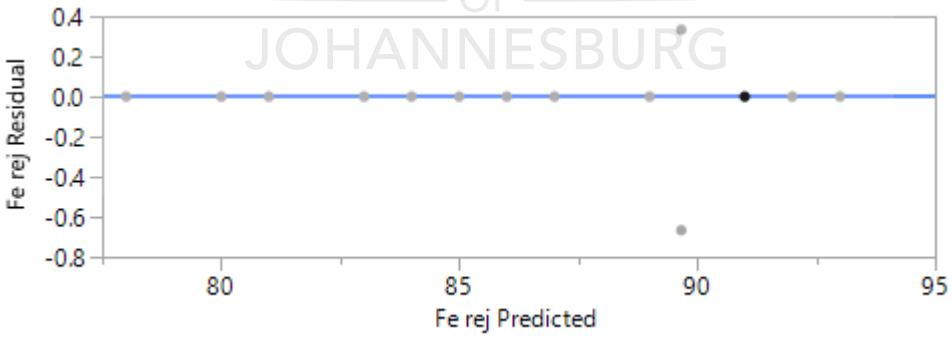

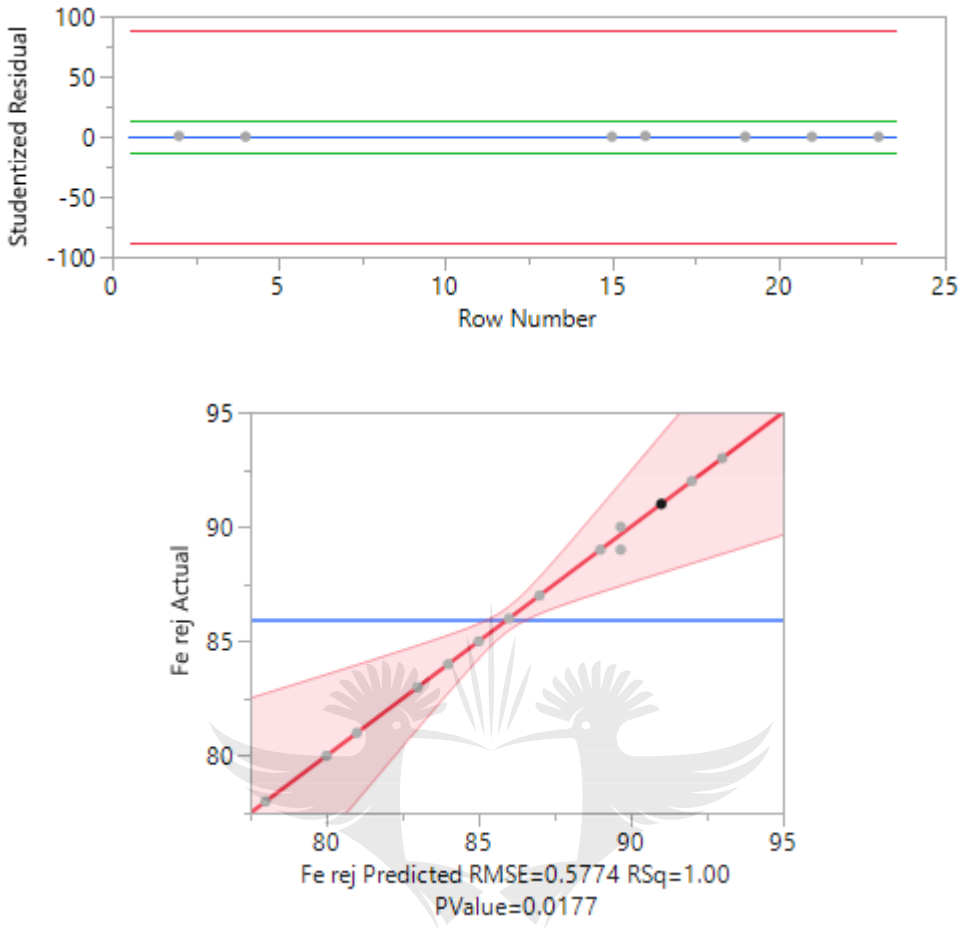

Figure B2: a) Residual, b) Studentised residual and c) Actual vs Predicted values of Fe^{3+}rejection

Table B-3: ANOVA for Response Surface Quadratic Model for effects of input parameters

Analysis of Variance Table for Mg^{2+} response

Source	Nparm	DF	Sum of Squares	F Ratio	Prob > F
Pressure(10,20)	1	1	85.289773	85.2898	0.0115*
CNT loading(0.2,0.4)	1	1	3.541138	3.5411	0.2006
Fe conc(1000,2000)	1	1	1.533542	1.5335	0.3412
Mg conc(100,200)	1	1	42.393121	42.3931	0.0228*
Al conc(100,200)	1	1	68.674032	68.6740	0.0143*
Pressure*Pressure	1	1	1.121284	1.1213	0.4006
Pressure*CNT loading	1	1	3.886563	3.8866	0.1874
CNT loading*CNT loading	1	1	58.632474	58.6325	0.0166*
Pressure*Fe conc	1	1	15.737017	15.7370	0.0581
CNT loading*Fe conc	1	1	1.901073	1.9011	0.3019
Fe conc*Fe conc	1	1	5.566830	5.5668	0.1423
Pressure*Mg conc	1	1	22.647186	22.6472	0.0414*
CNT loading*Mg conc	1	1	0.927380	0.9274	0.4372
Fe conc*Mg conc	1	1	8.188899	8.1889	0.1035
Mg conc*Mg conc	1	1	0.635165	0.6352	0.5090
Pressure*Al conc	1	1	0.257771	0.2578	0.6621
CNT loading*Al conc	1	1	3.495819	3.4958	0.2024
Fe conc*Al conc	1	1	14.465652	14.4657	0.0627
Mg conc*Al conc	1	1	22.729226	22.7292	0.0413*
Al conc*Al conc	1	1	5.280077	5.2801	0.1484

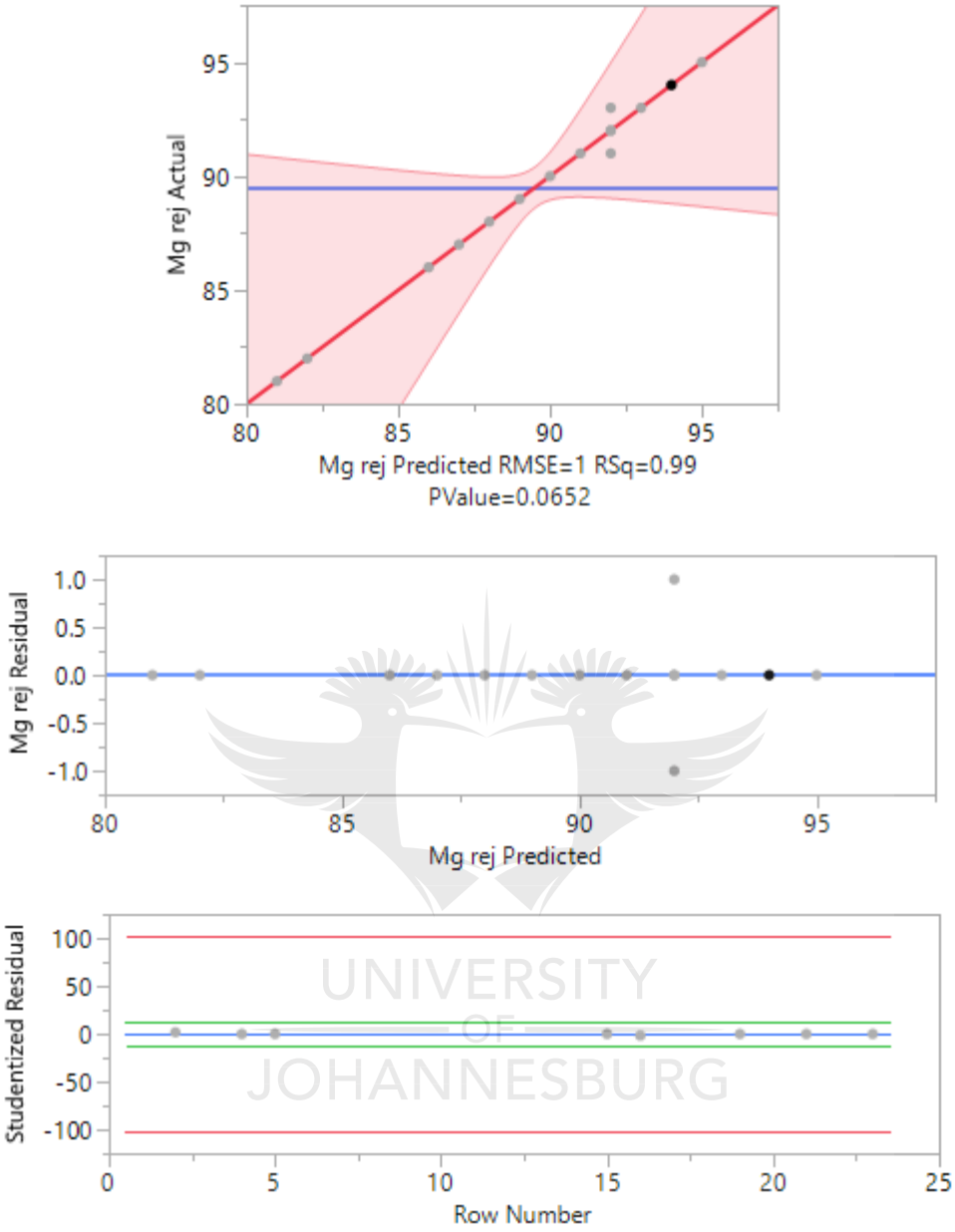

Figure B3: a) Residual, b) Studentised residual and c) Actual vs Predicted values of Mg^{2+}rejection

Table B-4: ANOVA for Response Surface Quadratic Model for effects of input parameters

Analysis of Variance Table for Flux response

Source	Nparm	DF	Sum of Squares	F Ratio	Prob > F
Pressure(10,20)	1	1	9.085422	2.7674	0.1184
CNT loading(0.2,0.4)	1	1	13.418814	4.0873	0.0628
Fe conc(1000,2000)	1	1	14.289846	4.3526	0.0557
Mg conc(100,200)	1	1	40.667807	12.3871	0.0034*
Al conc(100,200)	1	1	37.728824	11.4919	0.0044*
Pressure*Pressure	1	1	18.221036	5.5500	0.0336*
Pressure*Fe conc	1	1	18.655671	5.6824	0.0318*
CNT loading*Fe conc	1	1	13.837012	4.2147	0.0593
Pressure*Mg conc	1	1	16.696472	5.0856	0.0407*
Fe conc*Mg conc	1	1	10.521849	3.2049	0.0951
Pressure*Al conc	1	1	14.346899	4.3700	0.0553
Fe conc*Al conc	1	1	17.344477	5.2830	0.0375*
Al conc*Al conc	1	1	16.834031	5.1275	0.0400*

APPENDIX C1: COST TABLES AND GRAPHS

Table C1: Membrane costing variables

M-01			
Cost Indices		Exchange rate	
2018	2018	USD	ZAR
		$1	R18,4457*
Cost in ZAR,2018		R	92400

*Average dollar exchange rate in 2018

Table C2: Pump costing variables

P-01			
Cost Indices		Exchange rate	
2004	2018	USD	ZAR
		$1	R18,4457*
Power [kW]		2,908	
a		6900	
b		206	
n		0,9	
Cost in ZAR,2018		R	205409,6

P-02			
Cost Indices		Exchange rate	
2004	2018	USD	ZAR
		$1	R18,4457*
Power [kW]		29,321	
a		6900	
b		206	
n		0,9	
Cost in ZAR,2018		R	183806,7

APPENDIX C2: RESULTS OF MONTE CARLO SIMULATION FOR 5000 ITERATIONS

a)

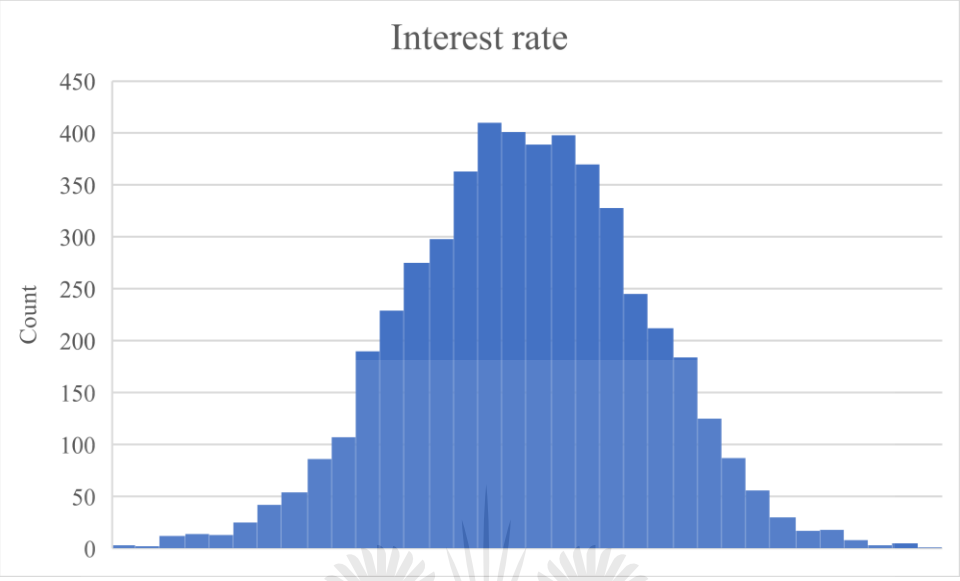

b)

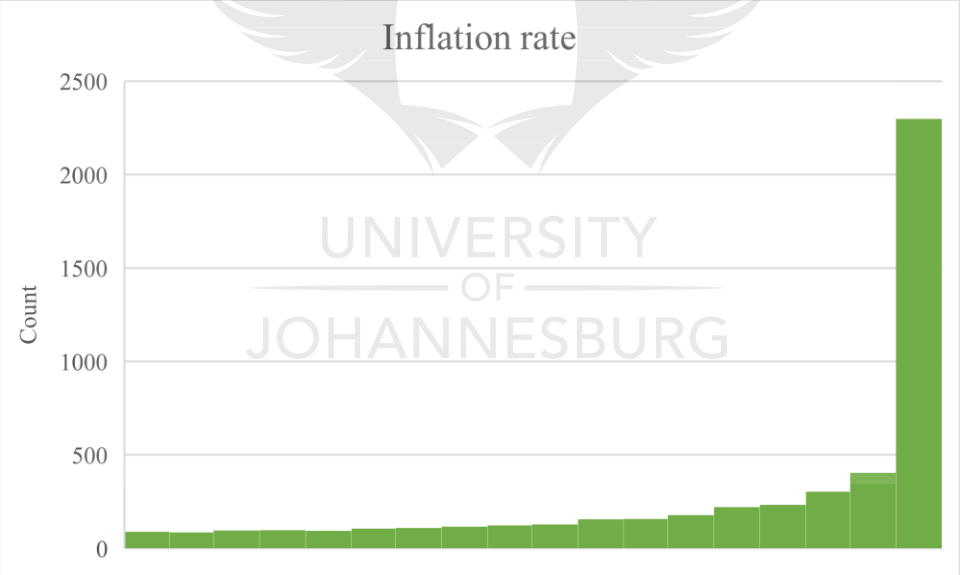

c)

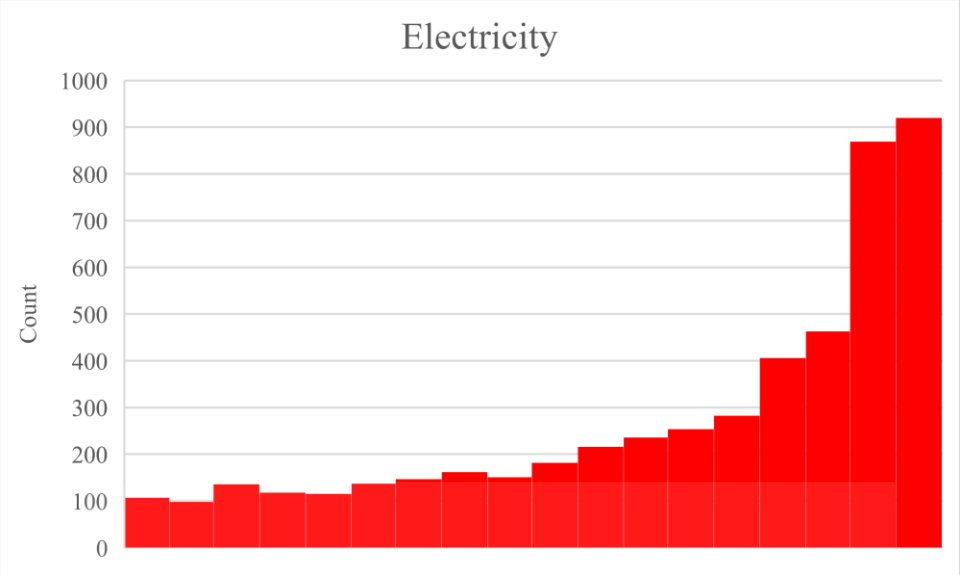

d)

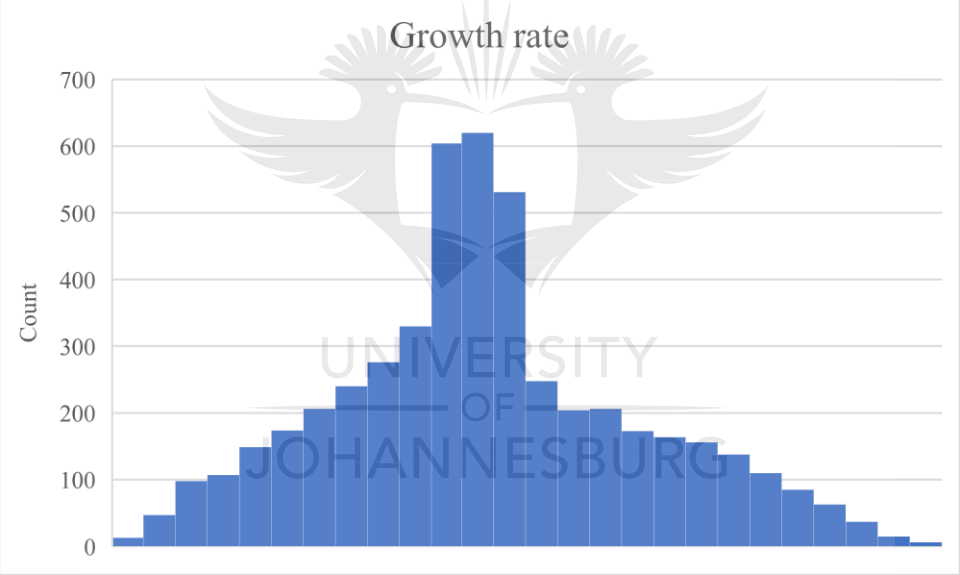

Figure C2: Distributions for a) interest rate, b) Inflation, c) Electricity and d) growth rate

* Interest rate, inflation and electricity were based on probability distributions of historical data while growth rate was based on estimates of compound annual growth rate for Nanofiltration and Reverse Osmosis markets.

APPENDIX D1: SUBMITTED MANUSCRIPT

Manuscript Details

Manuscript number	JPCE_2020_162
Title	Process optimization through Response Surface Methodology for treatment of acid mine drainage using carbon nanotubes-infused thin film nanocomposite membranes
Article type	Full length article

Abstract

The current work illustrates the use of Central Composite Design (CCD) and RSM to gain insight into the effect of five process factors (pressure, MgSO4 concentration, Fe2(SO4)3 concentration, Al2(SO4)3 concentration and CNT loading) on the treatment of synthetic AMD solution with TFN membrane. Performances of polyamide TFN membranes with different multi-walled carbon nanotube (MWCNT) loading were tested to determine optimum loading under different operating conditions. The treatment efficiency was examined in terms of flux and rejection and based on these results and the optimum region from RSM was selected. The five previously mentioned process variables were investigated, and regression models were built, while data on permeate flux behaviour, MgSO4 rejection, Fe2(SO4)3 rejection, and Al2(SO4)3 rejection as the response values were collected. Predicated models were in good agreement with experimental data and the results showed that pressure and CNT loading are the main effects that influence the process. The optimal conditions were a pressure of 20 bars and a CNT loading of 0.3%. Under these conditions, a permeate flux of 83%, 94% MgSO4 rejection, 92% Fe2(SO4)3 rejection, and 89% Al2(SO4)3 rejection have been observed. RSM models demonstrate the ability to overcome limitations of conventional experimental methods by accounting for interactions between the main factors which affect the process. RSM is applied as a novel method to optimise process conditions of CNT- infused TFN membranes in the removal of heavy metal ions from AMD.

Keywords	Response surface methodology; Acid mine drainage; thin film nanocomposite membrane; Multi-walled carbon nanotubes
Corresponding Author	Keneiloe Sikhwivhilu
Corresponding Author's Institution	Mintek
Order of Authors	Selaelo Ramokgopa, Keneiloe Sikhwivhilu, Kapil Moothi, Richard Moutloali

Submission Files Included in this PDF

File Name [File Type]

Ramokgopa et al_JPCE_Cover Letter.pdf [Cover Letter]

Ramokgopa et al_JPCE_Highlights.docx [Highlights]

Ramokgopa et al JPCE_Manuscript.docx [Manuscript File]

Ramokgopa et al_JPCE_Declaration.pdf [Conflict of Interest]

To view all the submission files, including those not included in the PDF, click on the manuscript title on your EVISE Homepage, then click 'Download zip file'.

Process optimization through Response Surface Methodology for treatment of acid mine drainage using carbon nanotubes-infused thin film nanocomposite membranes

Selaelo Kholofelo Ramokgopa,[a,b], Keneiloe Sikhwivhilu[b], Richard Motlhaletsi Moutloali[c], Kapil Moothi[a#]*

[a]University of Johannesburg, Department of Chemical Engineering, Doornfontein 2028, Johannesburg, South Africa

[b]DSI/Mintek Nanotechnology Innovation Centre, Advanced Materials Division, Mintek, Randburg, 2125, South Africa

[c]University of Johannesburg, Department of Chemical Sciences, Doornfontein 2028, Johannesburg, South Africa

Abstract

The current work illustrates the use of Central Composite Design (CCD) and RSM to gain insight into the effect of five process factors (pressure, $MgSO_4$ concentration, $Fe_2(SO_4)_3$ concentration, $Al_2(SO_4)_3$ concentration and CNT loading) on the treatment of synthetic AMD solution with TFN membrane. Performances of polyamide TFN membranes with different multi-walled carbon nanotube (MWCNT) loading were tested to determine optimum loading under different operating conditions. The treatment efficiency was examined in terms of flux and rejection and based on these results and the optimum region from RSM was selected. The five previously mentioned process variables were investigated, and regression models were built, while data on permeate flux behaviour, $MgSO_4$ rejection, $Fe_2(SO_4)_3$ rejection, and $Al_2(SO_4)_3$ rejection as the response values were collected. Predicated models were in good agreement with experimental data and the results showed that pressure and CNT loading are the main effects that influence the process. The optimal conditions were a pressure of 20 bars and a CNT loading of 0.3%. Under these conditions, a permeate flux of 83%, 94% $MgSO_4$ rejection, 92% $Fe_2(SO_4)_3$ rejection, and 89% $Al_2(SO_4)_3$ rejection have been observed. RSM models demonstrate the ability to overcome limitations of conventional experimental methods by accounting for interactions between the main factors which affect the process. RSM is applied as a novel method to optimise process conditions of CNT- infused TFN membranes in the removal of heavy metal ions from AMD.

Keywords: Response surface methodology, Acid mine drainage, thin film nanocomposite membrane, Multi-walled carbon nanotubes

20th WaterNet/WARFSA/GWPSA Symposium

∗ Corresponding authors: [*]keneiloes@mintek.co.za, [#]kmoothi@uj.ac.za

Introduction

Acid Mine Drainage is the acidic runoff generated from mining activities by the chemical reaction of sulphur-bearing minerals with water and oxygen to form sulphuric acid where AMD is generated [1-3]. Heavy metals are leached out in the process and are carried into rivers, seas and other bodies of water even contaminating soil and underground water [4-6]. According to Durube et al. [7], mining activities account for most of the environmental pollution by heavy metals, especially the pollution of natural water sources. The treatment of AMD is a complex

task due to the excessive volumes of AMD that are formed [8]. It is considered as an interminable process that is difficult to control and has high treatment costs [3, 8, 9]. Toxic heavy metals from mine wastewaters to be treated include copper, zinc, magnesium, iron, aluminium, cadmium and lead [10,15,65]. Heavy metals are toxic, carcinogenic and non-biodegradable [11-13]. Due to the toxic effects of heavy metal pollution, chemical precipitation, oxidation, reduction, coagulation, solvent extraction and absorption have been employed for the removal of heavy metal ions [16]. However, these methods are not efficient to achieve removal standards set out by the World Health Organisation (WHO) [2,8,15]. In addition, the above-mentioned methods are expensive and produce toxic by-products [16,65]. There is a need to develophighly competitive separation processes with improved selectivity and cost benefit for the treatment of AMD [17].

Recently, owing to their promising features such as excellent effluent quality, stable permeate flux, low concentration polarization, and higher retention, thin film nanocomposite (TFN) [15] membranes have proved to be effective for the treatment of AMD [15-16]. Attention has been focused on developing TFN membranes with improved rejection and flux [17,18]. The inclusion of MWCNTs has made a meaningful contribution in the fabrication of TFN membranes as they can enhance the wet zone of the top active layer, speed up diffusion of monomers to the interface and prevent the rapid change of pH in reaction by acting as a buffering agent [19]. Furthermore, CNT-infused TFN membranes have been shown to increase permeate flux while also increasing affinity for heavy metal rejection [17,15,19]. Generally, operating pressure and feed concentration, are key factors in AMD treatment [20,65]. Moreover, CNT loading has been shown to affect membrane performance [21]. Considering that there are multiple factors which influence process performance, it is essential to choose an appropriate experimental design method that can allow optimum parameters to be selected [22]. To this end, Response Surface Methodology (RSM) is used to develop empirical models for optimisation of TFN membrane for AMD treatment.

RSM is a collection of mathematical and statistical techniques used to solve multi-variate problems in order to optimise a response [22-23]. RSM has been successfully used in science, engineering and related fields, especially for researching interactions between process factors and process optimisation [21,24,27]. RSM is principally advantageous in estimating multiple parameters and their interactions with fewer experimental trials [28]. RSM extends the limitations of experiments in the design space by accounting for effects and interactions of the process parameters.

RSM facilities process optimisation through establishment of the relationship between input variables and the responses, determining the extent to which these variables influence the process and lastly optimising process parameters through a regression model [25,26,30]. Second order models are widely used for the optimisation of multiple responses in a process through the least squares' method [30,31]. CCD is used for the building of second order response surface models [31]. CCD designed under RSM was employed to determine the response matrix of pressure, heavy metal concentration and CNT loading on the efficiency of removal of heavy metal ions from

synthetic AMD solution. Significance of main effects and interactions were observed by ANOVA and the competence of the model was evaluated [32]. To date, RSM has been used in prediction and optimisation studies of heavy metal removal [22, 33-35], membrane filtration processes [36-37] and wastewater treatment [38-40]. However, the use of RSM for the parametric analysis of treatment of synthetic AMD solution with CNT-infused TFN membranes has not yet been explored, is thus the focus of this work. The aim of this work is to develop an empirical model through the non-linear multivariate regression of selected design variables (pressure, $MgSO_4$ concentration, $Fe_2(SO_4)_3$ concentration, $Al_2(SO_4)_3$ concentration and CNT loading) for process optimization.

Materials and methods

Materials

CNTs with an outer diameter of 6-13 nm and length from 2.5-20µm, with purity >98%, were purchased from Sigma Aldrich. Nitric acid (65%) and sulphuric acid (98%) were supplied by Ace Chemicals. Commercial LY ultrafiltration UF PES membranes with a MWCO of 100,000 Da were purchased from Synder Filtration (USA). For the preparation of polyamide TFC membrane n-hexane (anhydrous ≥99%) and the monomers Piperazine (PIP) and Trimesoyl chloride (TMC, 98%) were used as received from Sigma Aldrich. Sodium dodecyl sulphate (SDS) (98.5%) was purchased from Sigma Aldrich. Iron Sulphate $FeSO_4.7H_2O$, Aluminium Sulphate $Al_2(SO_4)_3.18H_2O$ and Magnesium Sulphate $MgSO_4$ salts for synthetic AMD synthesis were supplied by Rochelle Chemicals. Deionized (DI) water with a conductivity of 5.5µS/m at 25ºC was used in all experiments.

MWCNT preparation and characterisation

CNTs were oxidised using a mixture of 35% HNO_3 and 98% H_2SO_4 (3:1) (v/v) [41]. An amount of 2g of CNTs was added to 200ml of the solution and oxidation was carried out using a microwave digester operated at 150W. The reaction was carried out for 1hr at 70˚C [42]. The CNTs were then washed with DI water until pH 7 and dried in a vacuum oven at 60˚C for 12hr [43].

A JEOL-JEM 2100F high-resolution transmission electron microscopy (HR-TEM) was used to characterize the CNTs before and after oxidation. The CNT samples were sonicated in acetone in preparation for analysis. A few drops of the solution were placed on a carbon coated copper grid before viewing under 200kV. Low voltage is required to avoid damage to the nanotubes due to the electron beam [41]. Perkin Elmer Raman Station 400 equipped with a CCD detector was used to determine the graphitic structure of CNTs. Samples were characterised using a 1.96 eV excitation energy. Total Reflectance Fourier Transform Infrared Spectroscopy (ATR-FTIR) was used to study functional groups of the pristine and *f*-MWCNTs [43].

Preparation and characterisation of TFN membranes

Thin film composite membranes were prepared using a modified interfacial polymerisation process. In order to remove the glycerol used to preserve membrane pores of the commercial UF-PES support membrane, the membranes were immersed in an aqueous solution of 0.6 mol/L HCl for 40 min. The excess acid was neutralised by 0.5 mol/L NaOH solution [45]. Support membrane(s) were pre-treated by soaking them in 0.50% w/v of SDS overnight. SDS is an anionic surfactant and was used to clean the membranes before use [46]. The membrane(s) were then washed with distilled water for 1 hr and allowed to dry in a fume hood for 2 hr. The pre-treated membrane(s) were immobilized onto glass plates using double sided tapes and paper tapes; the paper tapes kept the double-sided tapes in place. The immobilised PES flat sheet membrane(s) were immersed in the organic solution of (0.40% w/v TMC) in hexane for 30 min, before immersion in the aqueous solution of DI water and PIP for 30 min. The membrane(s) were then immersed in the organic solution again for 30 min for further polymerisation and formation of the skin layer [47-48]. It is important to note that in order to maintain a uniform layer on the membrane surface, a rubber roller was used to remove residual droplets of aqueous solution on the top surface before immersing the membrane in the organic solution. PIP is an aliphatic diamine that is commonly used in the preparation of TFC membranes. [49]. PIP and TMC are polymerised on the membrane support to form the active layer of the membrane [77]. The reaction scheme of the amine with the acyl halide to form a polyamide thin layer is shown in Figure 1.

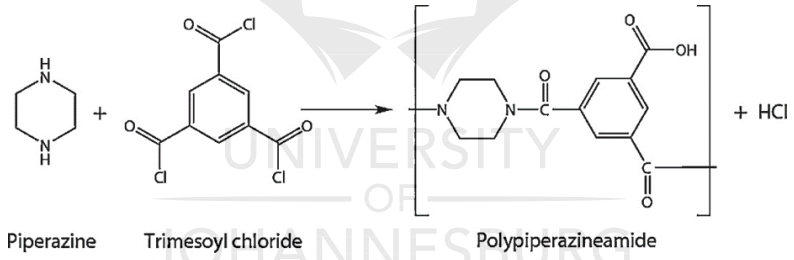

Figure 0-1: A scheme of cross-linking reaction between Piperazine and Trimesoyl chloride [76]

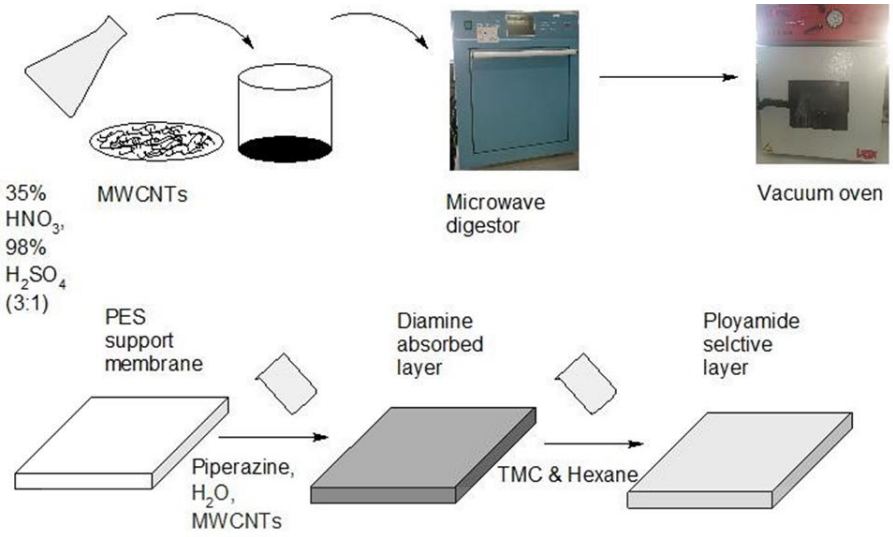

Figure 1: Preparation of CNT-TFN membranes

Preparation of synthetic AMD solution

Synthetic AMD solution was prepared based on heavy metals commonly found in gold AMD in South Africa [15]. Required amounts of $FeSO_4.7H_2O$ (which is expected oxidise to $Fe_2(SO_4)_3$ in acidic medium), $Al_2(SO_4)_3.18H_2O$ and $MgSO_4$ were weighed and dissolved in deionised water to give solution of 1000ml with 2000mg/L Fe^{3+}, 200mg/L Al^{3+} and 200mg/L Mg^{2+}. H_2SO_4 was added to ensure that the pH was below 3 (which is the typical level in AMD from gold mining activities in SA) to bring the SO_4^{2-} concentration to 6000mg/L [51].

Flux and rejection tests

The experiments were carried out using a crossflow filtration rig schematized in Fig 3. Heavy metal ions and DI water were used to prepare the feed salt solutions in desired concentrations. Membrane pure water permeability was determined using a crossflow filtration rig with a membrane area of 42 cm^2. The filtration rig consisted of a feed tank with a temperature controller, two pressure gauges (0-1500 psi) at the inlet and outlet of the membrane module, a flow meter on the retentate side, a low-pressure peristaltic pump and valves [52]. The electrical conductivity of the feed ad permeate solution were measured using a conductivity meter. Heavy metal salt rejection was measured as follows [53]:

$$R(\%) = 1 - \left(\frac{C_p}{C_f}\right) * 100 \quad (1)$$

where R is the percentage of ion rejection, C_p is the concentration of the permeate and is C_f the concentration of the feed.

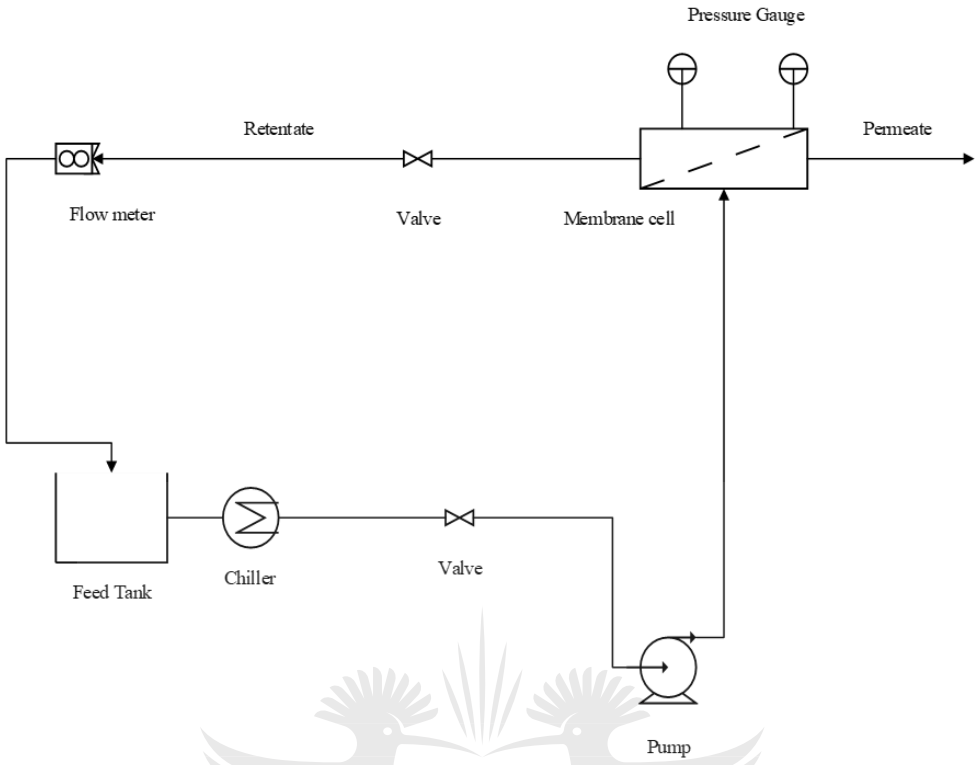

Figure 2: Experimental crossflow filtration rig

Design of experiments and RSM

The removal of heavy metal ions from AMD using a CNT-TFN membrane was designed by CCD using RSM. RSM is a statistical method that combines various statistical and mathematical techniques based on the multivariate linear model that consists of designing experiments to provide adequate and reliable methods of response [54]. This method had the best fit of data obtained from experimental design for determining the main and mutual effects between the effective parameters and used for developing, improving and optimising the process [55]. The main purpose of RSM is to determine the operational condition of the response that is affected by various factors of the process [56]. This method is widely used in Chemical engineering particularly to optimise membrane-based processes [57]. In this work the optimisation of removal of heavy metal ions from AMD was carried out by five parameters (pressure, CNT loading, $MgSO_4$ concentration, $Fe_2(SO_4)_3$ concentration, and $Al_2(SO_4)_3$ concentration). First, preliminary experiments were performed to determine independent factors in the study. The ranges and levels of the variables used in the experiments are listed in Table1.

Table 0-1: Levels of factors

Factors	Units	Level		
		Low (-1)	Centre (0)	High (+1)
Pressure	Bar	10	15	20
CNT loading	mg/ml	0,2	0,3	0,4
Mg conc.	Ppm	100	150	200
Fe conc.	Ppm	1000	1500	2000
Al conc.	Ppm	100	150	200

$MgSO_4$ rejection, $Fe_2(SO_4)_3$ rejection, $Al_2(SO_4)_3$ rejection and permeate flux were taken as the responses. The predicted optimal points of the 4 responses for the 5 independent variables are explained by the following quadratic equation [58-59]:

$$Y = b_0 + \sum_{i=1}^{n} b_i x_i + \sum_{i=1}^{n} b_{ii} x_i^2 + \sum_{i=1}^{n-1} \sum_{j=i}^{n} b_{ij} x_i x_j \quad (2)$$

Where Y is the predicted response, b_0 is the constant coefficient, b_i the linear coefficients, b_{ii} , b_{ij} the interaction coefficients and x_i, x_j are the coded levels of the factors studied. For statistical calculation, the relationship between coded and real values is [68]:

$$X_i = \frac{U_i - U_i^0}{\Delta U_i} \quad (3)$$

U_i is the real value of the independent variable, X_i is the independent variable coded value, U_i^0 is the independent variable real value in centre-point of the independent variable and ΔU_i is the step change in U_i. Factor levels are coded from low level (-1) to high level (+1) and centre points at 0.

In order to optimize as variables of this work 28 experiments were designed. The results of the CCD experimental design are illustrated in Table 2. Five axial points show the boundary region of experiments as shown in the pattern column of Table 2. One replicate was also added for reproducibility of results [75]. The coded variables of the multiple regression analysis were based on Eq. (3). A, B, C, D and E were used to represent coded values for pressure, $MgSO_4$ concentration, $Fe_2(SO_4)_3$ concentration, $Al_2(SO_4)_3$ concentration and CNT loading respectively.

Table 0-2: Experimental design with coded values

Pattern	A	B	C	D	E	Pressure (bar)	MWCNT (%)	$Fe_2(SO_4)_3$ (ppm)	$MgSO_4$ (ppm)	$Al_2(SO4)_3$ (ppm)
−−−++	-1	-1	-1	1	1	10	0,2	1000	100	150
+++−+	1	1	1	-1	1	15	0,3	1500	150	150
A0000	1	0	0	0	0	10	0,2	1500	150	100
−−+−+	-1	-1	1	-1	1	10	0,4	2000	100	100
000A0	0	0	0	1	0	15	0,2	1500	150	200
−++−−	-1	1	1	-1	-1	20	0,4	1500	200	100
0000a	0	0	0	0	-1	10	0,4	2000	200	200
0A000	0	1	0	0	0	20	0,4	2000	150	150
0a000	0	-1	0	0	0	15	0,3	2000	200	100
++−−−	1	1	-1	-1	-1	20	0,4	1000	200	200
00A00	0	0	1	0	0	10	0,4	1000	200	100
−−−−−	-1	-1	-1	-1	-1	15	0,4	1000	100	100
+−−+−	1	-1	-1	1	-1	10	0,2	1000	200	200
−+−+−	-1	1	-1	1	-1	10	0,2	2000	200	150
000a0	0	0	0	-1	0	10	0,3	1500	150	150
+−+++	1	-1	1	1	1	15	0,3	1500	100	150
a0000	-1	0	0	0	0	15	0,2	1000	200	100
0	0	0	0	0	0	15	0,4	1000	150	150
+−+−−	1	-1	1	-1	-1	15	0,3	1500	100	150
00a00	0	0	-1	0	0	20	0,2	1500	200	150
++++−	1	1	1	1	-1	10	0,2	2000	100	200
−++++	-1	1	1	1	1	20	0,3	1000	150	100
0000A	0	0	0	0	1	15	0,3	1500	150	150
0	0	0	0	0	0	10	0,4	1000	100	200
+−−−+	1	-1	-1	-1	1	20	0,2	2000	100	100
−−++−	-1	-1	1	1	-1	20	0,2	1000	100	200
++−++	1	1	-1	1	1	20	0,3	2000	200	200
−+−−+	-1	1	-1	-1	1	20	0,4	1500	100	200

Results and discussion

TEM of pristine and oxidized CNTs

Figure 4 shows the TEM images of pristine and microwave oxidised CNTs at different magnifications. The amount of amorphous carbon and metal catalyst (red arrows) in and around the pristine CNTs (Figure 4(a)) was reduced compared to the oxidised CNTs (Figure 4(b)). The agglomeration of CNTs was also reduced for microwave-assisted oxidation (Figure 4(e)) compared to the pristine CNTs (Figure 4(d)). Figure 4(c) shows the CNTs after microwave oxidation at higher magnification. From Figure 4(c) the walls of the CNTs are visible and no damage or defects on the tube walls were observed. Therefore, the CNTs stayed intact after oxidation, making microwave oxidation a viable method for CNT oxidation. According to Xin and Li [63], defects on the CNT walls may cause the electrical conductivity of the CNTs to decrease which could affect their performance in the membrane composite.

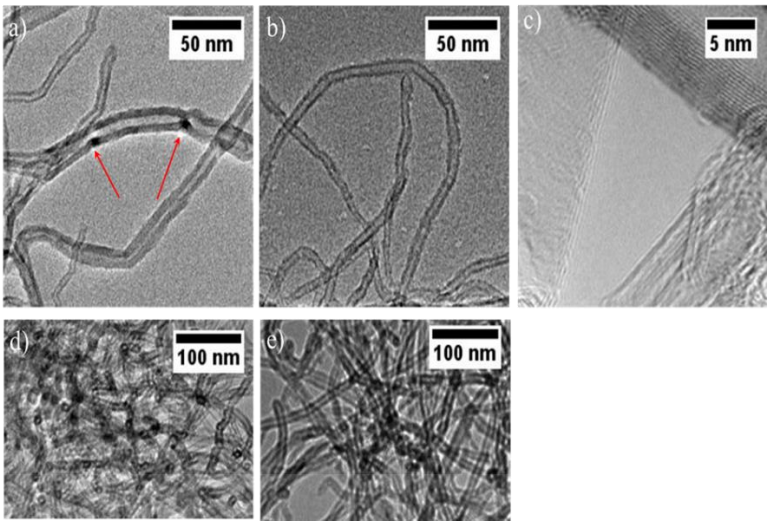

Figure 0-2: TEM of (a), (d) pristine and (b), (c), (e) microwave oxidised MWCNTs

Raman Analysis of pristine and oxidized CNTs

The results of the Raman Spectroscopy for microwave-oxidised (*f*-CNT) and pristine CNTs are shown in Figure 5. The first peak which appears at 1320 cm^{-1} is known as the D band, arises due to the sp^3 hybridized carbons in the nanotube walls and is an indication of the disordered carbon atoms in the walls. The second peak appearing at 1580 cm^{-1}, is known as the G band and is related to the tangential stretching of the sp^2 bonded carbons in the graphene sheets [69]. The I_D/I_G ratio shown in Table 3 indicates that the intensity of the D band to G band increases after oxidation which is an indication that the tubes became less graphitic and crystalline, and more disordered. The I_D/I_G ratio is a good indication of the defects on a CNT sample [42]. Therefore, the more defects on the CNT surface, the higher the I_D/I_G ratio. In the case of chemical oxidation, the surface defects are from the attachment of -COOH groups to the CNT walls.

Table 0-3: Raman of pristine and oxidised CNTs

	G	D	I_G	I_D	I_D/I_G
Pristine	1580	1320	365	200	0.54
f-MWCNT	1580	1320	372	320	0.86

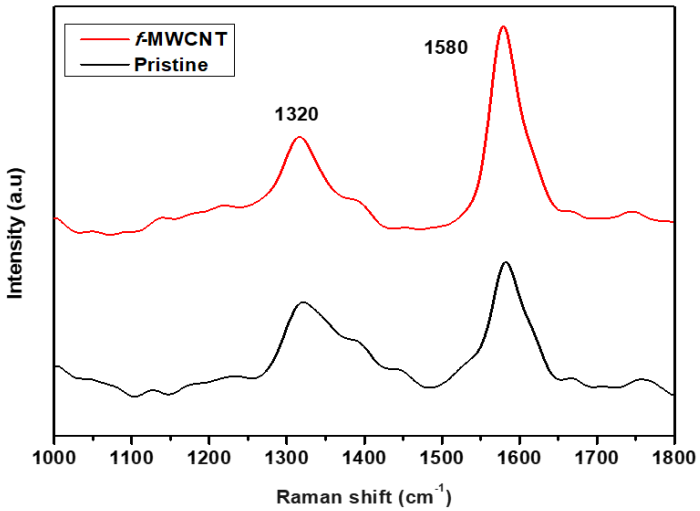

Figure 0-3: Raman spectra of pristine (a) and oxidised (b) CNTs

FTIR of pristine and oxidised CNTs

The ATR-FTIR spectra of pristine and oxidized CNTs is shown in Figure 6. The broad peak observed at for the microwave oxidized CNTs 3288 cm^{-1} is associated with the O-H stretching of the functional groups on the tube walls. The peak observed at 1642cm^{-1} is associated with the C=O stretch of the carboxylic group. The peak at 1308cm^{-1} may be due to the asymmetric stretching of the C=C-OH bonds on the CNTs backbone. The ATR-FTIR confirmed that there were changes to the pristine CNT structure, mainly the appearance of carboxylic groups which confirm the functionalization of the CNTs.

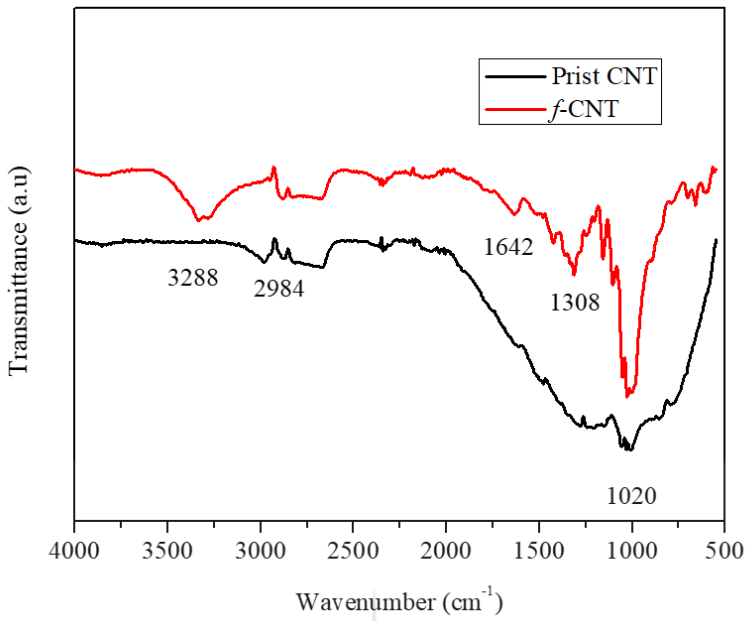

Figure 0-4: FTIR spectra of pristine (a) and oxidised (b) CNTs

FTIR of PES support and TFC membrane

Figure 7 shows FTIR peaks of (a) PES support membrane, pristine TFC membrane without CNT loading, and (b) the TFN membranes with different CNT loading. The PES support consists of benzene rings, ether and sulfone group. ATR-FTIR spectra over wave 1800-800cm $^{-1}$ show the support layer and the polyamide layers due to the penetration depth of >300nm which gives the chemical information of both the polyamide layer and the polyethersulfone layer [72]. The strong sharp band at 1093 cm^{-1}and 1243 cm^{-1} shows the symmetric and asymmetric stretching of the S=O bonds respectively. For the TFC membrane there was a shift to 1083 cm^{-1}and 1236 cm^{-1} respectively. The frequency of vibration is inversely proportional to the mass of the vibrating molecule; thus the shift to lower wave numbers indicates that the mass of the molecules was increased. The peak at 1715cm^{-1} shows the free carboxyl group. The bands at 1419 cm^{-1} and 2963 cm^{-1} correspond to C-H stretching [73]. At wave numbers of 4000-2600 cm^{-1} the penetration depth for the ATR-FTIR is <~200 nm which is ideal for analysing chemical properties of TFC polyamide layer [72].The TFC membrane peaks between 3000 cm^{-1} and 2800 cm^{-1} indicates the stretching of the $-CH_3$ and $-CH_2$ stretching vibrations [74]. No noticeable difference was observed in the spectra of the CNT-TFN membranes in comparison to that of the pristine TFC membrane, presumably due to the low loadings of CNTs used in the TFN membranes (Figure 7b).

a)

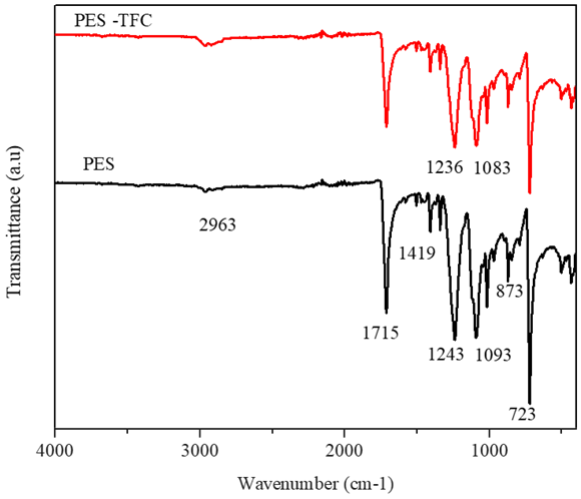

b)

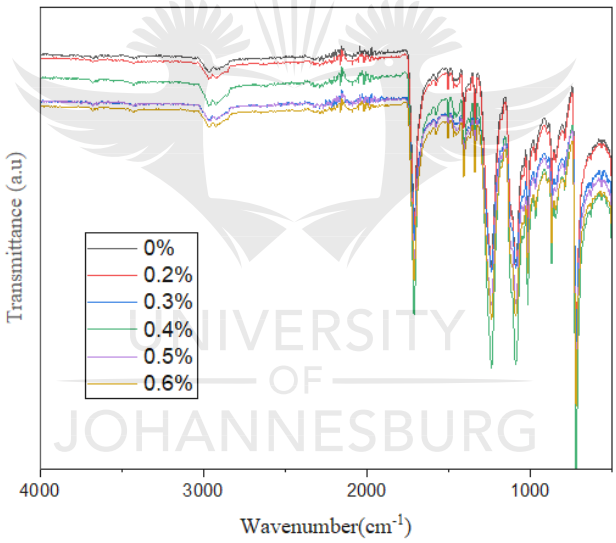

Figure 0-5: FTIR of (a) PES support membrane and TFC membrane and (b) membranes at different CNT loadings

Pure water flux

Pure water flux measurements as a function of pressure were carried out as shown in Figure 8. As expected, flux increase with an increase in transmembrane pressure (TMP) [62]. The flux increased for 0% to 0.3% CNT loading across all pressures studied (5-20) bar. This can possibly be due to the incorporated CNTs hindering the formation of a densely cross-linked polymer structure, thereby contributing to the enhancement of pure water flux compared to the pristine TFC membrane [48]. However, a decline in the flux as CNT loading was increased from 0.4% to 0.6% was observed across all pressures studied. When the amount of CNTs is higher than 0.3%, the distribution of CNTs across the membrane surface is not uniform and CNTs are not well dispersed leading to agglomeration of CNTs in solution and consequently on the membrane surface [63]. The clustered CNT bundles have a smaller specific surface area and lower interaction with the membrane surface [62], hence the observed decline in the water permeation rate at CNT loadings higher than 0.3% [63].

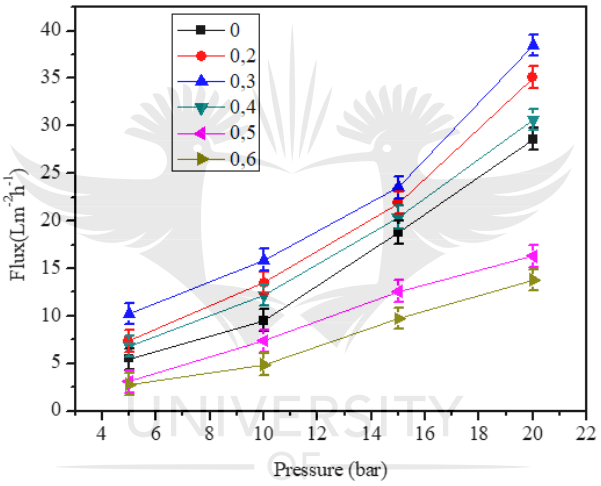

Figure 0-6: Pure water permeability of TFN membranes with different MWCNT loading

Flux and rejection studies

Effect of CNT loading on flux and rejection is shown in Figure 9. As CNT loading increased so did rejection and flux. There are more channels created on the membrane for permeation of the synthetic AMD solution through the incorporation of CNTs on the membrane [78]. The CNT- modified membrane surface provides adsorption sites for the heavy metal ions. However, no further increase in flux or rejection is observed for a loading greater than 0.5%. It can be understood that CNTs tend to agglomerate on the membrane surface at higher concentrations causing blockage of membrane pores and therefore reducing rejection.

a)

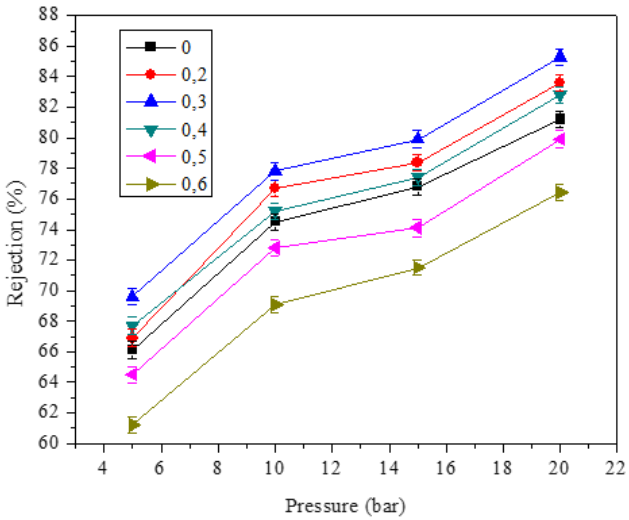

b)

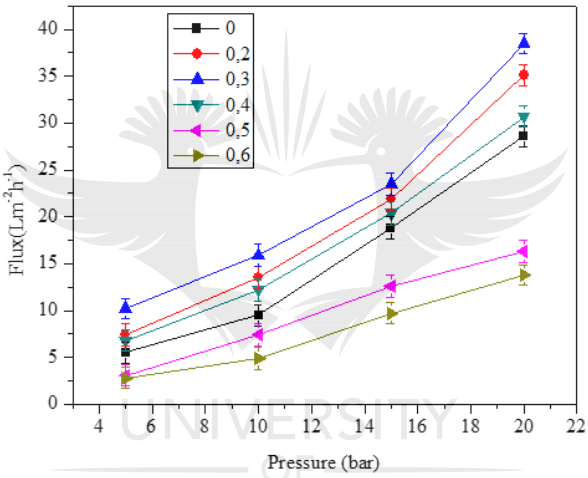

Figure 0-7: Rejection (a) and flux (b) of ternary salt solutions of 2000ppm $Fe_2(SO_4)_3$, 200 ppm$MgSO_4$ and 200 ppm $Al_2(SO_4)_3$ for TFN with 0% - 0.6% MWCNT

The rejection of heavy metal ions from synthetic AMD (Figure 10) depended primarily on ionic size and membrane permeability. The ionic size for Fe^{3+} is 73Radius/pm, while for Mg^{2+} is 79 Radius/pm and for Al^{3+} is 57 Radius/pm. According to [60], ionic permeability and the ionic size are inversely correlated therefore ions with a larger ionic size are expected to be less permeable through the membrane. The larger the positive charge of a cation, the smaller its radius because there are less electrons in its outer shell. Also, water molecules are more tightly held to smaller cations and therefore have a larger hydration radius [8]. For larger unhydrated ions, since the charge is more dispersed, the hydration water is held less strongly [60-61]. Magnesium has a large hydration radius as it is a small cation with a valence of 2. As a result, magnesium is closely bound to the water molecules around it as it approaches the membrane surface. The hydration shell around the magnesium ion prevents it from closely approaching the membrane surface therefore it is unable to pass through the membrane pores. Similarly, iron has a lower rejection than magnesium but higher than aluminium which correlates with the ionic size of the ions.

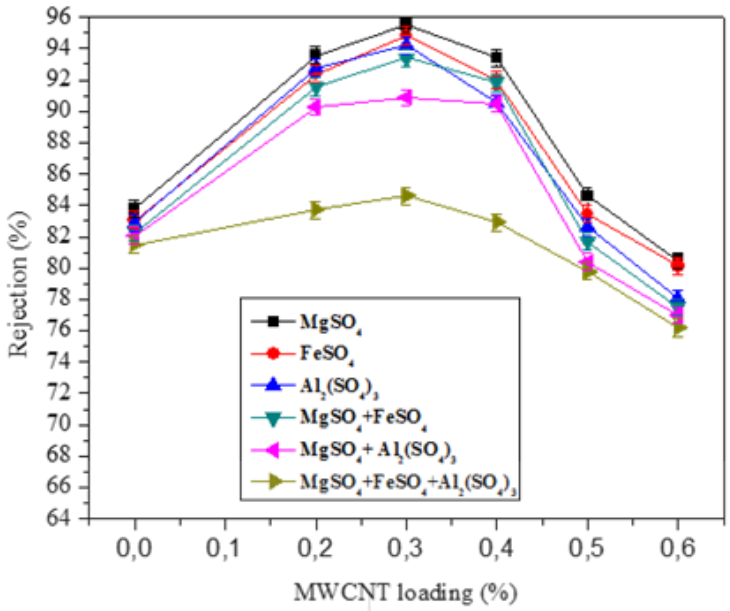

Figure 0-8: Rejection of single, binary and ternary solutions $Fe_2(SO_4)_3$, $MgSO_4$ and $Al_2(SO_4)_3$ for different MWCNT loadings at 20 bar

Permeate flux (presented in Figure 11) was lower than pure water flux (presented in Figure 8) for all observed heavy metals. This can be due to osmotic pressure build-up by the retained salt. Permeate flux was pressure dependent and tended to increase linearly with an increase in pressure according to Darcy's Law [64,68]. Flux as a function of pressure is shown as plotted in Figure 9 (b). As seen in the Figure 9 (b), flux increased with an increase in pressure due to an increase in driving force [65]. Furthermore, as shown in Figure 12, flux tended to decrease with an increase in feed concentration due to an increase in osmotic pressure.

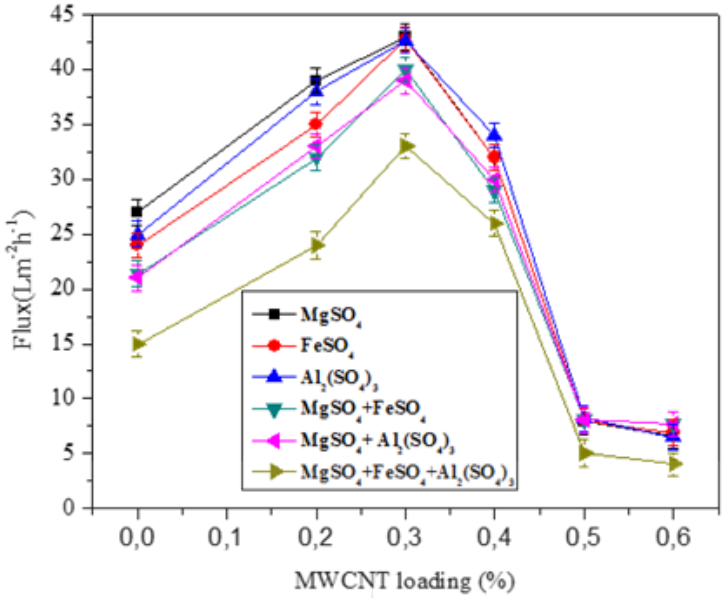

Figure 0-9: Flux of single, binary and ternary solutions $Fe_2(SO_4)_3$, $MgSO_4$ and $Al_2(SO_4)_3$ for different MWCNT loadings at 20 bar

a)

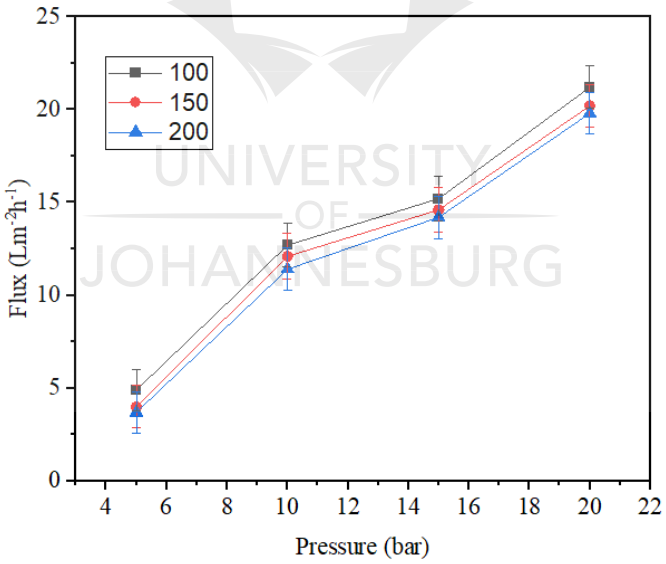

b)

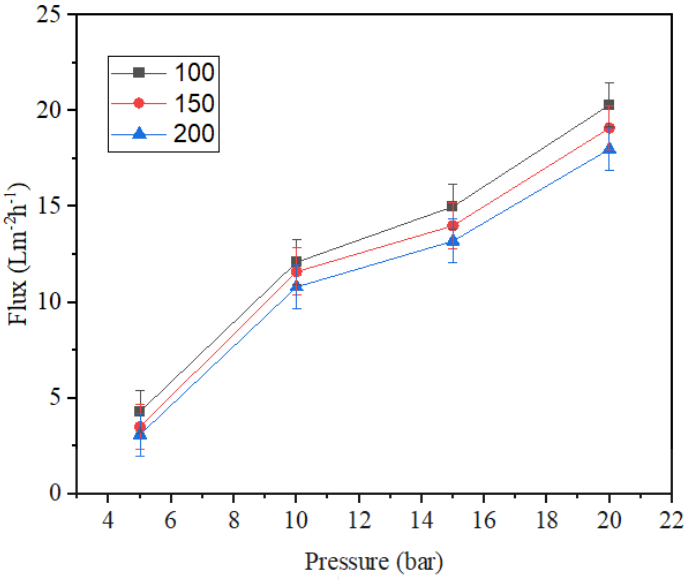

c)

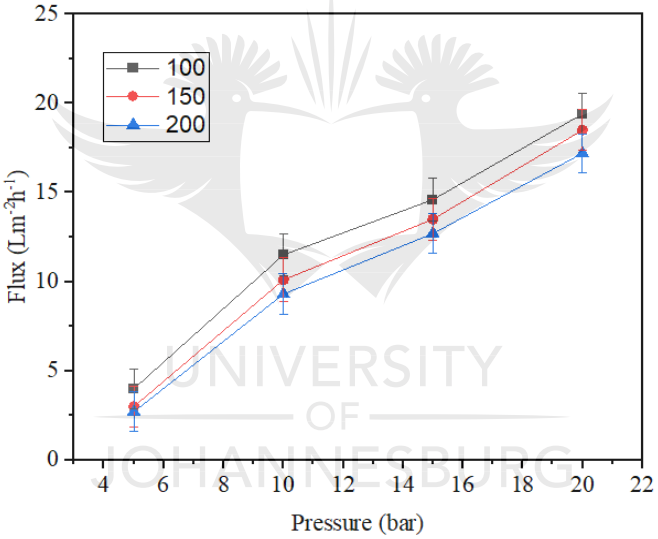

Figure 0-10: Flux for varying feed concentration of a) $MgSO_4$, b) $Fe_2(SO_4)_3$ and c) $Al_2(SO_4)_3$

In terms of the effects of feed concentration, the rejection tended to decrease with an increase in feed concentration as shown in Figure 13, which might be due to an increase in solute diffusion rate which is dependent on solute concentration. Therefore, it can be inferred that the increase in concentration caused an increase in species deposition or scaling on the surface [65]. The results showed that the rejection increases with increasing pressure and decreasing concentration, which could be explained on the basis of steric hindrance mechanism [66].

a)

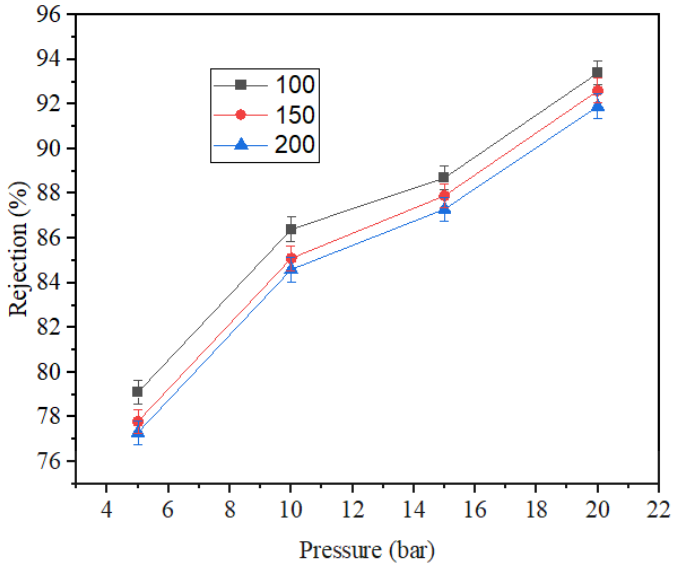

b)

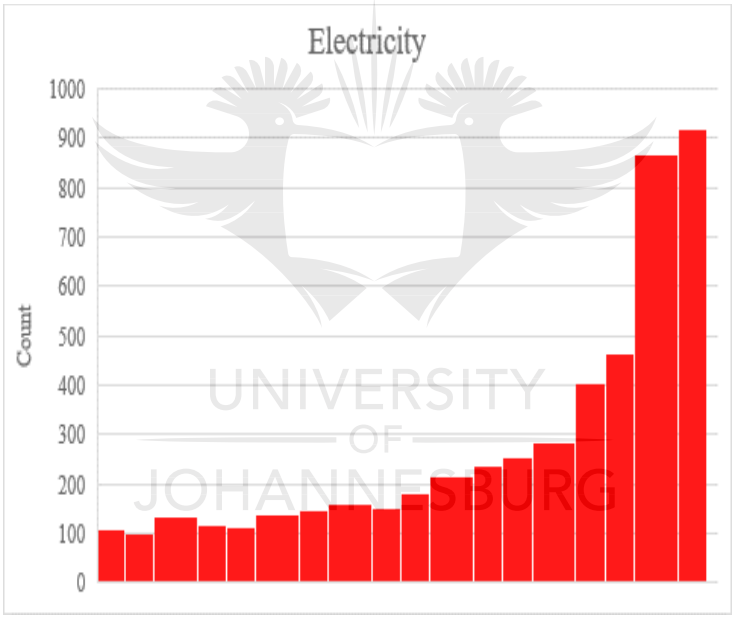

c)

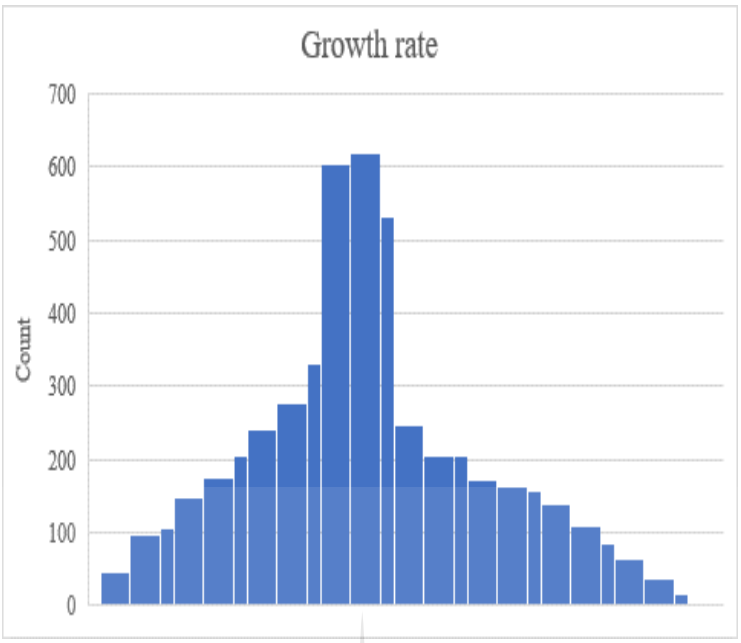

Figure 0-11: Rejection for varying feed concentration of a) $MgSO_4$, b) $Fe_2(SO_4)_3$ and c) $Al_2(SO_4)_3$

Process parameters can have a significant effect on the desired response to be optimized [27]. In the case of our study these responses were flux and rejection of the heavy metal ions. Input variables that did not lead to process optimization in the case of flux and rejection were eliminated from the study before optimization using RSM. Due to the small pore sizes a larger pressure is needed to push molecules through the membrane, hence smaller pressure of 5 bar showed lower rejection across all membranes studied. Also, as previously mentioned membranes with MWCNT loading < 0.4 % showed lower flux and rejection. Therefore, these values were not considered for further optimization studies using RSM.

Regression model and statistical analysis

The results of the effects of the input variables on the model are shown in Table 5. P-value is the actuarial factor that describes data variation around the mean while F-values (F-ratio and Prob F) enable evaluation of data on the level of significance of the variables. To validate a RS model from a statistical standpoint, the *F*-ratio should be as high as possible whereas the *P*-value should be as low as possible [75]. As shown in Table 4, P values less than 0.05 indicates that the variable is significant. Therefore, it is observed that $Fe_2(SO_4)_3$ concentration, pressure and CNT loading have the most significance on the process followed by$Al_2(SO_4)_3$ concentration and $MgSO_4$ concentration.

Table 0-4: Effects of interactions of studied factors

Source	LogWorth	PValue	
Fe conc(1000,2000)	3.899	0.00013	
Pressure*CNT loading	3.630	0.00023	
CNT loading(0.2,0.4)	3.579	0.00026	^
Fe conc*Fe conc	3.391	0.00041	
CNT loading*Mg conc	3.362	0.00043	
Pressure*Fe conc	3.297	0.00051	
CNT loading*Al conc	3.295	0.00051	
Pressure*Mg conc	3.174	0.00067	
Al conc(100,200)	3.014	0.00097	^
Al conc*Al conc	2.968	0.00108	
Pressure(10,20)	2.918	0.00121	^
CNT loading*CNT loading	2.892	0.00128	
Mg conc*Al conc	2.874	0.00134	
Mg conc*Mg conc	2.387	0.00410	
Fe conc*Al conc	2.332	0.00466	
Mg conc(100,200)	1.947	0.01129	^
Fe conc*Mg conc	1.936	0.01159	
Pressure*Al conc	1.296	0.05056	
Pressure*Pressure	1.163	0.06868	
CNT loading*Fe conc	0.558	0.27649	

Table 5 shows the ANOVA for the input variables of the process. As shown in Table 5, high F ratio indicate the statistical significance and so does a Prob> F value of less than 0.05. All interactions were shown to be significant apart from (Pressure *Al conc, Pressure*Pressure, CNT loading *Fe conc). Based on these results these effects were shown not to significantly affect the model.

Table 0-5: Effects of input parameters for RSM

Effect Tests

Source	Nparm	DF	Sum of Squares	F Ratio	Prob > F
Pressure(10,20)	1	1	275.2600	825.7799	0.0012*
CNT loading(0.2,0.4)	1	1	1263.6208	3790.862	0.0003*
Fe conc(1000,2000)	1	1	2639.2381	7917.714	0.0001*
Mg conc(100,200)	1	1	29.0364	87.1091	0.0113*
Al conc(100,200)	1	1	344.0474	1032.142	0.0010*
Pressure*Pressure	1	1	0.7259	2.1777	0.2780
Pressure*CNT loading	1	1	1421.6799	4265.040	0.0002*
CNT loading*CNT loading	1	1	259.3669	778.1006	0.0013*
Pressure*Fe conc	1	1	659.3521	1978.056	0.0005*
CNT loading*Fe conc	1	1	0.3852	1.1556	0.3949
Fe conc*Fe conc	1	1	819.0145	2457.044	0.0004*
Pressure*Mg conc	1	1	497.2206	1491.662	0.0007*
CNT loading*Mg conc	1	1	766.0339	2298.102	0.0004*
Fe conc*Mg conc	1	1	28.2527	84.7582	0.0116*
Mg conc*Mg conc	1	1	80.7486	242.2457	0.0041*
Pressure*Al conc	1	1	1.1229	3.3688	0.2079
CNT loading*Al conc	1	1	656.5204	1969.561	0.0005*
Fe conc*Al conc	1	1	71.0517	213.1551	0.0047*
Mg conc*Al conc	1	1	249.0413	747.1238	0.0013*
Al conc*Al conc	1	1	309.2775	927.8326	0.0011*

RSM optimisation

The 3D surface plots in Figure 13 for metal salts and heavy metal permeate flux were developed based on the quadratic interaction shown in Eq (2). The rejection efficiency increases with CNT loading because of the increased surface area provided for heavy metal absorption. A CNT loading of between 0.2 and 0.4 was chosen as higher loadings showed agglomeration of the CNTs. Furthermore, rejection also increased with an increase in pressure and decreased with an increase in heavy metal concentration. The response surfaces indicate that increasing both pressure and CNT loading will enhance the flux and rejection of the membrane as indicated by the optimum region (red). It is worth noting that the optimum loading for all three cases where both flux and rejection are optimised is at a CNT loading of 0.3% and a pressure of 20 bar a permeate flux of 83%, 94% $MgSO_4$ rejection, 92% $Fe_2(SO_4)_3$ rejection, and 89% $Al_2(SO_4)_3$ rejection was observed. The rejection of heavy metal ions follows the same trend as was observed from experiments, however values from the model were lower than experimental values. This is due to the second-degree interactions between process variables that cannot be accounted for in the preliminary experiments. Therefore, RSM offers a more accurate description of how the process outputs might be affected in industrial applications were more than one process variable is varied at a time. Industrial applications of membrane technology require higher rejection and good flux. Subsequently, TFN membranes can inferred to be best for industrial applications. The optimized values can be used for further process simulation and design studies.

a)

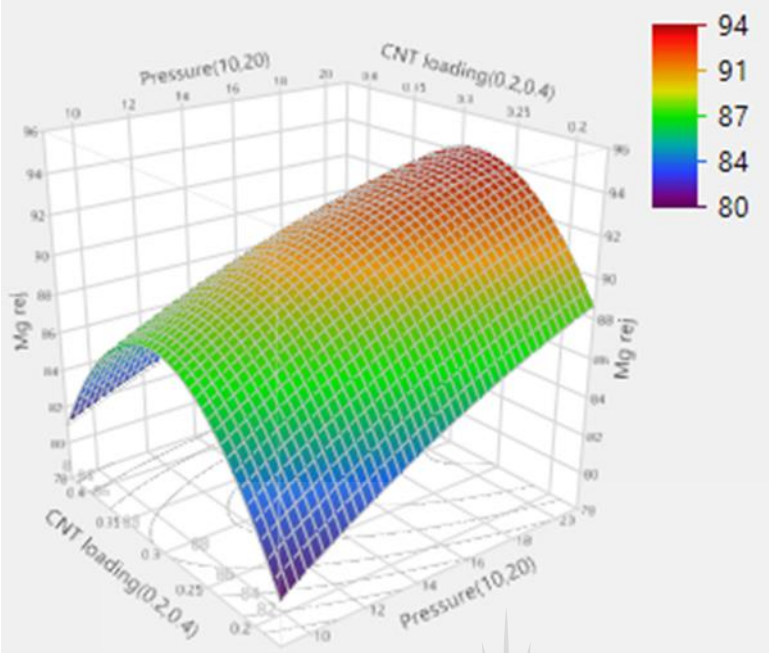

b)

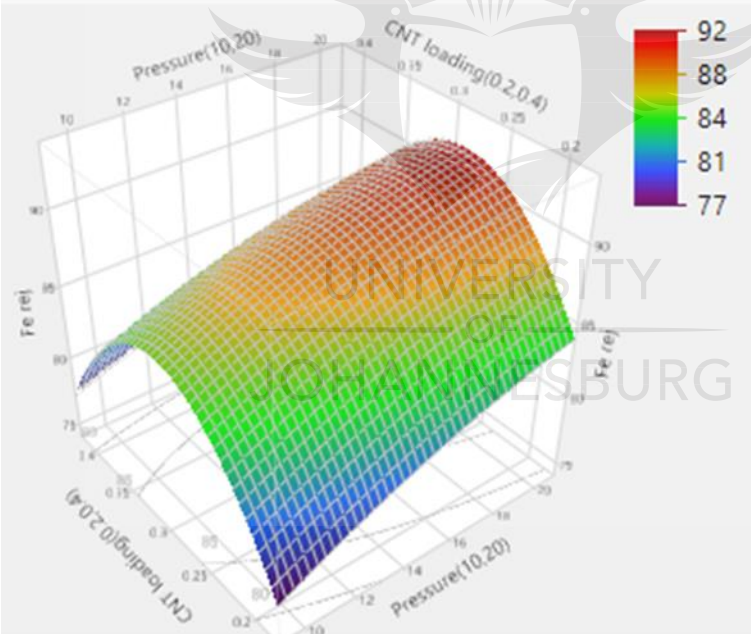

c)

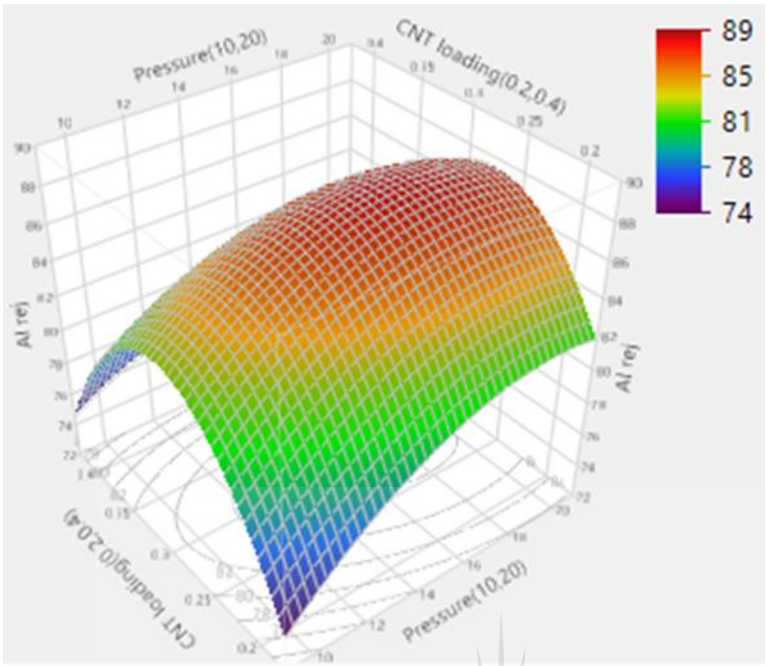

d)

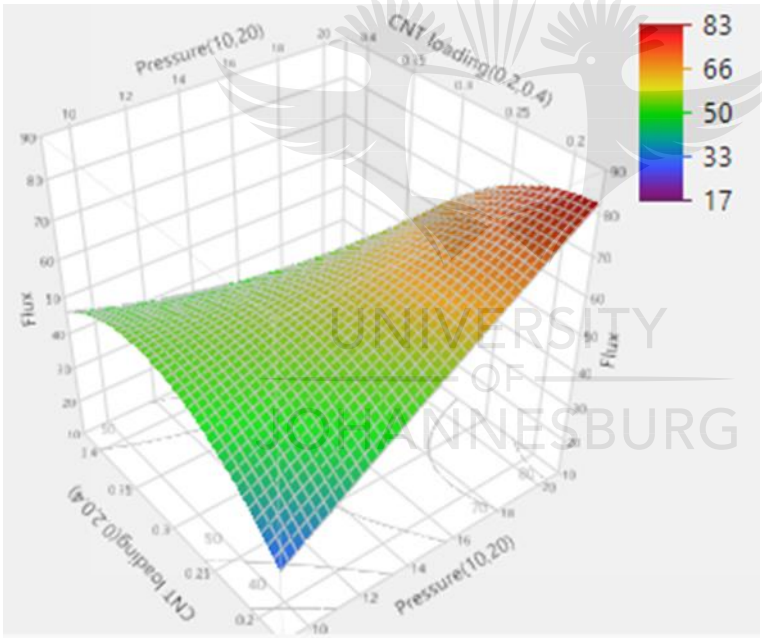

Figure 0-12: Response surface plots of the predicted performance of ternary solution for a) $MgSO_4$ rejection, b) $Fe_2(SO_4)_3$ rejection, c)$Al_2(SO_4)_3$ rejection and d) permeate flux

Conclusions

The present study investigated the effect of pressure, $MgSO_4$ concentration, $FeSO_4$/ $Fe_2(SO_4)_3$ concentration, $Al_2(SO_4)_3$ concentration and CNT loading on permeate flux and metal rejection. The significance of these effects was determined through CCD and RSM. From the study it was found that pressure, CNT loading, and heavy metal concentration (and their interactions with one another) influenced the process responses. Also, for the responses,

heavy metal rejection followed the sequence $MgSO_4$> $Fe_2(SO_4)_3$ > $Al_2(SO_4)_3$ in agreement with experimental observations. However, rejection values obtained from RSM were lower than experimental values due to the interactions of the effects. A similar observation was made when comparing permeate flux response to the experimental flux. In terms of the significance of effects on the responses, $Fe_2(SO_4)_3$ concentration was found to have a significant effect as was pressure and CNT loading. The $MgSO_4$ concentration and $Al_2(SO_4)_3$ concentration were found to have slightly less significance but still considerable effect on responses. Concerning process optimization, the optimal conditions were found to be a CNT loading of 0.3% and a pressure of 20 bar for maximum flux and rejection of all three heavy metals in solution.

Acknowledgements

The authors would like to thank the National Research foundation (NRF) of South Africa for providing a scholarship to S.K. Ramokgopa. The authors also wish to thank the University of Johannesburg and Mintek for funding the study.

References

[1] Akcil, A. and Koldas, S. (2006). Acid mine drainage (AMD): Causes, treatment and case studies. *Journal of Cleaner Production*, 14(12–13):1139-1145.https://doi.org/10.1016/j.jclepro.2004.09.006

[2] Mthetwa, V. (2014) Investigation of polyether sulfone (PES) hollow fibre membranes for the treatment of acid mine drainage. *University of Witwatersrand*. Johannesburg.

[3] Simate, G.S. and Ndlovu, S. (2014). Acid mine drainage: Challenges and opportunities. Journal of Environmental *Chemical Engineering*, 2(3):1785-1803.https://doi.org/10.1016/j.jece.2014.07.021

[4] Alloway, B.J. 2013, "Sources of heavy metals and metalloids in soils" in Heavy metals in soils *Springer*, pp. 11-50.

[5] Durand, J.F. (2012). The impact of gold mining on the Witwatersrand on the rivers and karst system of Gauteng and North West province, South Africa. *Journal of African Earth Sciences*, 68:24-43.https://doi.org/10.1016/j.jafrearsci.2012.03.013

[6] McCarthy, T.S. (2011). The impact of acid mine drainage in South Africa. *South African Journal of Science*, 107(5-6):1 http://dx.doi.org/10.4102/sajs.v107i5/6.712

[7] Duruibe, J.O., Ogwuegbu, M. and Egwurugwu, J.N. (2007). Heavy metal pollution and human biotoxic effects. *International Journal of Physical Sciences*, 2(5):112-118 t http://www.academicjournals.org/IJPS.

[8] Al-Rashdi, B., Johnson, D.J., Hilal, N. (2013). Removal of heavy metal ions by nanofiltration. *Desalination*, 315:2-17.https://doi.org/10.1016/j.desal.2012.05.022

[9] Qin, L., Ge, Y., Deng, B., Li, Z. (2017). Poly (ethylene imine) anchored lignin composite for heavy metals capturing in water. *Journal of The Taiwan Institute of Chemical Engineers*, 71:84-90.https://doi.org/10.1016/j.jtice.2016.11.012

[10] Lofrano, G., Carotenuto, M., Libralato, G., Domingos, R.F., Markus, A., Dini, L., Gautam, R.K., Baldantoni, D., Rossi, M. and Sharma, S.K. (2016). Polymer functionalized nanocomposites for metals removal from water and wastewater: An overview. *Water Research*, 92:22-37.https://doi.org/10.1016/j.watres.2016.01.033

[11] Jiwan, S. and Kalamdhad, A.S. (2011). Effects of heavy metals on soil, plants, human health and aquatic life. *International Journal of Research in Chemistry and Environment*, 1(2):15-21.

[12] Shojaeimehr, T., Rahimpour, F., Khadivi, M.A., Sadeghi, M. (2014). A modeling study by response surface methodology (RSM) and artificial neural network (ANN) on Cu2 adsorption optimization using light expended clay aggregate (LECA). *Journal of Industrial and Engineering Chemistry,* 20(3):870-880.https://doi.org/10.1016/j.jiec.2013.06.017

[13] Oncel, M.S., Muhcu, A., Demirbas, E. andKobya, M. (2013). A comparative study of chemical precipitation and electrocoagulation for treatment of coal acid drainage wastewater. *Journal of Environmental Chemical Engineering,* 1(4):989-995.https://doi.org/10.1016/j.jece.2013.08.008

[14] Hua, M., Zhang, S., Pan, B., Zhang, W., Lv, L. and Zhang, Q. (2012). Heavy metal removal from water/wastewater by nanosized metal oxides: A review. *Journal of Hazardous Materials,* 211:317-331.https://doi.org/10.1016/j.jhazmat.2011.10.016

[15] Tutu, H., McCarthy, T.S., Cukrowska, E. (2008). The chemical characteristics of acid mine drainage with particular reference to sources, distribution and remediation: The Witwatersrand basin, South Africa as a case study. *Applied Geochemistry*, 23(12):3666-3684.https://doi.org/10.1016/j.apgeochem.2008.09.002

[16] Al-Zoubi, H., Rieger, A., Steinberger, P., Pelz, W., Haseneder, R., Hartel, G. (2010). Optimisation study for treatment of Acid Mine Drainage using membrane technology. *Separation and Technology*, 14 (14): 2004-2016. https://doi.org/10.1080/01496395.2010.480963

[17] Oakes K., Shan Z., Kaliaperumal R., Zhang S.X., Mkandawire M. (2014) Nanotechnology in Contemporary Mine Water Issues. In: Hu A., Apblett A. (eds) Nanotechnology for Water Treatment and Purification. Lecture Notes in *Nanoscale Science and Technology*, vol 22. Springer, Cham.

[18] Mohammad, A.W., Teow, Y.H., Ang, W.L., Chung, Y.T., Oatley-Radcliffe, D.L. and Hilal, N. (2015). Nanofiltration membranes review: Recent advances and future prospects. *Desalination*, 356:226-254.https://doi.org/10.1016/j.desal.2014.10.043

[19] Al-Hobaib, A.S., Al-Sheetan, K.M., Shaik, M.R. and Al-Suhybani, M.S. (2017). Modification of thin-film polyamide membrane with multi-walled carbon nanotubes by interfacial polymerization. *Applied Water Science*, 7(8):4341-4350. https://doi.org/10.1007/s13201-017-0578-5

[20] Gherasim, C., Mikulek, P. (2014). Influence of operating variables on the removal of heavy metal ions from aqueous solutions by nanofiltration. *Desalination*, 343:67-74.https://doi.org/10.1016/j.desal.2013.11.012

[21] Zarrabi, H., Yekavalangi, M.E., Vatanpour, V., Shockravi, A. and Safarpour, M. (2016). Improvement in desalination performance of thin film nanocomposite nanofiltration membrane using amine-functionalized multiwalled carbon nanotube. *Desalination,* 39483-90.https://doi.org/10.1016/j.desal.2016.05.002

[22] Kirmizakis, P., Tsamoutsoglou, C., Kayan, B. andKalderis, D. (2014). Subcritical water treatment of landfill leachate: Application of response surface methodology. *Journal of environmental management,* 1469-15.https://doi.org/10.1016/j.jenvman.2014.04.037

[23] Gholami, R.M., Mousavi, S.M. and Borghei, S.M. (2012). Process optimization and modeling of heavy metals extraction from a molybdenum rich spent catalyst by aspergillus Niger using response surface methodology. *Journal of Industrial and Engineering Chemistry,* 18(1):218-224.https://doi.org/10.1016/j.jiec.2011.11.006

[24] Varala, S., Dharanija, B., Satyavathi, B., Rao, V.B. & Parthasarathy, R. (2016). New biosorbent based on deoiled karanja seed cake in biosorption studies of zr (IV): Optimization using Box–Behnken method in response surface methodology with desirability approach. *Chemical Engineering Journal,* 302:786-800. https://doi.org/10.1016/j.cej.2016.05.088

[25] Chauhan, G., Pant, K.K. and Nigam, K.D. (2013). Development of green technology for extraction of nickel from spent catalyst and its optimization using response surface methodology. *Green processing and synthesis,* 2(3):259-271. https://doi.org/10.1515/gps-2013-0016

[26] Muhamad, M.H., Abdullah, S.R.S., Mohamad, A.B., Rahman, R.A. &Kadhum, A.A.H. (2013). Application of response surface methodology (RSM) for optimisation of COD, NH3–N and 2, 4-DCP removal from recycled paper wastewater in a pilot-scale granular activated carbon sequencing batch biofilm reactor (GAC-SBBR). *Journal of Environmental Management,* 121:179-190. https://doi.org/10.1016/j.jenvman.2013.02.016

[27] Marchetti, P., Butté, A. and Livingston, A.G. (2013). Quality by design for peptide nanofiltration: Fundamental understanding and process selection. *Chemical Engineering Science,* 101:200-212. https://doi.org/10.1016/j.ces.2013.06.014

[28] Shojaeimehr, T., Rahimpour, F., Khadivi, M.A. & Sadeghi, M. (2014). A modeling study by response surface methodology (RSM) and artificial neural network (ANN) on Cu2 adsorption optimization using light expended clay aggregate (LECA). *Journal of Industrial and Engineering Chemistry,* 20(3):870-880. https://doi.org/10.1016/j.jiec.2013.06.017

[29] Moreno-Vilet, L., Bonnin-Paris, J., Bostyn, S., Ruiz-Cabrera, M.A. andMoscosa-Santillán, M. (2014). Assessment of sugars separation from a model carbohydrates solution by nanofiltration using a design of experiments (DoE) methodology. *Separation and Purification Technology,* 131:84-93. https://doi.org/10.1016/j.seppur.2014.04.040

[30] Chan, W. and Tsao, S. (2003). Fabrication of nanofiltration membranes with tunable separation characteristics using methods of uniform design and regression analysis. *Chemometrics and intelligent laboratory systems,* 65(2):241-256. https://doi.org/10.1016/S0169-7439(02)00141-7

[31] Bashir, M.J., Amr, S.A., Aziz, S.Q., Aun, N.C. and Sethupathi, S. (2015). Wastewater treatment processes optimization using response surface methodology (RSM) compared with conventional methods: Review and comparative study. *Middle-East Journal of Scientific Research*, 23(2):244-252.

[32] Auta, M. and Hameed, B.H. (2011). Optimized waste tea activated carbon for adsorption of methylene blue and acid blue 29 dyes using response surface methodology. *Chemical Engineering Journal,* 175:233-243. https://doi.org/10.1016/j.cej.2011.09.100

[33] Maher, A., Sadeghi, M. and Moheb, A. (2014). Heavy metal elimination from drinking water using nanofiltration membrane technology and process optimization using response surface methodology. *Desalination,* 352166-173. https://doi.org/10.1016/j.desal.2014.08.023

[34] Arshadi, M. and Mousavi, S.M. (2015). Multi-objective optimization of heavy metals bioleaching from discarded mobile phone PCBs: Simultaneous cu and ni recovery using Acidithiobacillus ferrooxidans. *Separation and Purification Technology,* 147:210-219. https://doi.org/10.1016/j.seppur.2015.04.020

[35] Ndiritu, S.W., Nzila, C. and Namango, S. (2017). Optimizing chemical extraction of heavy metals from anaerobically digested sewage sludge using response surface methodology. *Ijnres,* 4:17-26. https://doi.org/10.3390/met8010040

[36] Shintani, T., Akamatsu, K., Hamada, S., Nakagawa, K., Matsuyama, H. & Yoshioka, T. (2020). Preparation of monoamine-incorporated polyamide nanofiltration membranes by interfacial polymerization for efficient separation of divalent anions from divalent cations. *Separation and Purification Technology,* 116530. https://doi.org/10.1016/j.seppur.2020.116530

[37] Gozálvez-Zafrilla, J.M., Santafé-Moros, A. and García-Díaz, J.C. (2013). Crossed mixture–process design approach to model nanofiltration rejection for non-dilute multi-ionic solutions in a given range of solution compositions. *Desalination,* 31561-69. https://doi.org/10.1016/j.desal.2012.08.009

[38] Vebber, M.C., da Silva Crespo, J. and Giovanela, M. (2019). Self-assembled thin films of PAA/PAH/TiO2 for the photooxidation of ibuprofen. part I: Optimization of photoactivity using design of experiments and surface response methodology. *Chemical Engineering Journal,* 3601447-1458 https://doi.org/10.1016/j.cej.2018.10.189.

[39] Kirchem, D., Lynch, M.Á, Bertsch, V. and Casey, E. (2020). Modelling demand response with process models and energy systems models: Potential applications for wastewater treatment within the energy-water nexus. *Applied energy*, 260114321. https://doi.org/10.1016/j.apenergy.2019.114321

[40] Hasan, H.A., Abdullah, S.R.S., Kamarudin, S.K. Kofli, N.T. (2011). Response surface methodology for optimization of simultaneous COD, NH4 –N and Mn2 removal from drinking water by biological aerated filter. *Desalination,* 275(1-3):50-61. https://doi.org/10.1016/j.desal.2011.02.028

[41] Vatanpour, V., Safarpour, M., Khataee, A., Zarrabi, H., Yekavalangi, M.E. andKavian, M. (2017). A thin film nanocomposite reverse osmosis membrane containing amine-functionalized carbon nanotubes. *Separation and Purification Technology*, 184:135-143. https://doi.org/10.1016/j.seppur.2017.04.038

[42] Liu, Y., Li, Y. and Yan, X. (2008). Preparation, characterization, and application of l-cysteine functionalized multiwalled carbon nanotubes as a selective sorbent for separation and preconcentration of heavy metals. *Advanced Functional Materials*, 18(10):1536-154. https://doi.org/10.1002/adfm.200701433

[43] Shawky, H.A., Chae, S., Lin, S. and Wiesner, M.R. (2011). Synthesis and characterization of a carbon nanotube/polymer nanocomposite membrane for water treatment. *Desalination*, 272(1):46-50. https://doi.org/10.1016/j.desal.2010.12.051

[44] Snyder filtration https://synderfiltration.com

[45] Nan Shen, J., Chao Yu, C., Min Ruan, H., Jie Gao, C. and Van der Bruggen, B. (2013). Preparation and characterization of thin-film nanocomposite membranes embedded with poly (methyl methacrylate) hydrophobic

modified multiwalled carbon nanotubes by interfacial polymerization. *Journal of Membrane Science,* 442:18-26. https://doi.org/10.1016/j.memsci.2013.04.018

[46] Ang, W.S., Tiraferri, A., Chen, K.L. and Elimelech, M. (2011). Fouling and cleaning of RO membranes fouled by mixtures of organic foulants simulating wastewater effluent. *Journal of Membrane Science*, 376(1-2):196-206. https://doi.org/10.1016/j.memsci.2011.04.020

[47] Wu, H., Tang, B. and Wu, P. (2010). MWNTs/polyester thin film nanocomposite membrane: An approach to overcome the trade-off effect between permeability and selectivity. *The Journal of Physical Chemistry C,* 114(39):16395-16400 https://doi.org/10.1021/jp107280m.

[48] Wu, H., Tang, B. and Wu, P. (2013). Optimization, characterization and nanofiltration properties test of MWNTs/polyester thin film nanocomposite membrane. *Journal of Membrane Science*, 428:425-433. https://doi.org/10.1016/j.memsci.2012.10.042

[49] Gohil, J.M. and Ray, P. (2017). A review on semi-aromatic polyamide TFC membranes prepared by interfacial polymerization: Potential for water treatment and desalination. *Separation and Purification Technology*, 181:159-182. https://doi.org/10.1016/j.seppur.2017.03.020

[50] Lee, H.D., Kim, H.W., Cho, Y.H. and Park, H.B. (2014). Experimental evidence of rapid water transport through carbon nanotubes embedded in polymeric desalination membranes. *Small*, 10(13):2653-2660. https://doi.org/10.1002/smll.201303945

[51] Masindi, V., Gitari, M.W., Tutu, H. and DeBeer, M. (2015). Efficiency of ball milled south african bentonite clay for remediation of acid mine drainage. *Journal of Water Process Engineering*, 8:227-240. https://doi.org/10.1016/j.jwpe.2015.11.001

[52] Yokwana, K. (2014). *Towards the synthesis of doped carbon nanotube/polysulfone nanofiltration membranes for the removal of organic pollutants from water*. MTech. Thesis. University of Johannesburg. Johannesburg.

[53] Zhou, C., Shi, Y., Sun, C., Yu, S., Liu, M. and Gao, C. (2014). Thin-film composite membranes formed by interfacial polymerization with natural material sericin and trimesoyl chloride for nanofiltration. *Journal of Membrane Science,* 471:381-391. https://doi.org/10.1016/j.memsci.2014.08.033

[54] Kadel, S., Persico, M., Thibodeau, J., Lainé, C. and Bazinet, L. (2019). Use of redundancy analysis and multivariate regression models to select the significant membrane properties affecting peptide migration during electrodialysis with filtration membranes. *Separation and Purification Technology,* 221114-125. https://doi.org/10.1016/j.seppur.2019.03.051

[55] Danmaliki, G.I., Saleh, T.A. and Shamsuddeen, A.A. (2017). Response surface methodology optimization of adsorptive desulfurization on nickel/activated carbon. *Chemical engineering journal,* 313:993-1003. https://doi.org/10.1016/j.cej.2016.10.141

[56] Cheng, R., Li, G., Cheng, C., Liu, P., Shi, L., Ma, Z. & Zheng, X. (2014). Removal of bacteriophage f2 in water by nanoscale zero-valent iron and parameters optimization using response surface methodology. *Chemical Engineering Journal,* 252:150-158. https://doi.org/10.1016/j.cej.2014.05.003

[57] Fan, J., Luo, J., Zhang, X., Zhen, B., Dong, C., Li, Y., Shen, J., Cheng, Y. & Chen, H. (2019). A novel electrospun β-CD/CS/PVA nanofiber membrane for simultaneous and rapid removal of organic micropollutants and heavy metal ions from water. *Chemical Engineering Journal,* 378122232. https://doi.org/10.1016/j.cej.2019.122232

[58] Aghaei, F. and Jalilzadeh Yengejeh, R. (2017). Investigation of effective parameters on the performance of NF membrane in simultaneous removal of cr (VI) and cu from contaminated water. *Pollution*, 3(3):383-394. https://jpoll.ut.ac.ir

[59] Murugesan, A., Vidhyadevi, T., Kalaivani, S.S., Thiruvengadaravi, K.V., Ravikumar, L., Anuradha, C.D. and Sivanesan, S. (2014). Modelling of lead (II) ion adsorption onto poly (thiourea imine) functionalized chelating resin using response surface methodology (RSM). *Journal of water process engineering,* 3:132-143. https://doi.org/10.1016/j.jwpe.2014.06.004

[60] Tansel, B., Sager, J., Rector, T., Garland, J., Strayer, R.F., Levine, L., Roberts, M., Hummerick, M. and Bauer, J. (2006). Significance of hydrated radius and hydration shells on ionic permeability during nanofiltration in dead end and cross flow modes. *Separation and Purification Technology*, 51(1):40-4. https://doi.org/10.1016/j.seppur.2005.12.020

[61] Rivas, B.L., Pereira, E.D., Palencia, M. and Sánchez, J. (2011). Water-soluble functional polymers in conjunction with membranes to remove pollutant ions from aqueous solutions. *Progress in Polymer Science*, 36(2):294-322. https://doi.org/10.1016/j.progpolymsci.2010.11.001

[62] Rahimpour, A., Jahanshahi, M., Mortazavian, N., Madaeni, S.S. and Mansourpanah, Y. (2010). Preparation and characterization of asymmetric polyethersulfone and thin-film composite polyamide nanofiltration membranes for water softening. *Applied Surface Science*, 256(6):1657-1663. https://doi.org/10.1016/j.apsusc.2009.09.089

[63] Xin, F. and Li, L. (2011). Decoration of carbon nanotubes with silver nanoparticles for advanced CNT/polymer nanocomposites. *Composites Part A: Applied Science and Manufacturing*, 42(8):961-967. https://doi.org/10.1016/j.compositesa.2011.03.024

[64] Al-Zoubi, H., Rieger, A., Steinberger, P., Pelz, W., Haseneder, R., Hartel, G. (2010). Optimisation study for treatment of Acid Mine Drainage using membrane technology. *Separation and Technology*, 14 (14): 2004-2016. https://doi.org/10.1080/01496395.2010.480963

[65] Pino, L., Vargas, C., Schwarz, A. and Borquez, R. (2018). Influence of operating conditions on the removal of metals and sulfate from copper acid mine drainage by nanofiltration. *Chemical engineering journal,* 345:114-125. https://doi.org/10.1016/j.cej.2018.03.070

[66] Yang, W., Xu, H., Chen, W., Shen, Z., Ding, M., Lin, T., Tao, H., Kong, Q., Yang, G. and Xie, Z. (2020). A polyamide membrane with tubular crumples incorporating carboxylated single-walled carbon nanotubes for high water flux. *Desalination*, 479:114330. https://doi.org/10.1016/j.desal.2020.114330

[67] Suresh, K., Pugazhenthi, G. and Uppaluri, R. (2016). Fly ash based ceramic microfiltration membranes for oil-water emulsion treatment: Parametric optimization using response surface methodology. *Journal of water process engineering,* 13:27-43. https://doi.org/10.1016/j.jwpe.2016.07.008

[68] Salahi, A., Noshadi, I., Badrnezhad, R., Kanjilal, B. and Mohammadi, T. (2013). Nano-porous membrane process for oily wastewater treatment: Optimization using response surface methodology. *Journal of environmental chemical engineering,* 1(3):218-225. https://doi.org/10.1016/j.jece.2013.04.021

[69] Singh, C., Srivastava, S., Ali, M.A., Gupta, T.K., Sumana, G., Srivastava, A., Mathur, R.B. and Malhotra, B.D., (2013). Carboxylated multiwalled carbon nanotubes based biosensor for aflatoxin detection. *Sensors and Actuators B: Chemical*, 185:258-264. https://doi.org/10.1016/j.snb.2013.04.040

[70] Hilal, N., Al-Zoubi, H., Darwish, N.A. and Mohammad, A.W. (2005). Characterisation of nanofiltration membranes using atomic force microscopy. *Desalination*, 177(1-3):187-199. https://doi.org/10.1016/j.desal.2004.12.008

[71] Shawky, H.A., Chae, S., Lin, S. and Wiesner, M.R. (2011). Synthesis and characterization of a carbon nanotube/polymer nanocomposite membrane for water treatment. *Desalination*, 272(1):46-50. https://doi.org/10.1016/j.desal.2010.12.051

[72] Tang, C.Y., Kwon, Y. and Leckie, J.O. (2009). Effect of membrane chemistry and coating layer on physiochemical properties of thin film composite polyamide RO and NF membranes: I. FTIR and XPS characterization of polyamide and coating layer chemistry. *Desalination*, 242(1-3):149-167. https://doi.org/10.1016/j.desal.2008.04.003

[73] Rezania, H.J., Vatanpour, V., Shockravi, A. and Ehsani, M. (2019). Study of synergetic effect and comparison of novel sulfonated and carboxylated bulky diamine-diol and piperazine in preparation of negative charge NF membrane. *Separation and Purification Technology*, 222:284-296. https://doi.org/10.1016/j.seppur.2019.04.043

[74] El-Arnaouty, M.B., Eid, M. and Abdel Ghaffar, A.M. (2015). Radiation synthesis of stimuli responsive micro-porous hydrogels for controlled drug release of aspirin. *Polymer-Plastics Technology and Engineering*, 54(12):1215-1222. https://doi.org/10.1080/03602559.2014.1003229

[75] Khayet, M., Cojocaru, C. and Essalhi, M. (2011). Artificial neural network modeling and response surface methodology of desalination by reverse osmosis. *Journal of Membrane Science,* 368(1-2):202-214. https://doi.org/10.1016/j.memsci.2010.11.030

[76] Dalwani, M., Benes, N.E., Bargeman, G., Stamatialis, D. and Wessling, M. (2011). Effect of pH on the performance of polyamide/polyacrylonitrile based thin film composite membranes. *Journal of Membrane Science*, 372(1-2):228-238. https://0-doi-org.ujlink.uj.ac.za/10.1016/j.memsci.2011.02.012

[77] Misdan, N., Lau, W.J., Ismail, A.F., Matsuura, T. and Rana, D., 2014. Study on the thin film composite poly (piperazine-amide) nanofiltration membrane: Impacts of physicochemical properties of substrate on interfacial polymerization formation. *Desalination*, *344*, pp.198-205.https://0-doi-org.ujlink.uj.ac.za/10.1016/j.desal.2014.03.036

[78] Anand, A., Unnikrishnan, B., Mao, J., Lin, H. and Huang, C. (2018). Graphene-based nanofiltration membranes for improving salt rejection, water flux and antifouling–A review. *Desalination,* 429:119-133. https://doi.org/10.1016/j.desal.2017.12.012